T I M E A N D F R E Q U E N C Y D O M A I N

M O D E L L I N G O F T H E

P I E Z O E L E C T R I C T R A N S D U C E R

PRESENTED BY

GORDON HAYWARD

Vol II

In the fulfilment of the requirement for the degree of Doctor of Philosophy of the University of Strathclyde

Department of Electronic Science and Telecommunications

December 1981 Glasgow

A P P E N D I X A

A.1 FUNDAMENTAL PIEZOELECTRIC RELATIONSHIPS

In general, an elastic solid has 36 values of elastic constant, corresponding to 6 components of stress and 6 components of strain. However, the present context considers only one longitudinal component of stress, relating to one value of strain along only one axis of the crystal; namely its thickness direction. That is, any changes in mechanical (and electrical) quantities occur only in the one direction. Hooke's law, relating stress to strain, may now be expressed as follows (for the x-direction),

$$\Gamma = Y \frac{\partial \xi}{\partial x}$$

Γ is the stress in N/m^2,
Y is Young's modulus of elasticity in N/m^2.

$$\Gamma = YS_x \qquad S_x = \frac{\partial \xi}{\partial x}$$

is the strain, where ξ is the particle displacement.

Secondly, employing the relationship between electrical displacement, electric field strength and charge polarisation in a dielectric,

$$D = \varepsilon_o E + P = \varepsilon E$$

where D is the electrical displacement or surface charge density in coulombs per square metre (C/m^2),

ε_o is the permittivity of free space,

ε is the permittivity of the dielectric material (Farads/metre),

P is the polarisation, or induced surface charge density in C/m^2, and

E is the electric field in the dielectric (V/m).

Consider a piezoelectric crystal placed between two electrodes. The crystal is then subjected to a compressive stress, resulting in a strain, S_x, developed in the material. The strain is given by,

$$S_x = \frac{\Gamma}{Y^E}$$

where Y^E indicates that the elastic modulus was measured under conditions of constant electric field.

The applied stress also produces a polarisation of charge, P_p, in the crystal. Defining d as the charge density produced per applied mechanical stress, then

$$P_p = d\Gamma$$

where d is expressed in Coulombs per Newton.

Consequently, the total dielectric displacement in a piezoelectric crystal which is simultaneously subjected to an applied electric field and mechanical stress is given by,

$$D = \epsilon_o E + P_D + P_p$$

where P_D is the dielectric polarisation and P_p is the piezoelectric polarisation. This then results in an expression for D, viz:

$$D = \epsilon E + P_p, \text{ or}$$

$$D = \epsilon_\Gamma E + d\Gamma$$

ϵ_Γ indicates that the permittivity was measured under conditions of constant stress. The above equation describes the electric displacement D, in a piezoelectric crystal which is simultaneously subjected to an applied electric field E, and a mechanical stress, Γ.

In addition, if an electric field is applied to a mechanically free crystal, then a strain is introduced within the crystal. Since the direct and inverse piezoelectric effects are assumed to be equal and opposite, then the induced strain is related to the applied field by the piezoelectric constant, d, ie

$$S_x = dE$$

where, in this case, d is the strain developed per applied

electric field in metres per volt. Consequently, in the general case for both an electric field and mechanical stress applied simultaneously to the crystal, the total strain included in the material is given by,

$$S_x = \frac{\Gamma}{Y^E} + dE$$

The previous two equations can be expressed in a somewhat different manner if, instead of keeping the stress constant for the measurement of permittivity, the strain is kept constant by mechanically clamping the crystal. For this case, we define:

e = charge density developed/applied mechanical strain

where e is expressed in Coulombs per metre^2. In this case, the piezoelectric constant, e, represents the direct effect. For the indirect effect we have,

e = stress developed/applied electric field

where e is expressed in Newtons/volt/metre.

In an analogous manner to the case for constant stress, the following two piezoelectric equations are obtained

$$D = \varepsilon^{S_x} E + eS_x \qquad \text{(Direct effect)}$$

$$\Gamma = Y^E S_x + eE \qquad \text{(Inverse effect)}$$

where ε^{Sx} indicates that the permittivity was measured under conditions of constant strain.

To summarise, there are four basic piezoelectric relations. Two describe the direct and inverse effects for the material permittivity measured under conditions of constant stress (a mechanically free crystal). The remaining two describe the effects for the permittivity measured under conditions of constant strain (a mechanically clamped crystal). In all four equations the elastic constant is measured under conditions of constant electric field.

Mason (A2) pointed out that when the piezoelectric equations are expressed in the previous manner, the elastic, dielectric and piezoelectric constants can vary widely with temperature, plating conditions and conditions of strain. He expressed the piezoelectric relationships in terms of charge and introduced the boundary condition of constant electrical displacement. This condition can be approximately realised when a piezoelectric crystal is electrically isolated. That is, when the electrodes are open circuit. In this case, Hooke's law can be expressed as:

$$T = Y^{D} S_{x}$$

where Y^{D} is the elastic modulus measured under conditions of constant electrical displacement (or constant free charge density).

The free surface charge must also induce a component of strain in the material, which gives rise to a piezoelectric component of stress. This stress component is related to the displacement D by the piezoelectric constant h, where h is defined as the stress developed per applied surface charge density, in Newtons per Coulomb.

This then leads to the relationship describing the inverse effect

$$T = Y^D S_x - hD$$

Similarly under mechanically clamped (constant strain) conditions we have the relationship,

$$E = D/\epsilon^{S_x}$$

In this case, defining h as the electrical field developed per applied mechanical strain, the relationship for the direct effect can be obtained.

$$E = -hS + D/\epsilon^{S_x}$$

A.2 ELECTRICAL AND MECHANICAL BOUNDARY CONDITIONS

In general, the elastic or mechanical boundary conditions are of importance during the converse piezoelectric effect, that is, when an electric field is being impressed upon the crystal. Similarly, the electrical boundary conditions are usually considered during conditions of applied mechanical

stress, ie the direct piezoelectric situation. Both of these cases have been neatly summarised by Cady (A1) when he stated that, 'The resultant polarisation produced in a piezoelectric plate by the application of an electric field depends on the mechanical relaxation of the plate', and 'The resultant strain produced in a piezoelectric plate due to the application of a mechanical stress depends on the electrical relaxation of the plate.'

In general, two extremes of mechanical boundary condition exist, these being defined as free (constant external stress) and clamped (constant external strain).

For the case of the mechanically free crystal, the crystal is considered to be free from all external stress. This condition may be realised by placing the piezoelectric material in a surrounding medium which has infinite compliance, such as a vacuum, or even air. Consequently, when an electric field is applied, the resultant polarisation is purely dielectric and the resultant strain is due entirely to the inverse piezoelectric effect. Measurements of the dielectric constant of piezoelectric transducers are usually performed with the devices in the mechanically free condition. Consequently, under the assumption that all mechanical and electrical relations are linear, then the same value of dielectric constant would be observed if the mechanical stress system is not zero, but is held constant.

In the case of the mechanically clamped piezoelectric transducer, the strain is held at a constant value by applying a mechanical stress which counteracts strains set up by an applied electric field due to the inverse effect. Consequently, no net mechanical displacement can take place. Although theoretically feasible, this condition is extremely difficult to achieve in practice. Another technique is to rigidly mount all of the crystal surfaces, so that there is no net mechanical motion.

There are similarly two extremes of electrical boundary condition, these being defined as free (constant electric field) and clamped (constant electrical polarisation or constant electrical displacement).

The electrically free piezoelectric crystal can be realised by rendering the entire plate surfaces equipotential. In the case of a piezoelectric disc, this condition can be achieved by simply short-circuiting the electrodes. There is thus no measurable electric field in the crystal and if the material is now mechanically stressed, any resultant polarisation within the crystal is due entirely to the direct effect. Static measurements of the elastic constants are generally made with the piezoelectric material in the electrically free state. Also, assuming all electromechanical relations to be linear, the value of elastic constant would be the same as that for which the electric field was maintained constant.

The electrically clamped condition of constant electrical polarisation, (or according to Mason (A2) constant electrical displacement), can be achieved by applying a counter-field of suitable intensity that it neutralises the polarisation induced directly by an applied mechanical stress. This situation can be approximated by allowing the electrodes to be open circuit, whereby the piezoelectric polarisation due to an applied strain gives rise to polarisation charges, from which all lines of force turn back through the crystal. The net effect is to produce a depolarising field of the correct magnitude to make the resultant polarisation and displacement zero both inside and outside of the crystal.

A.3 SECONDARY PIEZOELECTRIC ACTION

When a piezoelectric crystal is subject to mechanical stress, a polarisation of electrical charge is produced within the crystal, due to the direct piezoelectric effect. This generally gives rise to an electric field within the material, the form and magnitude of which depends on the system boundary conditions. The direction of the electric field is such as to oppose the direction of the incident mechanical stress. It is also possible that the electric field, by virtue of the converse piezoelectric effect, can cause extra components of strain to arise within the crystal. Such secondary components of strain are additional to those introduced by the incident mechanical stress.

An applied electric field induces a primary polarisation of charge in the piezoelectric material, which through the converse effect, introduces a state of strain within the crystal. The resultant stress magnitude is dependent on external boundary conditions and has a direction opposite to that of the incident electric field. It is also possible that the mechanical stress may produce a secondary polarisation of charge within the crystal, resulting in an additional component of electric field.

REFERENCES

A1 CADY

A2 MASON, W. P., Electromechanical transducers and wave filters (2nd Edit), Van Nostrand, New York, 1948.

A P P E N D I X B

GENERAL ELECTRICAL LOADING CONDITIONS FOR THE PIEZO-ELECTRIC TRANSDUCER

The nature of the electrical load plays an important role in determining the output waveshape in both transmitting and receiving modes. It is desired to model transducer behaviour under the majority of electrical loading conditions likely to be encountered in practice and hence determine how variations in these parameters modify transducer performance.

A general case of the transducer operating in pulse-echo mode is considered. That is, the same transducer is employed as a transmitter and receiver, with the resultant complications in electrical load conditions. The principal loading elements for a transducer operating in this manner are shown in figure B1 and the main features may be summarised as follows.

B.1 Transmitter Output Impedance (Z_o)

In the case of CW or gated CW operation, this network comprises the output resistance of the generator, in series with any capacitive or inductive coupling components which may be present. In pulse excitation systems the output characteristics involve more complex R-C networks which

determine the time constant and pulse repetition frequency (prf). However, as described in Appendix C, these may also be characterised by an output resistance in series with inductive or capacitive coupling components.

B.2 The Connecting Cable

For those applications where significant lengths of lossy interconnecting cable are involved, a lumped transmission line equivalent circuit may be employed in order to evaluate the resultant signal attenuation. However, for the present purpose it is assumed that the transducer and adjoining stages are situated in close proximity and hence interconnecting effects may be neglected. That is, the cable is of a low loss type and its length is restricted to less than two metres. In practice the majority of transmitters conform to this situation and when operating in the receiving mode, driving of longer cable lengths is usually achieved via a buffer stage situated in close proximity to the transducer.

B.3 The Matching Network (Z_E)

This may be part of a pulse shaping network comprising a resistor or the parallel combination of a resistor and an inductor. The matching network may also form part of an electrical tuning system designed to match the transducer to the electrical load in order to improve power transfer.

The tuning element normally consists of an inductor connected in series or in parallel with the transducer.

B.4 The Amplifier Protection Network

This is incorporated in pulse-echo systems in order to protect the amplifier from the excitation voltage. In many practical systems an electronic switch, (usually a switching FET) which remains non-conducting during the firing period is employed. The switch is then turned on, effectively linking transducer to amplifier for the receiving mode. Such devices are designed to have very low conducting resistances (<2Ω) and can isolate or block voltages up to 1 kV.

B.5 The Receiver Coupling Network

This is assumed to comprise a coupling capacitor which may, or may not be present, depending on the particular application.

B.6 The Amplifier Input Impedance

The input impedance of any successive amplifying stage may be regarded as consisting of the parallel combination of a resistor and a capacitor. However, the input capacitance of a wideband receiving stage is very much less than either of the transducer capacitances (typically <1 pf) and hence this component may be neglected. The input impedance thus consists of a pure resistance, which may vary from 50Ω to

10 MΩ, depending on the application.

In addition, the following points should be noted concerning differences in electrical loading between the transmitting and receiving modes.

B.6i Transmitting mode

The pre-amplifier characteristics are not included, since the receiver is assumed to be isolated during the excitation period. This may arise as a result of physical separation as in separate transmit-receive systems, or because of suitable protection circuitry when operating in the pulse-echo mode. Consequently, the transducer is assumed to be loaded by the impedances Z_o and Z_E, as shown in figure B.2a.

B.6ii Receiving mode

For pulsed operation, the electronic pulser is assumed non-conducting at the instant when the pressure signal is received. It may thus be considered on open circuit during the reception interval. In addition, the protection circuit is assumed ideal, ie a short circuit during the reception interval. Electrical loading for the receiver is shown in figure B.2b.

A P P E N D I X C

TRANSMITTING CIRCUITRY

C.1 CW Operation

The transducer is assumed to be driven from a voltage generator acting as a continuous wave source (CW) or providing pulsed sinusoidal packets from one half to several cycles in duration. This latter mode is termed gated CW operation. Both techniques are extensively employed in transducer calibration studies involving the determination of piezoelectric parameters and in the measurement of transducer beam characteristics. Gated CW is extensively employed in sonar, underwater communications and in applications where the power spectrum is required to be contained within a narrow band. It is also used in some non-destructive testing applications where high energy may constitute a primary requirement.

In all cases, the transducer is electrically driven from a wave generator or power amplifier possessing a specific output impedance over the operating frequency range. This is invariably resistive and often matched for 50Ω operation. It should be noted that the exciting waveform need not be a pure sinusoid, the stimulus may be a step function or periodic square wave train; but invariably a sinusoidal forcing function is employed.

C.2 Pulsed or Transient Operation

In this instance, the transducer is stimulated by the rapid deposition of a quantity of charge on the electrodes. This method is extremely common in NDT and biomedical applications where short duration, high intensity bursts of ultrasound are required. It has also found widespread use in acoustic imaging and ultrasonic spectroscopy, where a primary requirement is for wideband acoustic signals.

A typical electronic pulser of this type is shown in figure C.1. In the figure, a blocking capacitor, C_B, is charged to the HT potential via a resistor R. Depending on the particular application, the HT voltage may vary from 5 V to 3 kV. The switch S_1 is a fast electronic device which, when activated, results in a transference of charge from the blocking capacitor to the transducer and its associated electrical load, Z_E. Suitable types of switches include valves, thyristors, avalanche and VMOS (switching FET) transistors; the individual characteristics of which are briefly presented in Section C.4.

C.3 Analysis of Transient Operation

The electronic switch may be characterised by its turn on time (t_o) and internal resistance when in the conducting state (R_{on}), both of which may vary widely from device to device. For example, turn on time ranges from a few nanoseconds up to several microseconds for some of the slower

thyristors. In some devices, Ron may assume values of 10-20Ω, but in the more modern thyristors and switching FETS, this value is negligible, being as low as 0.3Ω in some instances. Consequently, in the present analysis the switch is assumed to possess zero on resistance and a finite turn on time. It should be noted however that provision is made for including internal resistance in the simulation package describing the piezoelectric transmitter.

From figure C.1 it may be observed that this mode of operation is equivalent to applying a ramp function to the blocking capacitor C_B. The ramp function descends from HT volts to zero volts in a time equal to t_o; and is assumed to remain at zero volts for the remainder of the firing interval. The equivalent circuit and input waveform are shown in figure C.2, where, for analytic convenience, the transducer has been replaced by its static capacitance, C_o. Since the transducer impedance may be regarded as equivalent to the impedance of this capcitance, modified by secondary piezoelectric effects, the main features of the pulser transducer configuration may readily be observed. The resistor R is assumed much greater than R_E, and hence has little influence on circuit operation. Consequently, the input voltage may be described as follows:

$$e_{in} = \frac{-V_m t}{t_o} + \frac{V_m (t - t_o)}{t_o}$$

where V_m = HT volts.

This is equivalent to applying a negative going ramp function at t = 0 and then adding to it a positive going ramp function at $t = t_o$. As a result, the Laplace Transform of the input voltage may be described by the following equation:

$$e(S) = \frac{-V_m}{S^2 t_o} (1 - e^{-St_o}) \qquad 1$$

In addition, the transfer function relating e and V_o may be expressed by,

$$\frac{V_o(S)}{e(S)} = \frac{S^2 R_E L_E C_B}{S^2 R_E L_E (C_o + C_B) + SL_E + R_E}$$

therefore

$$V_o(S) = \frac{-V_m}{t_o} (1 - e^{-St_o}) \left(\frac{1}{S^2 a + Sb + c} \right)$$

where

$$a = \frac{C_o + C_B}{C_B}, \quad b = \frac{1}{R_E C_B}, \quad c = \frac{1}{L_E C_B}$$

Completing the square in this equation gives,

$$V_o(S) = \frac{-V_m}{t_o a} (1 - e^{-St_o}) \left(\frac{1}{(S + \alpha)^2 + \omega^2} \right)$$

where

$$\alpha = b/2a, \quad \omega^2 = C/a - b^2/4a^2$$

This equation has a standard inverse Laplace Transform which may be expressed as follows:

$$V_o(t) = \frac{-V_m e^{-\alpha t}}{t_o a \omega} \{\sin \omega t - e^{\alpha t_o} \sin \omega(t - t_o)\} \qquad \text{——— 2}$$

$$\alpha = \frac{1}{2R_E(C_o + C_B)}$$

$$\omega = \left\{ \frac{1}{L_E(C_o + C_B)} - \frac{1}{4R_E^2(C_o + C_B)^2} \right\}^{\frac{1}{2}}$$

The main characteristics of equation 2 may be summarised as follows.

C.3i Over damping in the system

In this case ω is imaginary, ie

$$L_E > 4R_E^2(C_o + C_B)$$

This results in a wide pulse across the transducer, and hence is not normally encountered in practice.

C.3ii Underdamping

ω is real and hence,

$$L_E < 4R_E^2(C_o + C_B)$$

This produces a ringing waveform across the transducer, the frequency of which depends on the relative values of R, L_E and C_B. In practice, these components may be selected to optimise the ringing frequency for the particular transducer, thereby maximising the output pressure. Operation thus tends to be narrowband.

C.3iii Critical damping

ω is zero, and

$$L_E = 4R^2(C_o + C_B)$$

This condition is difficult to achieve in practice, as some degree of overshoot is usually evident. However, very narrow pulses can be achieved across the transducer and this form of excitation is suitable for wideband applications.

C.3iv The effect of pulser turn on time

At $t = t_o$, the voltage across the static capacitance is given by,

$$V_o(t) = \frac{-V_m e^{-\alpha t_o}}{a} \left\{\frac{\sin \omega t_o}{\omega t_o}\right\}$$

For t_o equal to zero; that is, an ideal switch,

$$V_o(t) = -V_m C_B/(C_o + C_B)$$

This is the maximum value of voltage which may be applied to the transducer system, for fixed values of C_o and C_B. Consequently, increasing the turn on time serves to reduce the applied voltage signal, hence reducing the efficiency of the configuration. The effect of varying pulser turn on time is shown in figure C.3; for two values of turn on time, equal to 10 and 200 ns. The improvement in applied voltage for the faster device is clearly observed.

C.4 Practical Switching Devices

C.4i Valves

Although capable of handling large amounts of current and possessing very fast switching times, valves have been largely superceded by solid state devices in pulsed ultrasonic applications. However, they are still used in some high intensity applications where high voltages and fast turn on times are required. For example, the Krytron KN-22 can switch 1.5 kV in under 20 ns and is comparable in size with most commercially available solid state devices.

C.4ii Avalanche transistor

Bipolar transistors operating in the avalanche mode are characterised by fast switching times (10-100 ns) and low values of 'ON' resistance (<10Ω typically). However, they are limited by the maximum value of HT voltage which the transducer is capable of holding; commercially available

types being restricted to approximately 300 V. Although higher voltages are possible by cascading devices, the associated circuitry becomes more complex in order that simultaneous conduction is ensured.

C.4iii Silicon controlled rectifier (SCR)

These devices are commonly used in ultrasonic pulser applications, where speed, energy and reliability are a primary requirement. However, as an ultrasonic transmitter, SCRs suffer from the following disadvantages:

a. Commercially available thyristors are limited in speed and there is invariably a trade-off between HT voltage and turn on time. In addition, SCRs with turn on times less than 100 ns tend to be expensive.

b. The internal resistance is high, in the region of 20Ω for many devices.

c. The SCR is difficult to turn off. The most common method of achieving turn off is to ensure that the 'ON' current through the device is less than the stipulated holding current. This is normally performed by selecting a high enough value of resistance R in the HT chain and as a result, often comprimises the pulse repetition rate of the system. Turn off time of the thyristor can be as high as 100 μs in some instances. However, it should be noted that recent developments in thyristor technology

have produced the gate controlled device, which may be switched on or off from the gate terminal. However, switching times are still relatively slow when compared with avalanche transistors and FETs.

C.4iv The switching MOSFET

In the last two years, high power mosfets (C1) have become commercially available and these devices, with their high operating voltages (1 kV), very fast switching times (10 ns) and low 'ON' resistance (0.3Ω) are expected to supercede both thyristors and avalanche transistors in ultrasonic pulser circuits.

A typical example outlining the performance characteristics of these devices is the International Rectifier IRF 830, which is capable of handling peak currents of 7A (3A continuous) and operates up to 500 V with a rated switching time of 30 ns. The resistance in the conducting state is only 1.3Ω and consequently, this switch approximates closely to the ideal situation. That is, a device possessing zero internal resistance and capable of producing a step function of voltage.

Although faster devices are commercially available they tend to be more expensive and hence the IRF 830 was employed in all of the experimental work concerning transient operation. The results of these investigations are presented in chapters VI and VII. A circuit diagram showing

the operational mode of this device is shown in figure C.4. This circuit was employed in the experimental investigations of chapters VI and VII.

REFERENCE

C1 VMOS Power FET Design Catalogue, Siliconix Ltd, January 1979.

A P P E N D I X D

TRANSDUCER CHARACTERISTICS

Physical characteristics of the various thickness mode transducers used in the experimental work are shown in tables D.1 and D.2. Four different values of electrical resonant frequency were selected (0.5, 1, 2 and 4 mHz), thereby permitting a wide range of diameter/thickness ratios to be studied. The frequencies of mechanical resonance were calculated from the transit times, by dividing the corresponding thickness with the longitudinal wave velocity.

It should be noted that variations of 5, 10 and 20 per cent are not uncommon in the elastic, piezoelectric and dielectric constants respectively. In addition, the following tolerance variations in physical dimensions and frequency are quoted by the transducer manufacturers.

Thickness variation ± 0.5 mm
Diameter variation ± 0.15 mm
Frequency variation ± 7 per cent

Where possible, individual crystal dimensions were carefully measured using a micrometer and without exception, all crystals were found to be well within the tolerance range. The individual values of free capacitance were checked at 1 kHz by means of a Wayne-Kerr Bridge (Universal Bridge B224) and in some instances deviations up to 15 per cent

were encountered. Direct measurement of clamped capacitance proved extremely difficult and was confined to those transducers possessing a diameter to thickness ratio of greater than 20:1. Consequently, measurement of C_o was confined to the higher frequency devices (2 mHz and 4 mHz) and this was performed at a frequency equivalent to twice the mechanical resonance, when no secondary action takes place.

In these instances, the clamped capacitance may be obtained from the voltage transfer characteristic by means of the following method.

Consider a voltage generator, possessing an output resistance R_o, driving a capacitive load of value C_o. The ratio of input voltage (V_i), to the measured voltage across the capacitance (V_o) is thus given by,

$$\left|\frac{V_o}{V_i}\right| = \left|\frac{1}{1 + j\omega R_o C_o}\right|$$

Let $x = \left|\frac{V_o}{V_i}\right|$

therefore

$$x^2 = \frac{1}{1 + \omega^2 R_o^2 C_o^2}$$

therefore

$$C_o = \left(\frac{1 - x^2}{x^2}\right)^{\frac{1}{2}} \frac{1}{2\pi f R_o}$$

If the load is a piezoelectric transducer, then at a frequency equivalent to twice the mechanical resonance, the transducer impedance is equal to the impedance of the device static capacitance. Consequently, the static capacitance may be obtained from the following formula:

$$C_o = \left(\frac{1 - x^2}{x^2}\right)^{\frac{1}{2}} \frac{1}{4\pi f_2 R_o}$$

where

$$x = \left|\frac{V_o}{V_i}\right|$$

measured at two times mechanical resonance.

$\left|\frac{V_o}{V_i}\right|$ is the normalised value of the transfer characteristic, as defined in chapter VI,

f_2 is the frequency of mechanical resonance, and

R_o is the output resistance of the voltage generator.

In almost every case, considerable deviation from the manufacturer's specified values were encountered. These may readily be observed from table D.2, where differences of 20 per cent between theoretical and measured values of clamped capacitance are evident.

For those transducers possessing lower diameter/thickness ratios, measurement of clamped capacity by means of this

technique is extremely difficult owing to unwanted, radial modes of vibration corrupting the results. In these instances, an estimate of clamped capacity was made from the voltage transfer characteristics, as described in chapter VI.

The various transducer parameters outlined in tables D.1 and D.2 may be summarised as follows:

a Transducer Material

The transducer material in every case was lead Zirconate Titanate (PZI-5A). It is characterised by a high electro-mechanical coupling coefficient and high charge sensitivity.

b Density

$$\rho = 7.75 \text{ kg/m}^3$$

c Compression Wave Velocity in the Thickness Direction

This is the longitudinal wave velocity in a direction parallel to the polar axis. It is measured under conditions of constant charge density.

$$V_t^D = 4350 \text{ m/sec}$$

d Acoustic Impedance (Per Unit Area)

$$Z_C = \rho V_t^D = 33.712 \times 10^6 \text{ kg/s-m}^2$$

e Free Relative Dielectric Constant

This is normally measured at a low frequency of around 1 kHz.

$$\varepsilon_{33}^{T} = 1700$$

It should be noted that this figure may be as low as 1300. Consequently, individual measurements should be performed on each crystal.

f Free Dielectric Loss Factor

This is usually measured at 1 kHz under conditions of low electric field.

$$\tan \delta = 0.02$$

This parameter increases under high field conditions. For example,

$$\tan \delta = 0.04 \quad \text{at } E = 1 \text{ kV/cm}$$

g Clamped Relative Dielectric Constant

This is normally measured at frequencies well above mechanical resonance, where inertia effects minimise secondary action.

$$\varepsilon_{33}^{S} = 830$$

This dielectric constant defines the transducer static capacity and hence the value is of great importance in verifying simulation results.

h Thickness Coupling Factor

This is the electromechanical coupling factor for a laterally clamped transducer operating in the thickness mode.

$$K = 0.486$$

i Piezoelectric Constant

$$h_{33} = 21.5 \times 10^8 \text{ V/m}$$

j Transducer Frequency Constant

This is defined as the product of the electrical resonant frequency and the thickness of a thin plate which is operating in the thickness mode.

$$N_3 t = 1890 \text{ Hz} - \text{metres}$$

k Elastic Stiffness

This is measured under conditions of constant charge density.

$$Y_{33}^D = 14.7 \times 10^{10} \text{ N/m}^2$$

$$K^2 = h_{33}^2 \ (\epsilon_{33}^S / Y_{33}^D)$$

The transducer data was obtained from the following production sheets:

Vernitron Bulletin 66047/A (January 1975)

Vernitron Bulletin 66011/F (January 1976)

Vernitron Bulletin 66017/B (March 1976)

Unilator Technical Ceramics Ltd, data sheet 'Piezoelectric Ceramics'.

Appendix E

Selected Program Listings

```
100 REM TIME AND FREQUENCY RESPONSE OF TRANSMITTER
110 PRINT "FREQUENCY(1) OR TIME(2)"
120 INPUT F8
122 PRINT "STEP(1) OR SIN (2) I/P"
123 INPUT F9
124 PRINT "AMP. OF STEP I/P?"
125 INPUT S4
130 PRINT "O/P IMP PARAMS?-R0(T1),CC(T2),LC(T3)"
140 INPUT T1,T2,T3
150 PRINT "MATCHING CCT PARAMS?-RM(T4),LM(T5)"
160 INPUT T4,T5
170 PRINT "TXDCR PARAMS?-K(S1),ZF(Z1),ZB(Z2)"
180 INPUT S1,Z1,Z2
190 REM OTHER TXDCR PARAMS-RF=R1,RB=R2,H=H1,C0=C9,ZC=Z3
200 Z3=33.712
210 H1=2.15*10^3
220 C9=0.00105
230 R1=(Z3-Z1)/(Z3+Z1)
240 R2=(Z3-Z2)/(Z3+Z2)
250 REM SAMPLING RATE
260 PRINT "TRANSIT TIME AND FREQ SAMPLING INTERVAL"
270 INPUT T,F
280 PRINT "NO OF SAMPLES?"
290 INPUT L
300 DIM X(L,2)
310 REM PLOTS I/P ADMITTANCE(YI) OR FBK ADMITTANCE(YF)
312 REM PLOTS CURRENTFBK FACTOR(ATF) OR TRANSFER FUNCTION(H)
314 REM PLOTS TOTAL AMOUNT OF CURRENT FEEDBACK(AT) OR TOTAL CURRENT(IT)
315 REM PLOTS FBK IMPEDANCE AMP AND PHASE(ZF,PHF)
316 REM SET FLAG FOR FREQUENCY PLOT
318 IF F8=2 THEN 335
320 PRINT "SET V=1(YI),2(YF),3(ATF),4(H),5(AT),6(IT),7(ZF) OR 8(PHF)"
330 INPUT V
332 GO TO 340
335 V=4
340 FOR I=1 TO L/2+1
350 M=I-1
360 W=2*PI*F*M
370 IF I=1 THEN 1020
380 REM EVALUATE DRIVING CCT O/P IMP (Z0=A1+JB1)
```

```
1130 C=1
1140 PRINT "WINDOW CO-ORDS-X1,X2,Y1,Y2"
1150 INPUT A1,A2,B1,B2
1160 PAGE
1170 WINDOW A1,A2,B1,B2
1180 VIEWPORT 10,100,10,90
1190 AXIS @C:(A2-A1)/10,(B2-B1)/10
1200 FOR I=1 TO L/2+1
1205 IF V=8 THEN 1214
1210 Y=SQR(X(I,1)*X(I,1)+X(I,2)*X(I,2))
1212 GO TO 1220
1214 SET DEGREES
1215 Y=ATN(X(I,2)/X(I,1))
1220 M=I-1
1230 O=F*M
1240 DRAW @C:O,Y
1250 NEXT I
1260 PRINT "ANOTHER COPY?-1(Y),2(N)"
1270 INPUT P4
1280 IF P4=2 THEN 1500
1290 GO TO 1080
1300 REM MANIPULATE AMP AND PHASE DATA
1310 K=L/2
1320 FOR I=L/2+2 TO L
1330 X(I,1)=X(K,1)
1340 X(I,2)=-X(K,2)
1350 K=K-1
1360 NEXT I
1365 PRINT "INSERT TAPE FOR DATA TRANSFER"
1370 PRINT "TYPE FILE NO"
1380 INPUT A$
1390 FIND VAL(A$)
1400 WRITE @33:L
1410 FOR I=1 TO L
1420 FOR J=1 TO 2
1430 WRITE @33:X(I,J)
1440 NEXT J
1450 NEXT I
1460 FOR I=1 TO L
1470 PRINT X(I,1),X(I,2),I
1480 NEXT I
1490 CLOSE
1500 END
```

```
854 W2=A3*(1+A8)+B3*B8
855 W3=B3*(1+A8)-A3*B8
856 W4=(1+A8)*(1+A8)+B8*B8
857 IF V=6 THEN 952
860 C=D3+B6
870 D=D4+B7
880 A9=(A*C+B*D)/(C*C+D*D)
890 B9=(B*C-A*D)/(C*C+D*D)
900 X(I,1)=A9
910 X(I,2)=B9
911 IF F9=2 THEN 920
912 REM STEP I/P
913 X(I,1)=-B9*S4/W
914 X(I,2)=+A9*S4/W
920 GO TO 1010
922 REM REM EVALUATE TOTAL FEEDBACK CURRENT
923 X(I,1)=A8
924 X(I,2)=B8
925 GO TO 1010
930 X(I,1)=A3
940 X(I,2)=B3
950 GO TO 1010
952 REM EVALUATE TOTAL CURRENT
953 X(I,1)=W2/W4
954 X(I,2)=W3/W4
955 GO TO 1010
960 X(I,1)=A4
970 X(I,2)=B4
972 X(I,1)=B4/(W*C9)
973 X(I,2)=-A4/(W*C9)
975 GO TO 1010
980 GO TO 1010
990 X(I,1)=A5
1000 X(I,2)=B5
1010 IF I=L/2+1 THEN 1040
1015 GO TO 1050
1020 W=1*10^-15
1030 GO TO 380
1040 X(I,2)=0
1050 NEXT I
1051 PRINT "MODIFY ARRAY DATA AT ZERO FREQ?-1(Y),2(N)"
1052 INPUT M1
1053 IF M1=2 THEN 1060
1054 X(1,1)=X(2,1)
1055 X(1,2)=0
1060 IF F8=2 THEN 1300
1070 REM FREQ DOMAIN PLOT
1080 PRINT "HARD COPY?-1 FOR YES,2 FOR NO"
1090 INPUT G8
1100 IF G8=1 THEN 1130
1110 C=32
1120 GO TO 1140
```

```
390 A1=T1
400 B1=W*T3-1/(W*T2)
410 REM EVALUATE MATCHING CCT IMP (ZE=A2+JB2)
420 A2=W*W*T4*T5*T5/(T4*T4+W*W*T5*T5)
430 B2=W*T5*T4*T4/(T4*T4+W*W*T5*T5)
440 REM EVALUATE I/P ADMITTANCE(YI=A3+JB3)
450 U1=-W*C9*B2
460 V1=W*C9*A2
470 U2=A1+A2-W*C9*B1*A2-W*C9*A1*B2
480 V2=B1+B2+W*C9*A1*A2-W*C9*B1*B2
490 A3=(U1*U2+V1*V2)/(U2*U2+V2*V2)
500 B3=(V1*U2-U1*V2)/(U2*U2+V2*V2)
510 IF V=1 THEN 930
520 REM EVALUATE THE FBK ADMITTANCE(YF=A4+JB4)
530 U3=-W*C9*(B1+B2)
540 V3=W*C9*(A1+A2)
550 A4=(U3*U2+V3*V2)/(U2*U2+V2*V2)
560 B4=(V3*U2-U3*V2)/(U2*U2+V2*V2)
570 IF V=2 THEN 960
575 IF V=7 THEN 972
580 REM EVALUATE THE CURRENT FBK FACTOR(ATF=A5+JB5)
590 U7=S1*S1*Z3/(C9*T*(Z3+Z1))
600 A5=B4*U7/(W*H1)
610 B5=-U7*A4/(W*H1)
620 IF V=3 THEN 990
630 REM EVALUATE THE VOLTAGE-FORCE TF(H=A9+JB9)
640 C3=1-COS(W*T)
650 C4=SIN(W*T)
660 C5=1-R2*COS(W*T)
670 C6=R2*SIN(W*T)
680 C7=1-R1*COS(W*T)
690 C8=R1*SIN(W*T)
700 D3=1-R1*R2*COS(2*W*T)
710 D4=R1*R2*SIN(2*W*T)
720 U8=S1*S1*Z3/((Z3+Z2)*C9*T)
730 E1=C3*C5-C4*C6
740 E2=C4*C5+C3*C6
750 E3=(C3*C7-C4*C8)*U8
760 E4=(C4*C7+C3*C8)*U8
770 E5=E1*U7+E3
780 E6=E2*U7+E4
790 A6=A3*E1-B3*E2
800 A7=B3*E1+A3*E2
810 P1=-H1*Z1/((Z3+Z1)*W)
820 A=P1*A7
830 B=-P1*A6
840 B6=(A4*E5-B4*E6)/(W*W)
850 B7=(B4*E5+A4*E6)/(W*W)
851 A8=(B6*D3+B7*D4)/(D3*D3+D4*D4)
852 B8=(B7*D3-B6*D4)/(D3*D3+D4*D4)
853 IF V=5 THEN 922
```

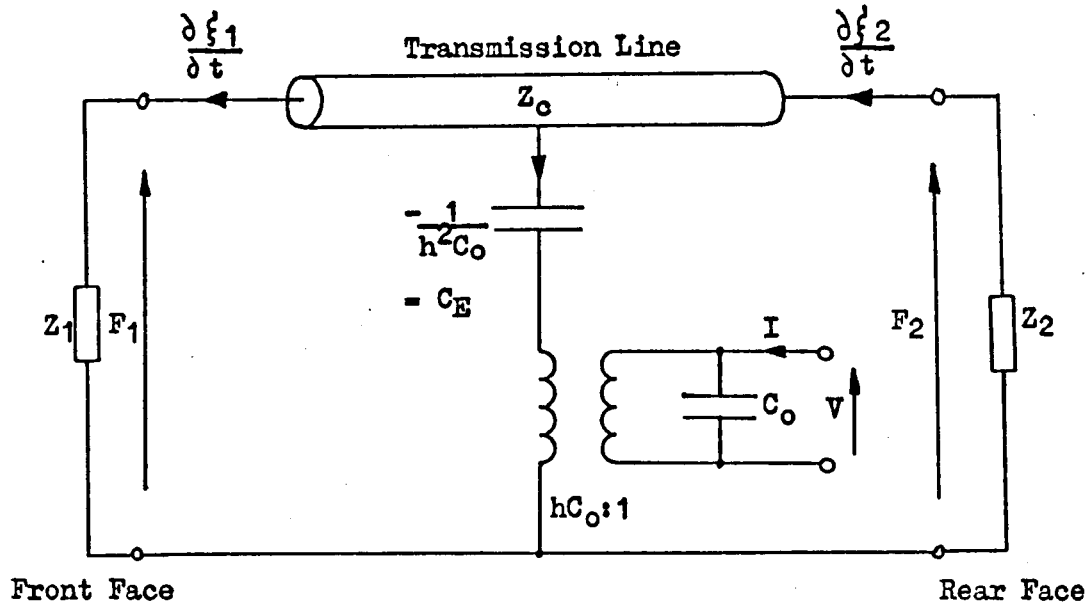

Fig. 2.1. Mason's Electromechanical Equivalent Circuit of a Thickness Mode Transducer

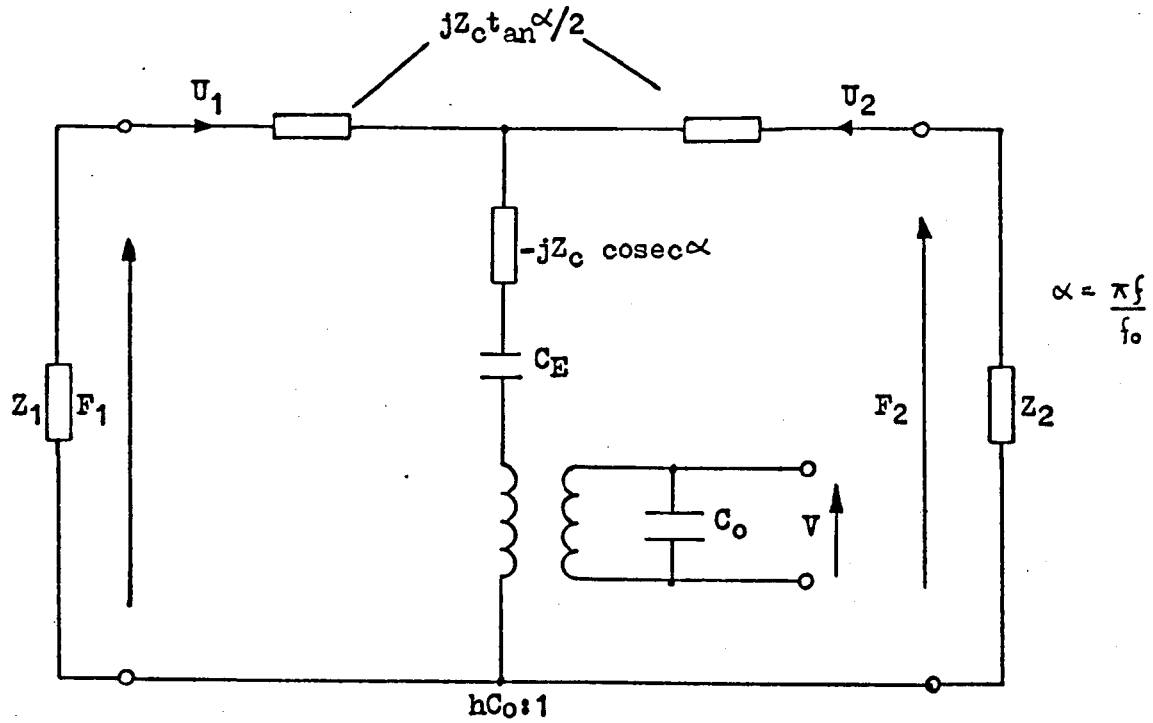

f_o = transducer mechanical resonant frequency

Fig. 2.2. Lumped Parameter Equivalent Circuit for a Piezoelectric Transducer

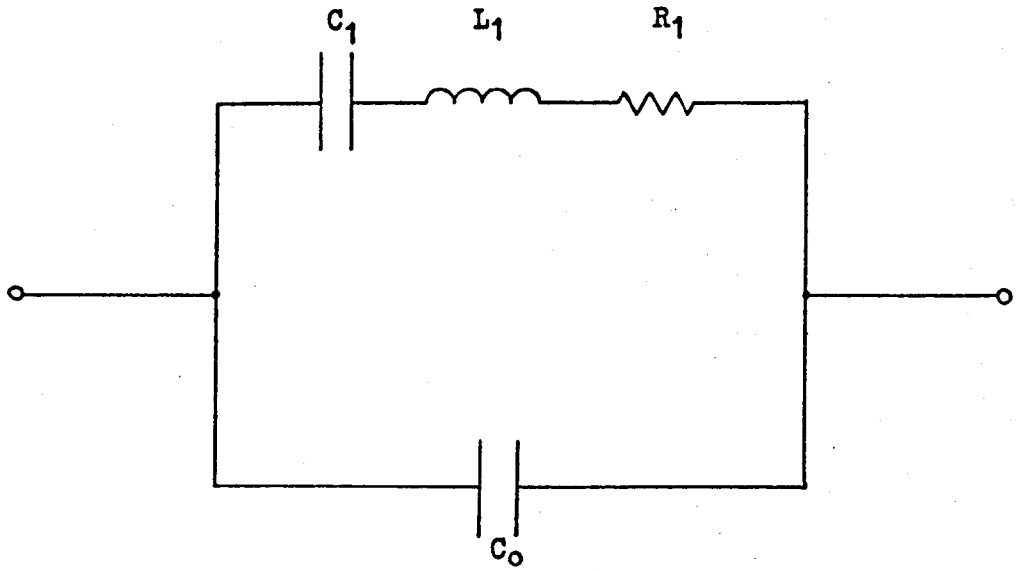

Fig. 2.3. Basic Lumped Parameter Equivalent Circuit

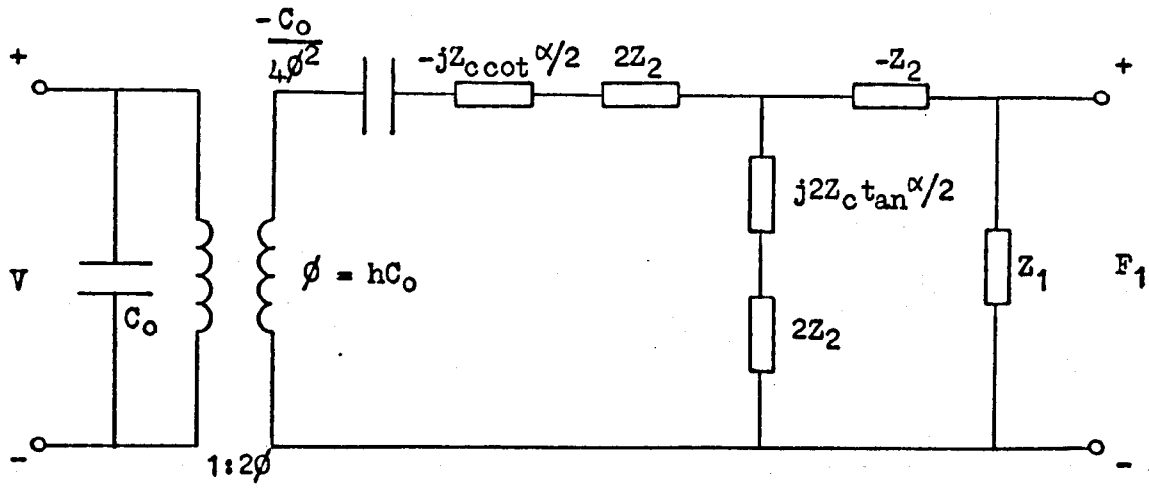

Fig. 2.4. Equivalent Circuit for the Piezoelectric Transducer (According to Kossof)

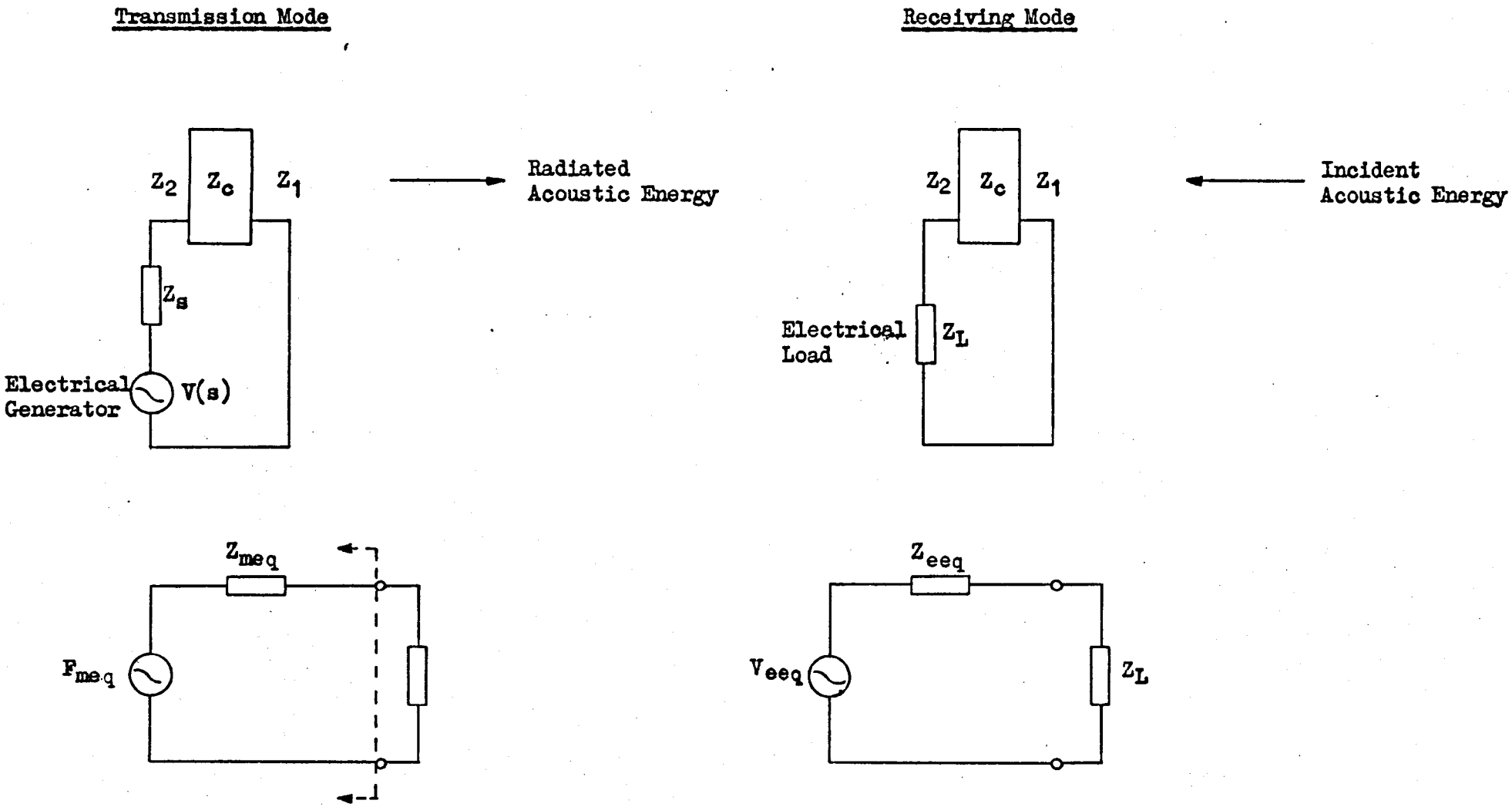

Fig. 2.5. Thevenin Equivalent Circuits for the Thickness Mode Transducer According to Martin and Sigelmann

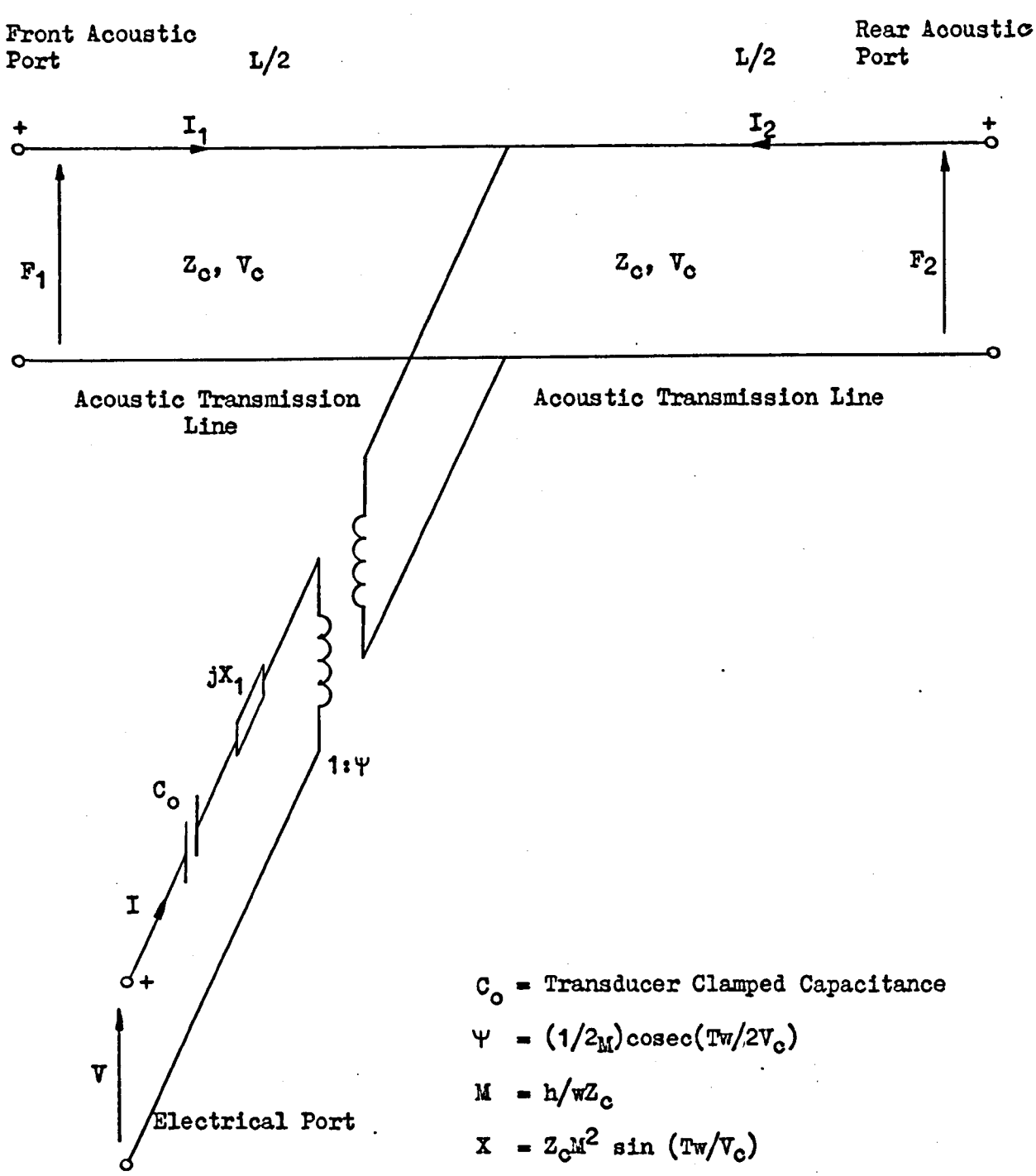

where w is the angular frequency

T is the time for longitudinal waves to travel through the transducer in its thickness direction

V_c is the velocity of longitudinal waves in the thickness direction

L is the transducer thickness.

Fig. 2.6. KLM Equivalent Circuit for a Thickness Mode Transducer

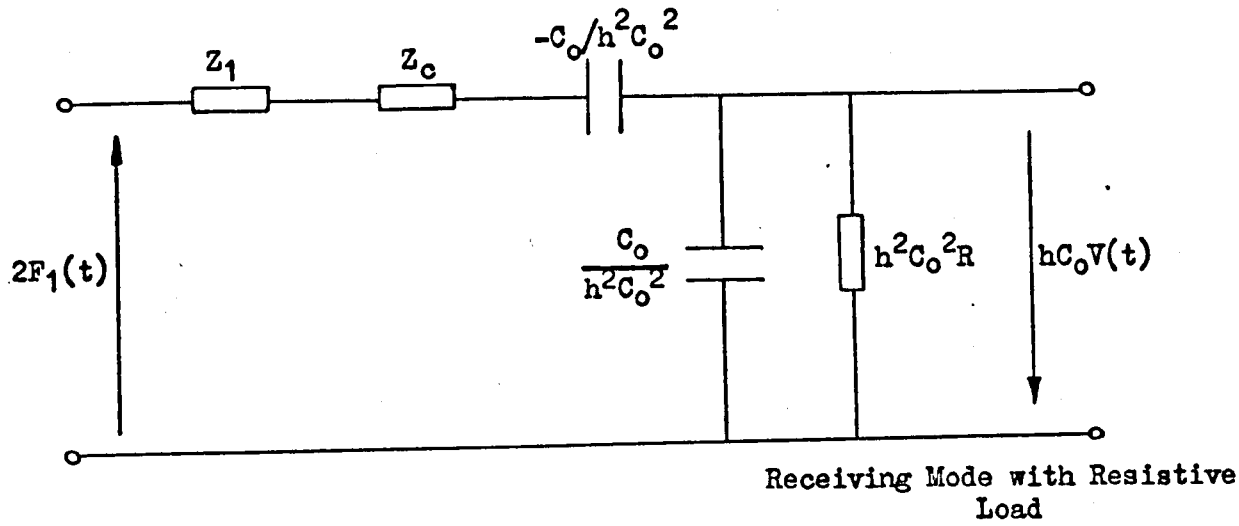

Receiving Mode with Resistive Load

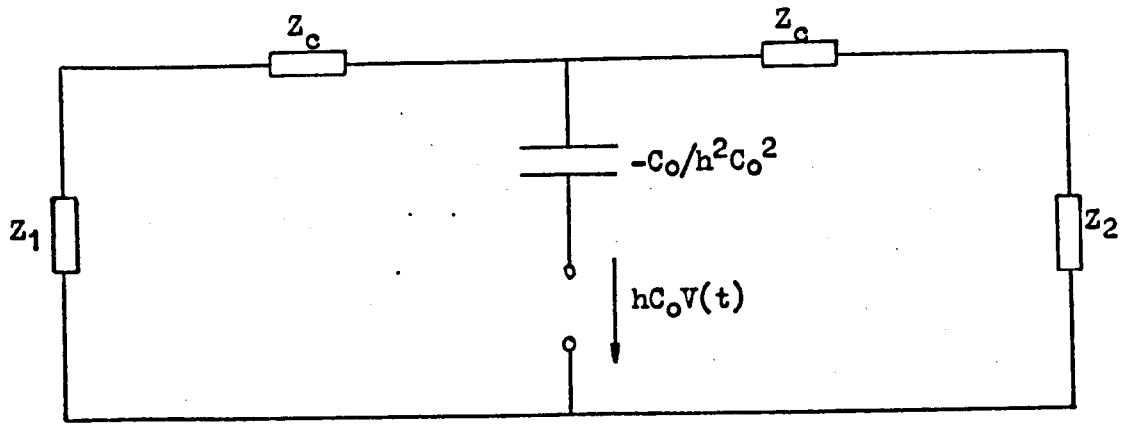

Transmitting Mode

Fig. 2.8. Equivalent Electrical Circuits of Redwood (Valid over the first Transit Internal)

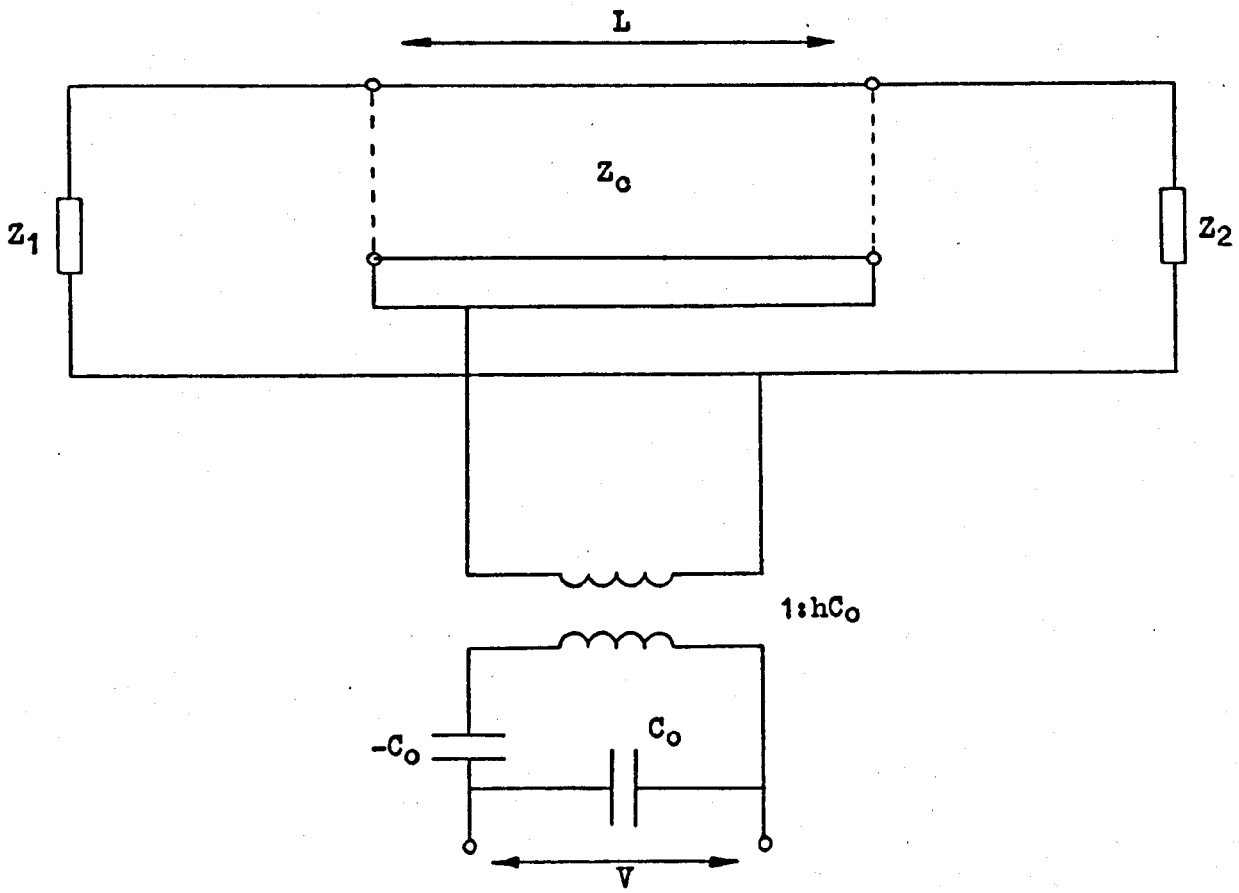

Fig. 2.9. Equivalent Electromechanical Circuit of the Piezoelectric Transducer for Transient Analysis (According to Filipczynski)

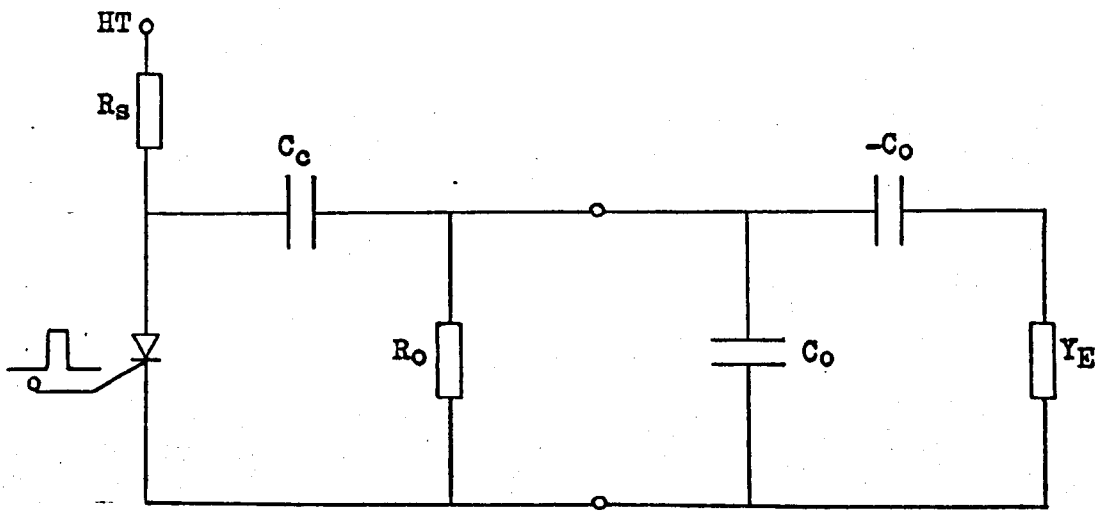

R_o and R_s are assumed very large

Y_E is the electrical admittance of the transducer

Fig. 2.10. Transmitting Circuit of Filipczynski

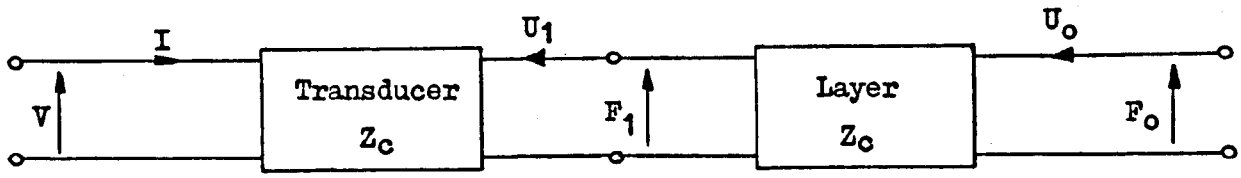

Fig. 2.11. Transducer Loaded at Front Face by Single Intermediate Layer of Finite Thickness (According to Sittig)

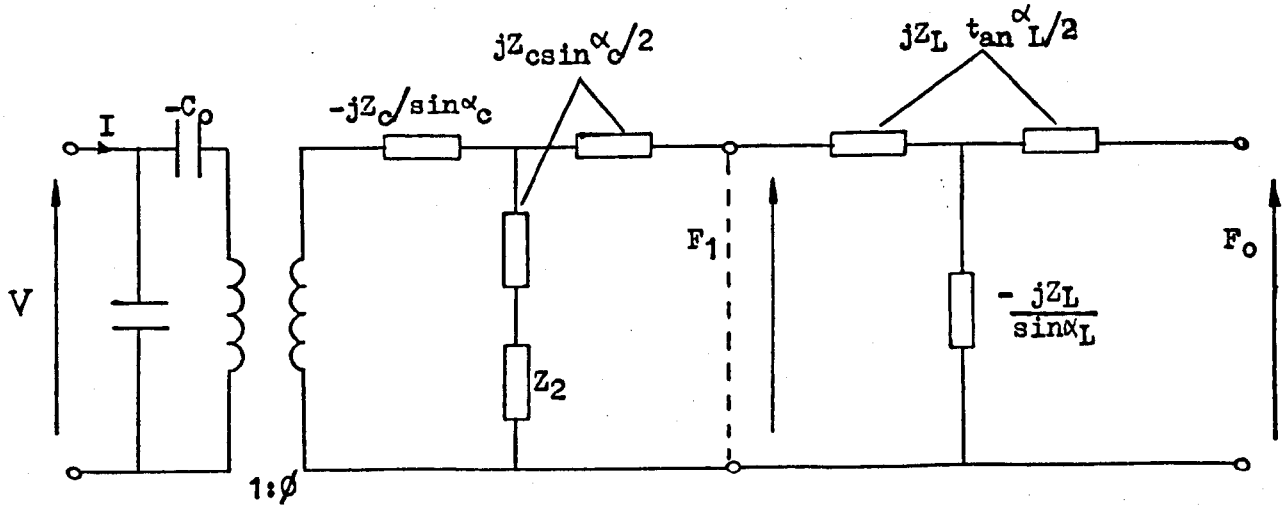

Active Layer (Transducer)

Inactive Layer

$\phi = hC_o$

$\alpha_c = f/f_c$ where $f_c = v_c/2L$

$\alpha_L = f/f_L$, $f_L = v_L/2l$

v_c = longitudinal velocity of sound in transducer

L = thickness of transducer

v_L = longitudinal velocity of sound in the layer

l = thickness of the layer

Fig. 2.12. Equivalent Electrical Representation of a Transducer and Single Layer (According to Sittig)

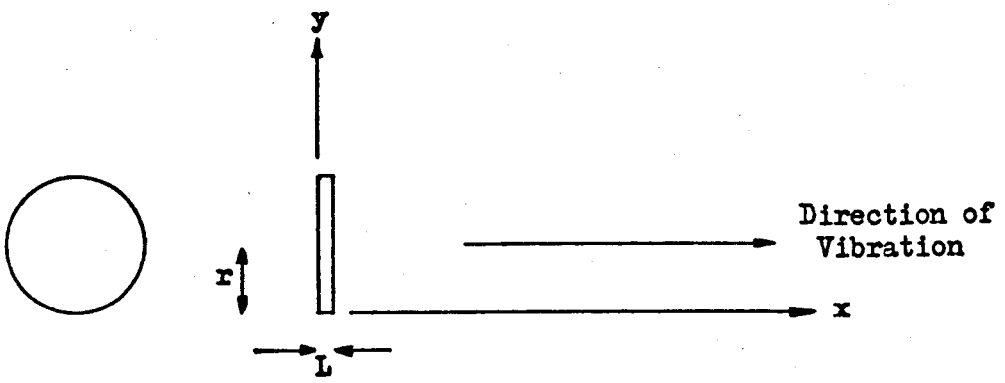

Fig. 3.1 Geometry of Disc Transducer

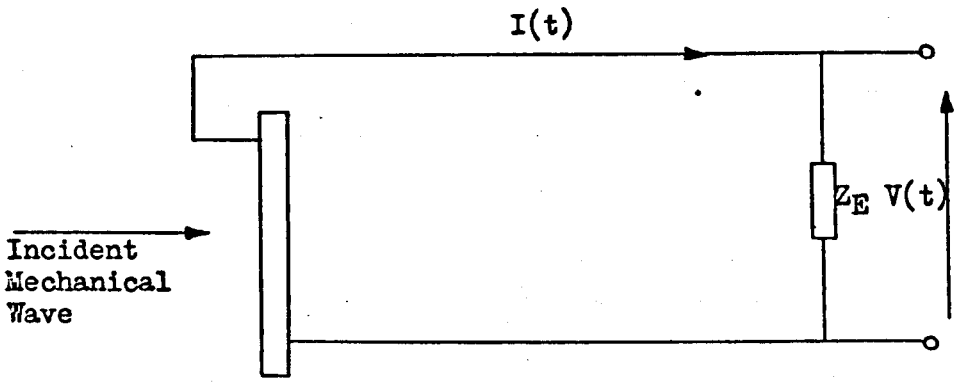

Fig. 3.2 Arbitrary Electrical Impedance Connected Across the Transducer Terminals

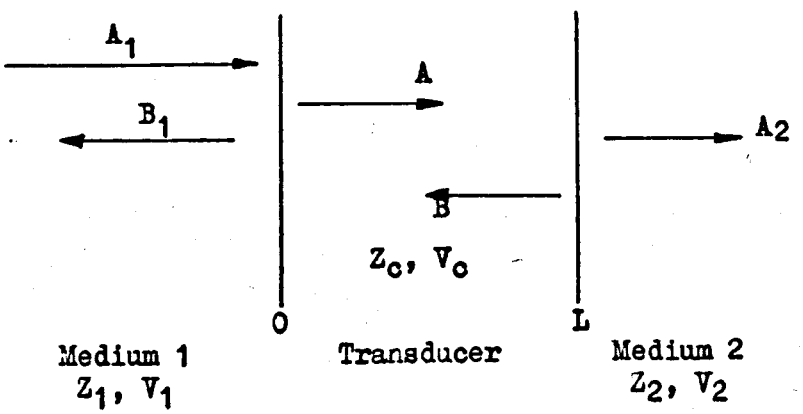

Fig. 3.3 Mechanical Boundary Conditions for the Transducer in Reception

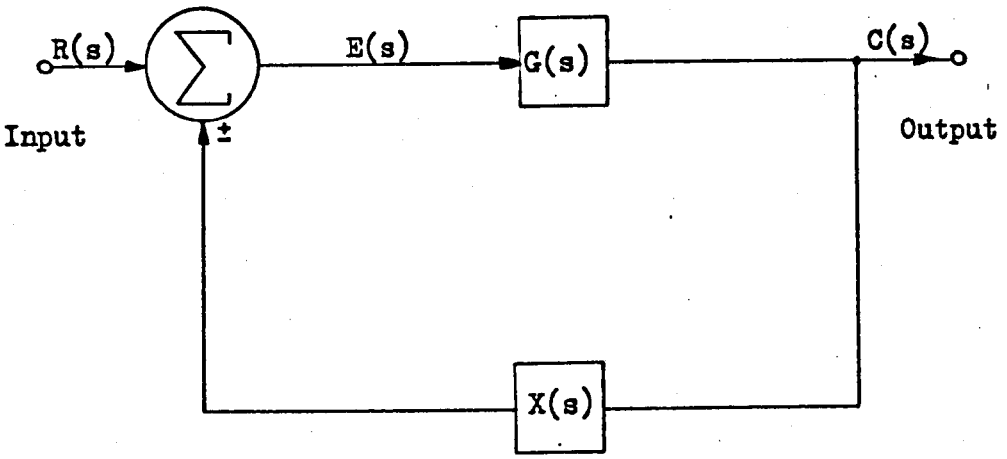

Fig. 3.4 Block Diagram of a Typical Feedback System

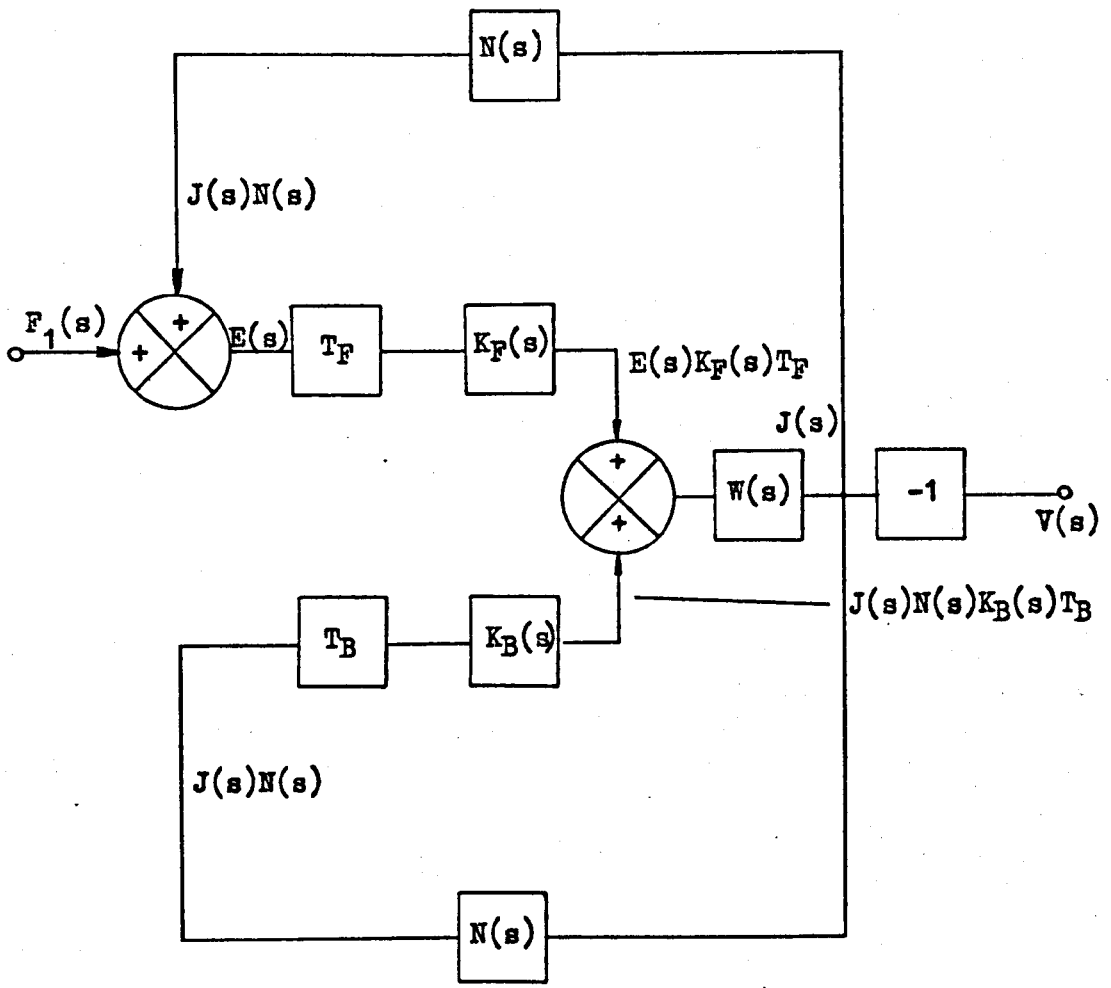

Fig. 3.5 Block Diagram of a Piezoelectric Receiver

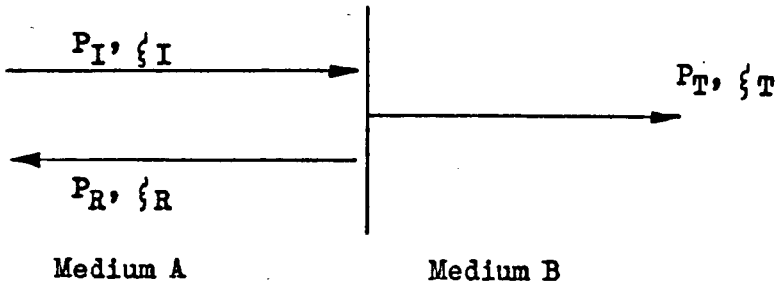

Fig. 3.6 Reflection and Transmission at Normal Incidence

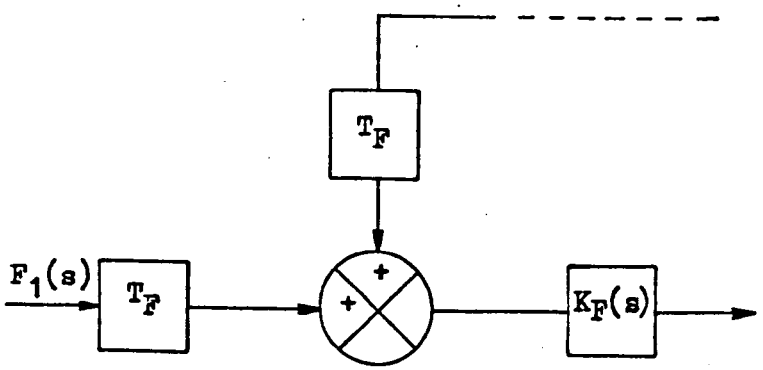

Fig. 3.7 Removal of the Block T_F from the Forward Loop

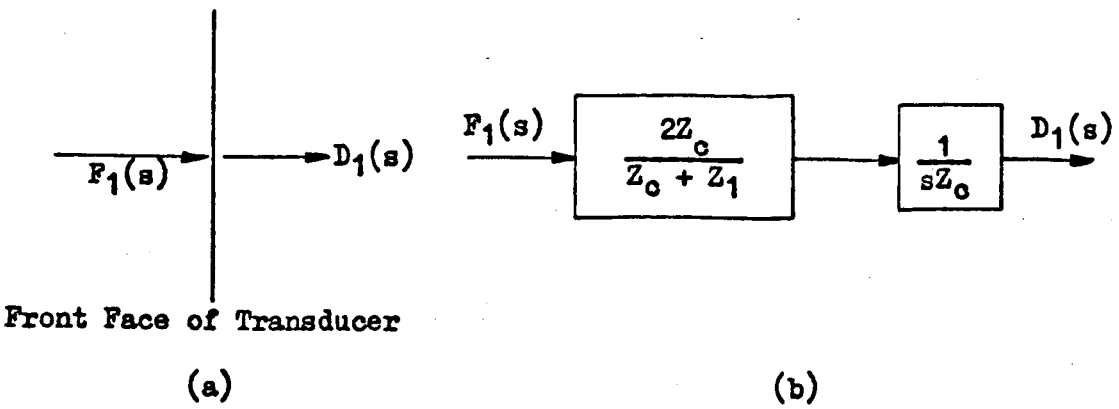

Fig. 3.8 Transmission Characteristics at the Transducer Front Face

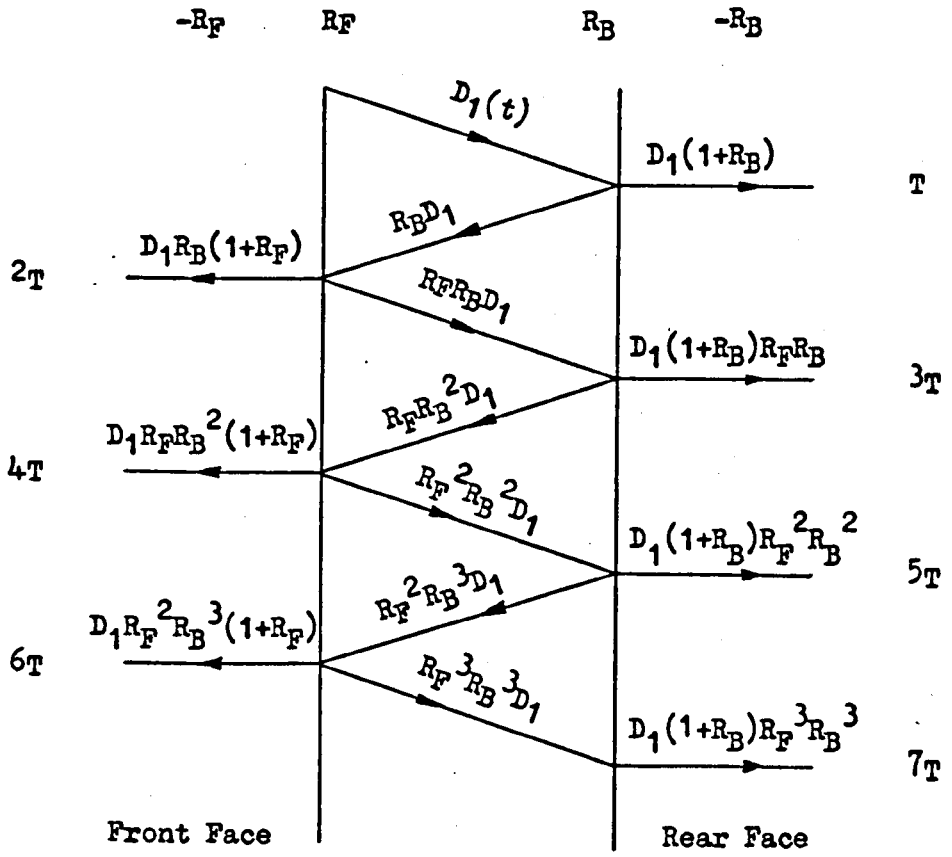

Fig. 3.9a Particle Displacements at the Transducer Faces

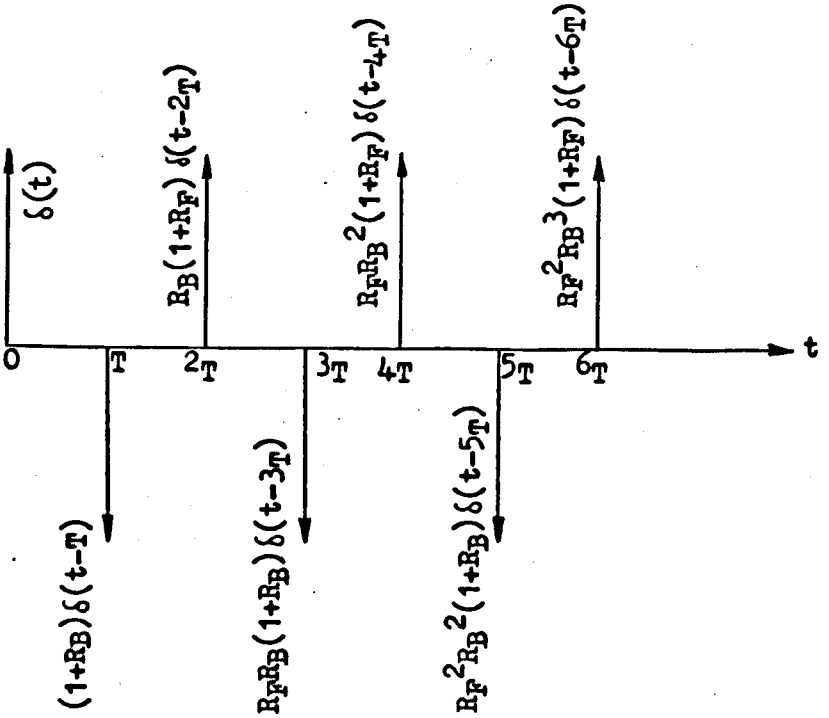

Fig. 3.9b Time Domain Representation of k_F

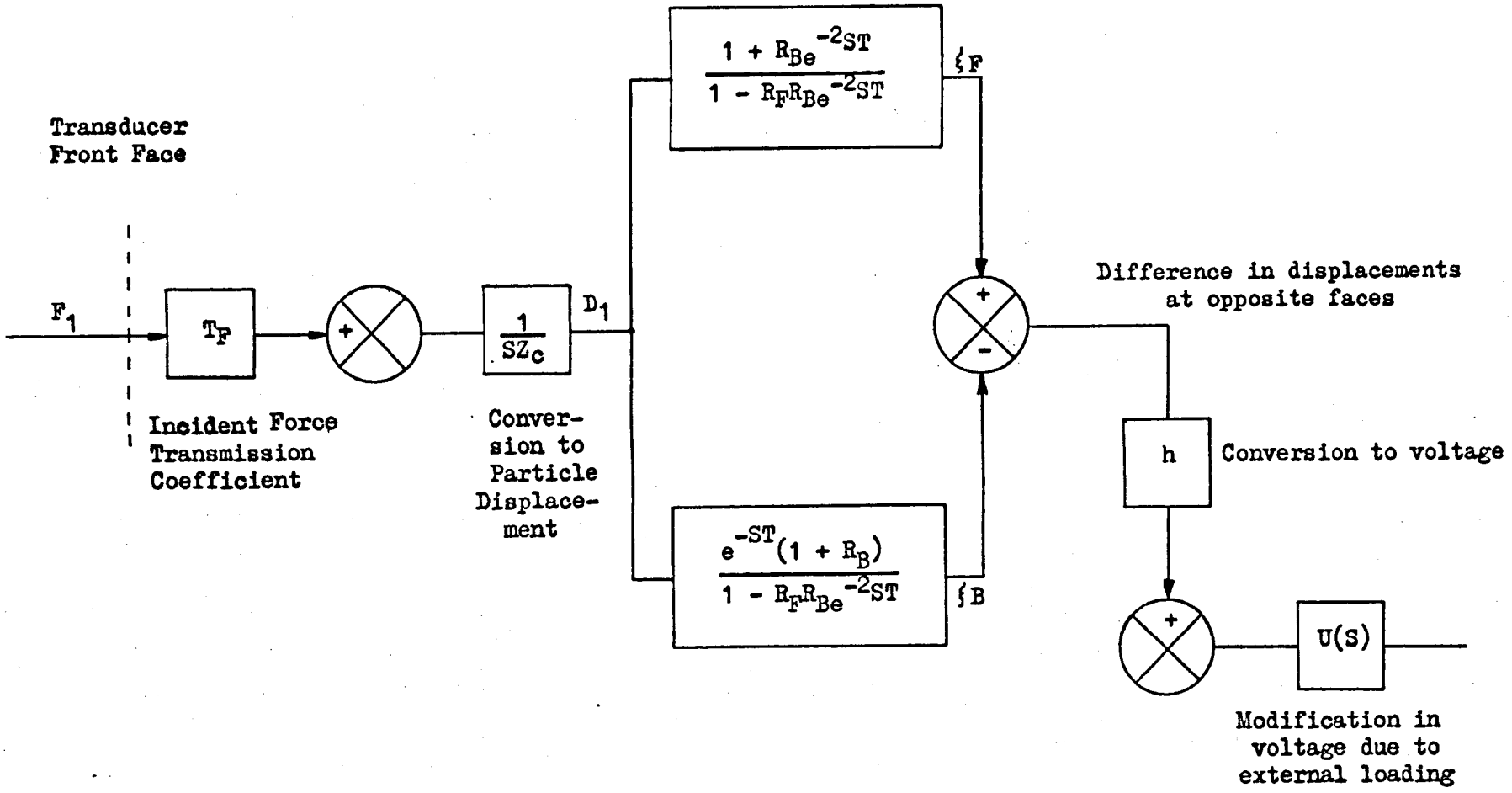

Fig. 3.10 Physical Interpretation of Transducer Front Face Forward Loop

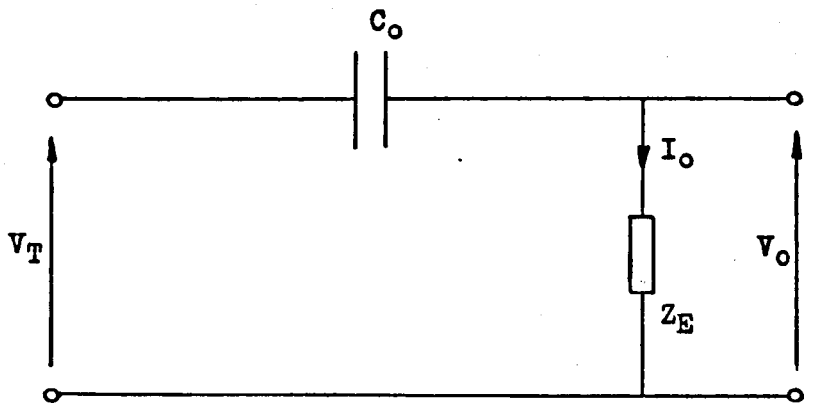

Fig. 3.11 Electrical Equivalent of Transfer Block U(S)

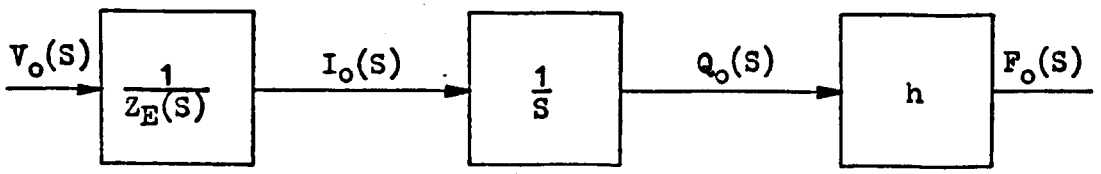

Fig. 3.12 Generation of Force in the Feedback Loop

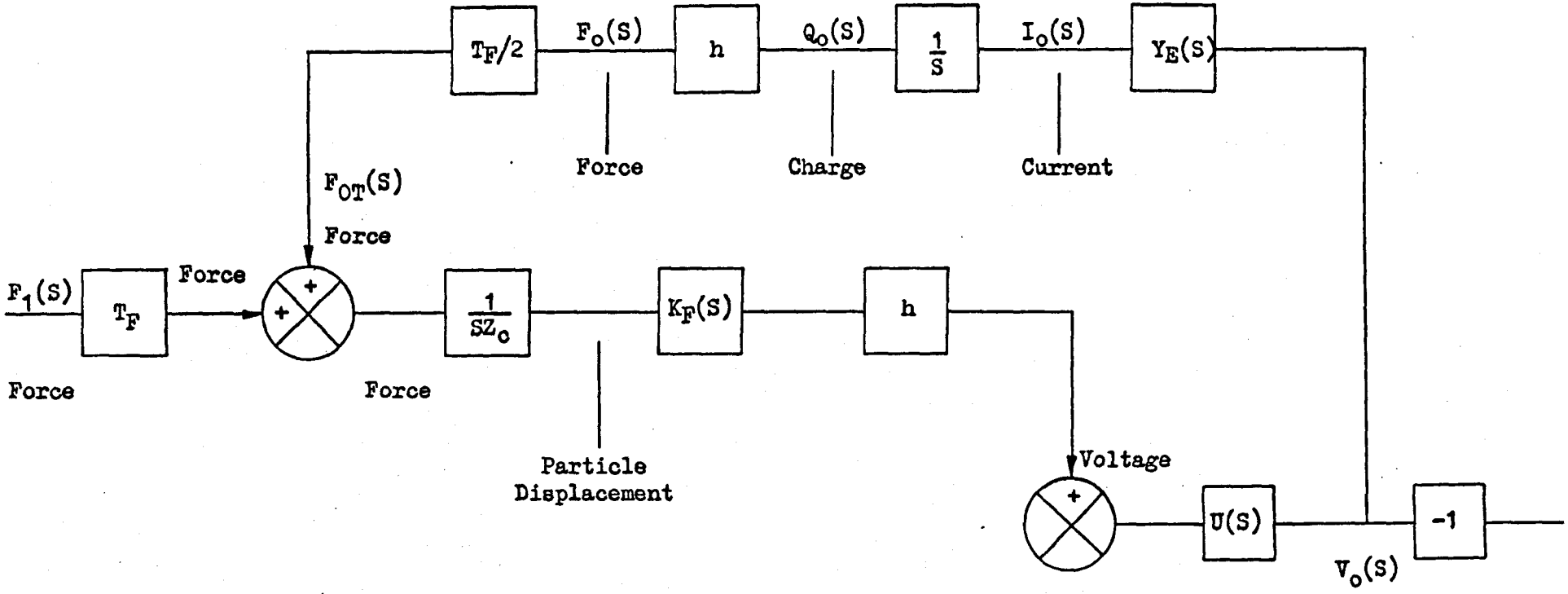

Fig. 3.13 Feedback System Relating to the Transducer Front Face

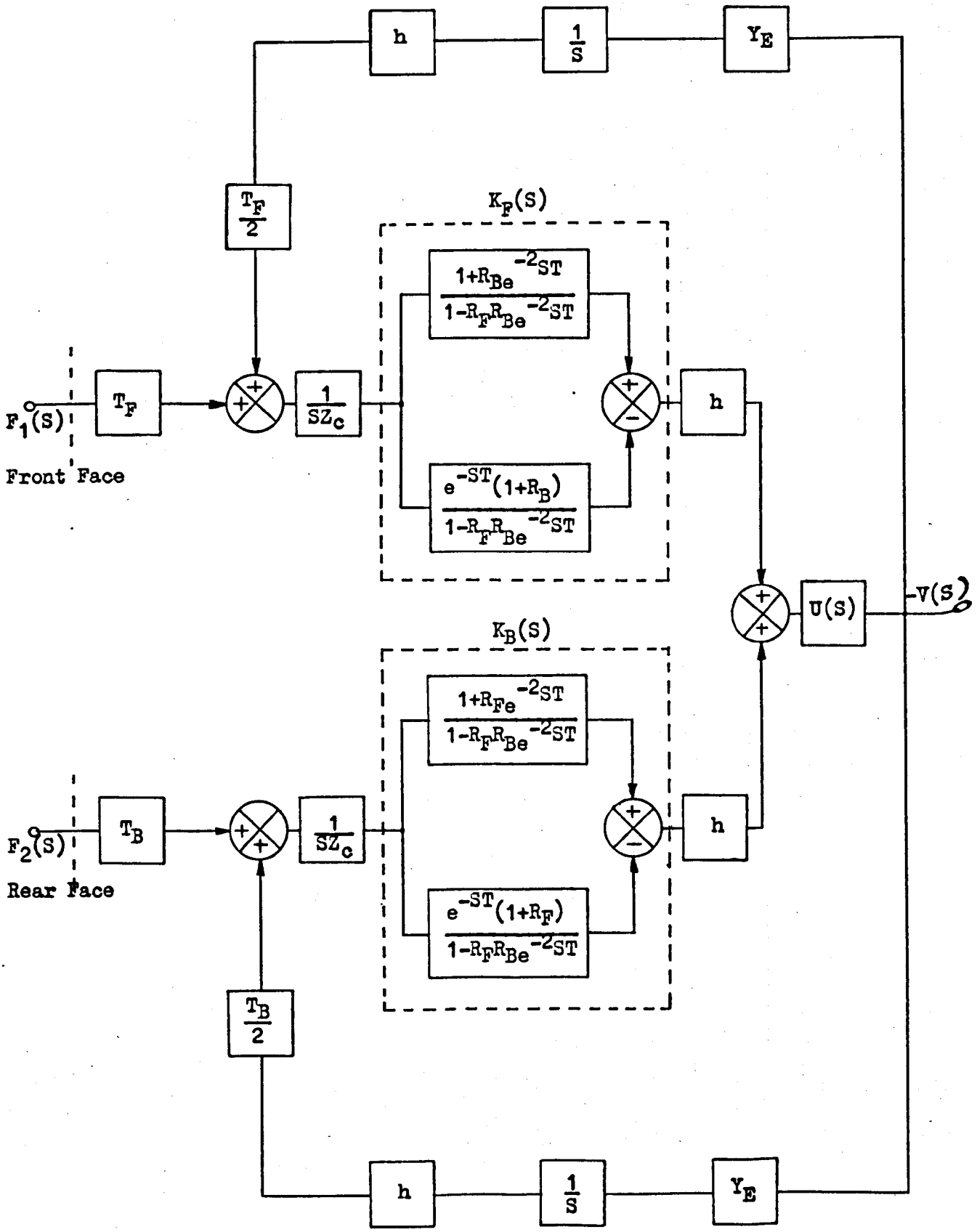

Fig. 3.14 Generalised Feedback Model for a Piezoelectric Transducer in the Receiving Mode

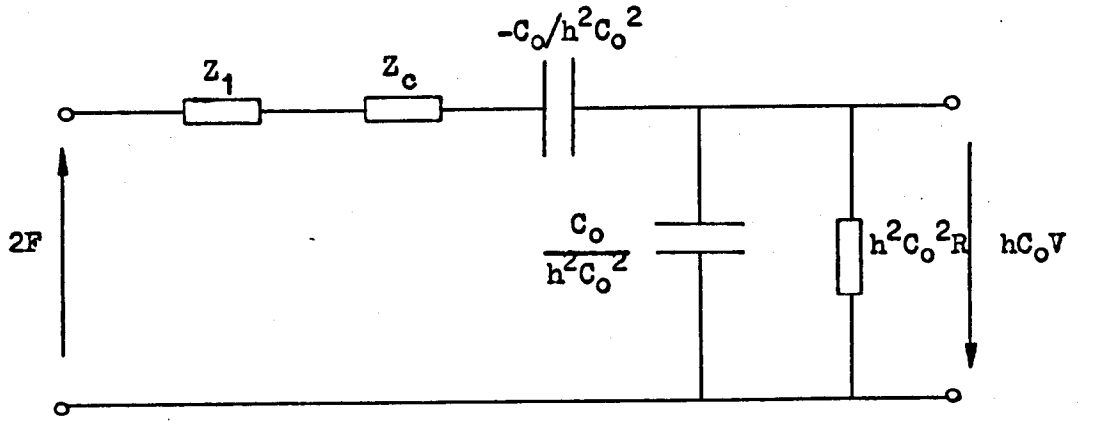

Fig. 3.15 Equivalent Electrical Circuit of Redwood

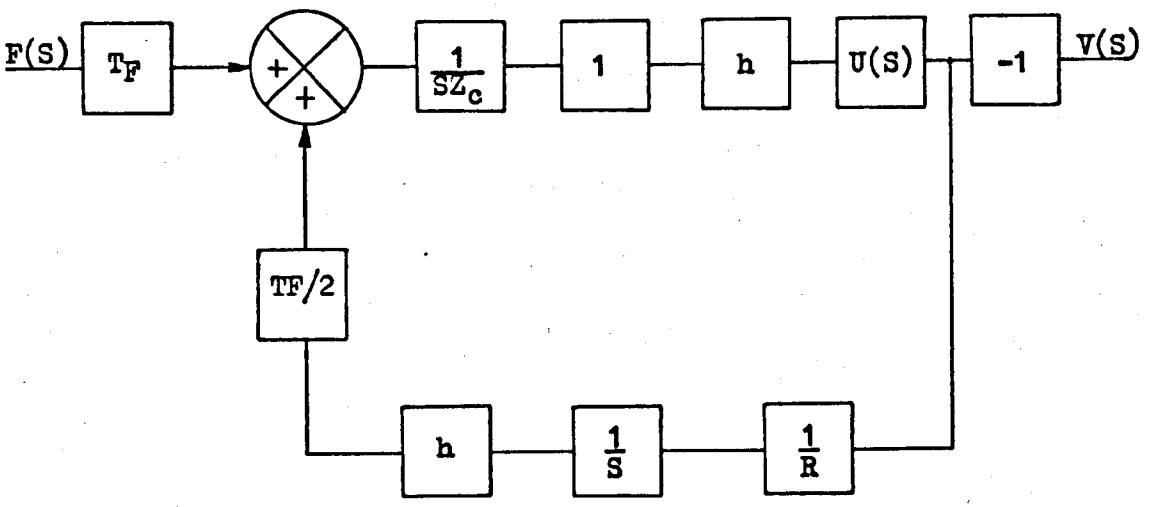

Fig. 3.16 Block Diagram of a Rigidly Backed Transducer with Resistive Loading during the First Transit Interval

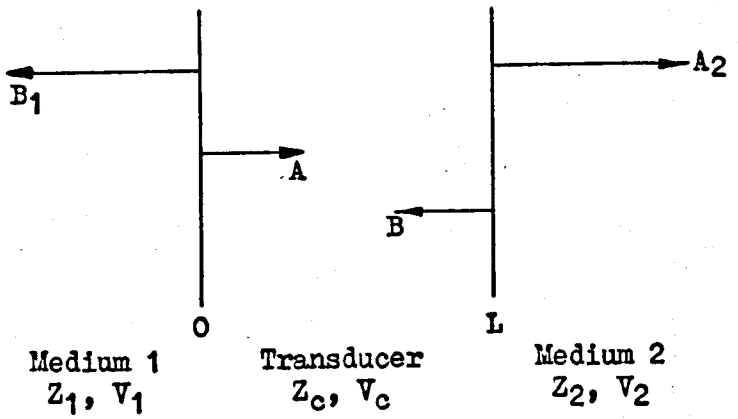

Fig. 4.1 Mechanical Boundary Conditions for the Transducer in Transmission

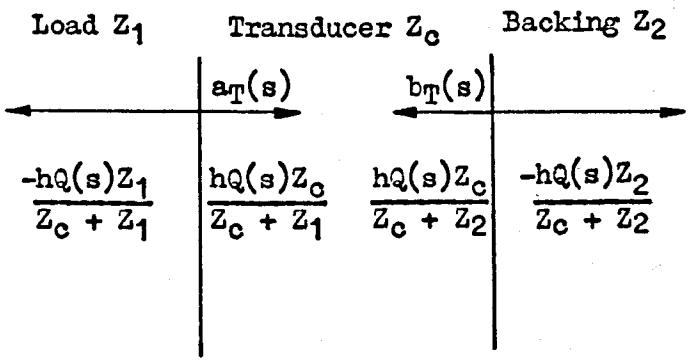

Fig. 4.2a. Initial Stress Waves Generated at the Transducer Faces

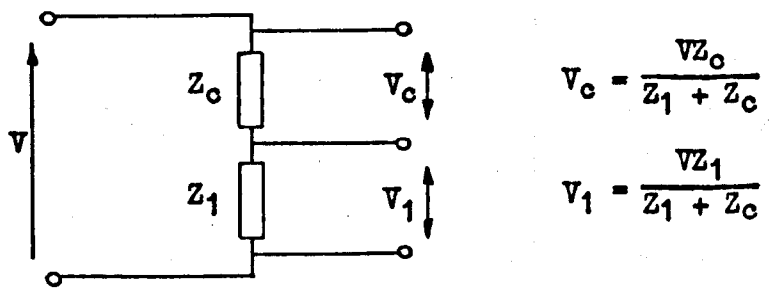

Fig. 4.2b. Electrical Analogy of the Initial Force Generation at the Transducer Front Face

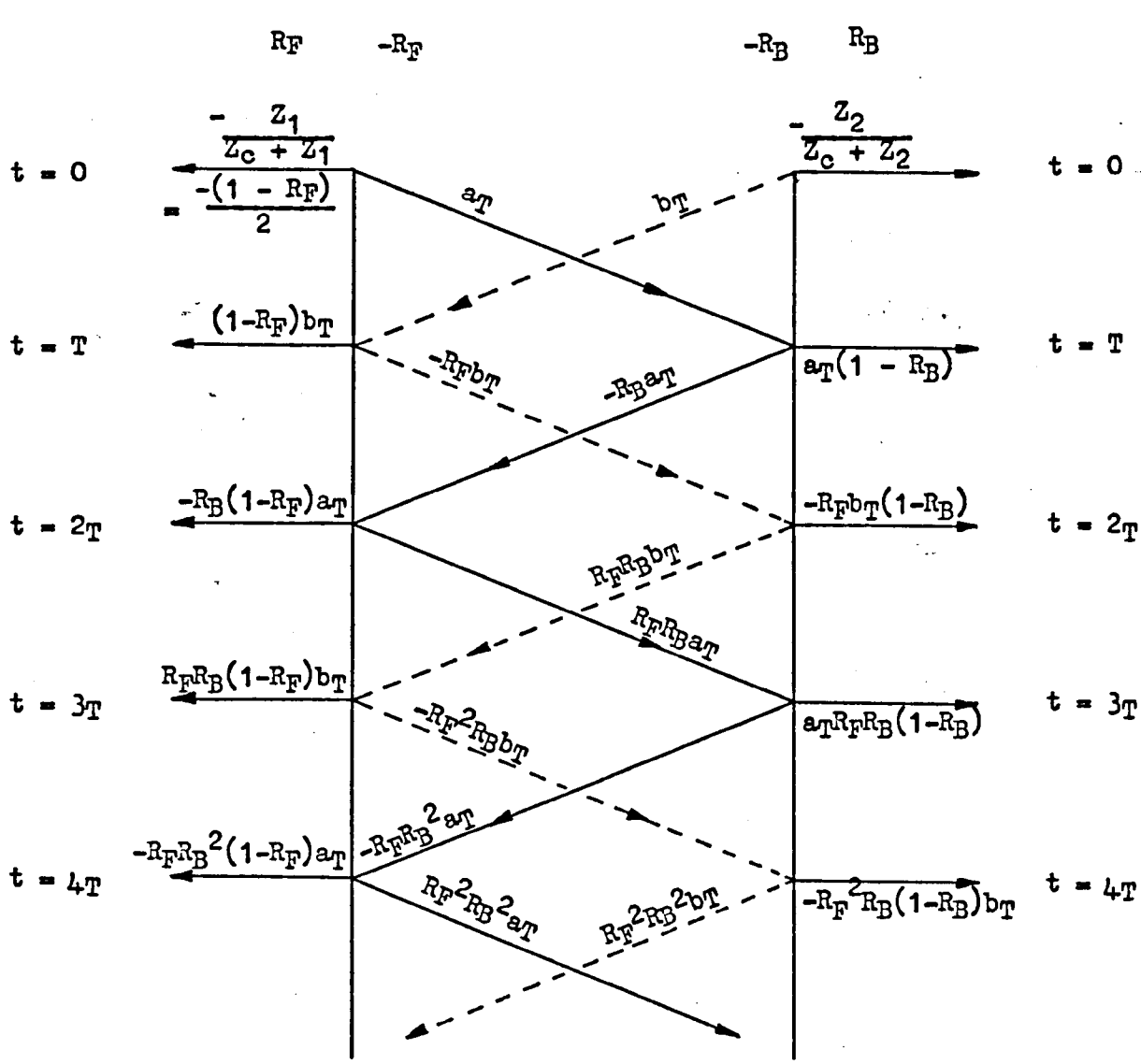

Fig. 4.3. Lattice Diagram of Forces Generated in the Transmission Mode

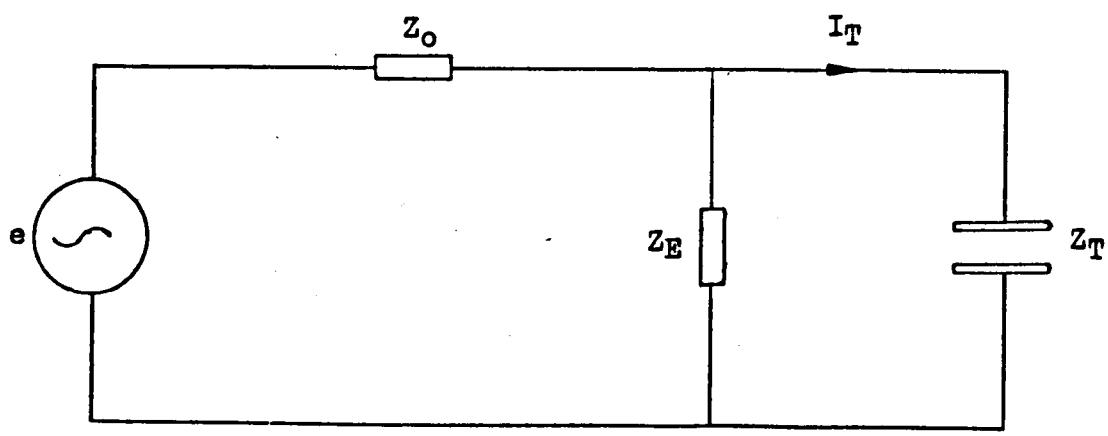

Fig. 4.4. General Transmitter Configuration

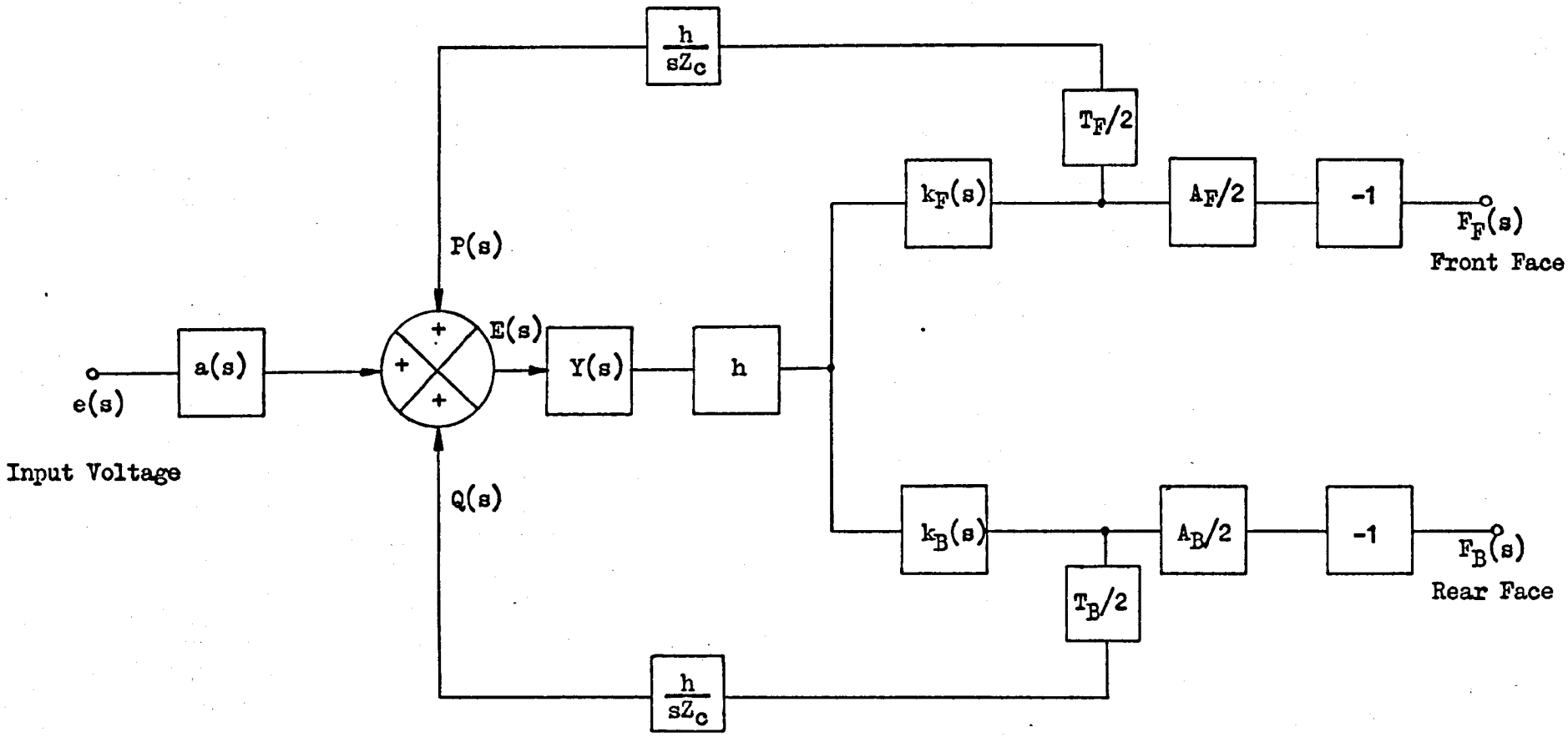

Fig. 4.5. General Block Diagram of the Piezoelectric Transmitter

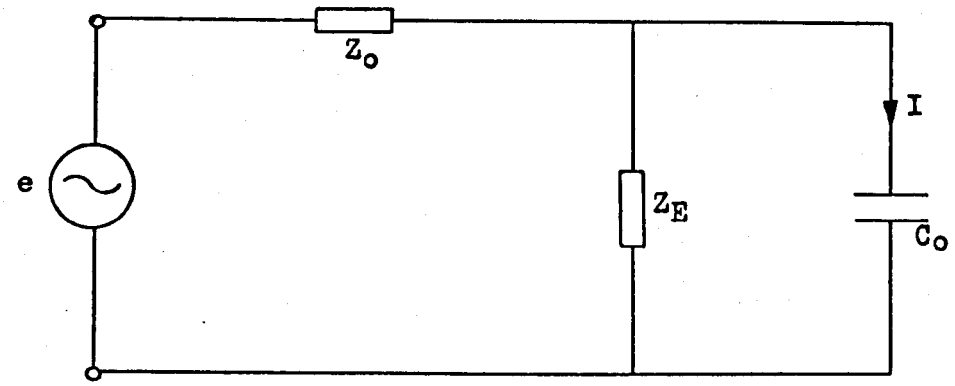

Fig. 4.6. Equivalent Electrical Circuit at the Transducer Input

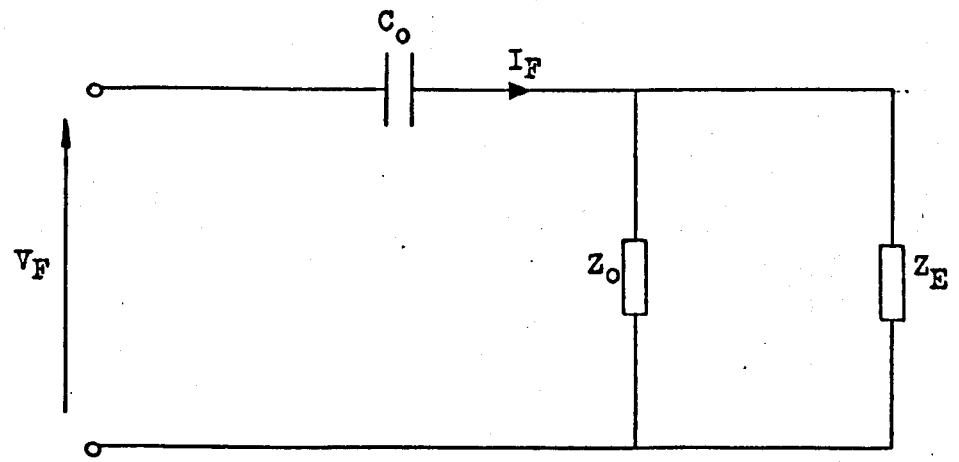

Fig. 4.7. Equivalent Electrical Circuit of Each Feedback Path

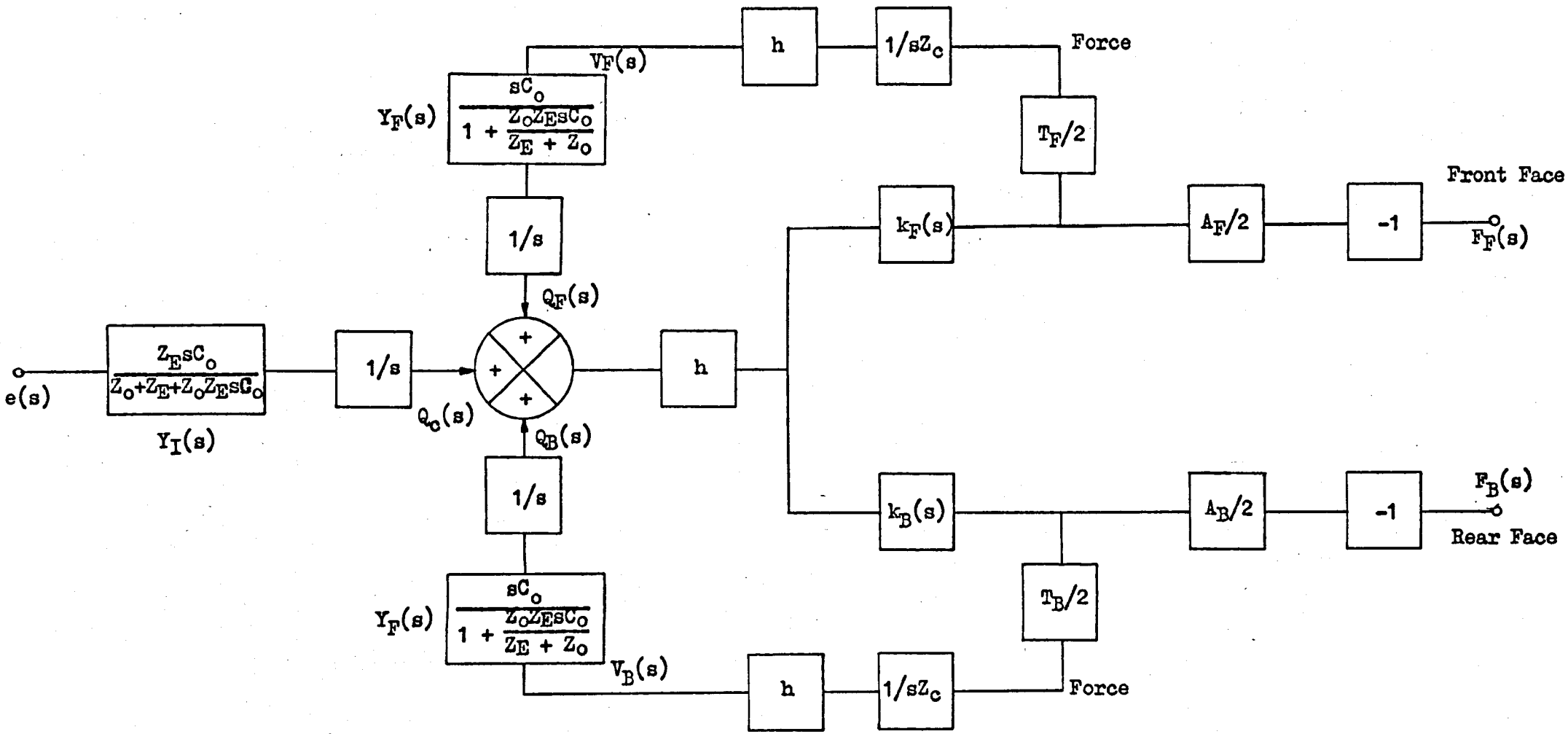

Fig. 4.8. Generalised Feedback Model for a Piezoelectric Transducer in the Transmitting Mode

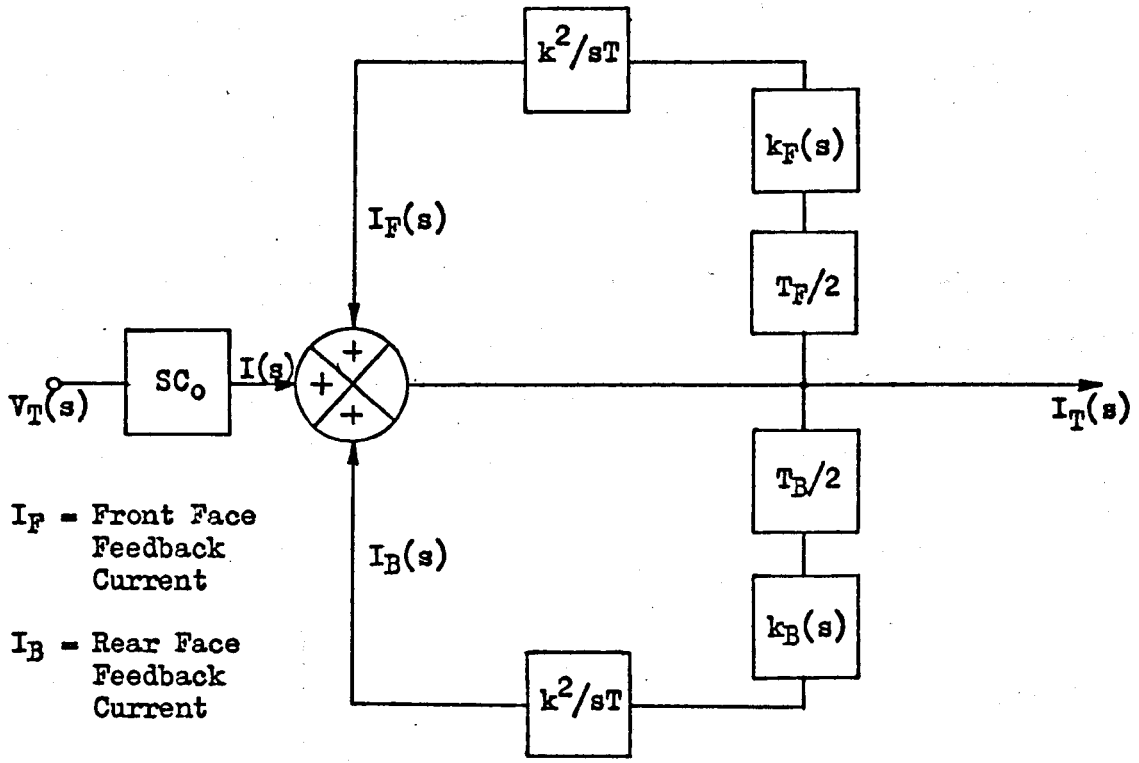

Fig. 5.1. Block Diagram Respresentation of the Transducer Admittance Function

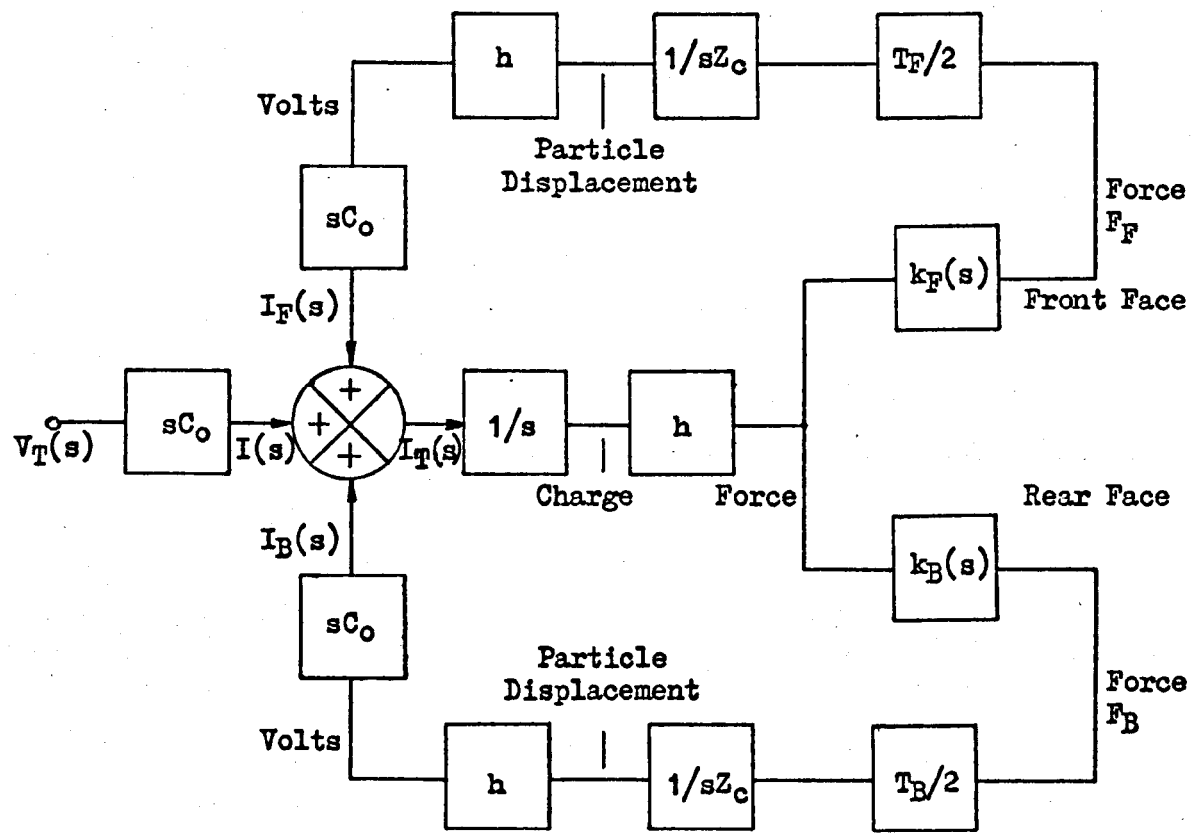

Fig. 5.2. Expanded Admittance Block Diagram

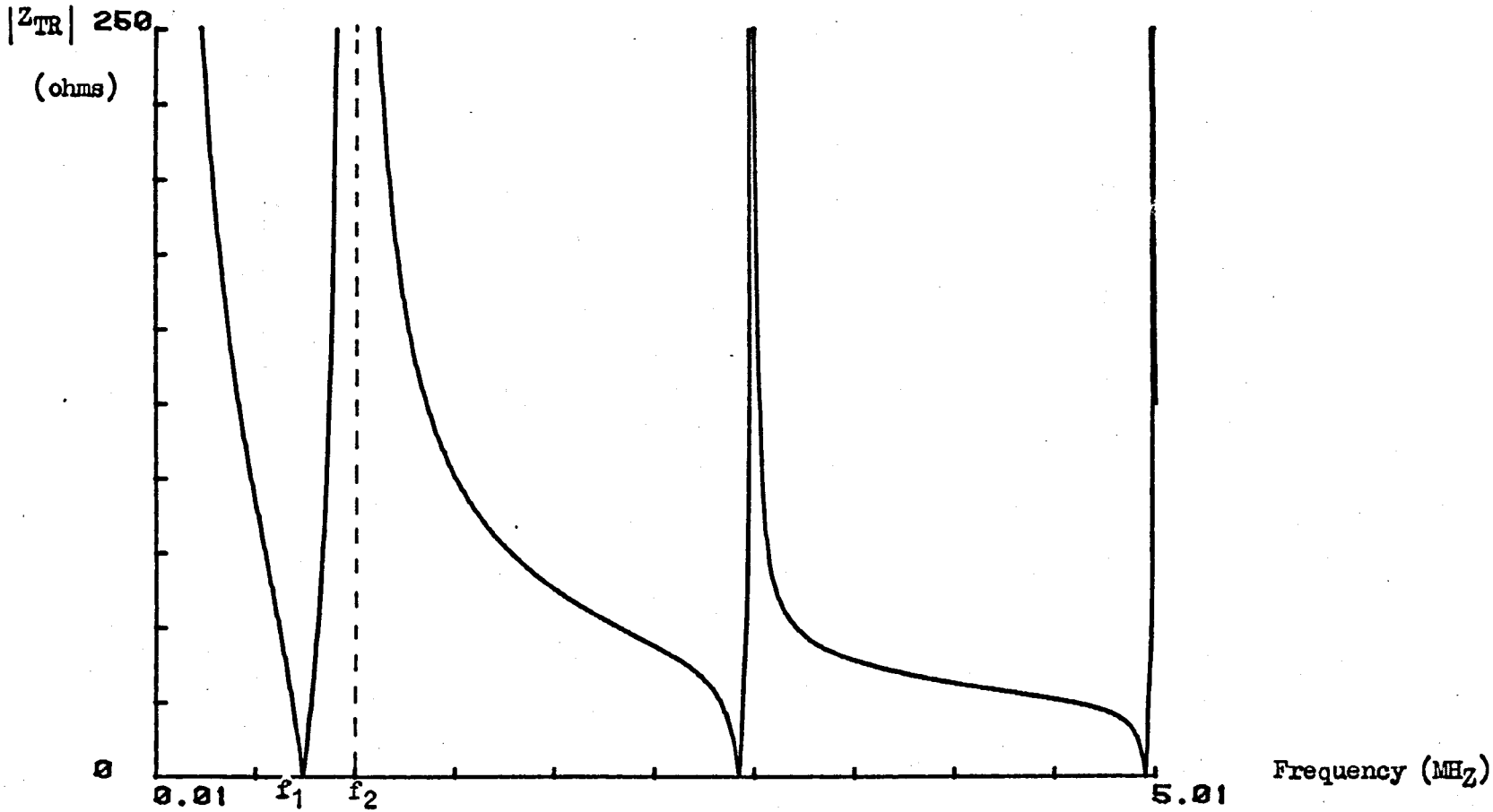

Fig. 5.3a. Magnitude of Resonator Impedance V_s Frequency

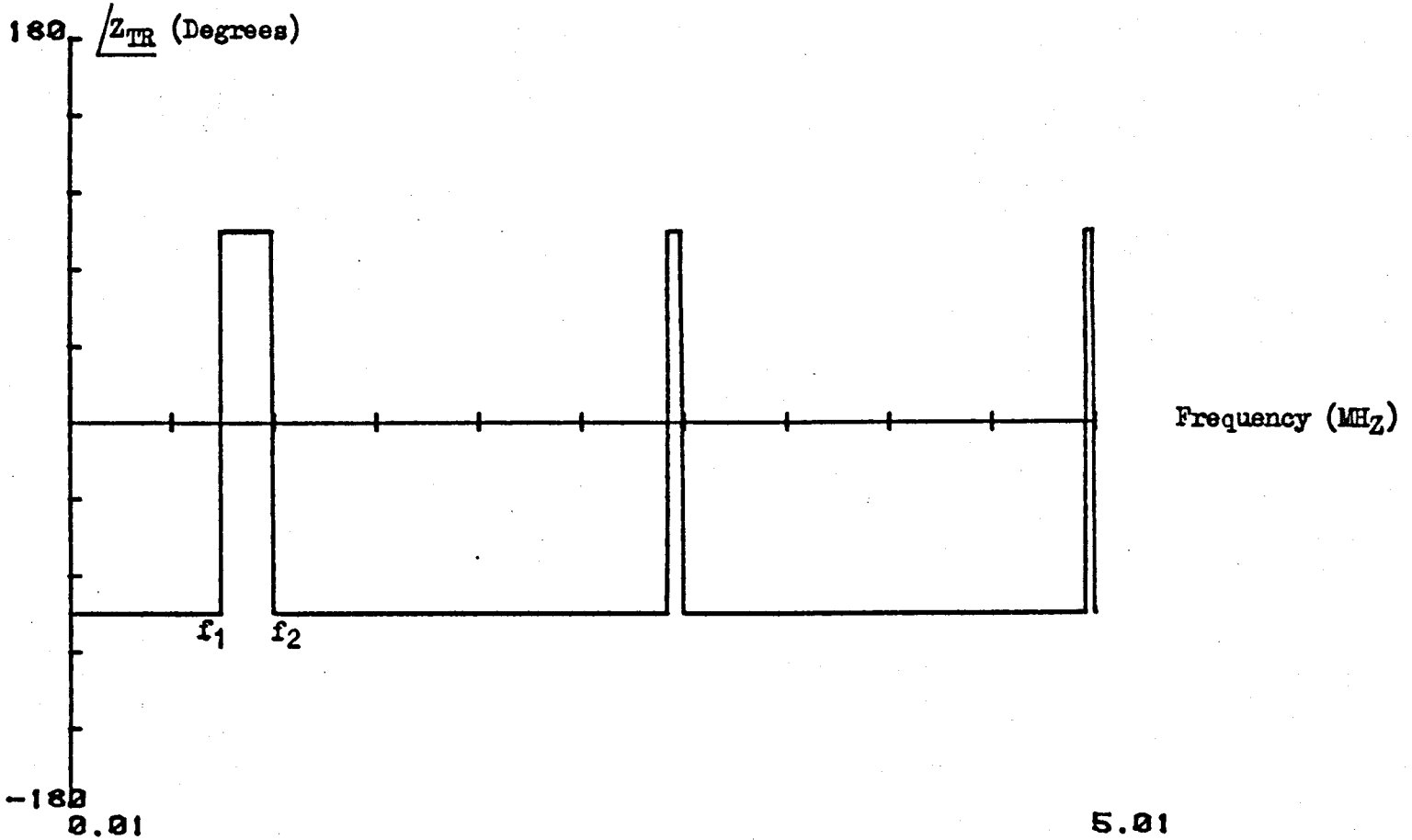

Fig. 5.3b. Phase of Resonator Impedance V_s Frequency

f_2 (MHz)	k^2	Z_c (kg/s m^2)	C_o (pf)
1	.5	33.712	1261

Table 5.1. Nominal Transducer Parameters

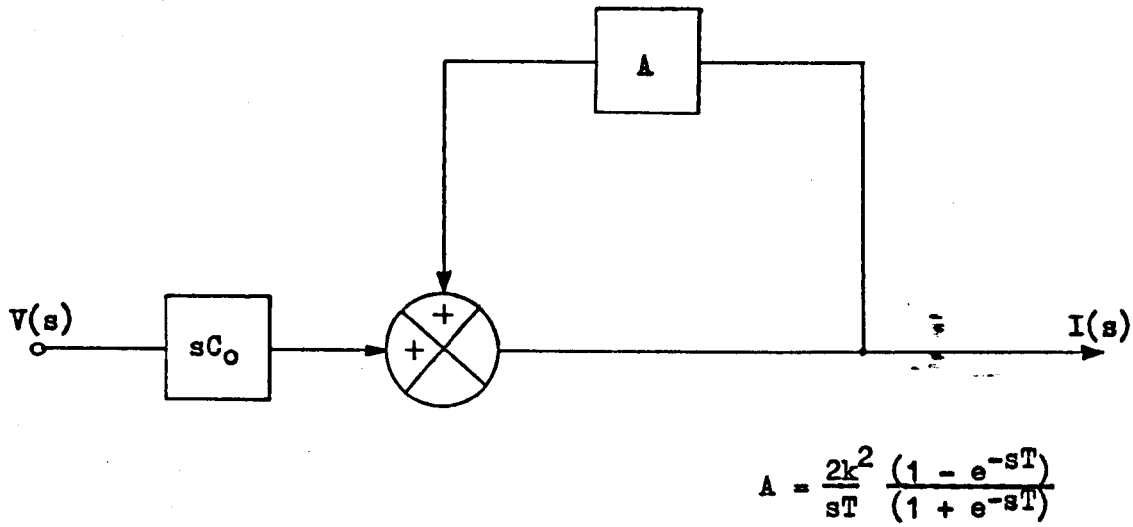

Fig. 5.4. Admittance Block Diagram of the Lossless Piezoelectric Resonator

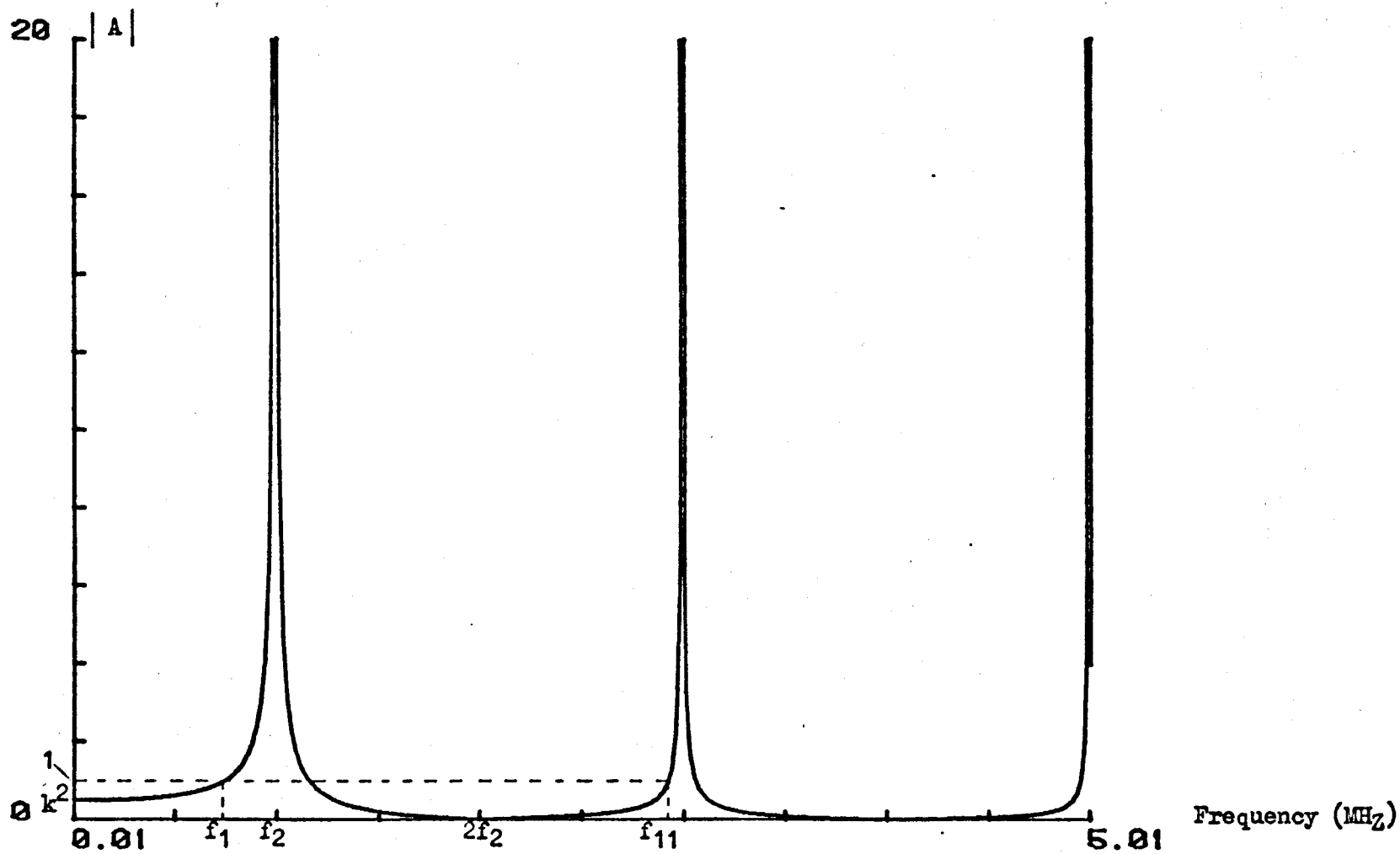

Fig. 5.5a. Magnitude Characteristics of the Resonator Feedback Factor

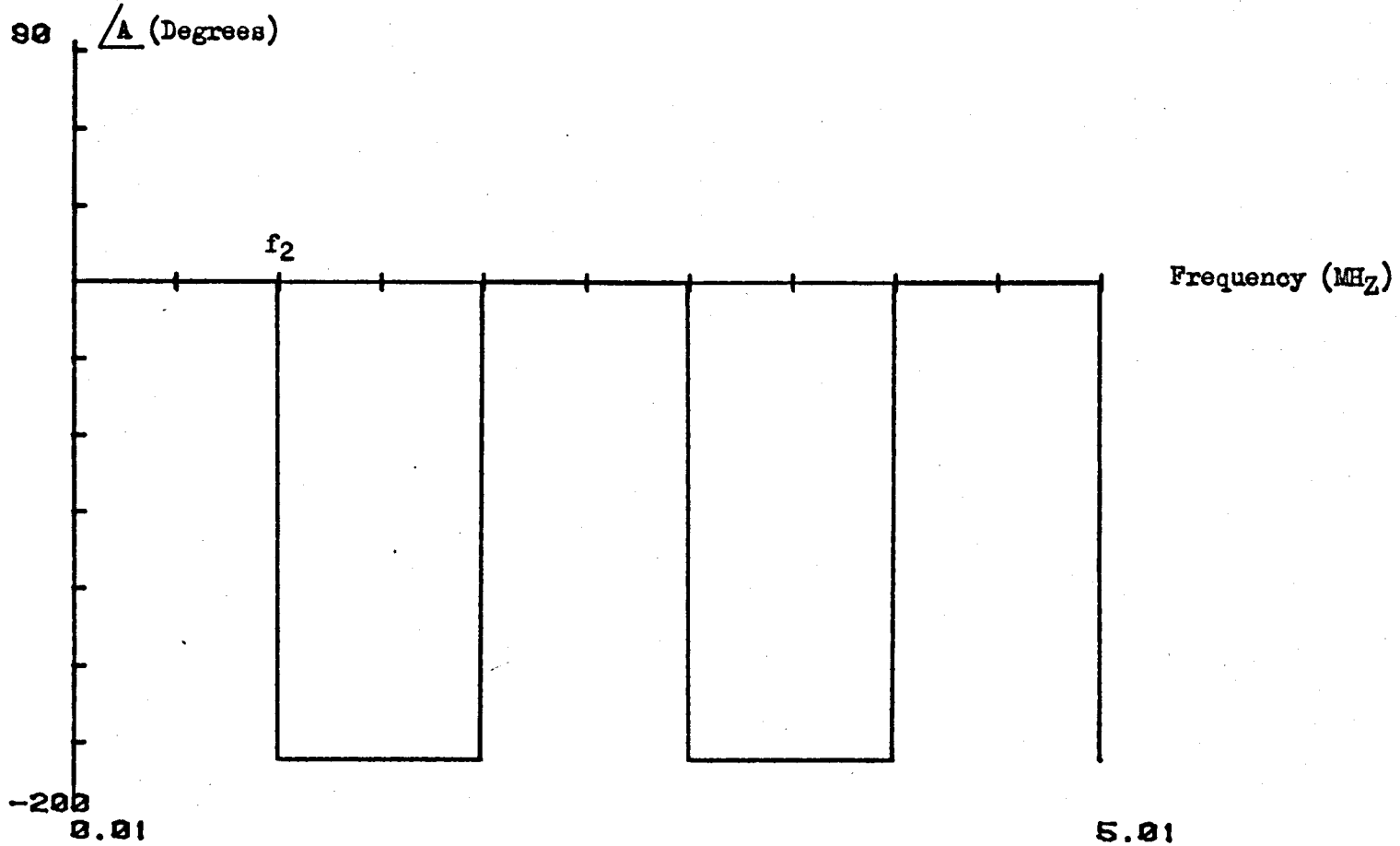

Fig. 5.5b. Phase Characteristics of the Resonator Feedback Factor

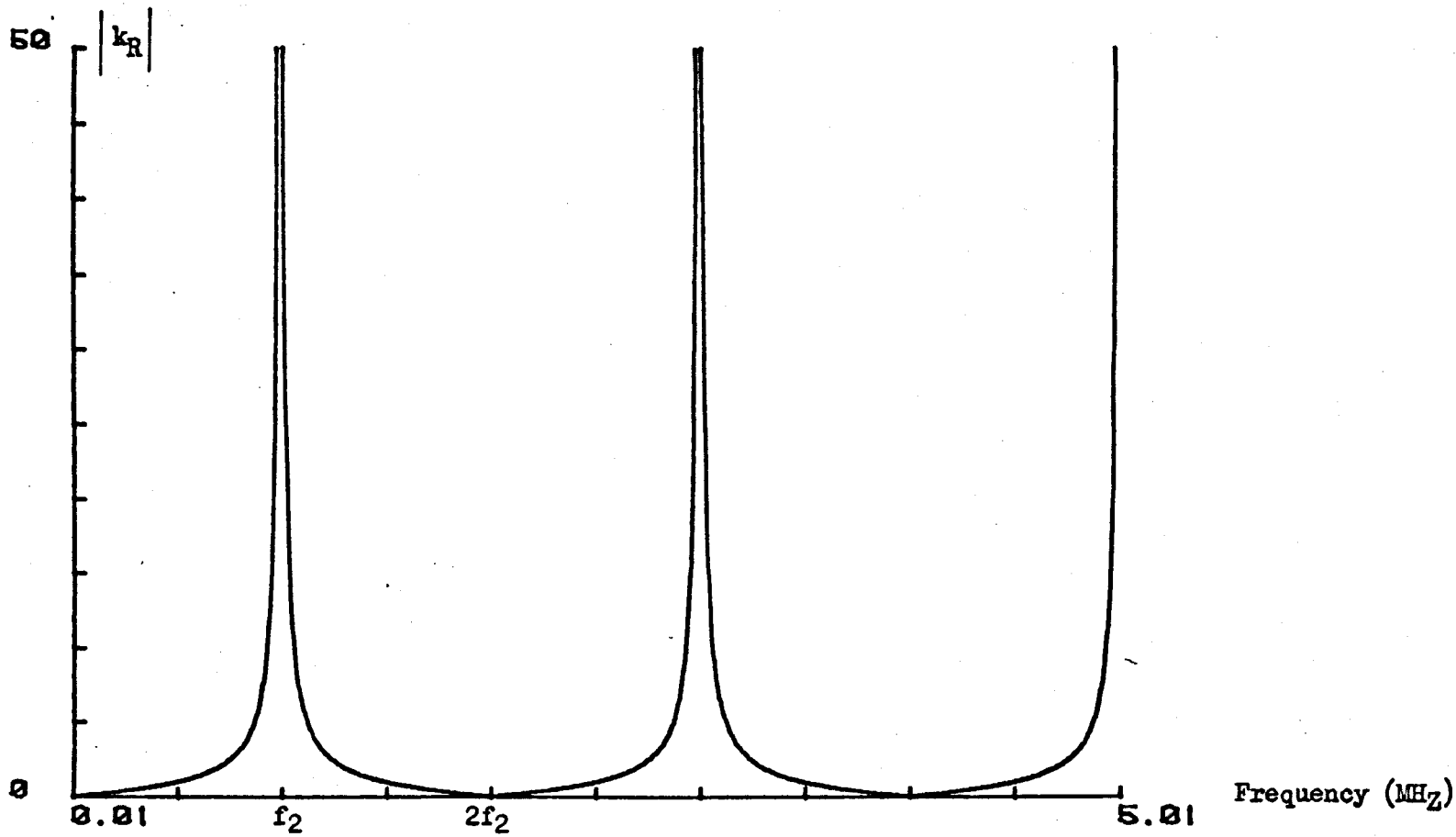

Fig. 5.6a. Magnitude Characteristics of the Resonator Reverberation Factor

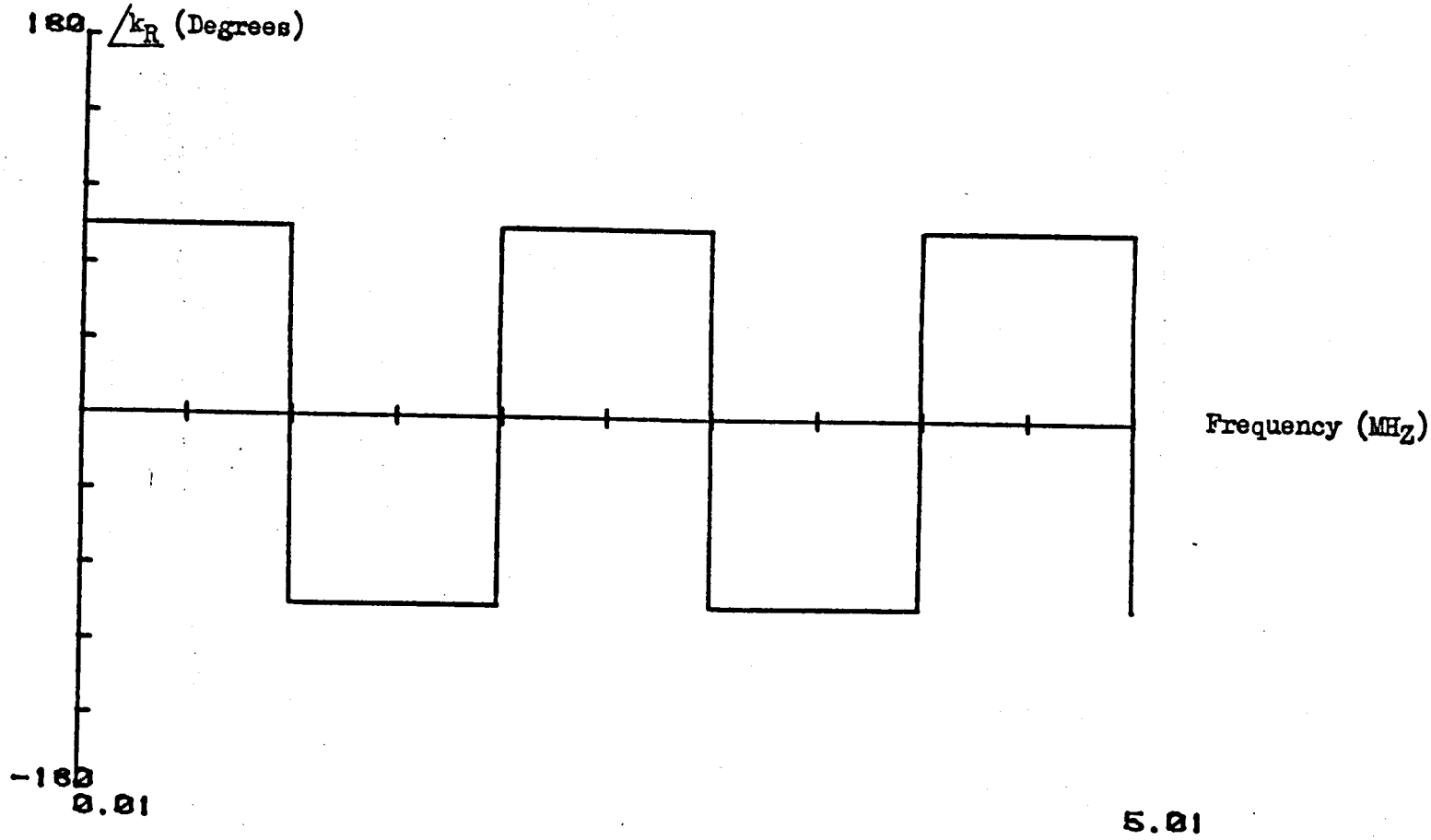

Fig. 5.6b. Phase Characteristics of the Resonator Reverberation Factor

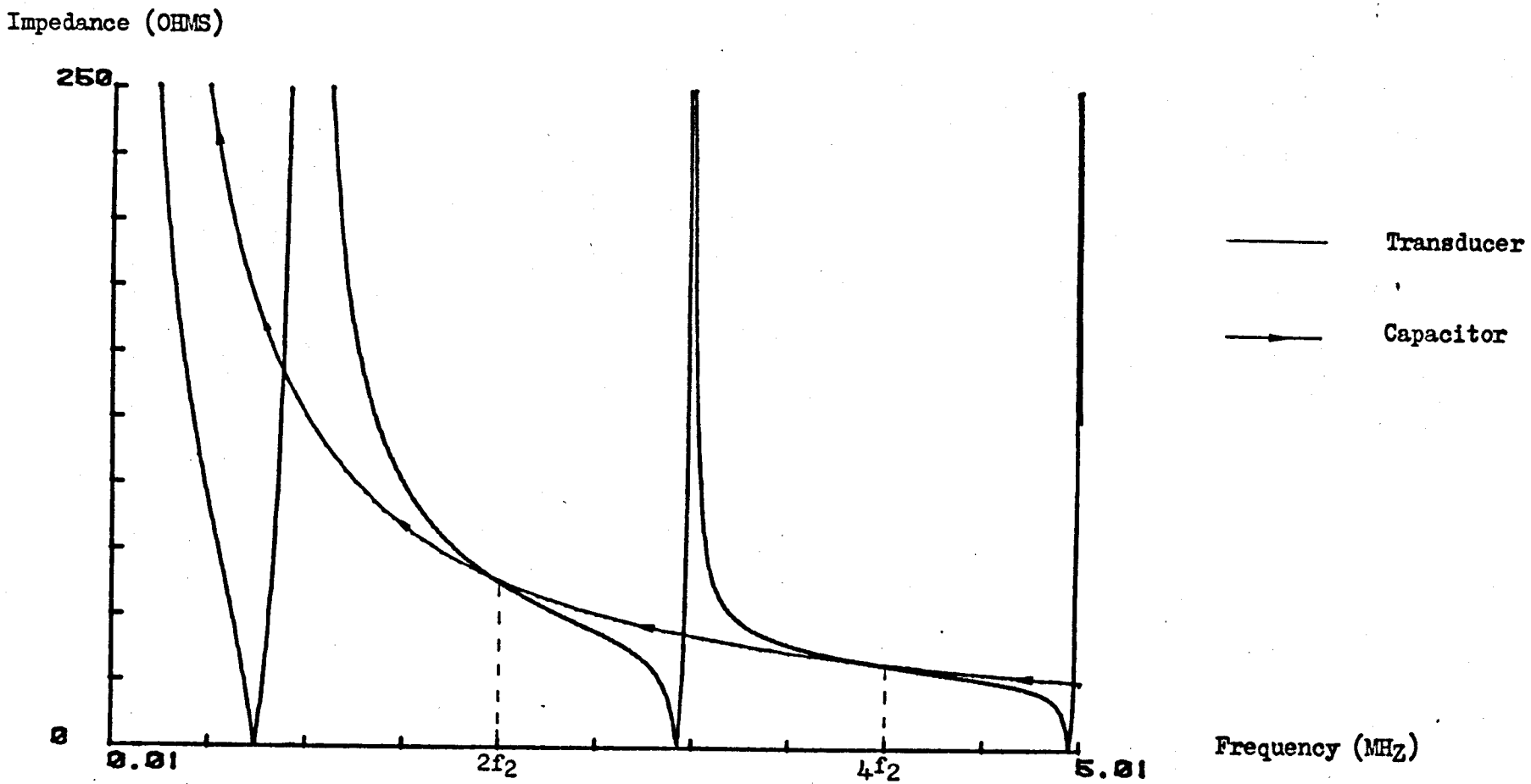

Fig. 5.7. Comparison Between Static Capacitance and Resonator Impedance Magnitudes

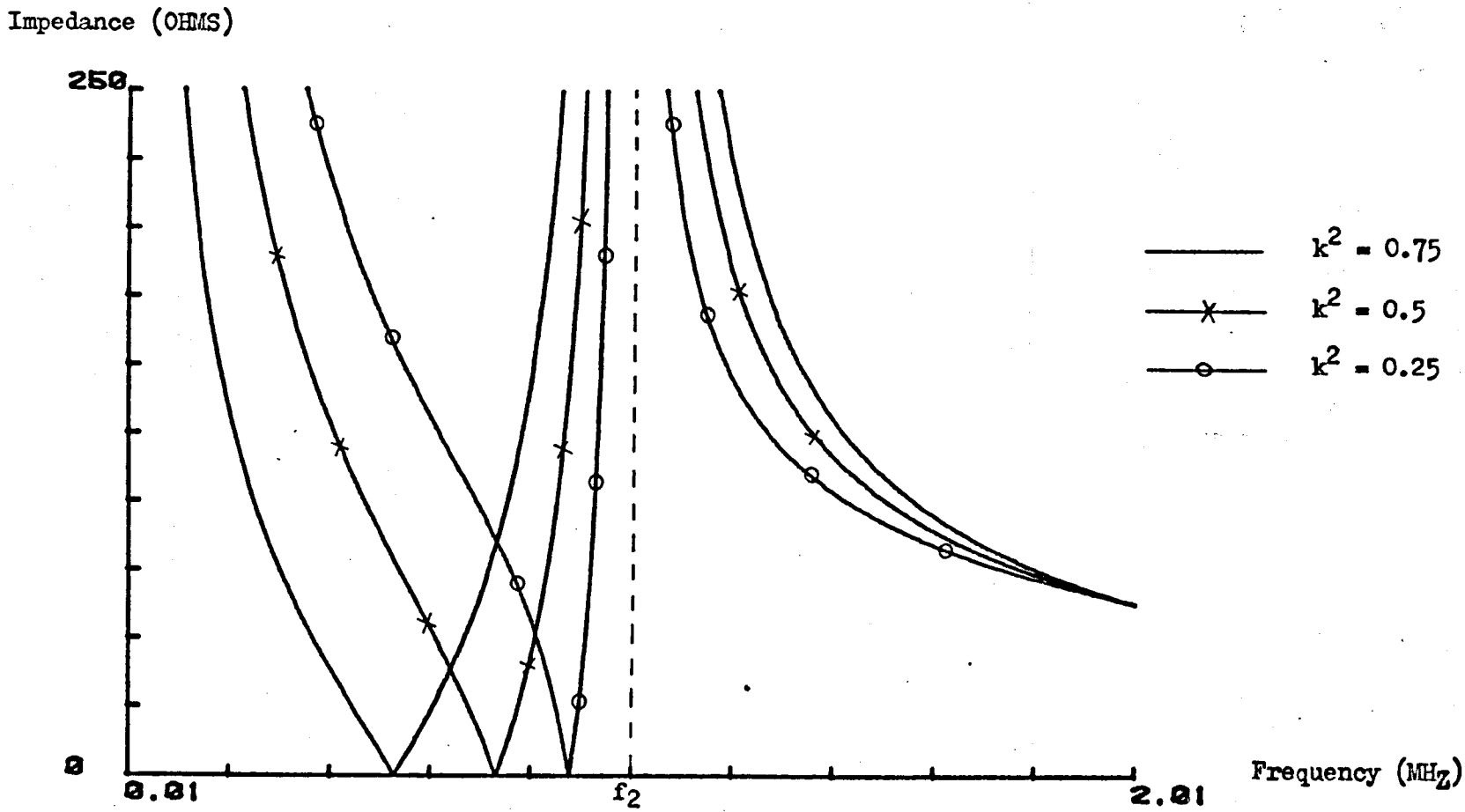

Fig. 5.8. Variation of Resonator Impedance Characteristic with Electromechanical Coupling Coefficient

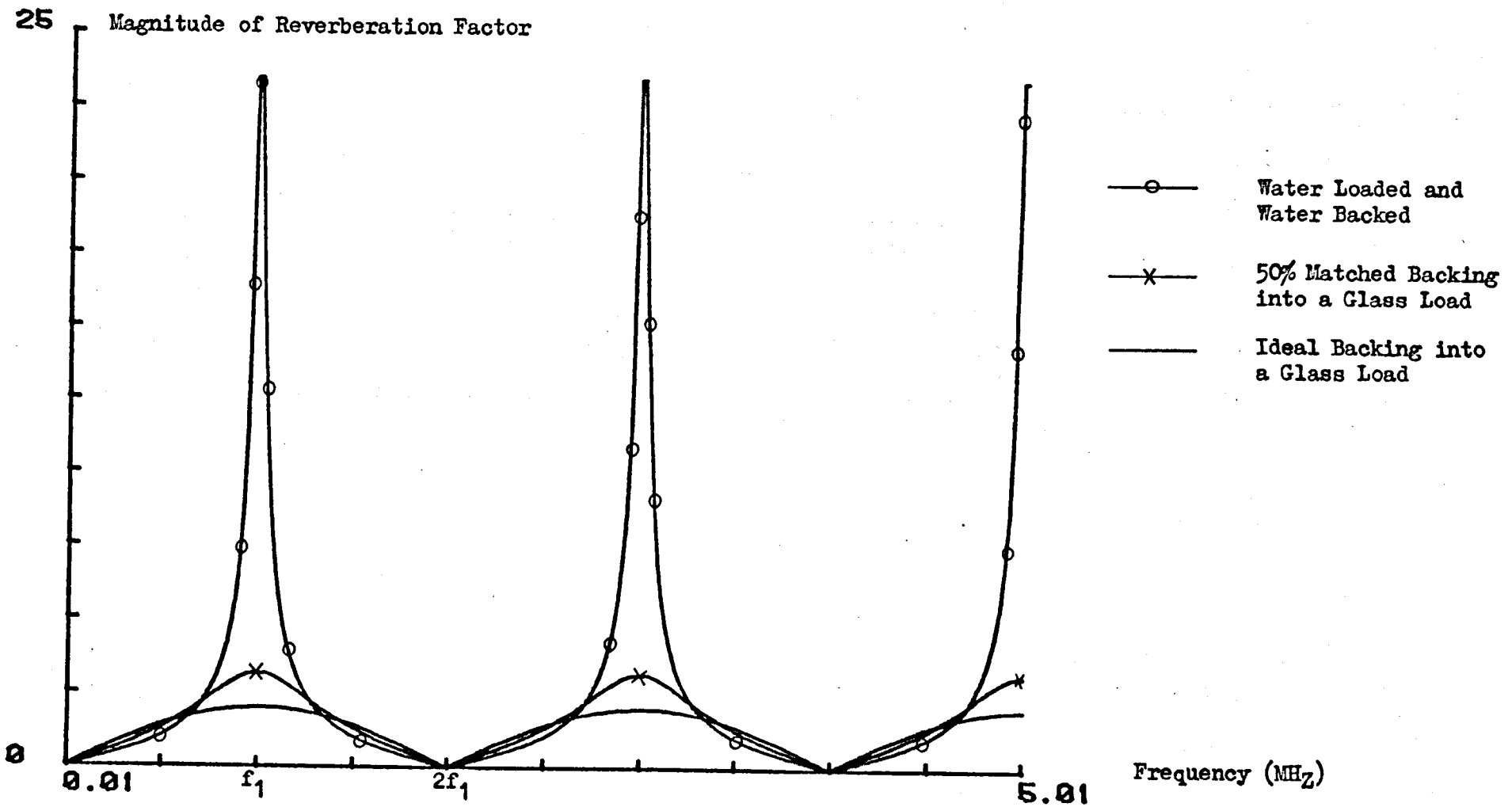

Fig. 5.9a. Magnitude of Reverberation Factor for a Loaded Transducer

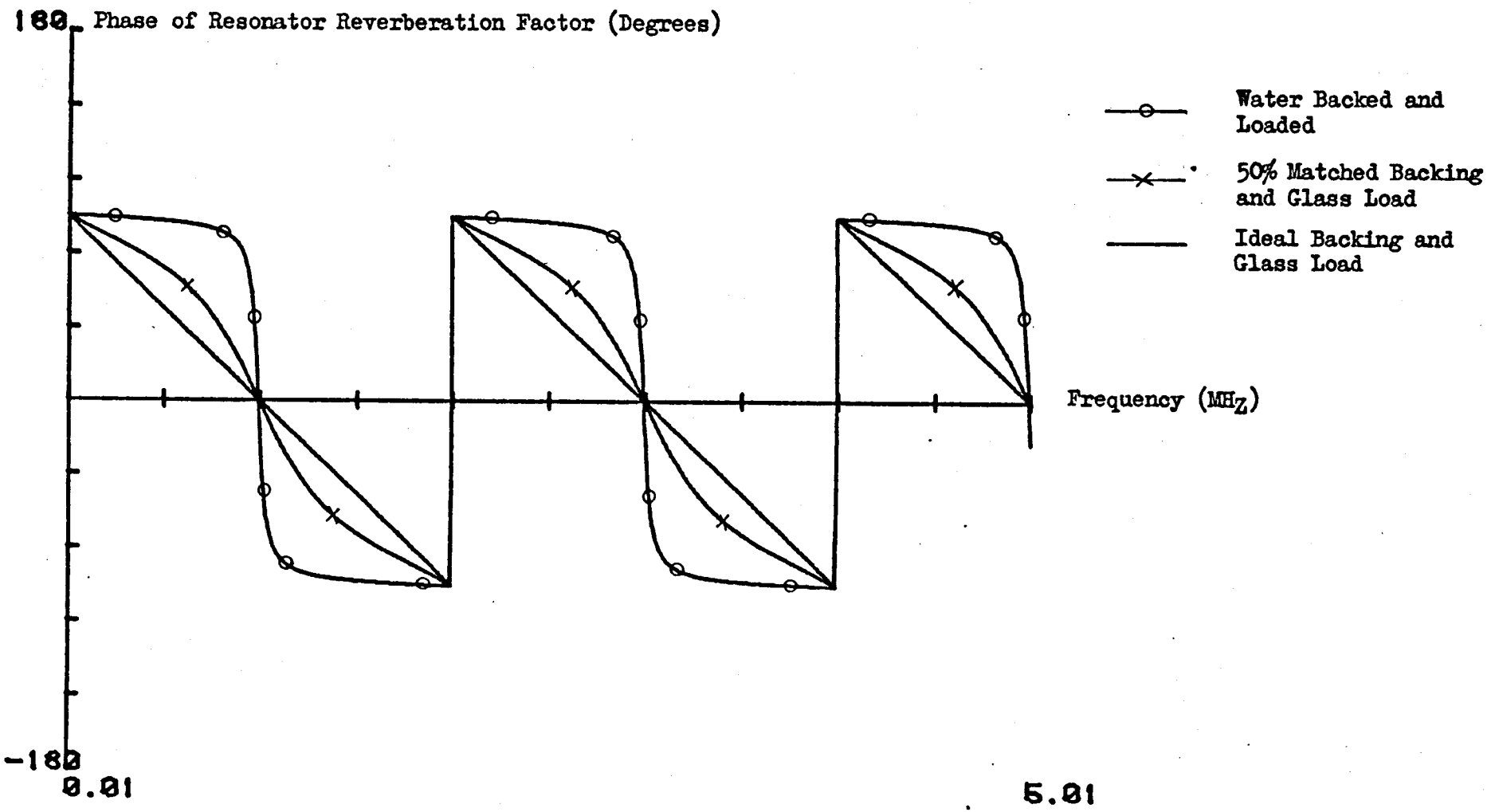

Fig. 5.9b. Phase of K_F for a Loaded Transducer

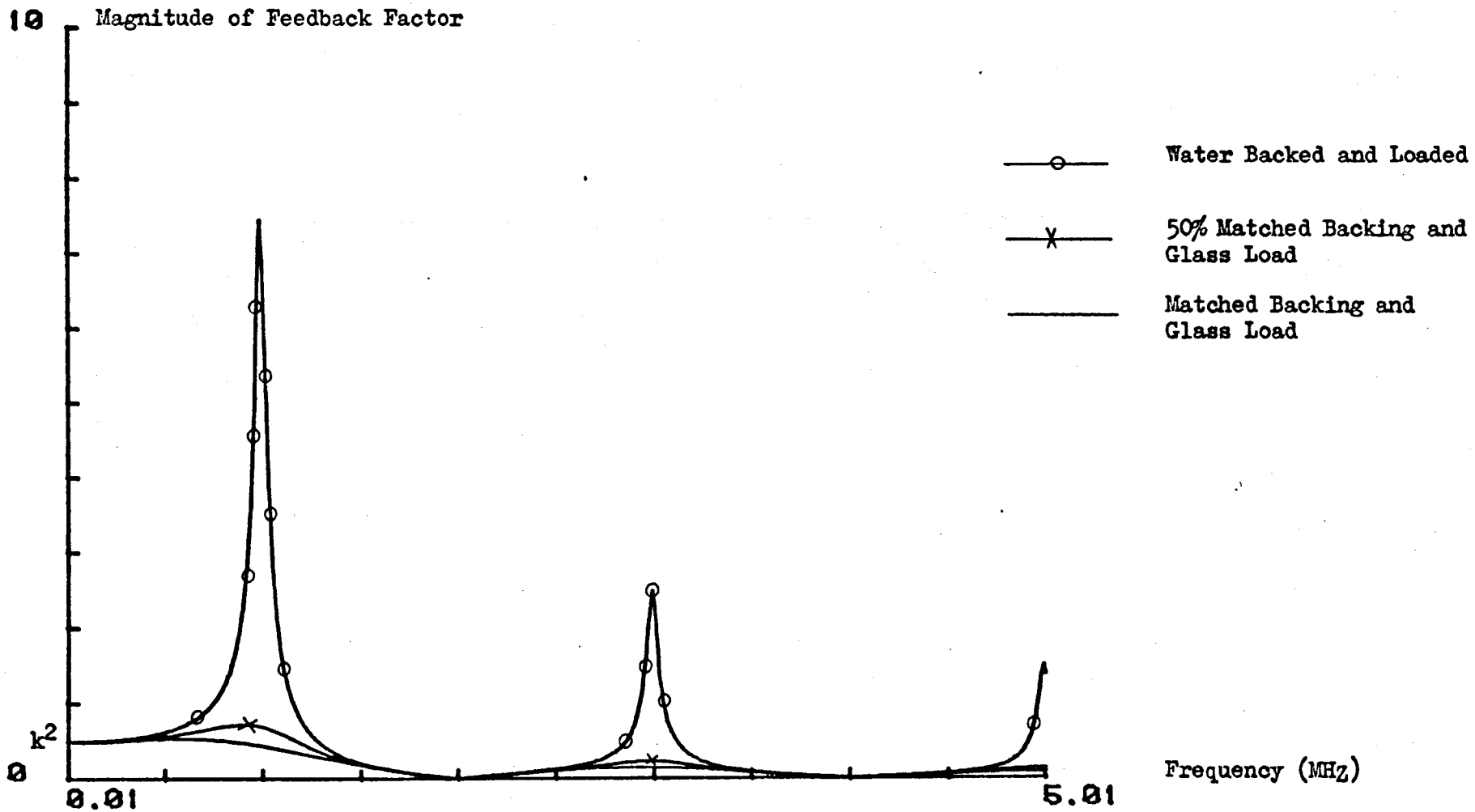

Fig. 5.10a. Variation in Feedback Factor with Mechanical Load

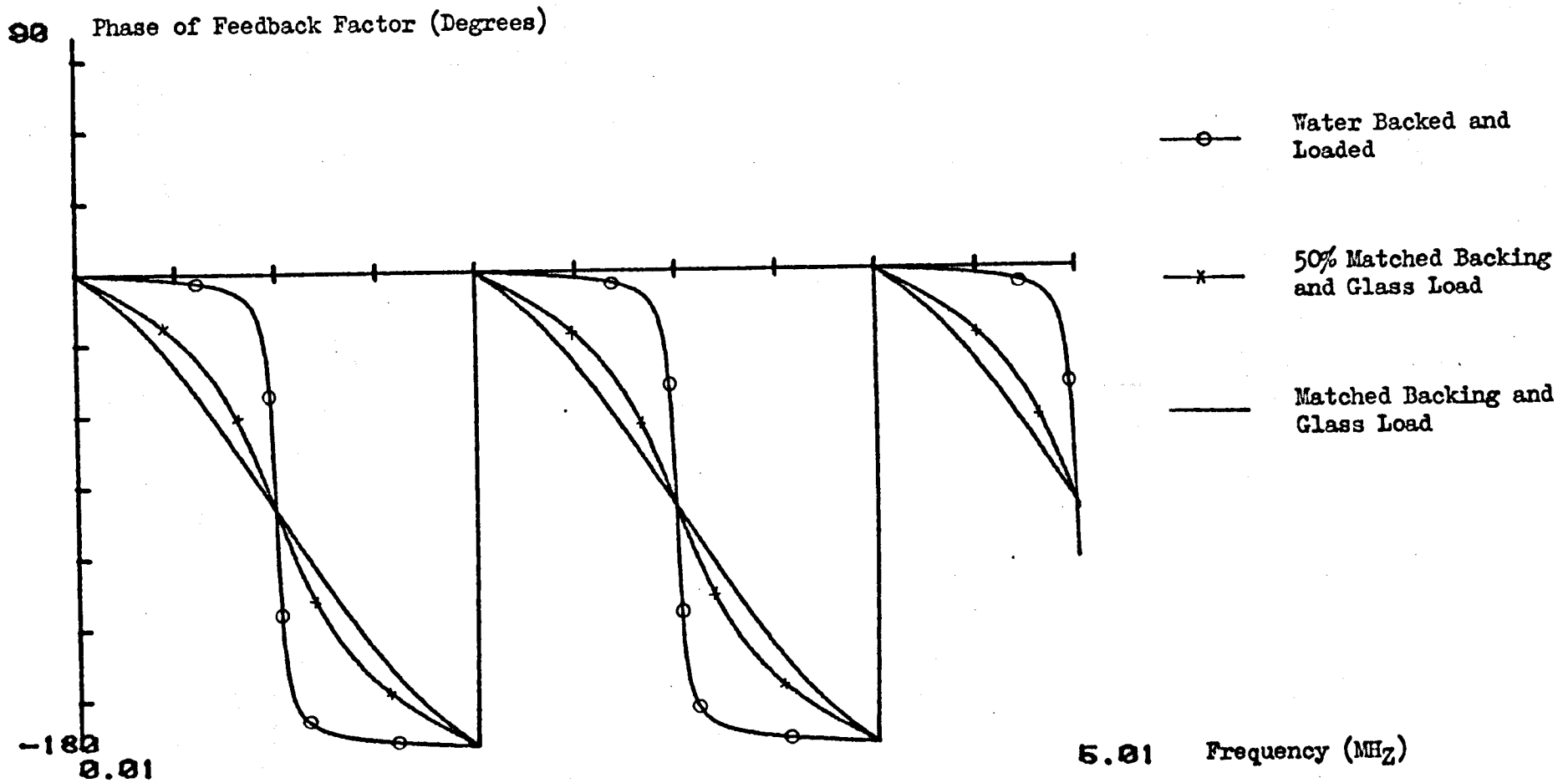

Fig. 5.10b. Variation in Phase of Total Feedback Factor with Mechanical Load

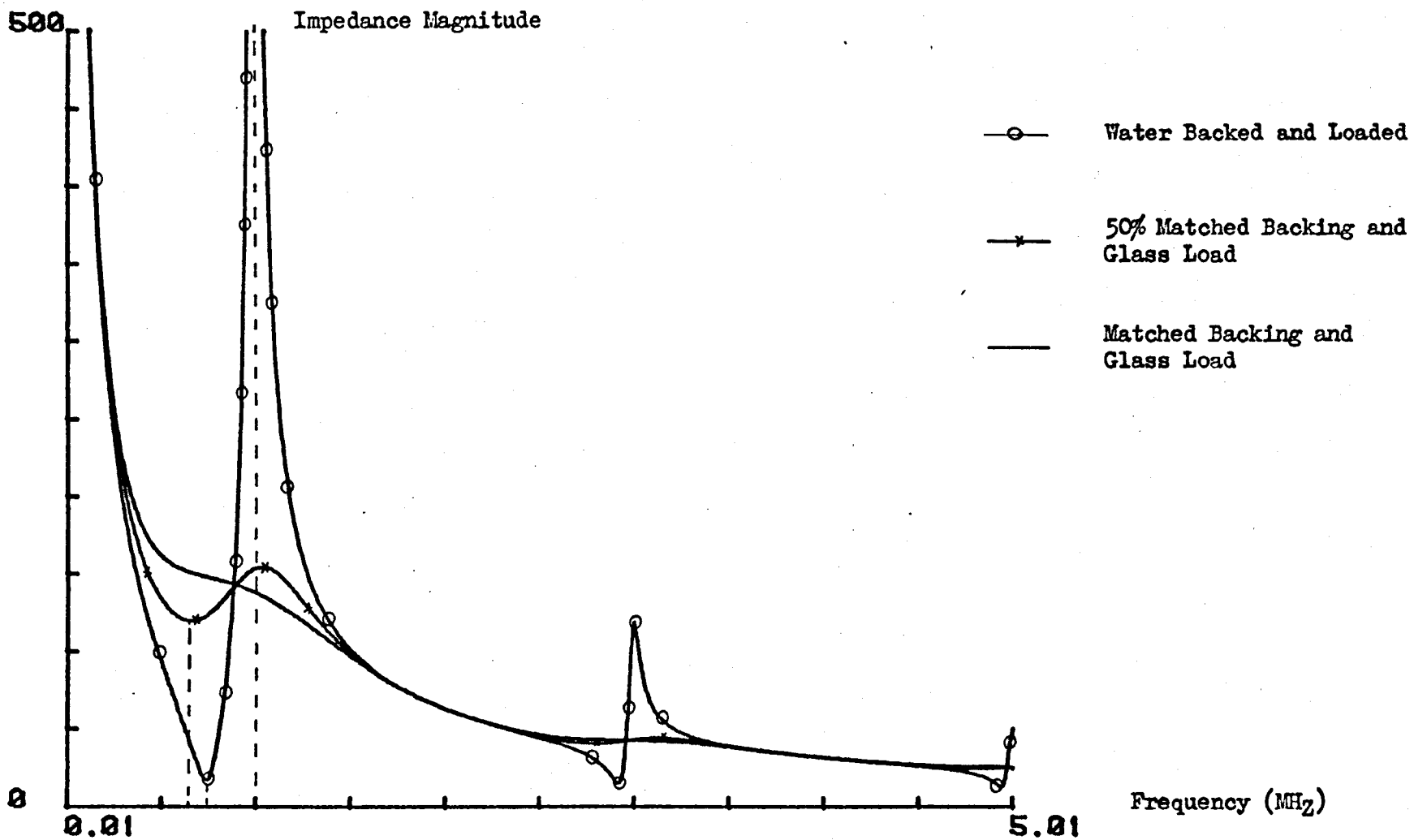

Fig. 5.11a. Variation of Electrical Impedance Magnitude with Mechanical Load

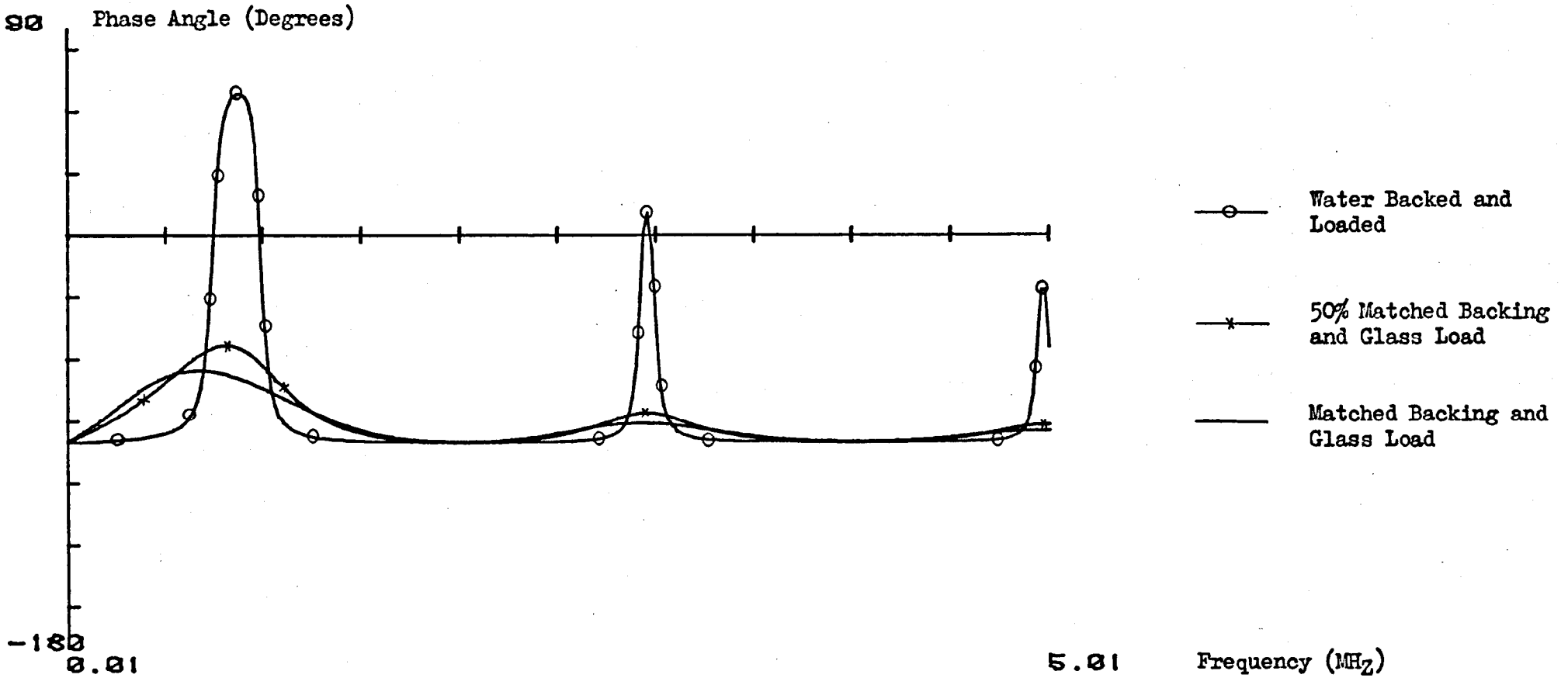

Fig. 5.11b. Variation of Electrical Impedance Phase with Mechanical Load

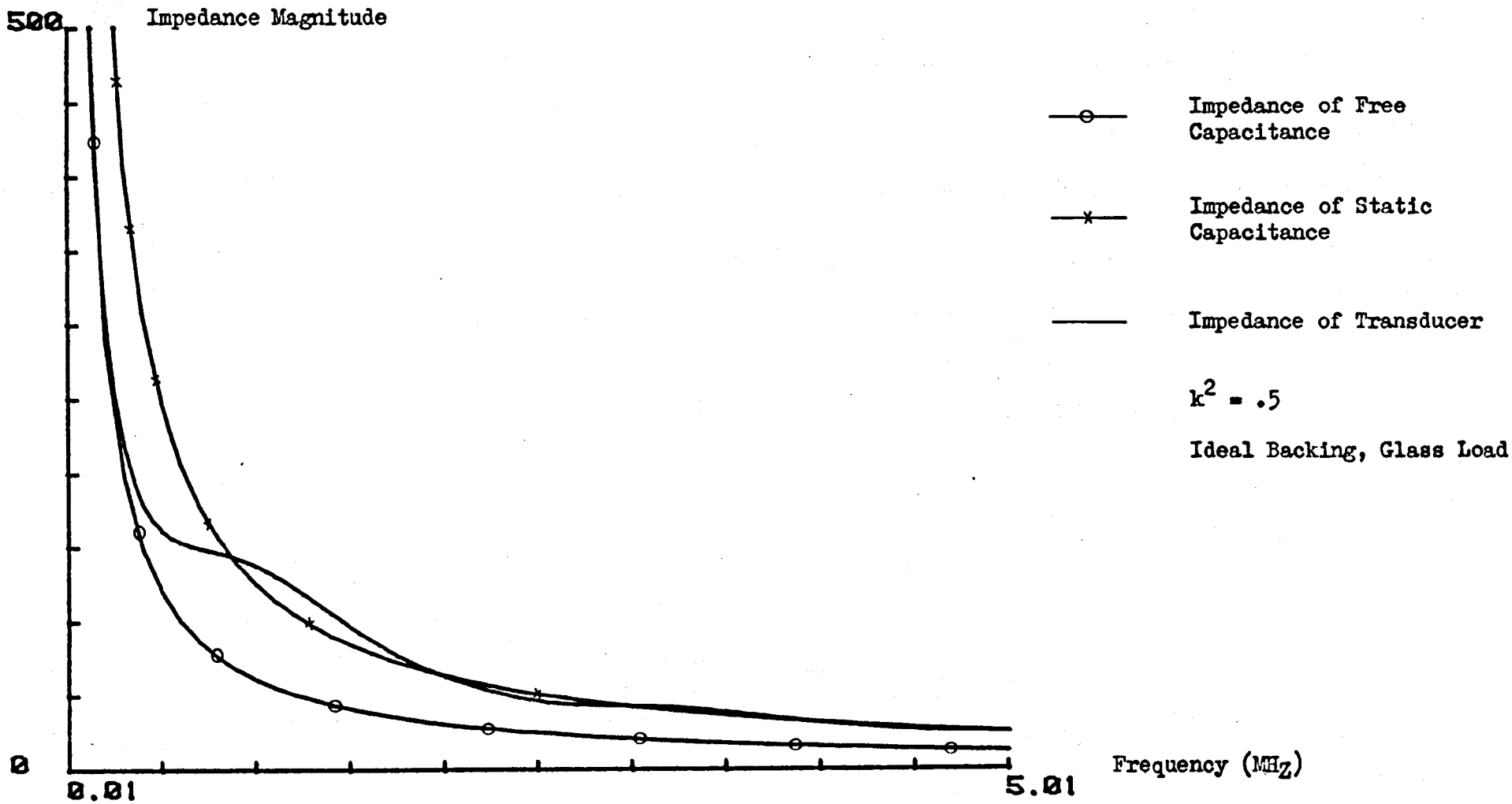

Fig. 5.12a. Comparison of Heavily Damped 1MHz Transducer Impedance with Device Capacitances

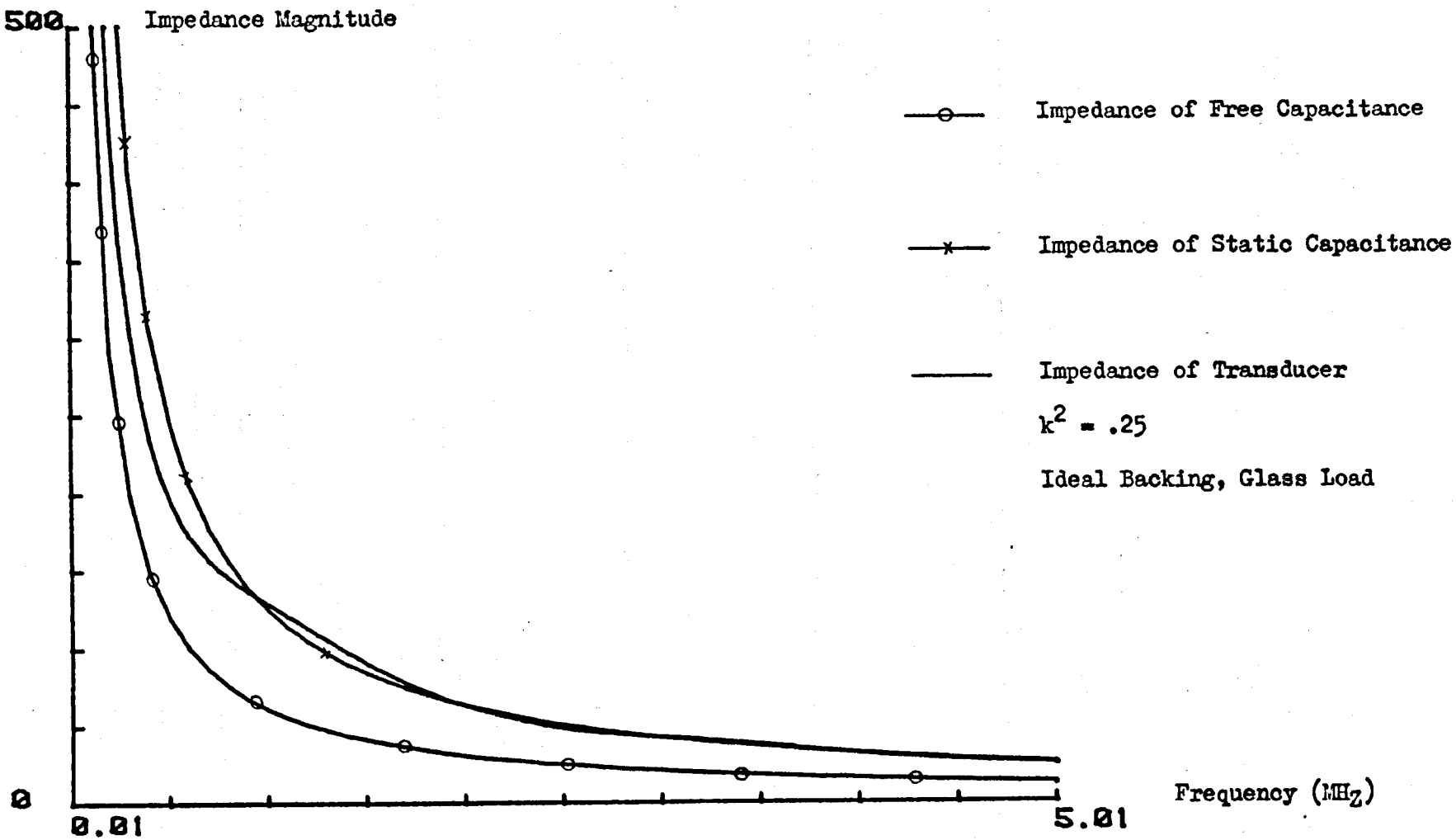

Fig. 5.12b. Comparison of Heavily Damped Transducer Impedance and Device Capacitances

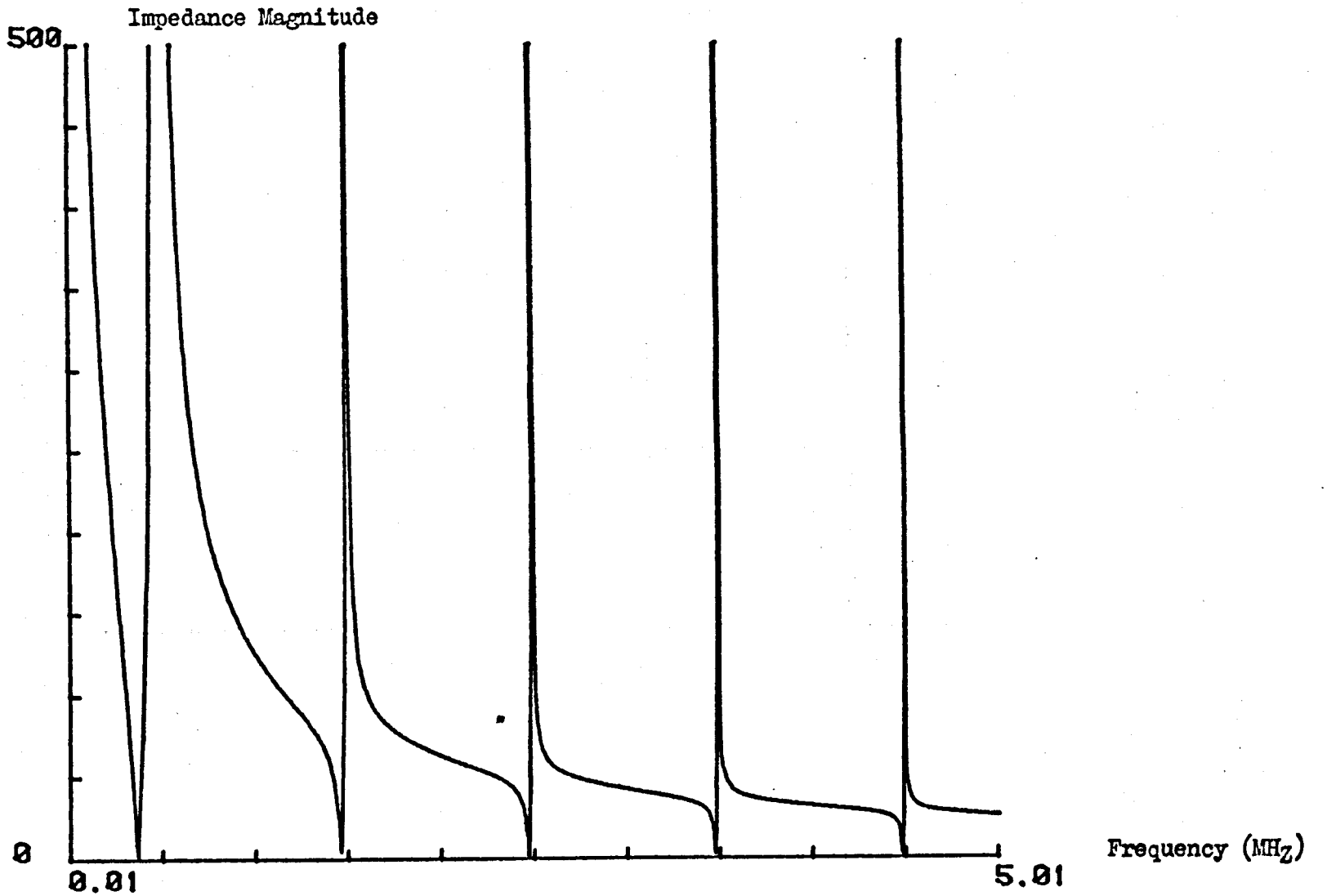

Fig. 5.13a. Impedance Magnitude Characteristic for a Rigidly Backed, Air Loaded Transducer

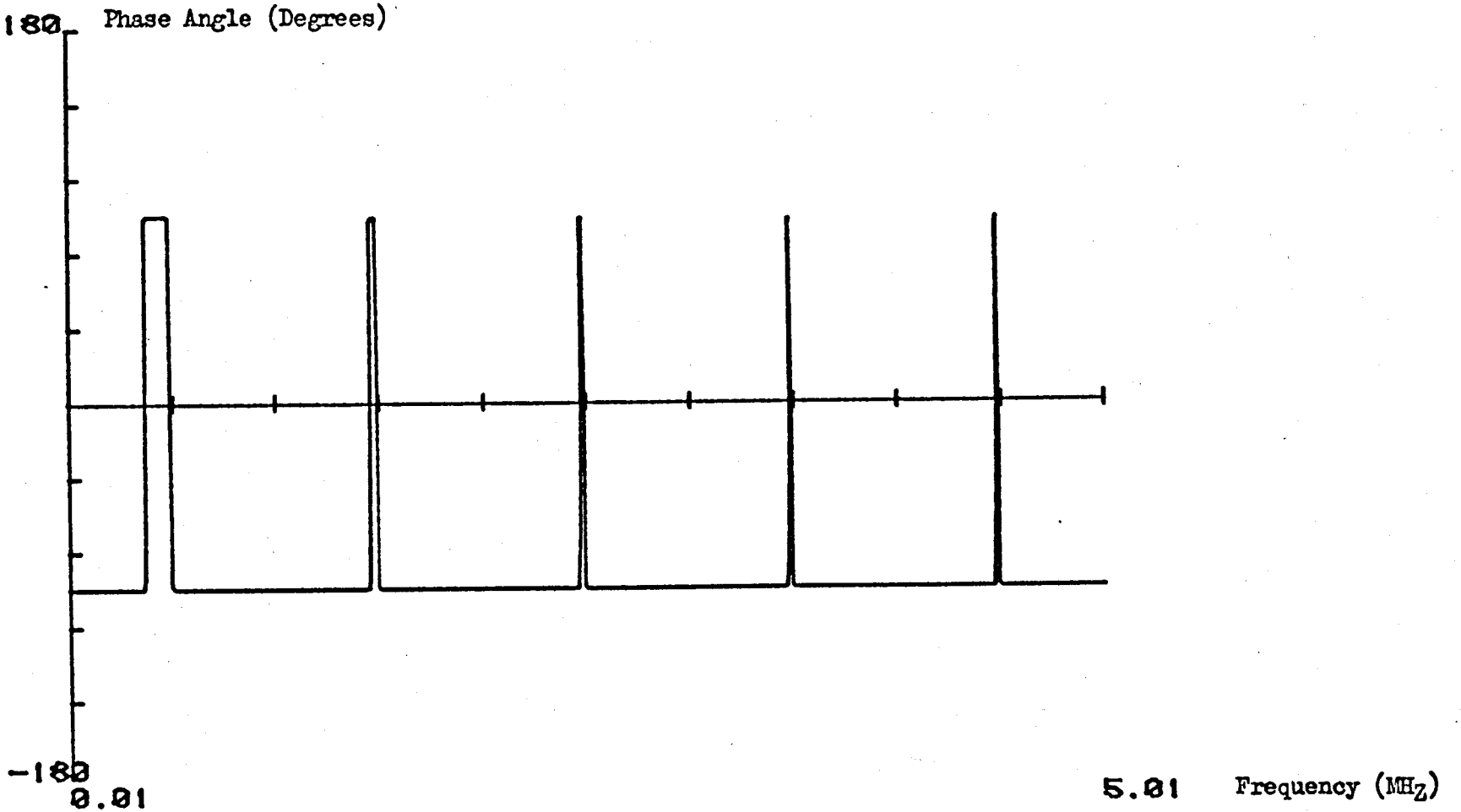

Fig. 5.13b. Impedance Phase Characteristic for a Rigidly Backed, Air Loaded Transducer

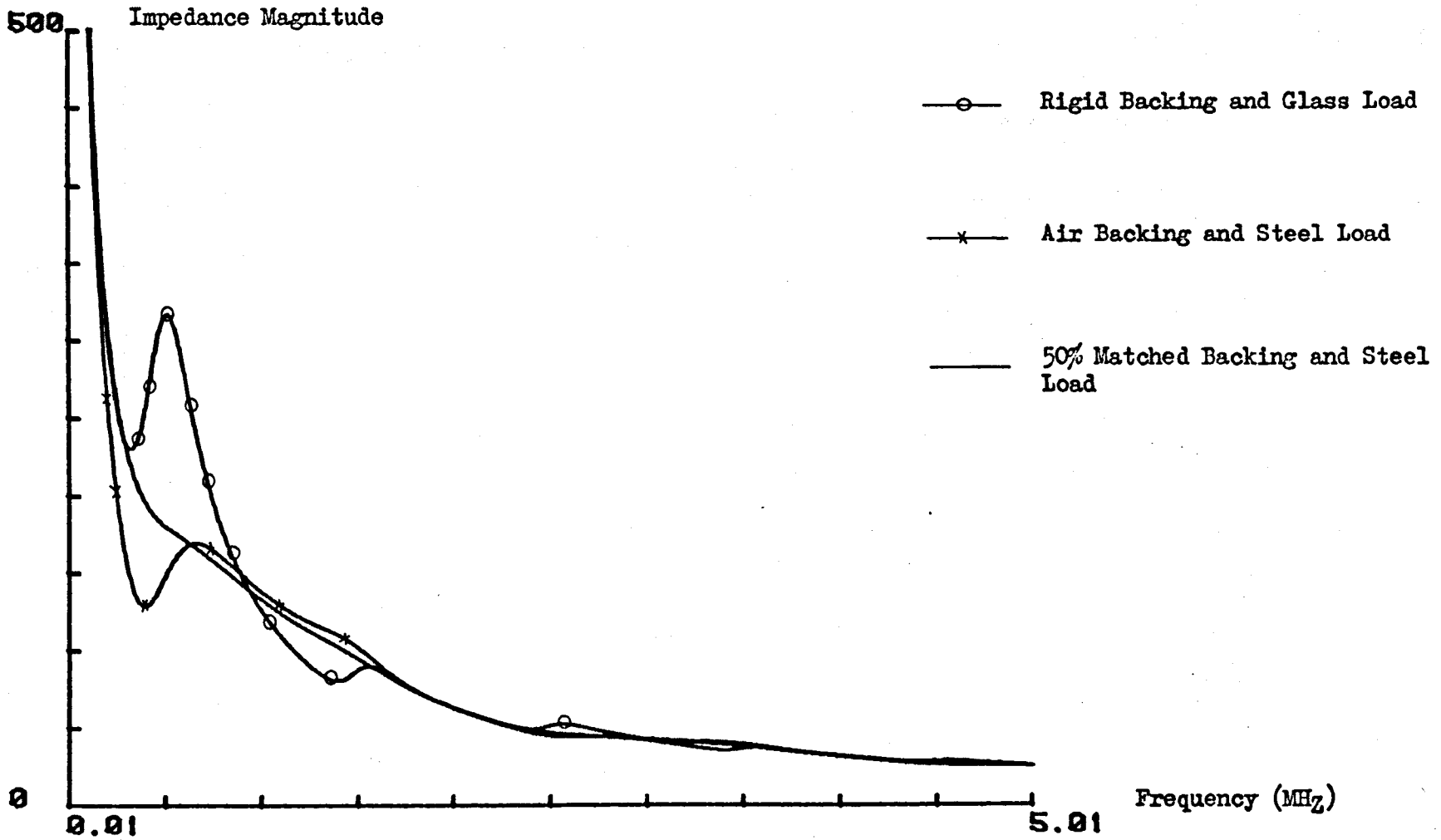

Fig. 5.14a. Impedance Magnitude Characteristics for Miscellaneous Mechanical Loading

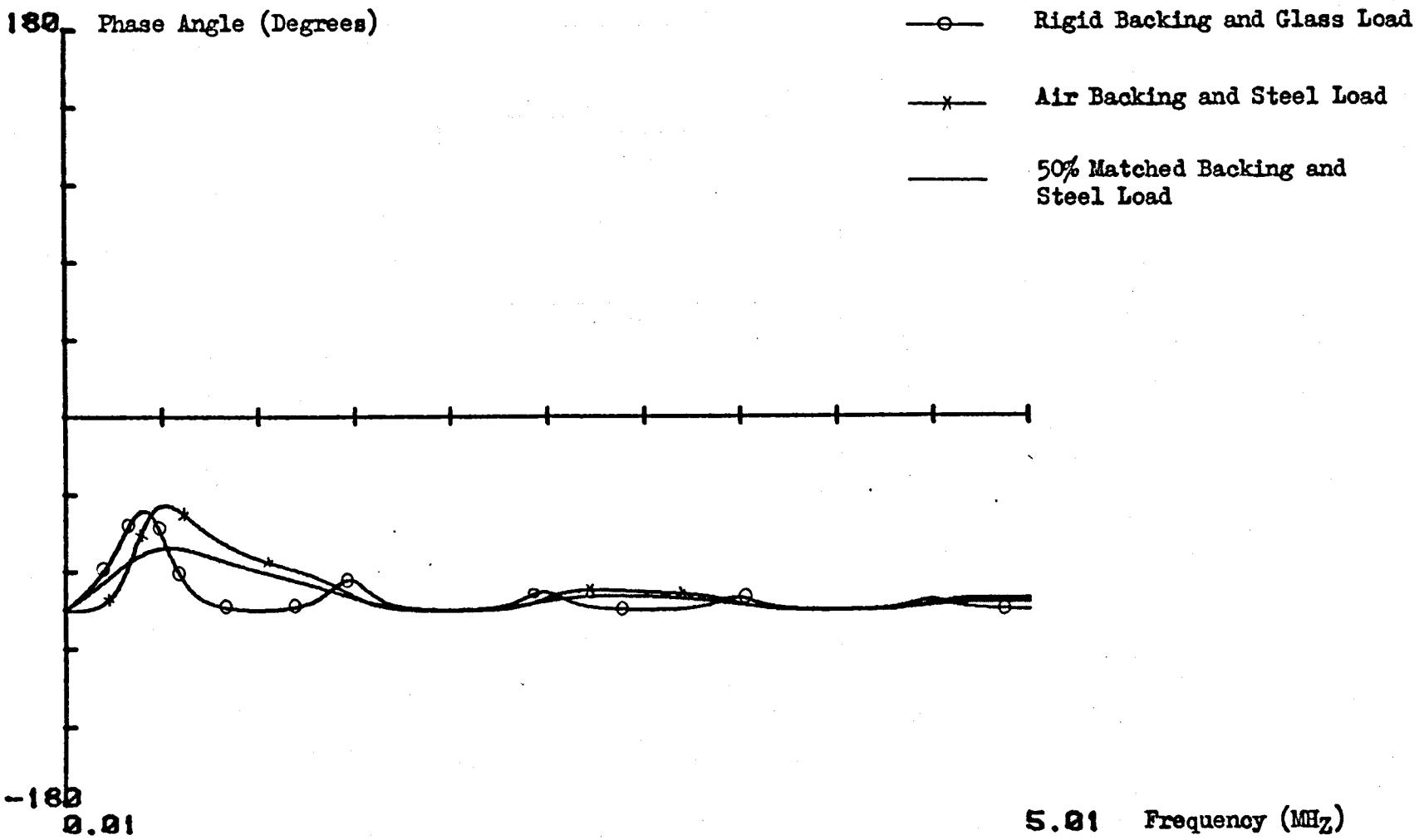

Fig. 5.14b. Impedance Phase Characteristics for Miscellaneous Acoustic Loadings

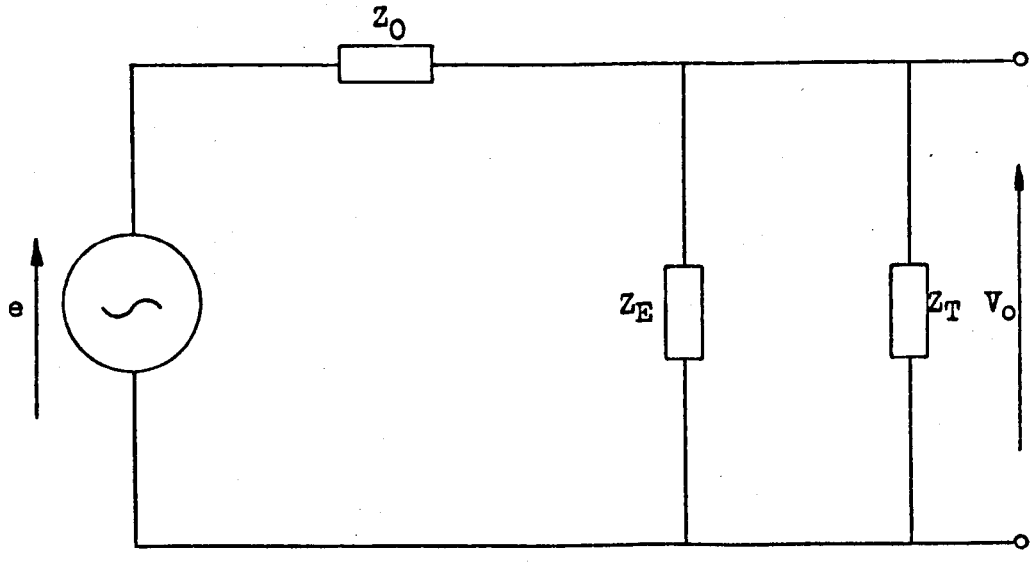

Fig. 6.1. Electrical Configuration for the Voltage Transfer Function

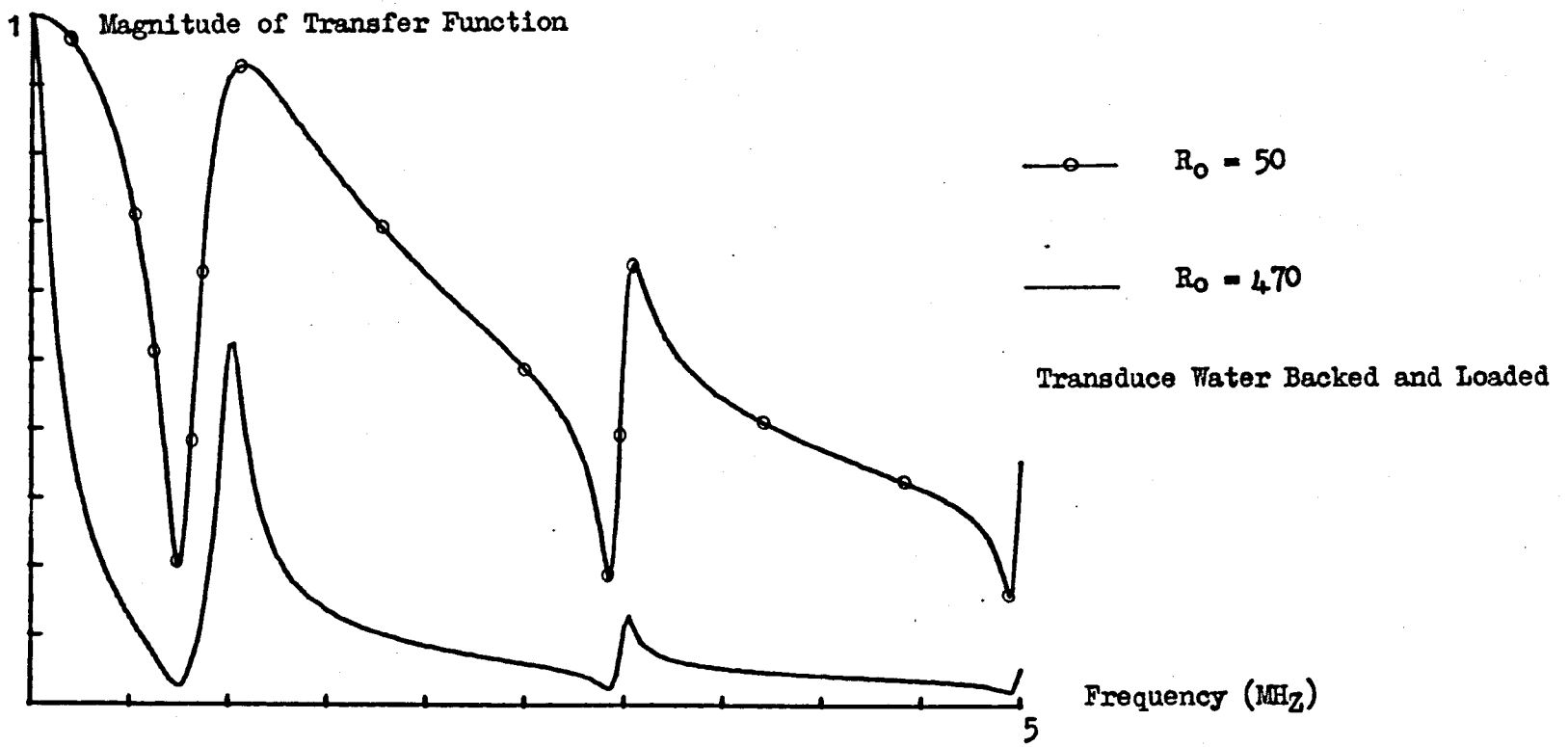

Fig. 6.2a. Frequency Characteristics of the Voltage Transfer Function for Different Values of Source Resistance

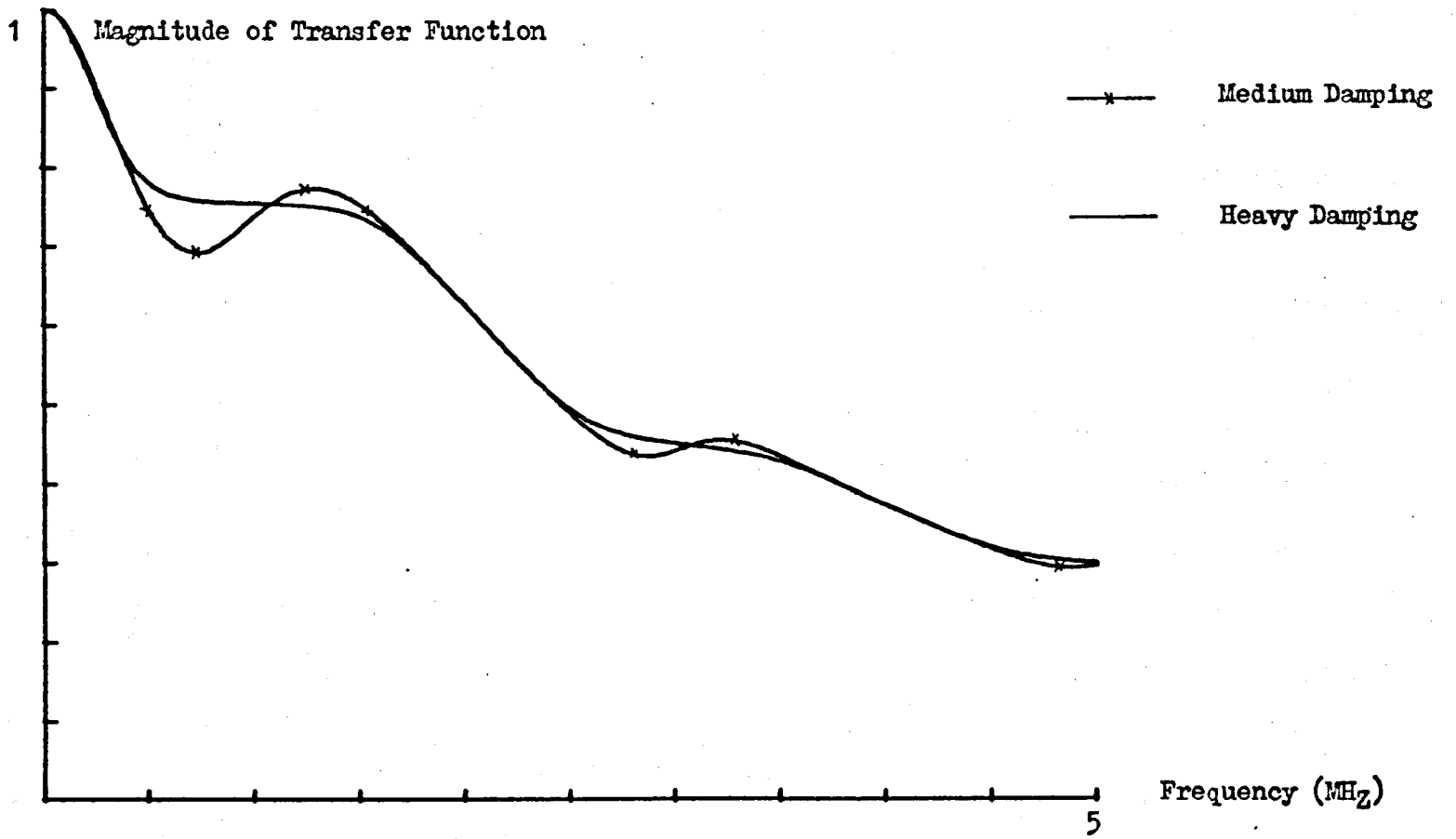

Fig. 6.2b. Frequency Response of the Voltage Transfer Function under Conditions of Medium and Heavy Damping (R_o = 50)

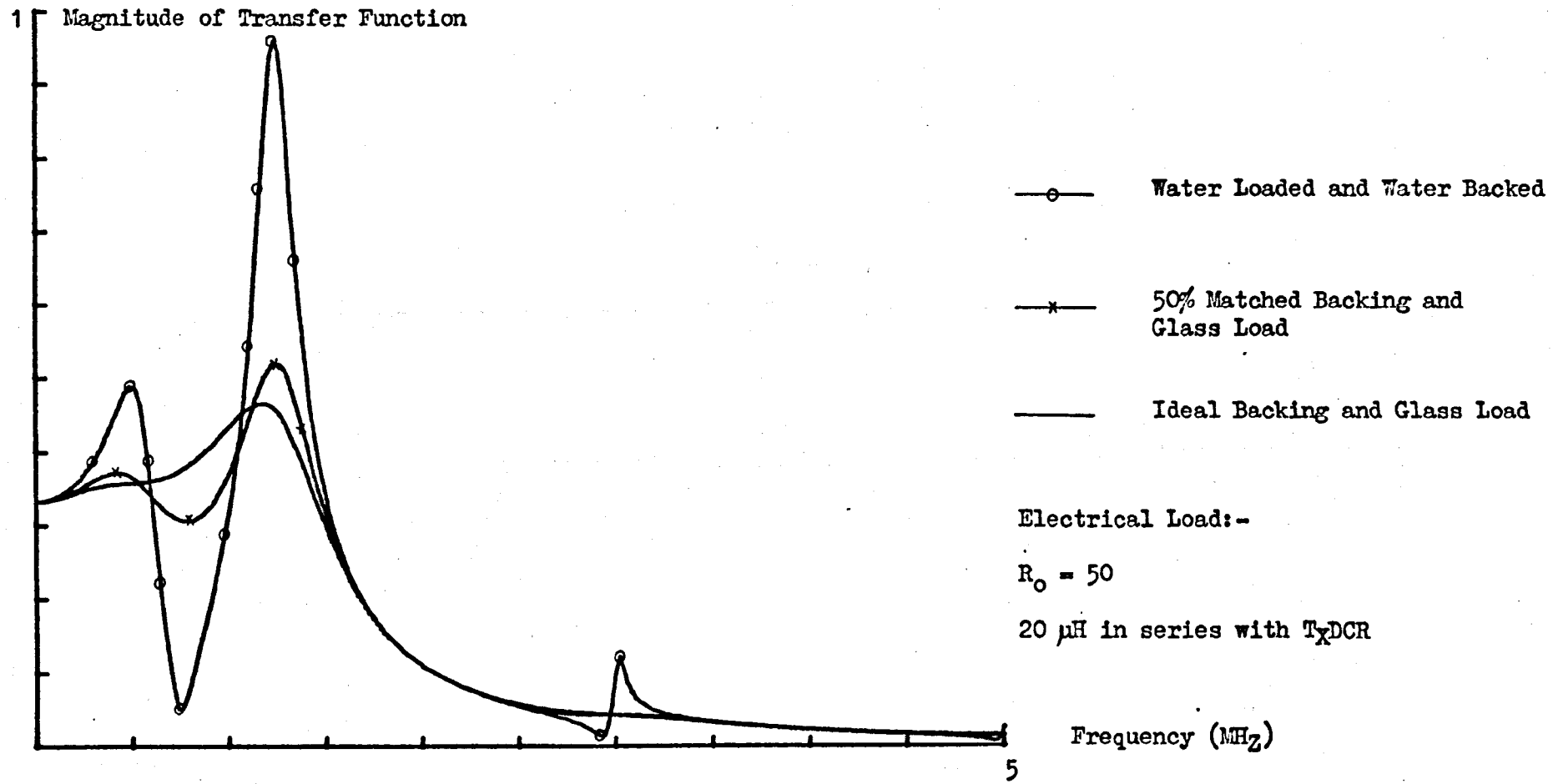

Fig. 6.2c. Frequency Response of the Voltage Transfer Function Response under Different Conditions of Mechanical Load

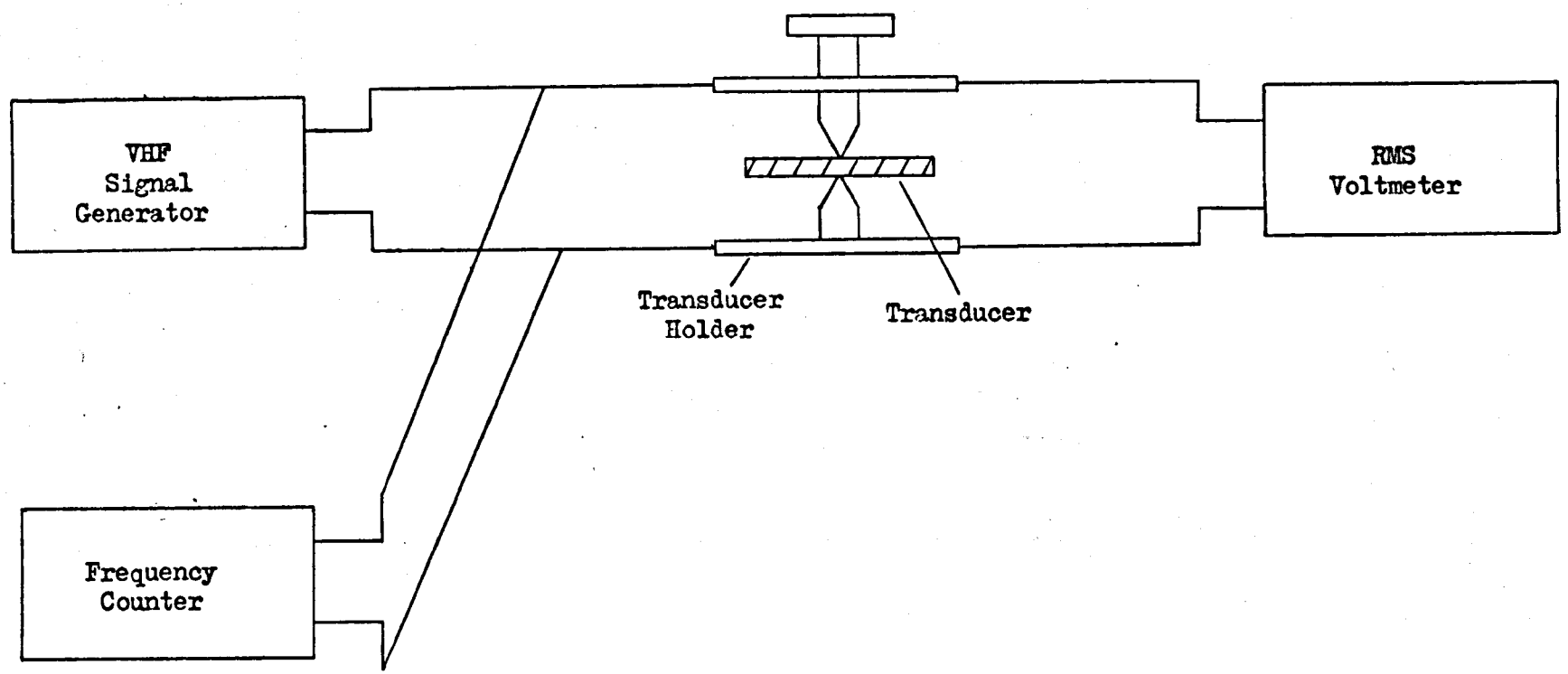

Fig. 6.3. Apparatus for CW Measurement of the Voltage Transfer Function

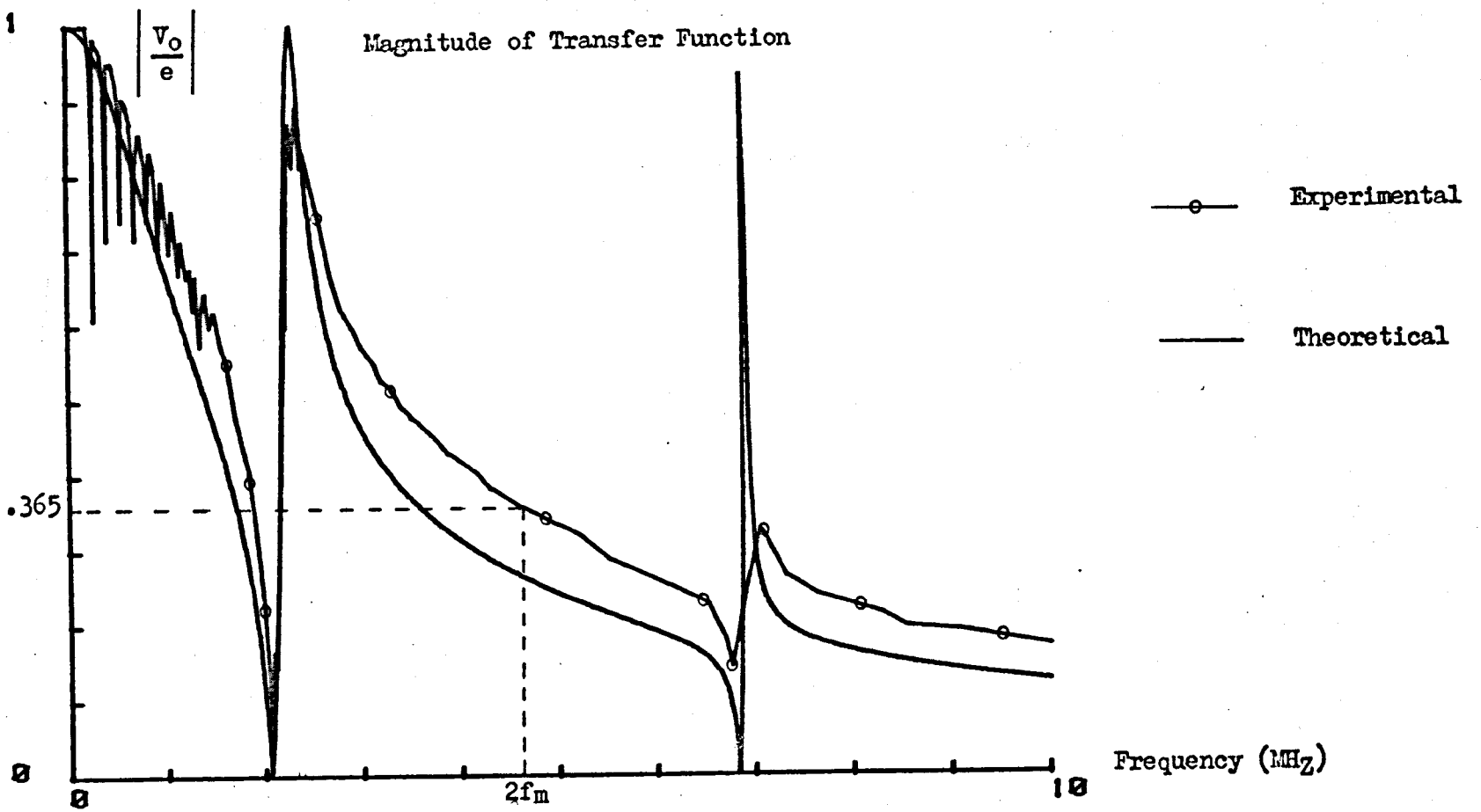

Fig. 6.4a. CW Voltage Response for the 2MHz Transducer

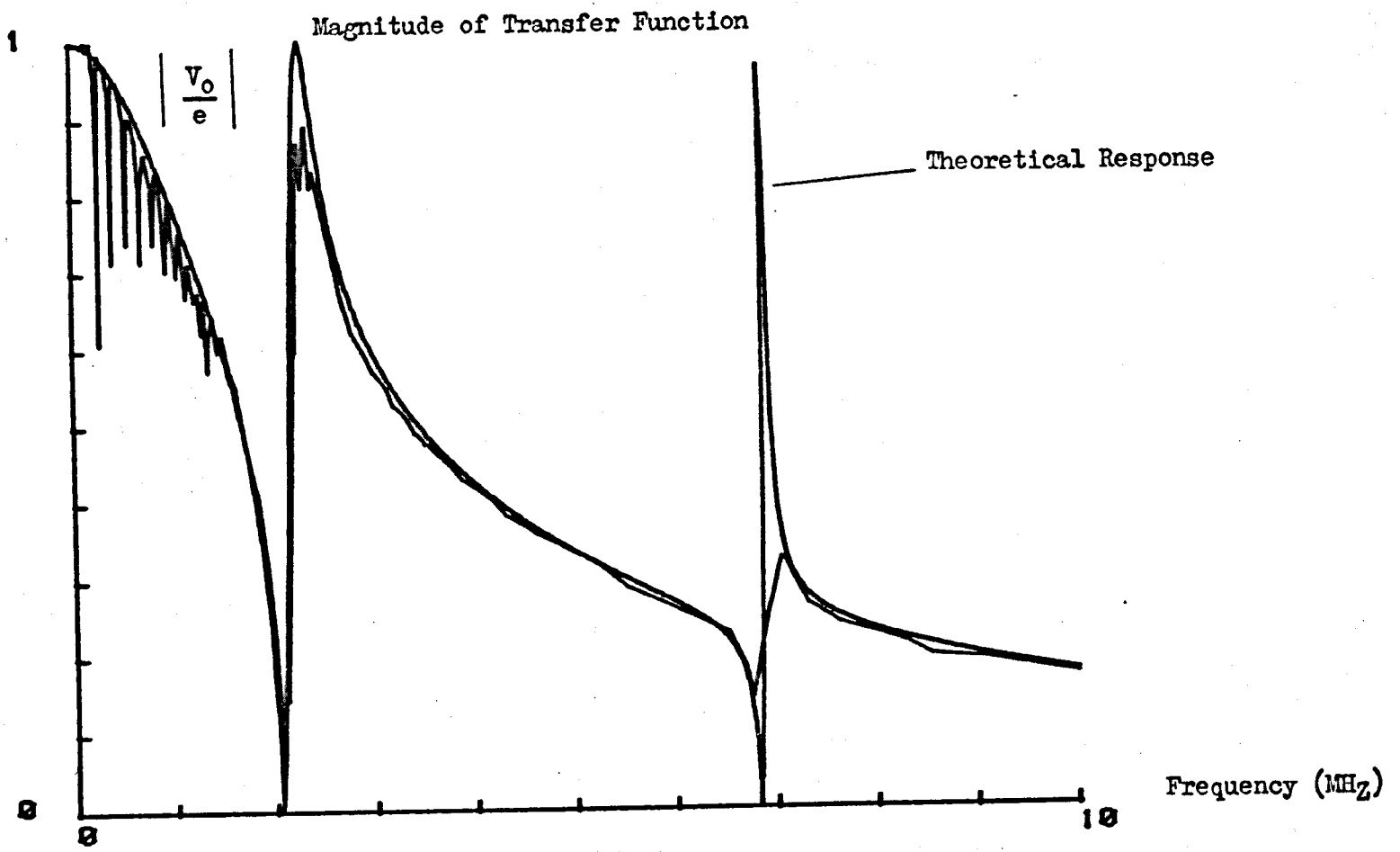

Fig. 6.4b. 2 MH_Z Response with Corrected Value of Static Capacitance

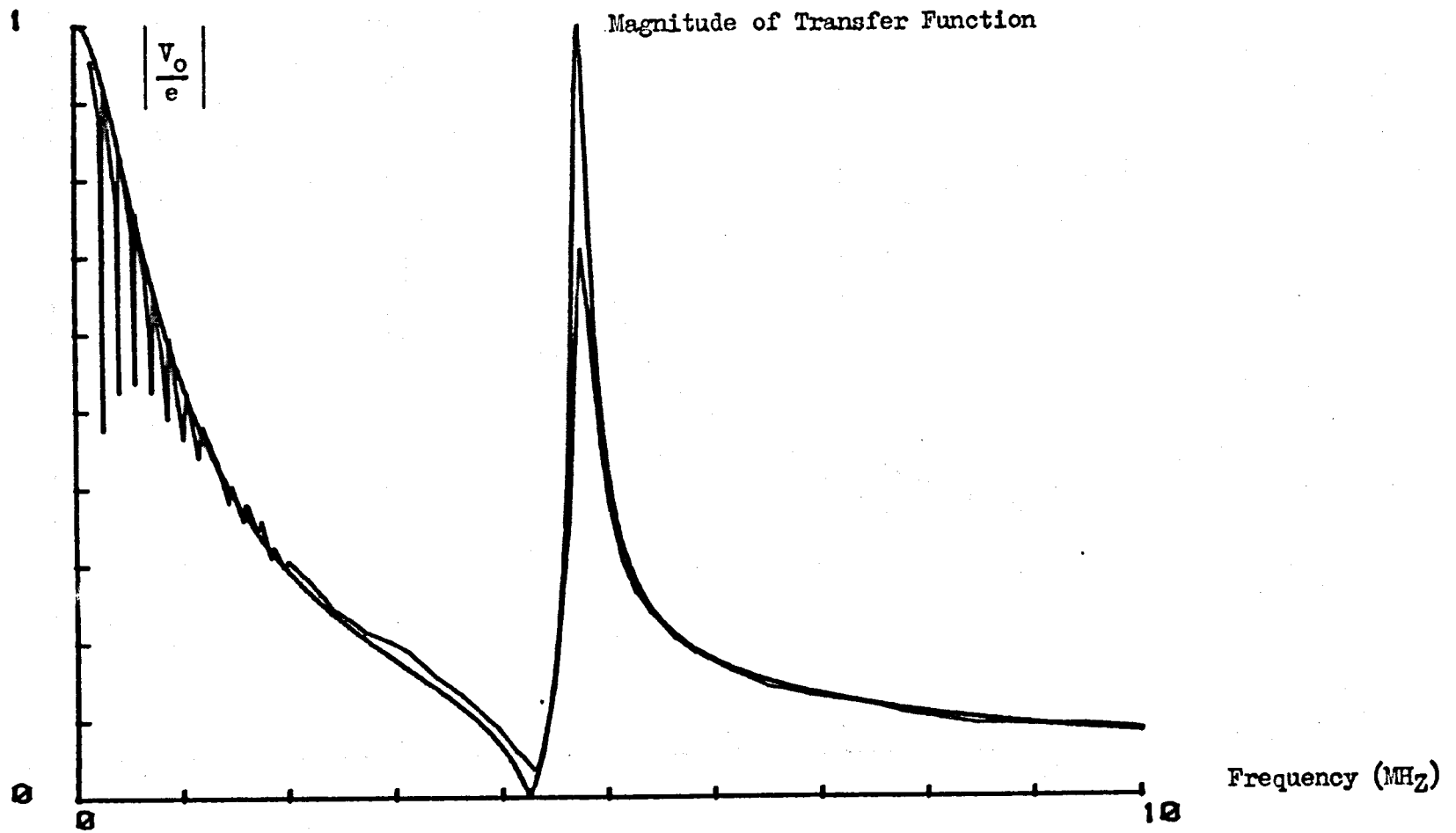

Fig. 6.4c. 4 MHz Transducer Response Characteristic (Mechanically Free Device)

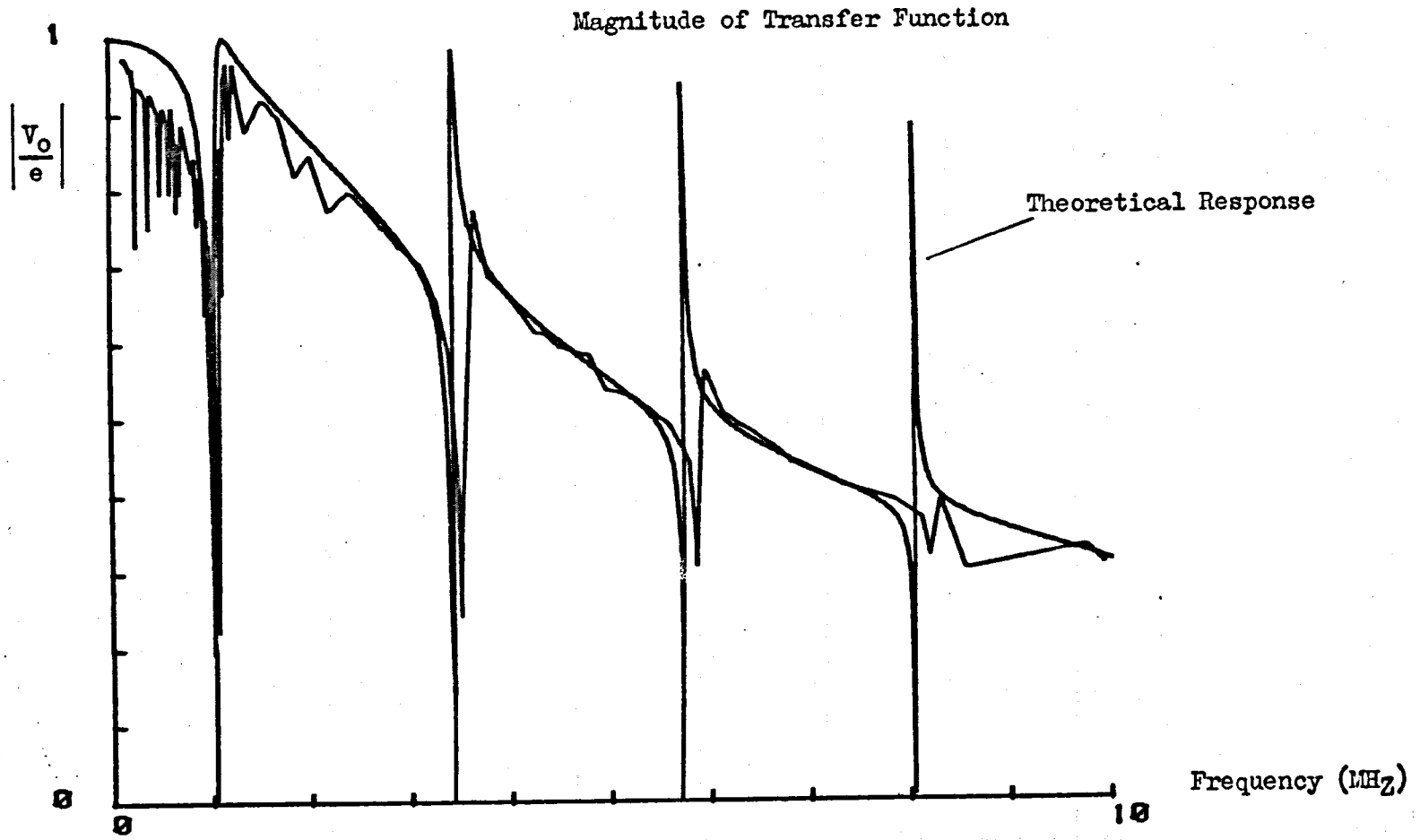

Fig. 6.4d. 1 MHz Transducer Voltage Response Characteristics (Mechanically Free)

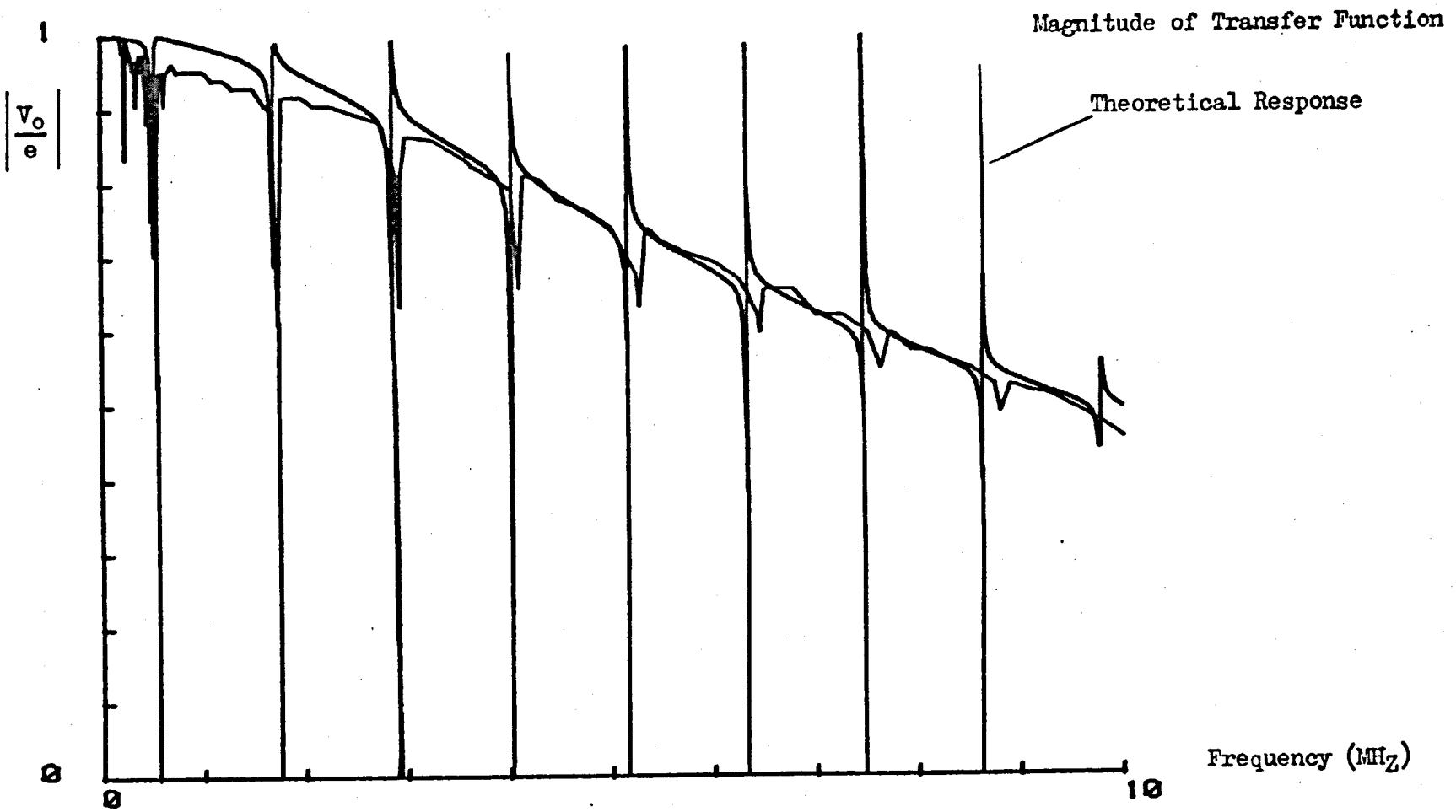

Fig. 6.4e. 0.5 MHz Transducer Voltage Response Characteristics
(Mechanically Free)

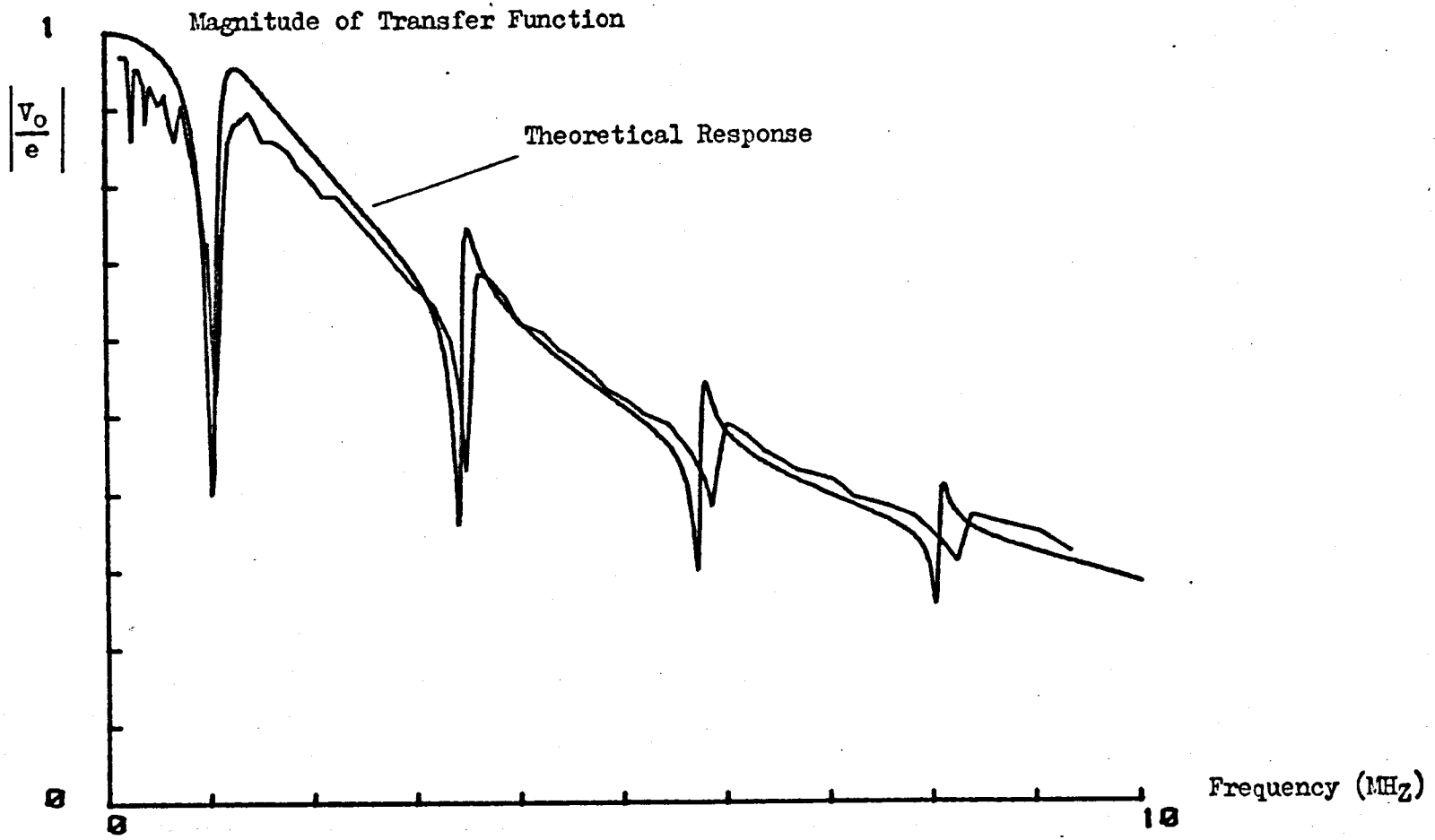

Fig. 6.5a. 1 MHz Transducer Voltage Response Characteristics
(Oil Loading and Oil Backing)

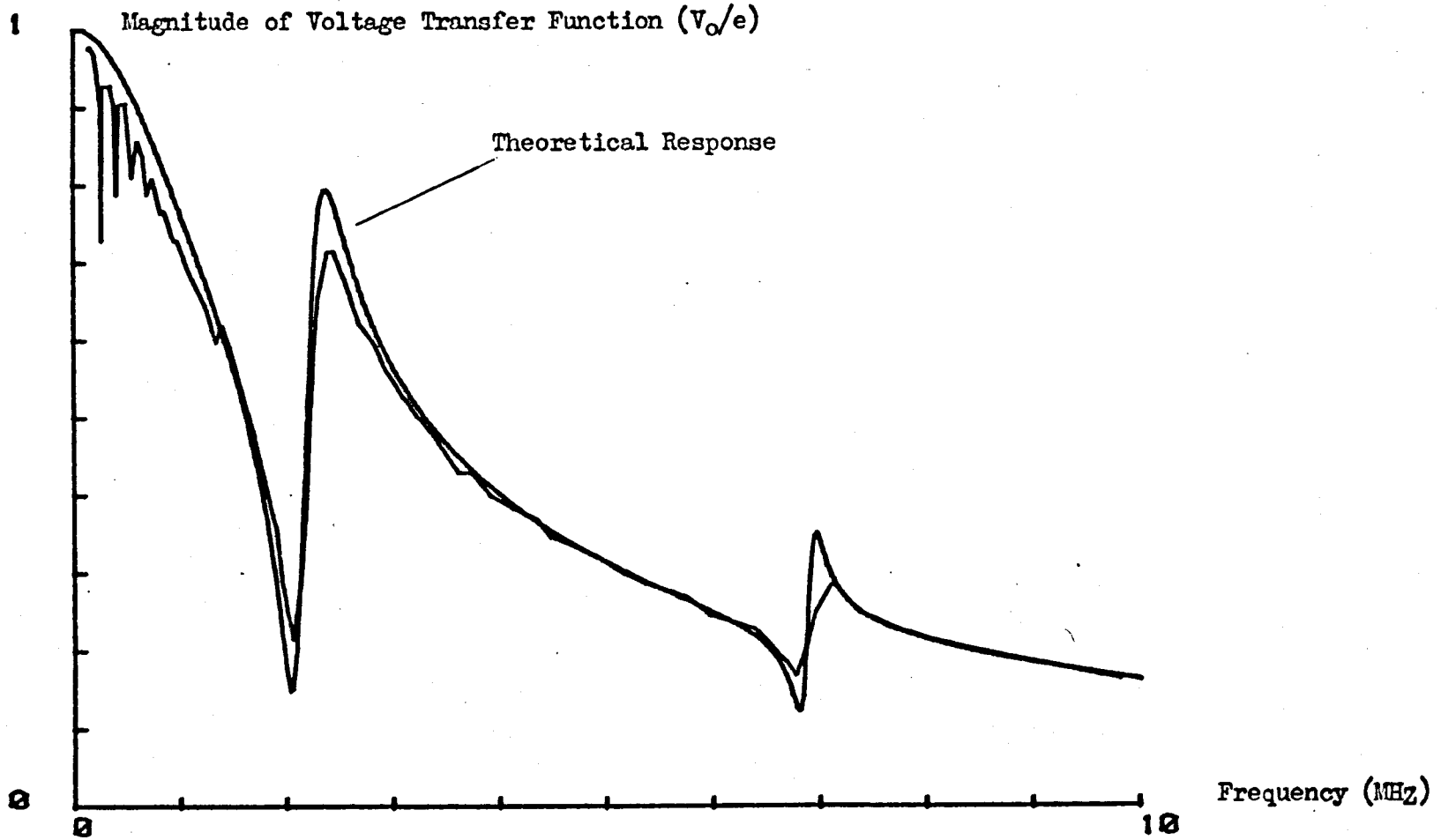

Fig. 6.5b. 2 MHz Transducer Voltage Response Characteristics (Oil Damping)

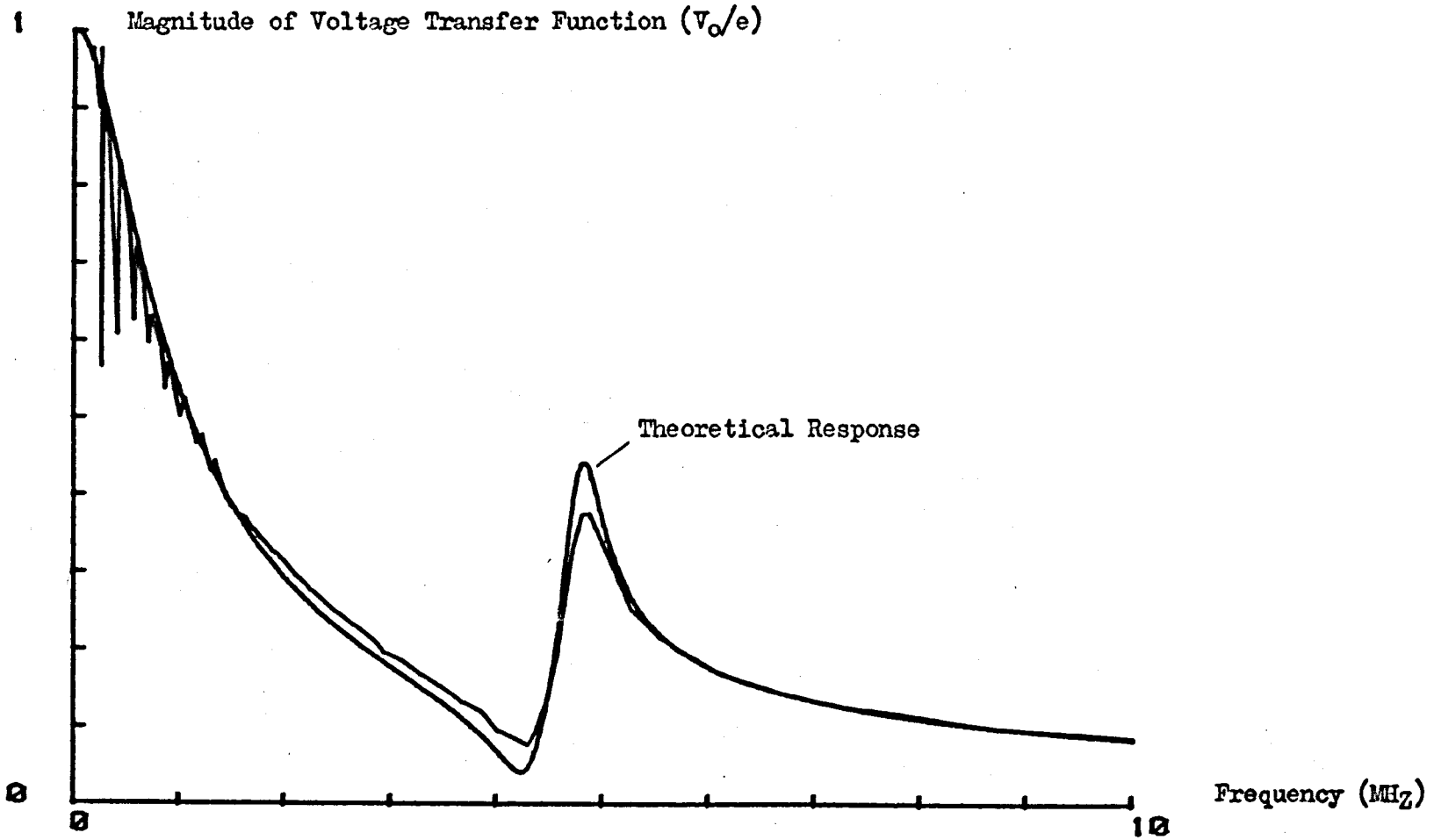

Fig. 6.5c. 4 MH_Z Transducer Response Characteristics (Oil Damping)

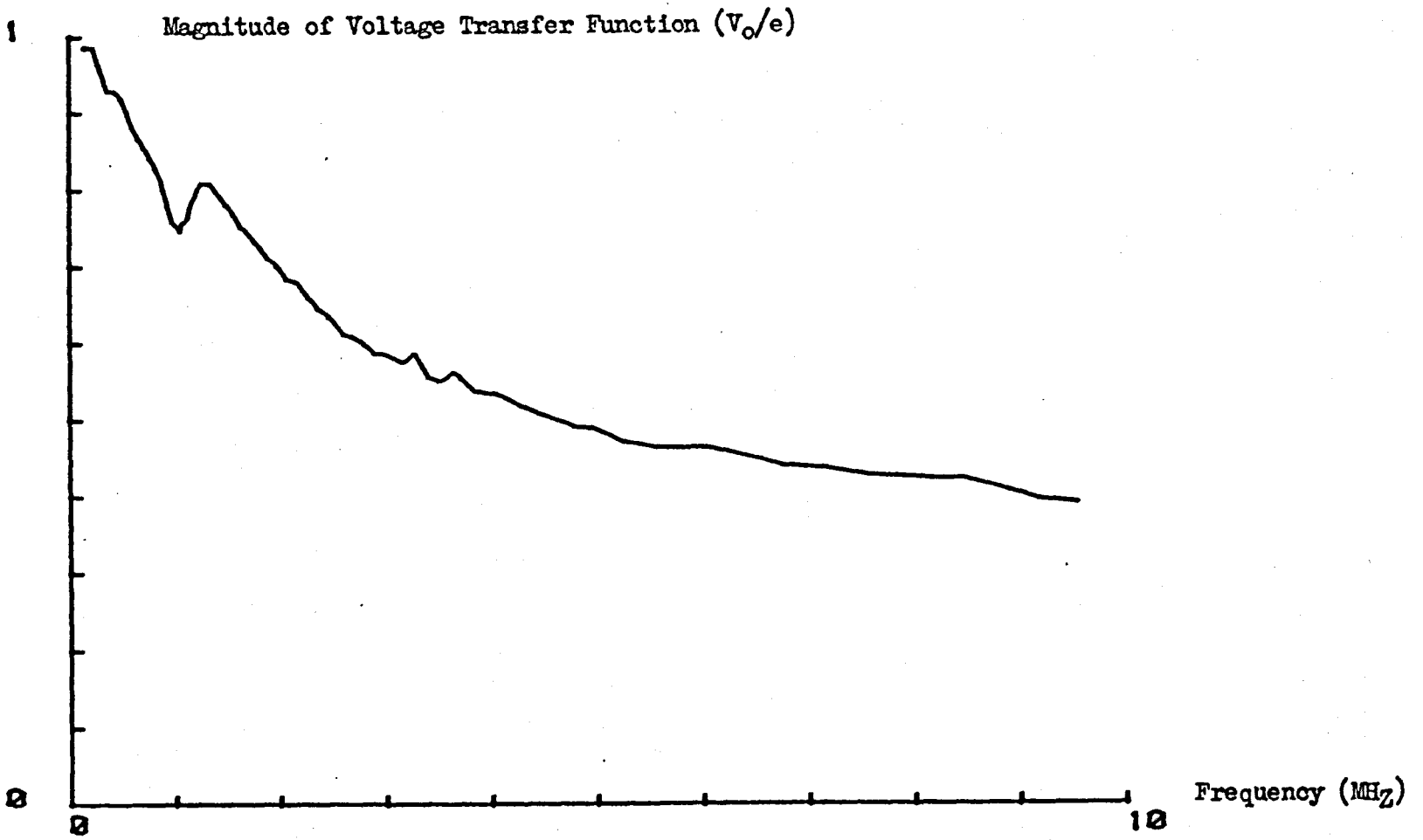

Fig. 6.5d. Response of a Commercially Available 1 MH_Z Probe (Solid Media at Both Faces)

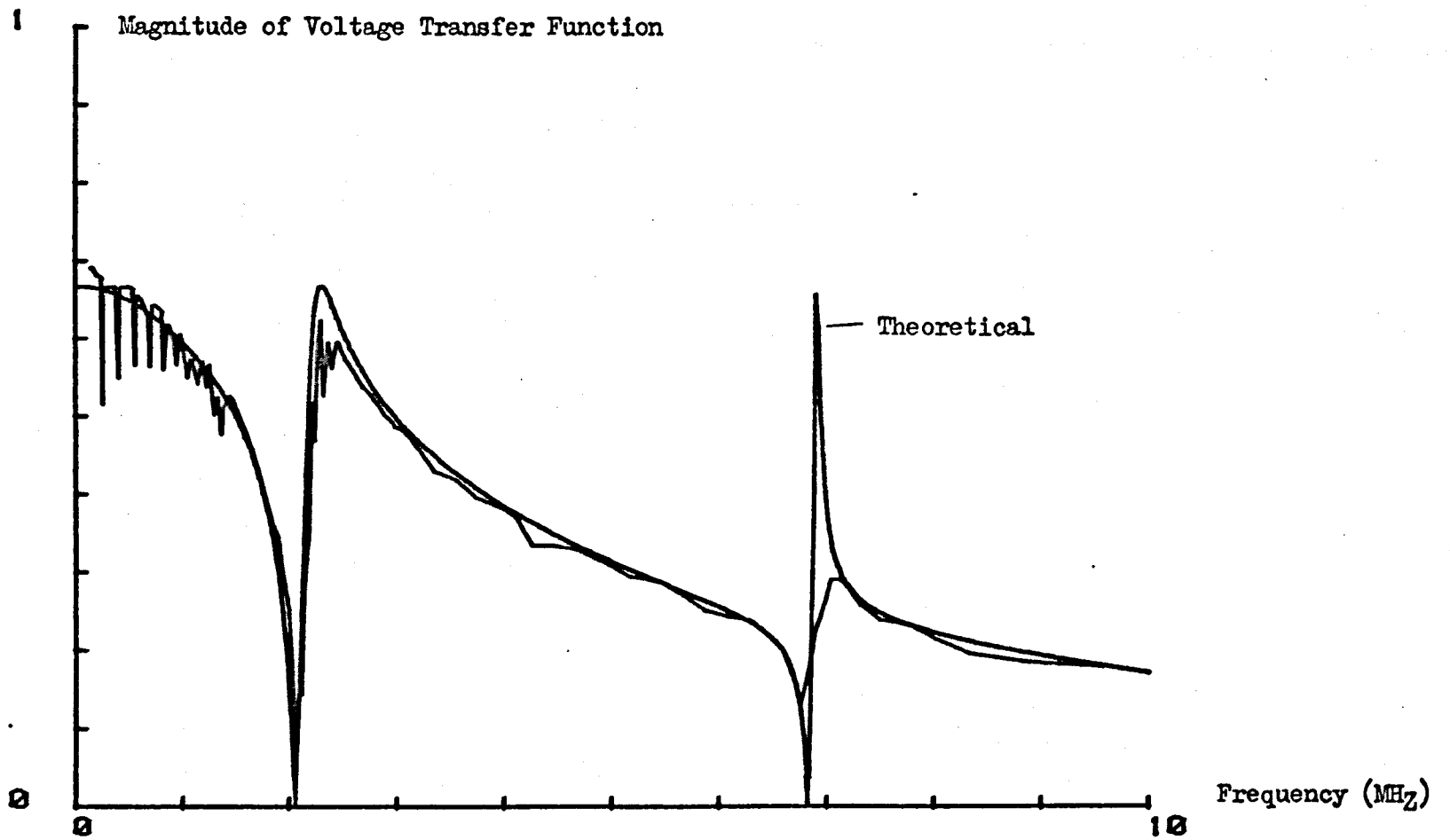

Fig. 6.6a. 2 MH_Z T_{XDCR} Response with 100Ω in Parallel with the Device (Mechanically Free)

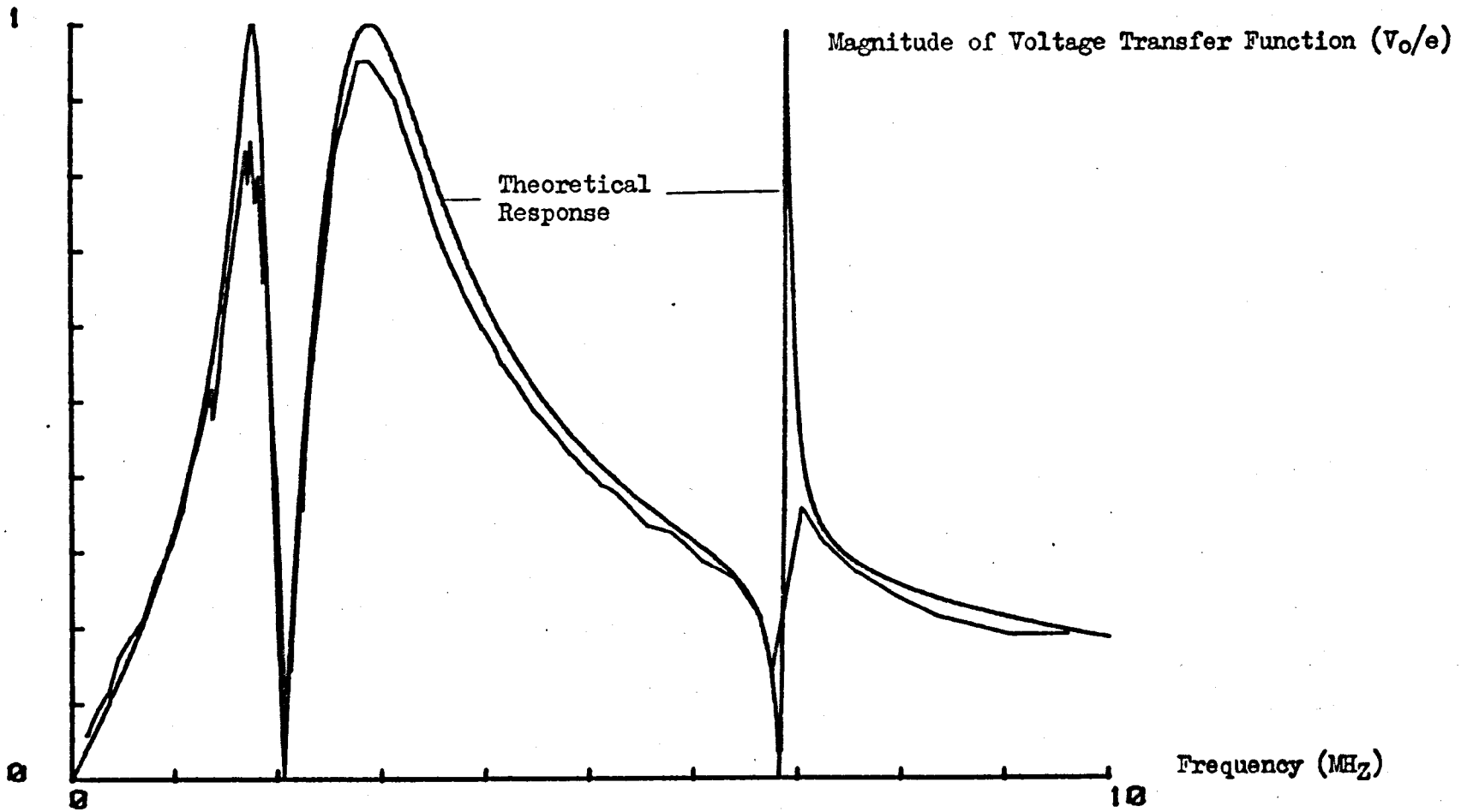

Fig. 6.6b. 2 MHz TXDCR Response with 2.2 μH in Parallel with the Device (Mechanically Free)

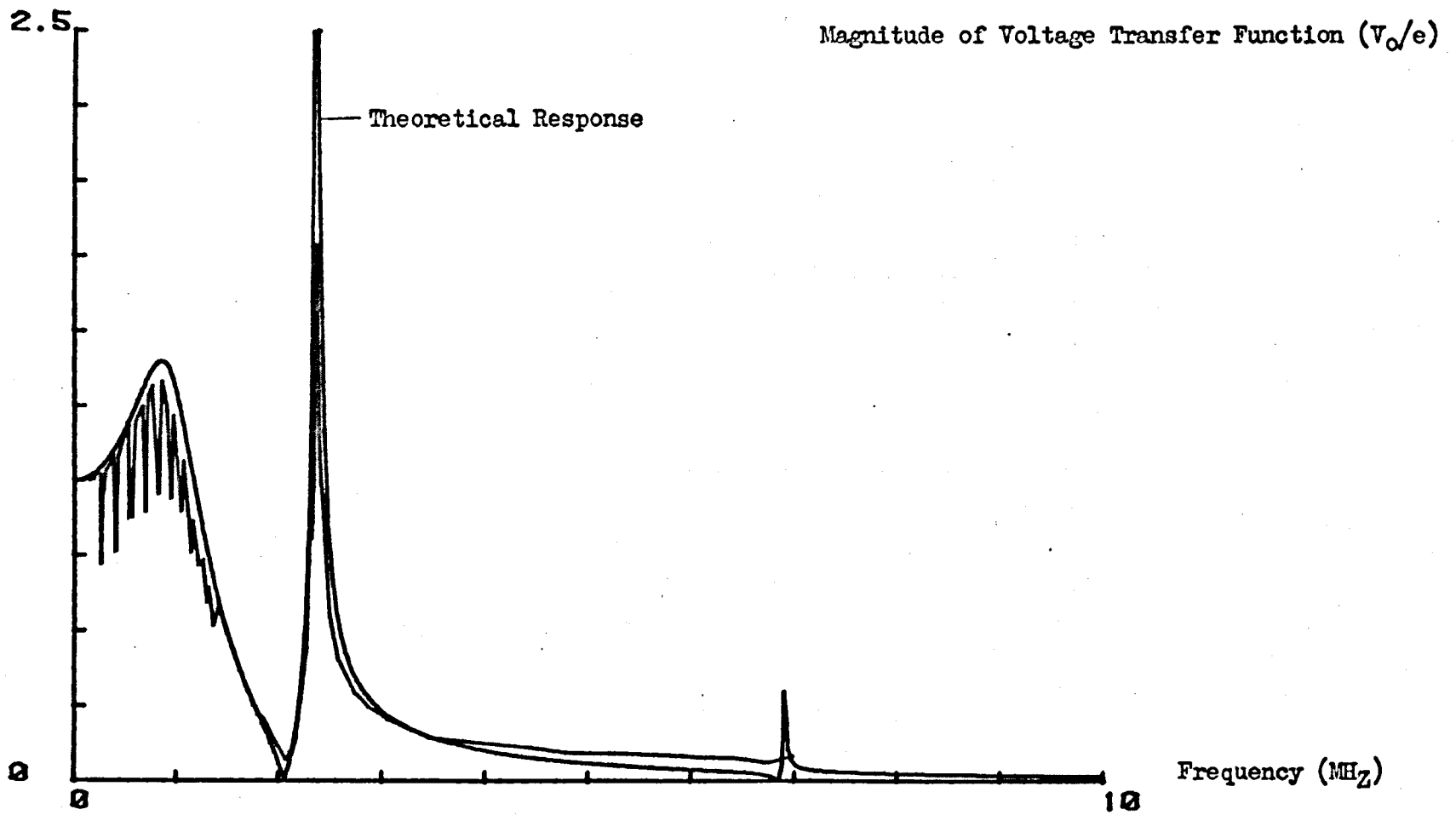

Fig. 6.6c. 2 MH_Z T_{XDCR} Response with 10 μH in Series with the Device (Mechanically Free)

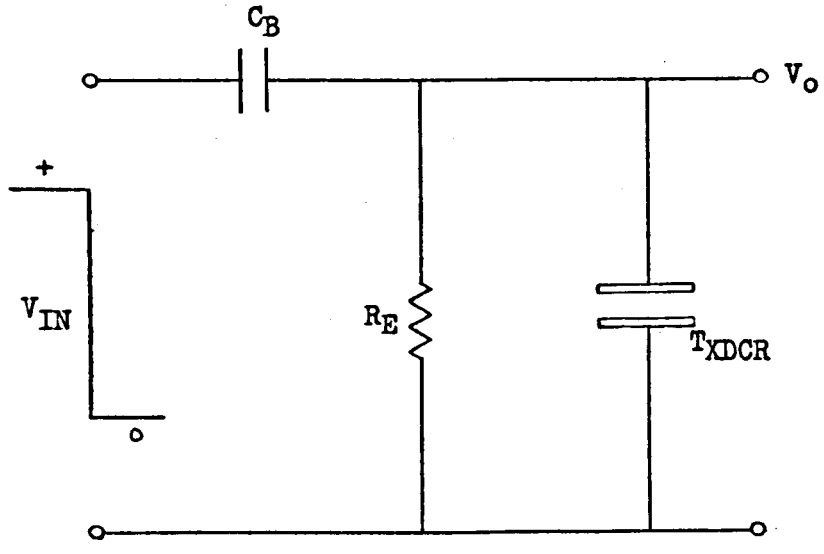

Fig. 6.7. Pulse Shaping Circuit for Voltage Step Excitation

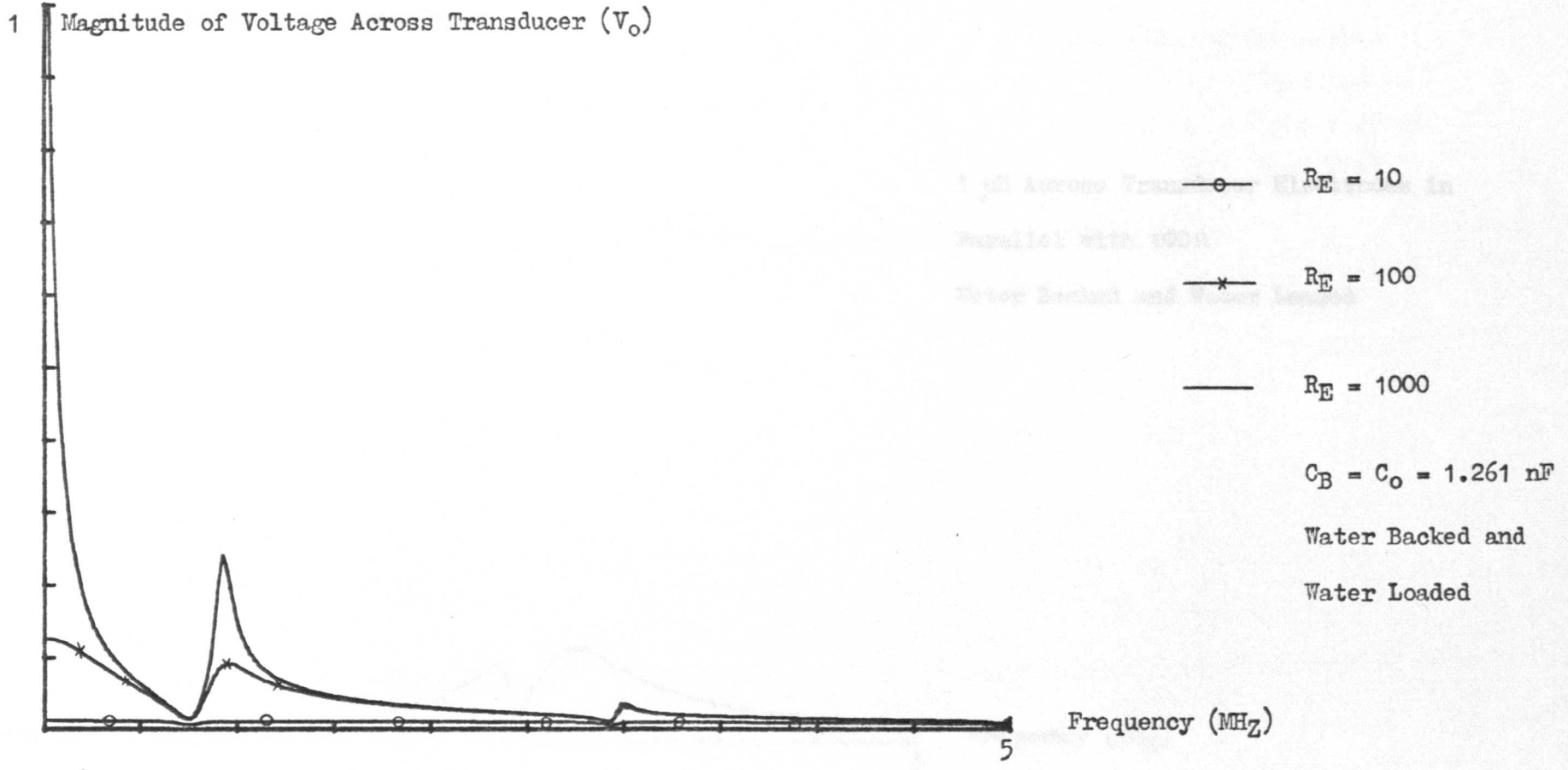

Fig. 6.8a. Frequency Spectrum of Measured Voltage Across Transducer for an Applied Step Input of Voltage

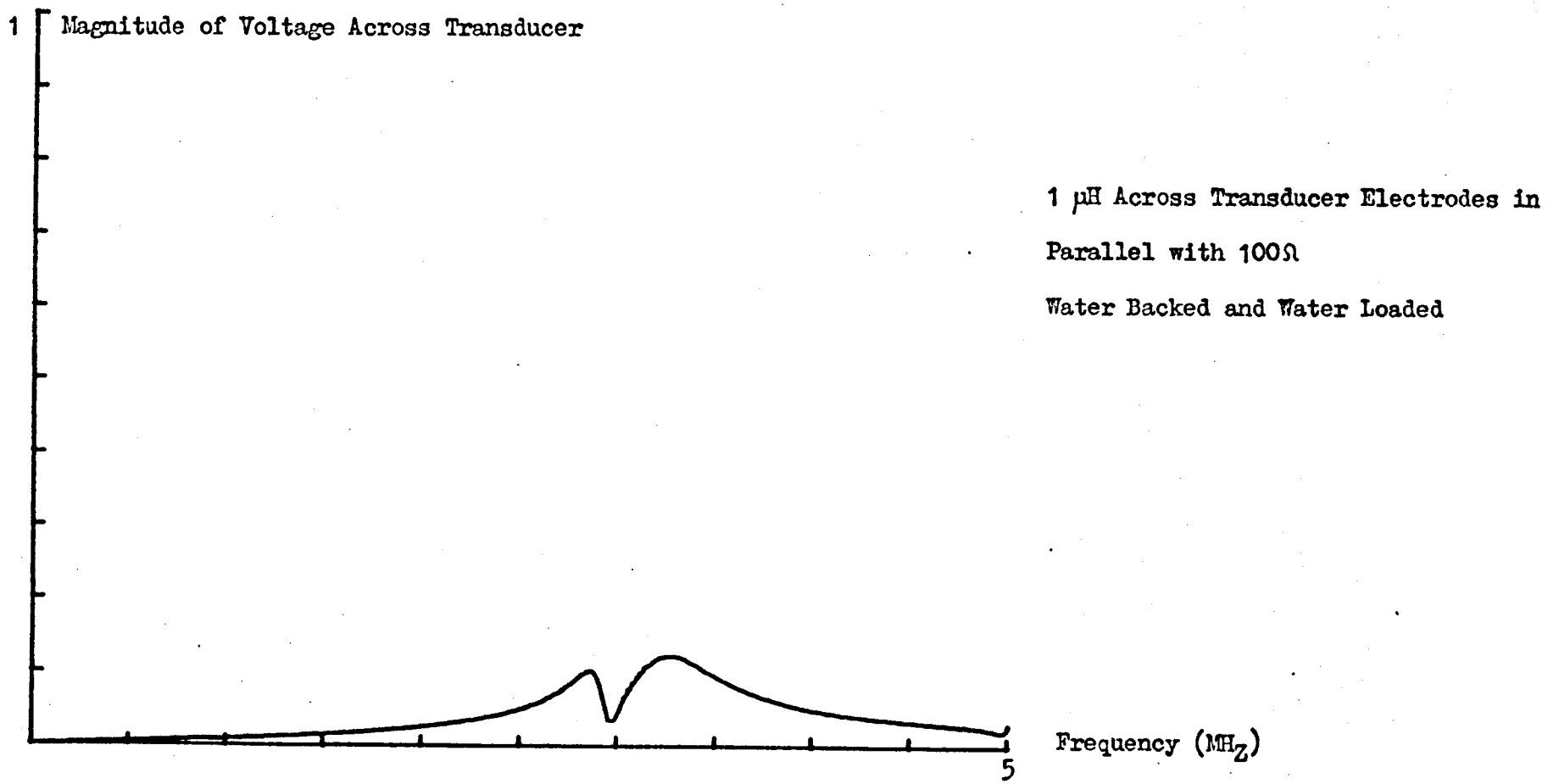

Fig. 6.8b. Spectrum of Measured Voltage Across T_{XDCR} with Inductive Shaping

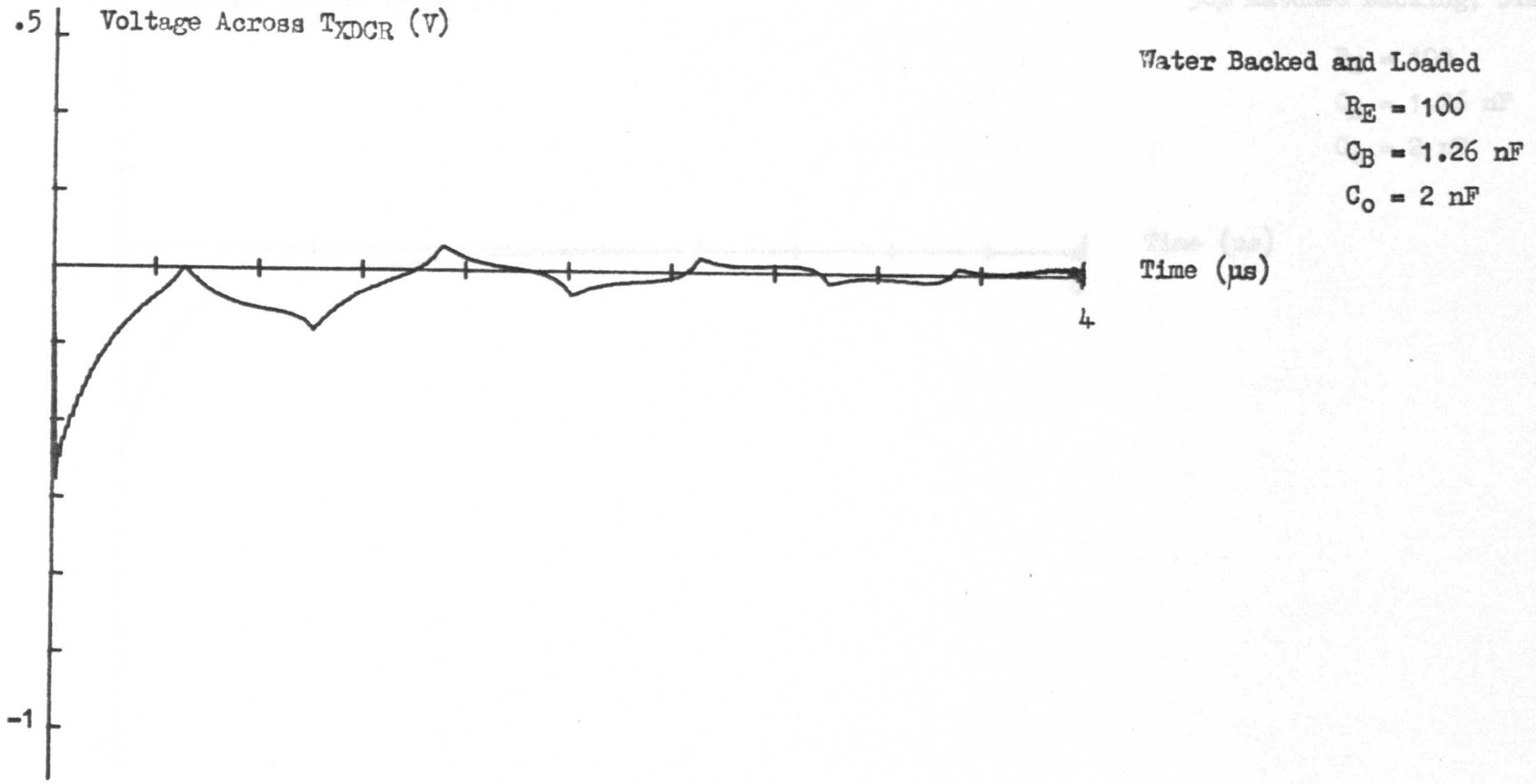

Fig. 6.9a. Time Domain Response for Lightly Backed Transduce
(Step I/P to Network)

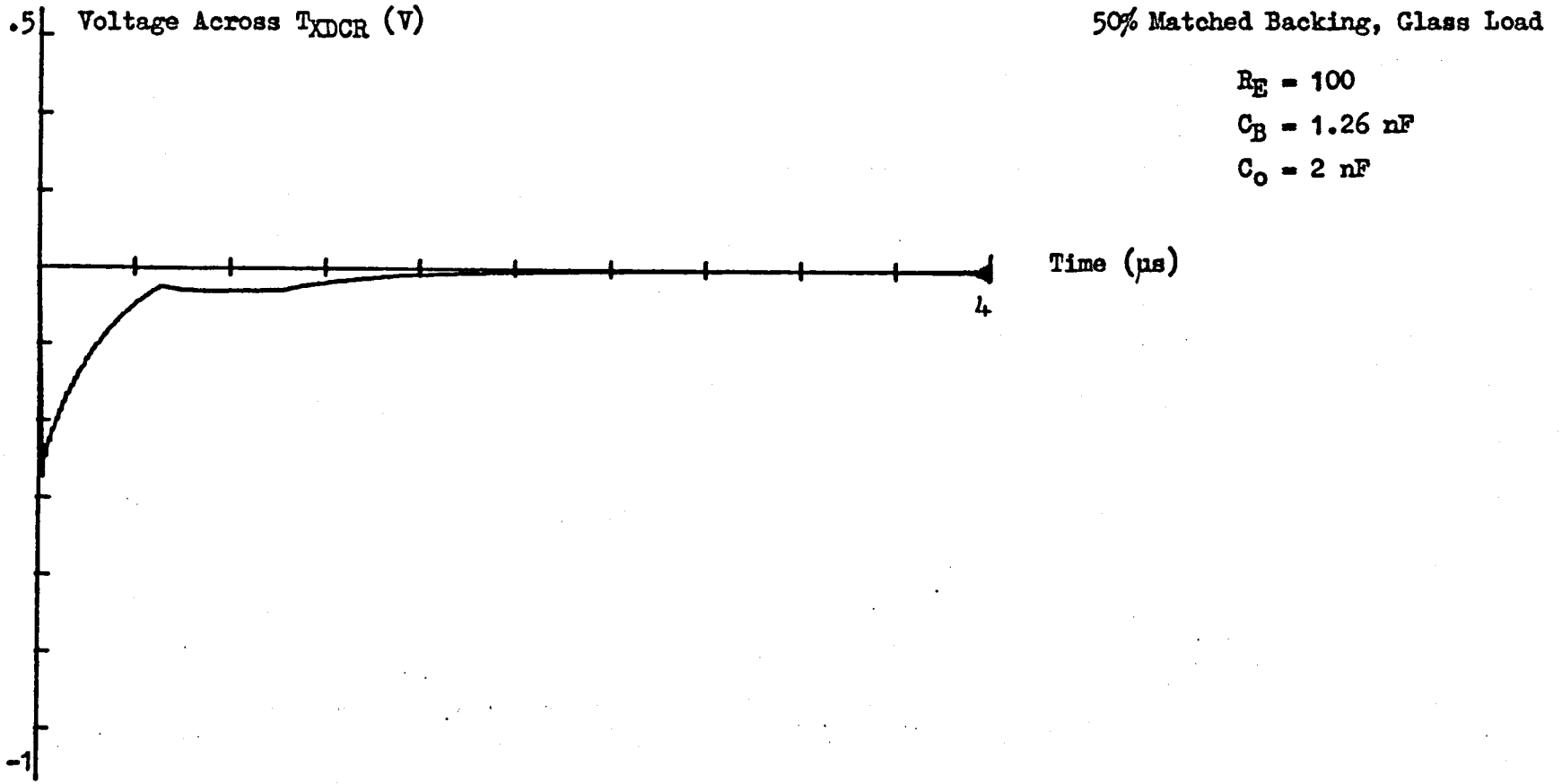

Fig. 6.9b. Time Domain Response for a Transducer Subject to Medium Loading (Step I/P to Network)

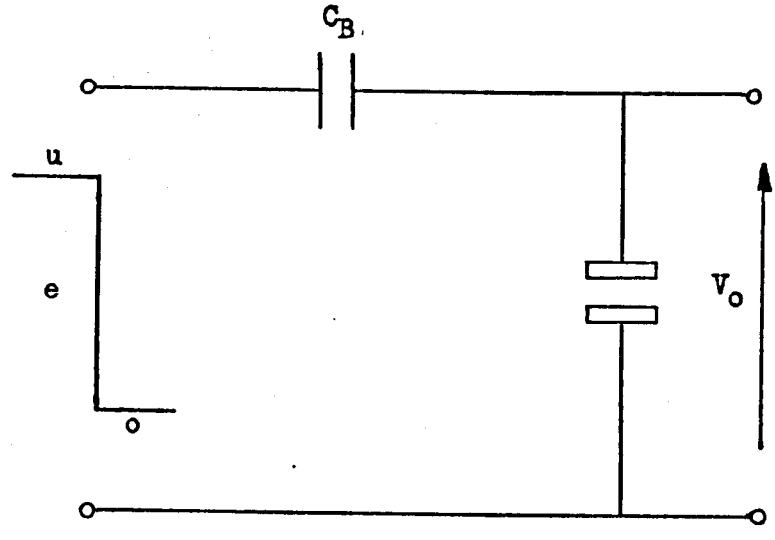

Fig. 6.10. Configuration for Constrained Time Domain Analysis

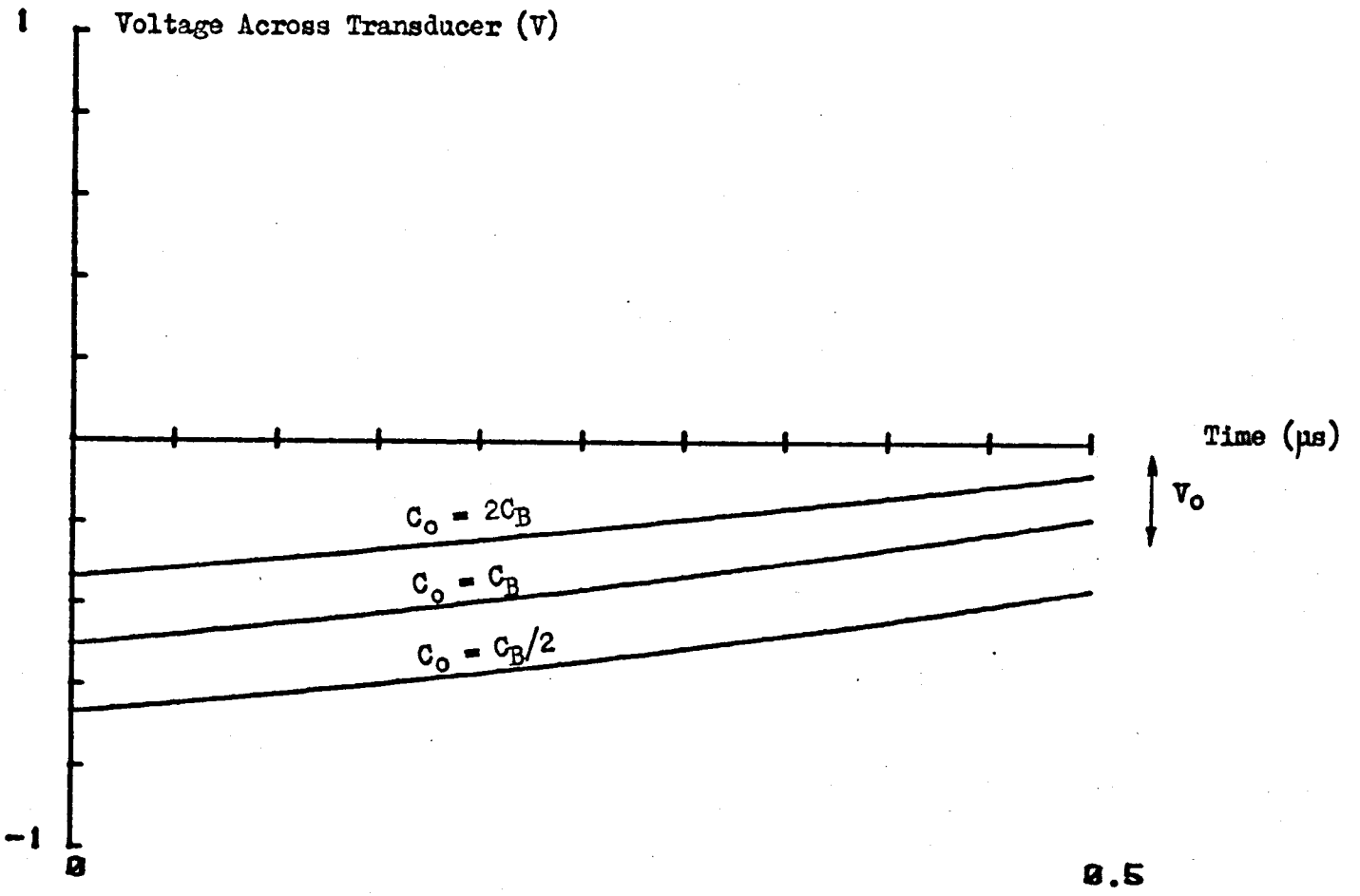

Fig. 6.11. Voltage Across T_{XDCR} for 1 Transit Interval (Mechanically Free)

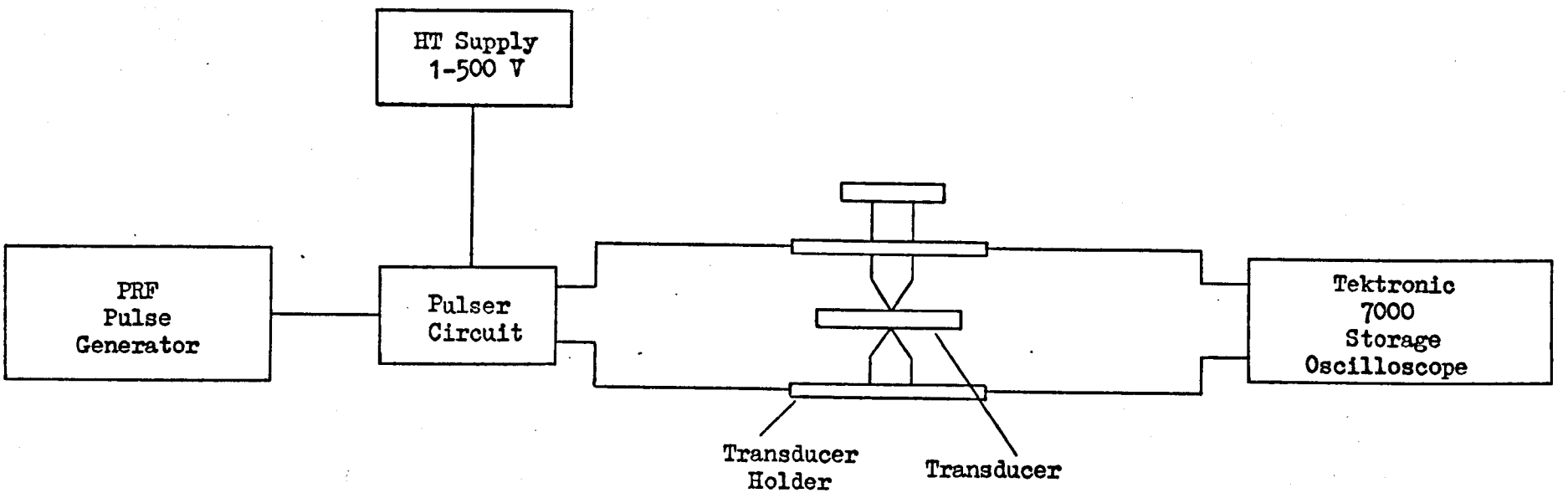

Fig. 6.12. Apparatus for Determination of Transient Response

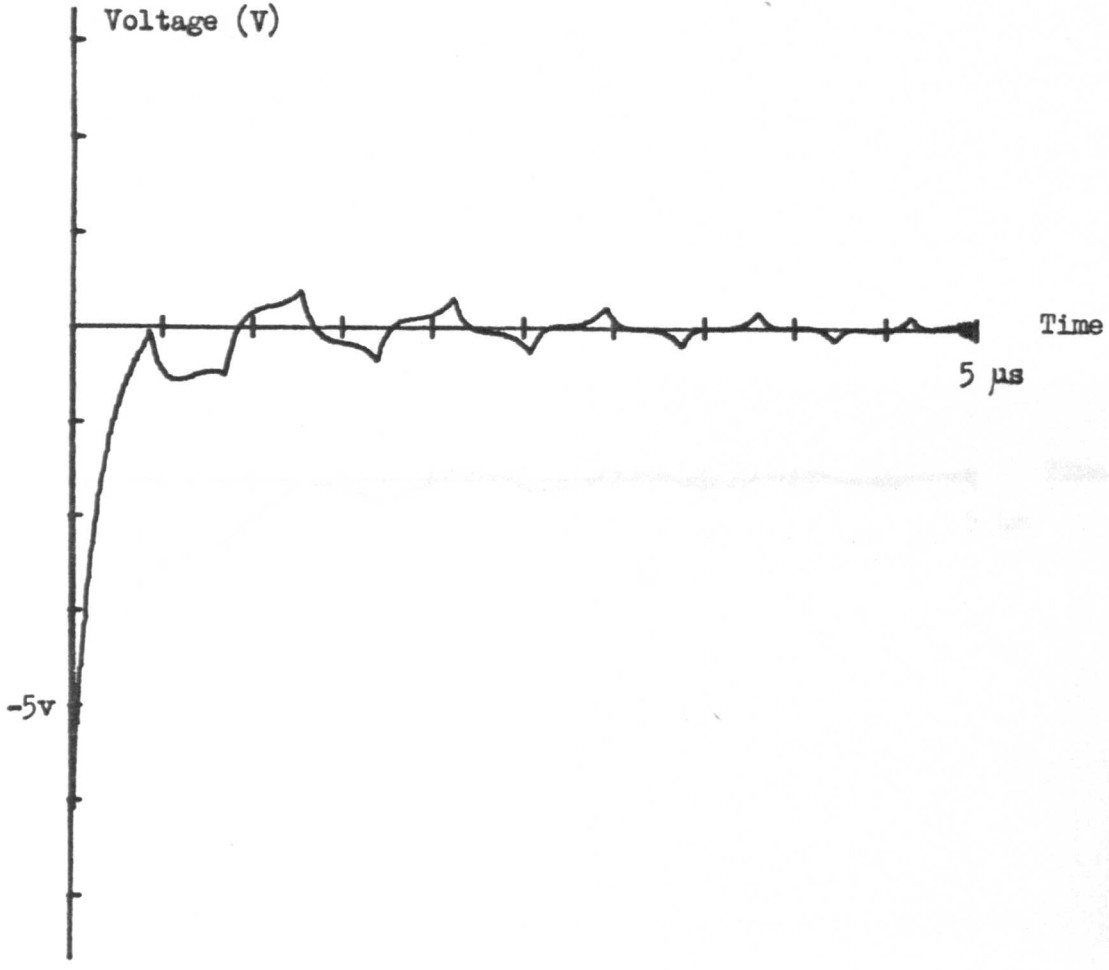

Fig. 6.13a. Theoretical and Simulated Transient Voltage Response Characteristics

C_B = 100 pF

C_o = 0.95 nF

R_{ON} = 1.3

V_{supply} = 50 V

R_E = 120

Transducer Electrical Resonance = 1 MH_Z

Light Damping (Oil Backed, Oil Loaded)

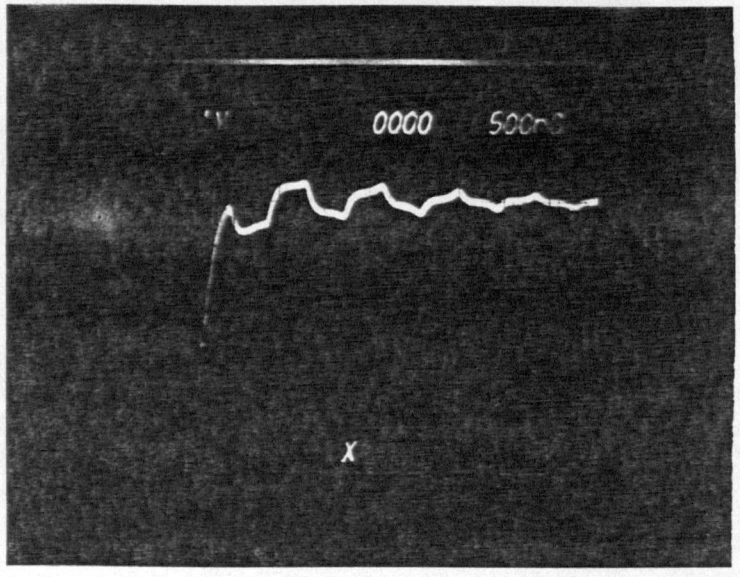

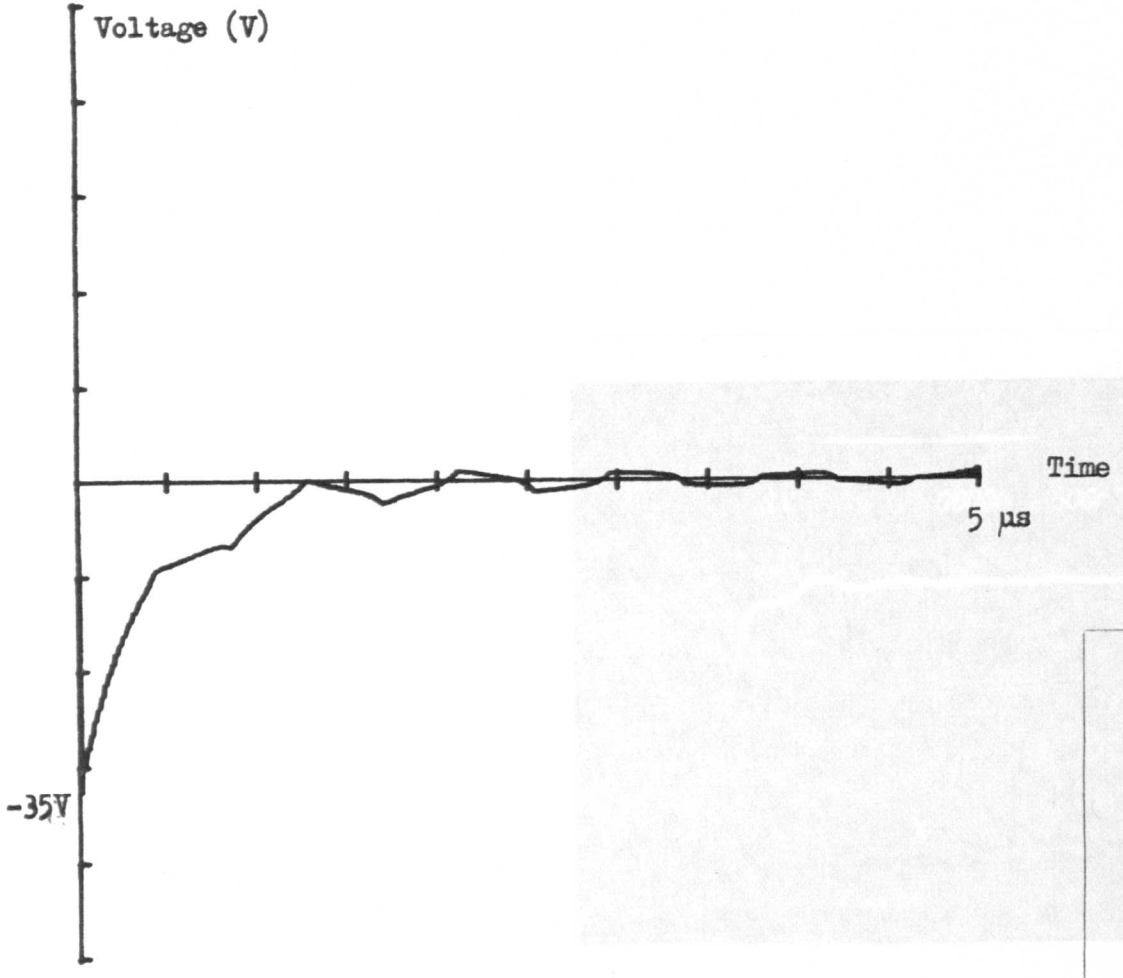

C_B = 2.2 nF

C_o = 0.95 nF

R_{ON} = 1.3

V_{supply} = 50 V

R_E = 120

Transducer Electrical Resonance = 1 MHz

Light Damping (Oil Backed, Oil Loaded)

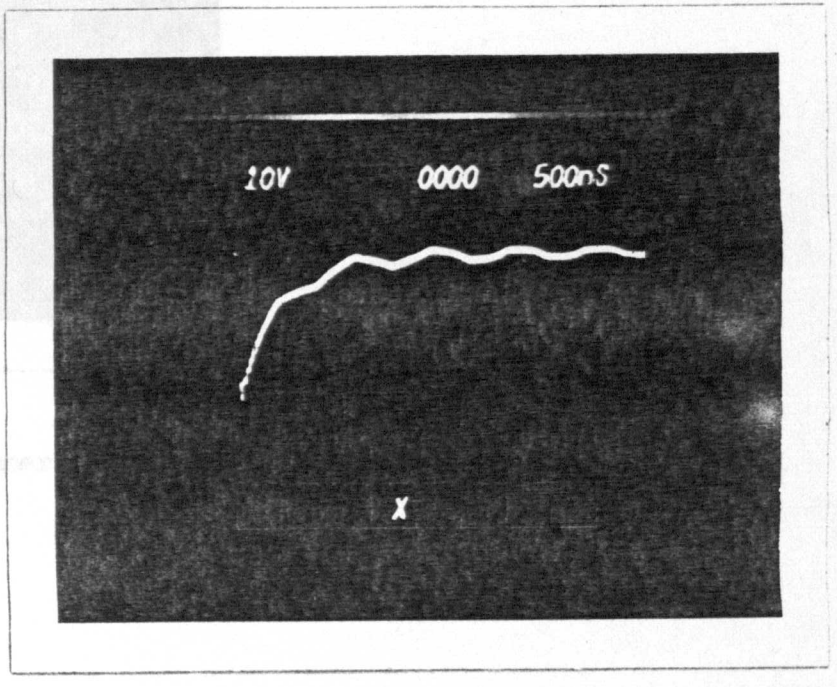

Fig. 6.13b. Theoretical and Simulated Transient Voltage Response Characteristics

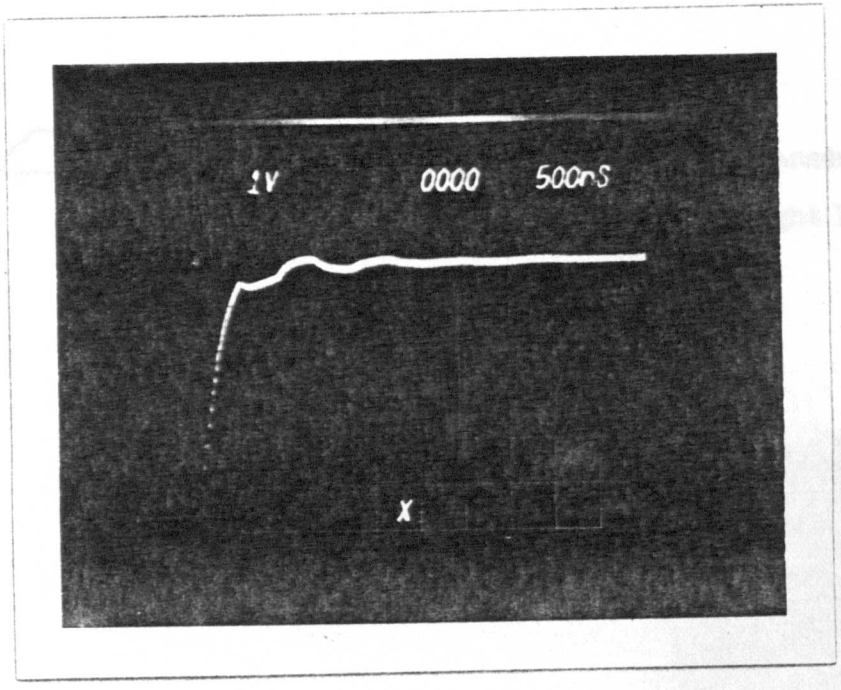

C_B = 100 pf

R_E = 120

Fig. 6.13c. Transient Voltage Response of a Commercially Available, 1 MH_Z Probe

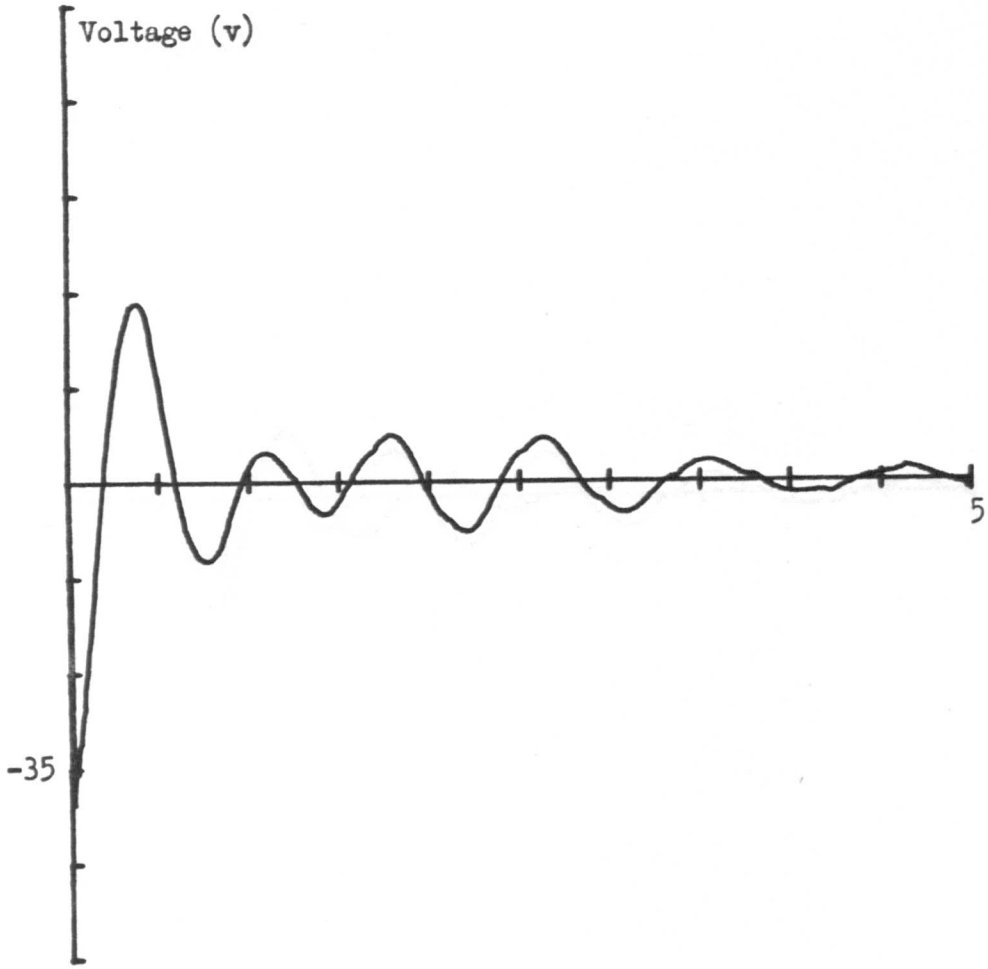

C_B = 2.2 nF
C_o = .95 nF
L_E = 4.7 μH
R_E = 120
R_o = 2
V_{supply} = 50V

Transducer Electrical Resonance = 1 MHz
Light Damping (Oil Backed, Oil Loaded)

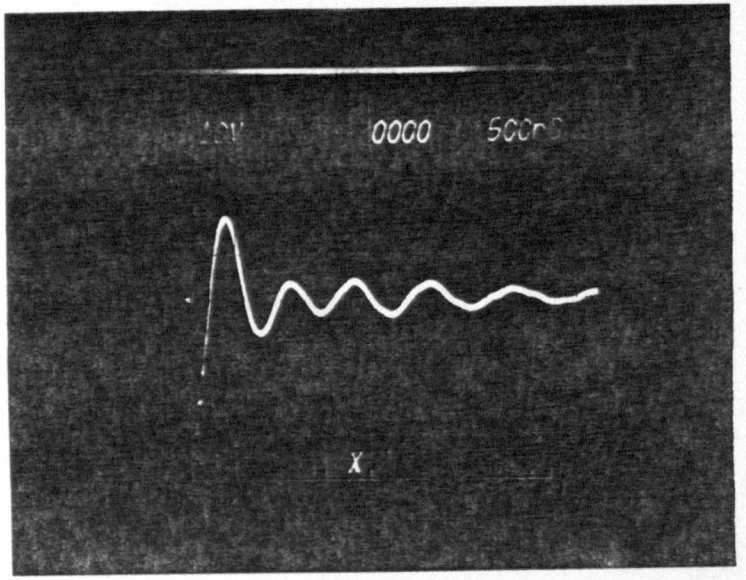

Fig. 6.14a. Theoretical and Simulated Transient Voltage Response Characteristics (Inductively Loaded Device)

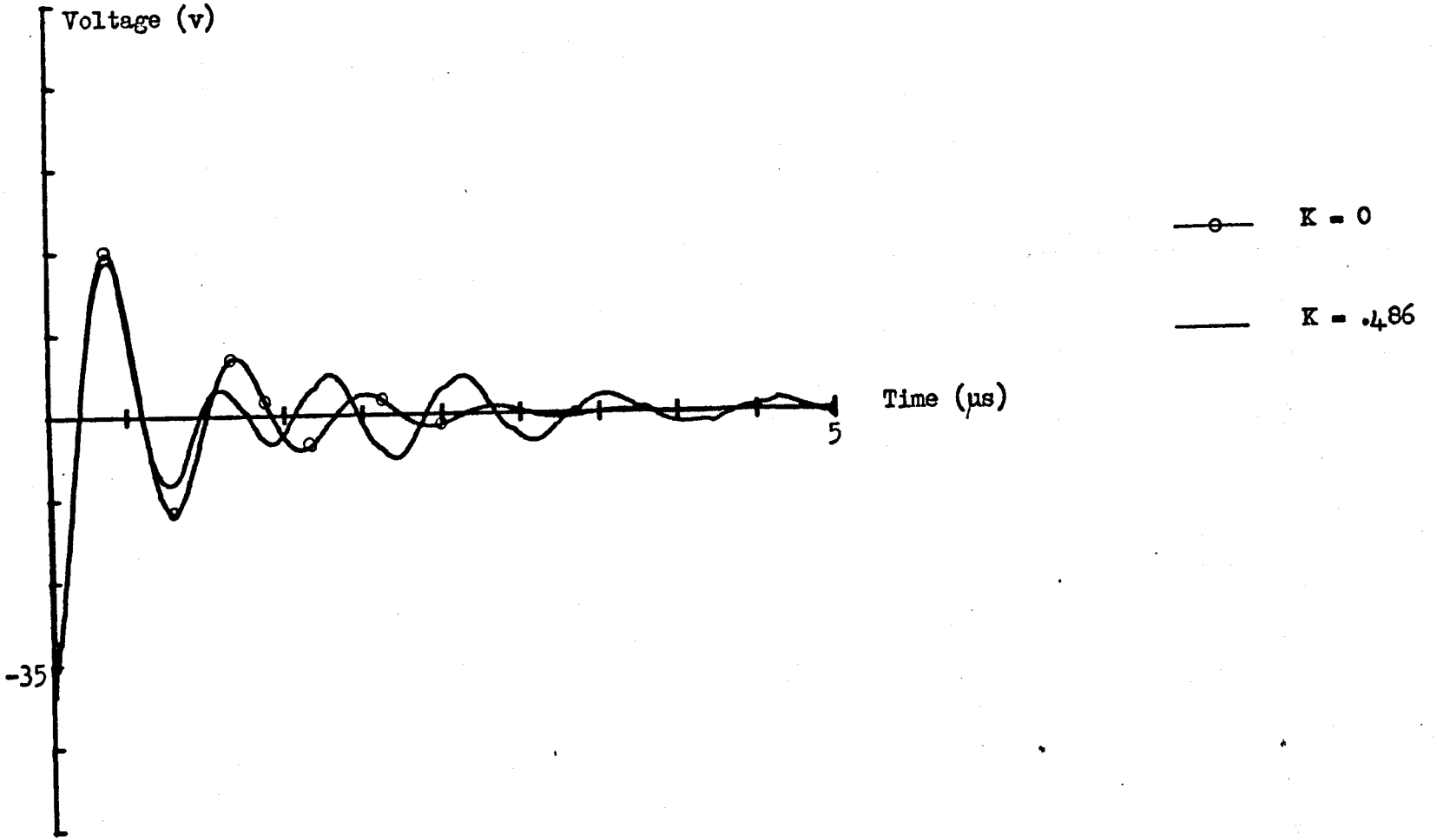

Fig. 6.14b. Comparison of Transient Response With and Without Feedback

4 MH_Z Transducer

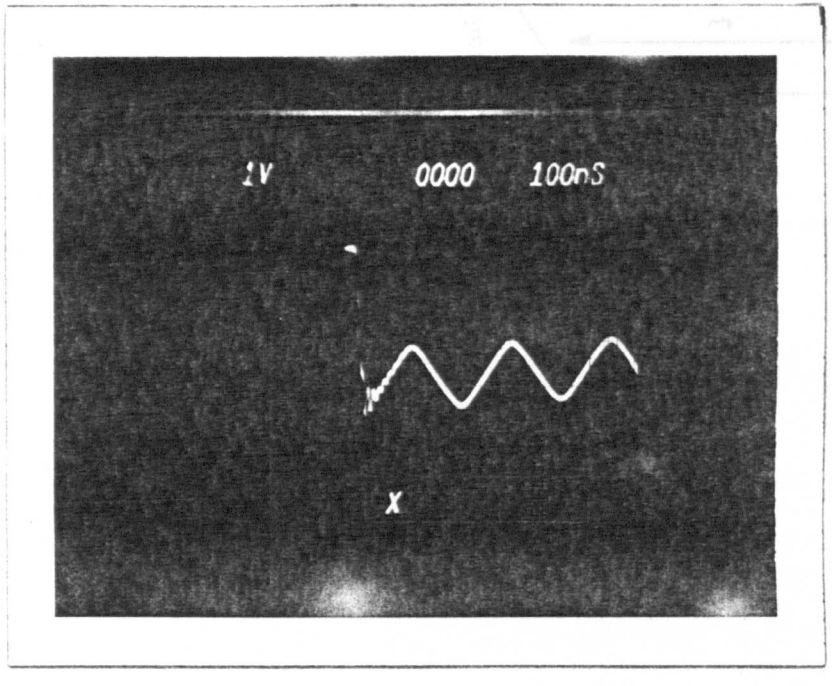

1 MH_Z Transducer

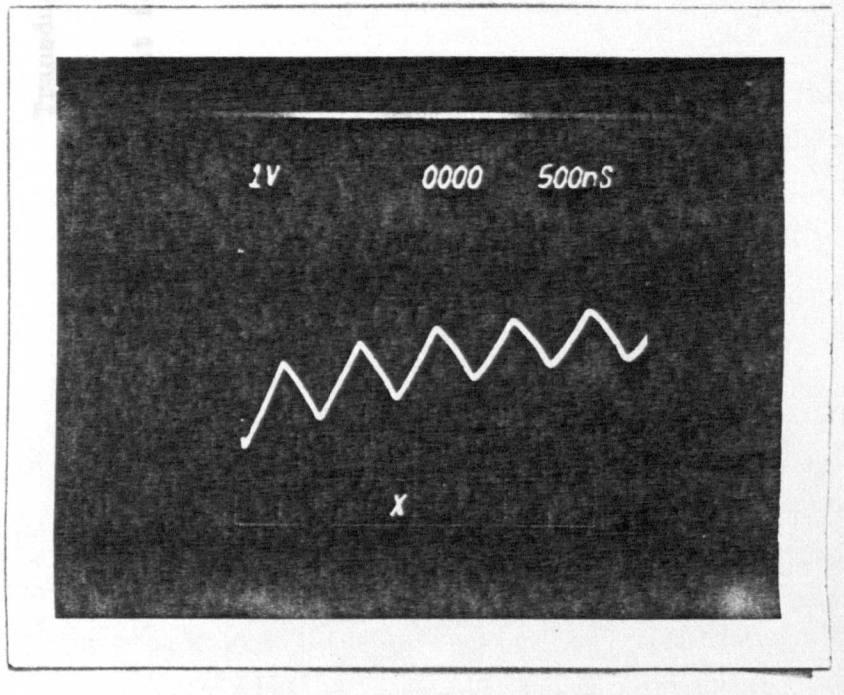

Fig. 6.15. Transient Response Characteristics of the 1 MH_Z and 4 MH_Z Transducers

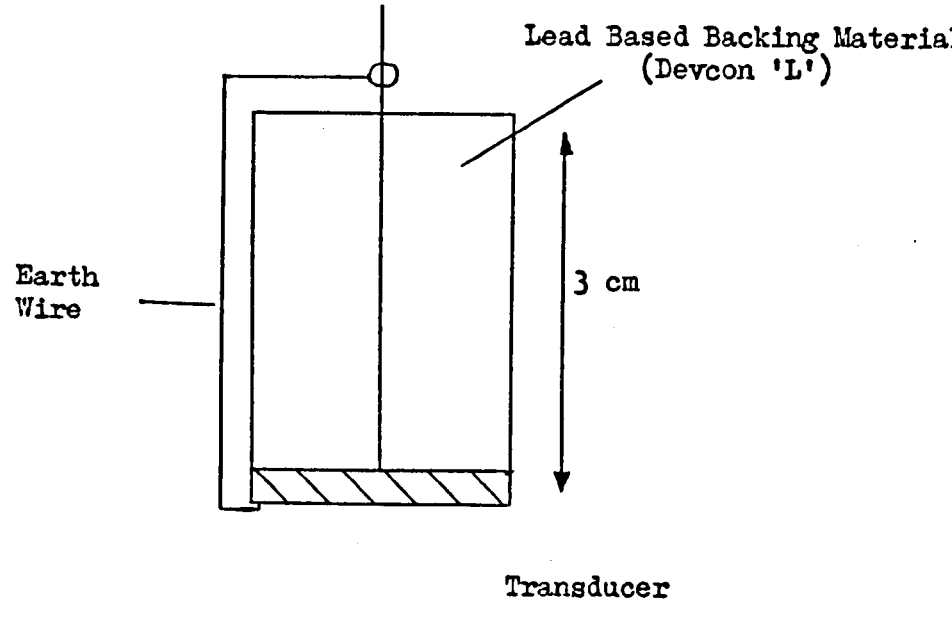

Fig. 6.16. Transducer Arrangement for Lead Based Backing Medium

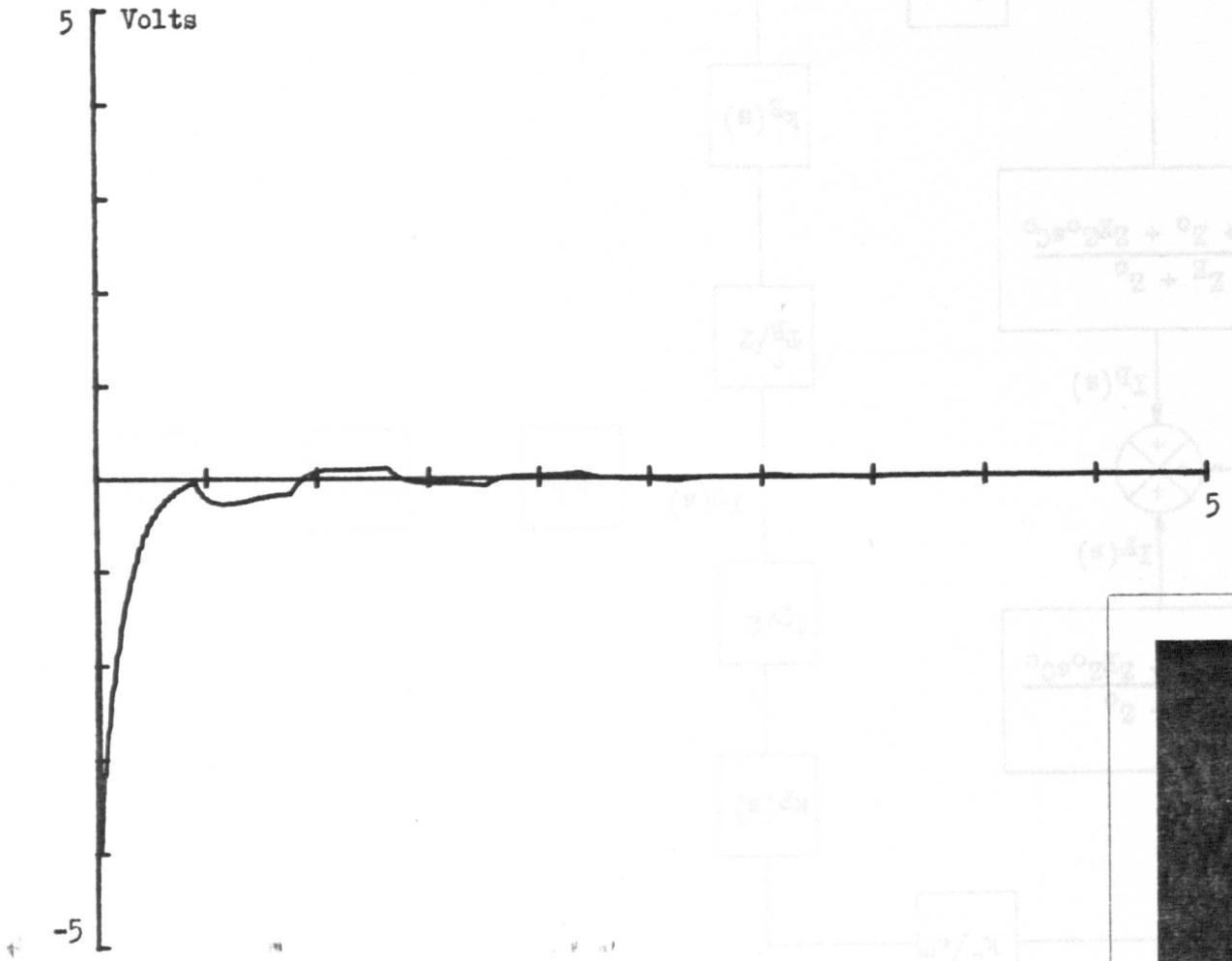

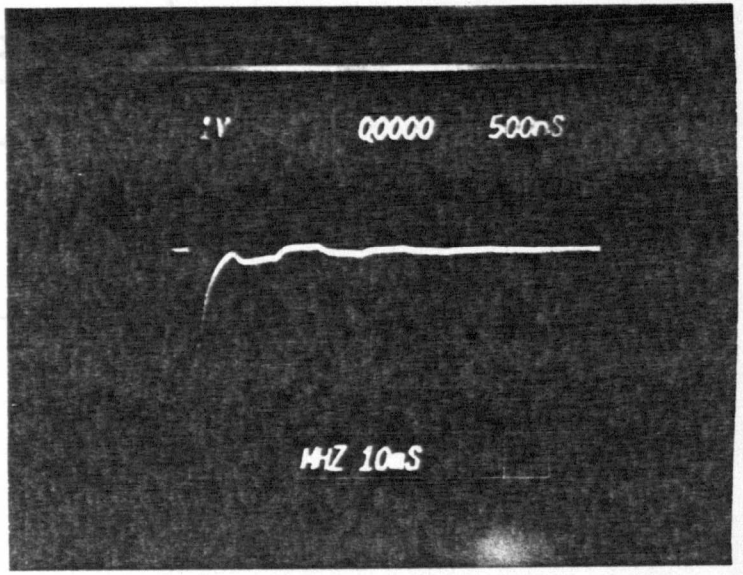

Fig. 6.17. Transient Voltage Response of a 1 MHz TXDCR Backed with 'Devcon L'

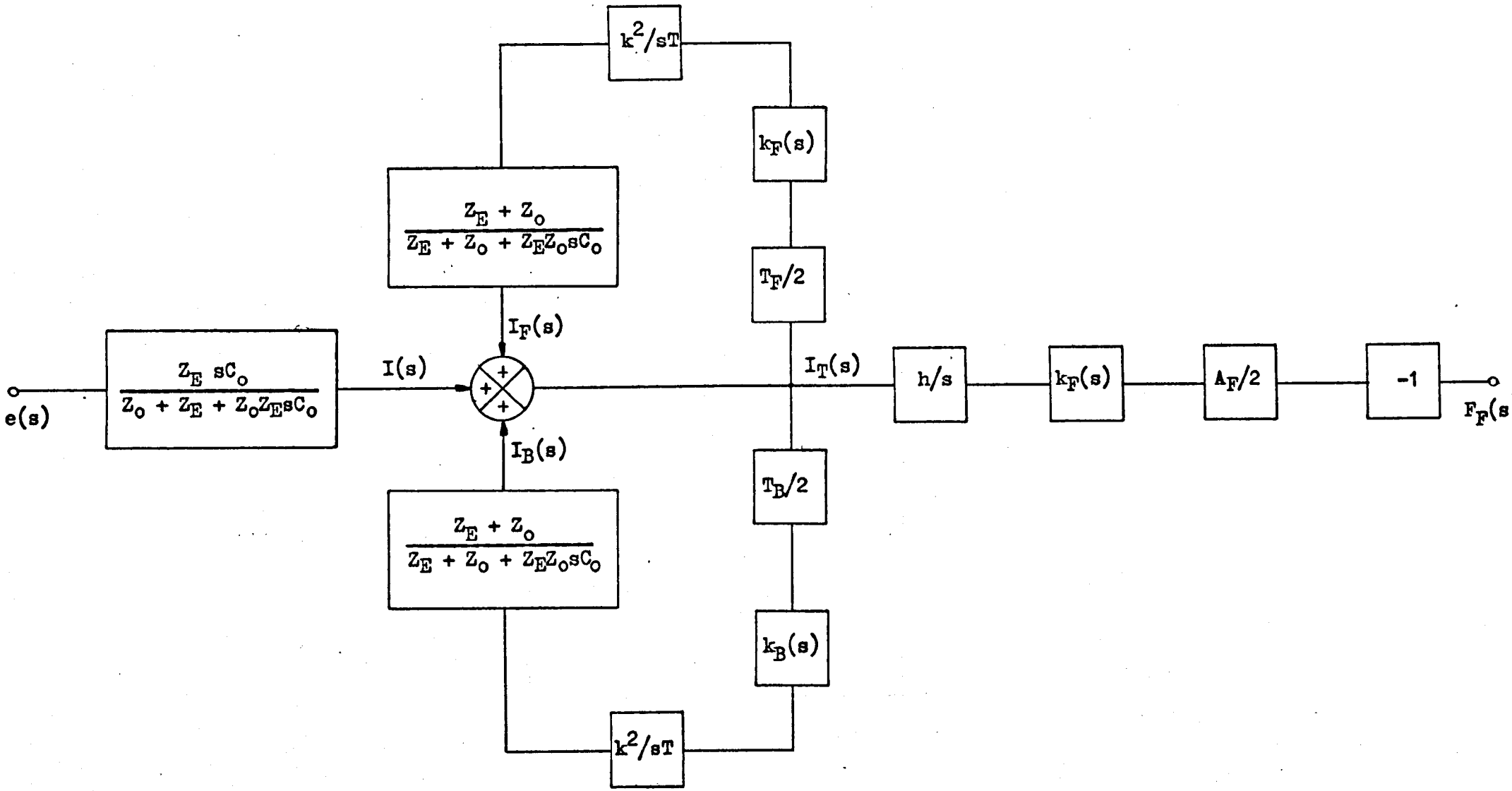

Fig. 7.1. Transmitter Block Diagram Showing Current as the Feedback Quantity

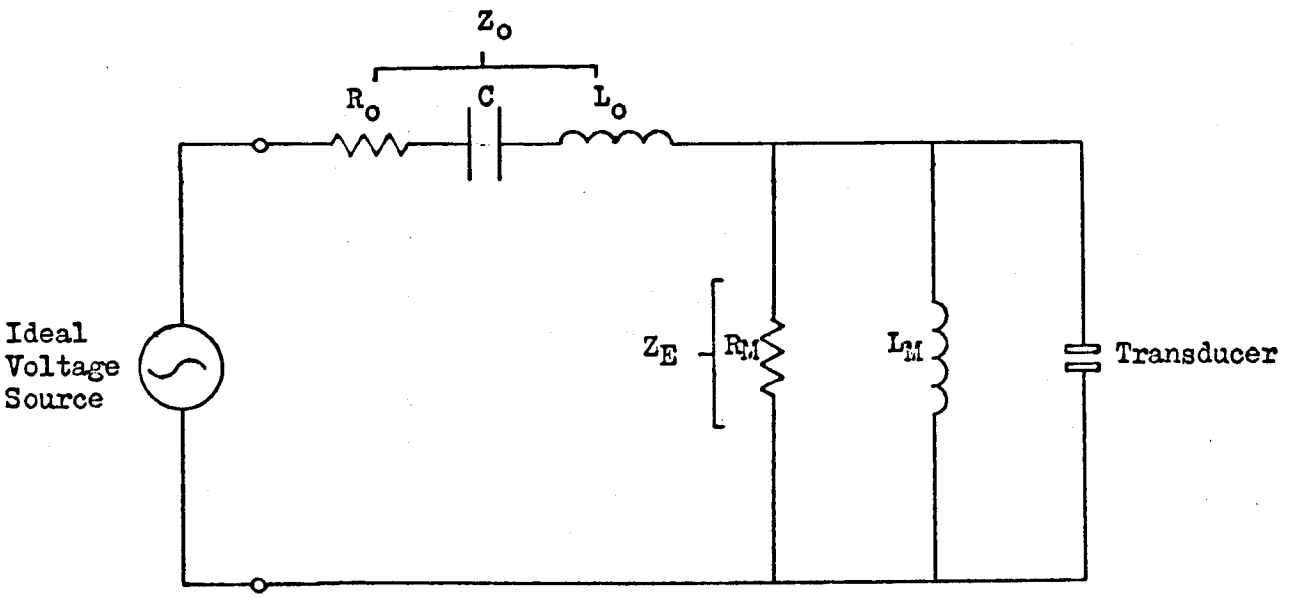

Fig. 7.2. General Circuit Load Configuration for the Transmitting Mode

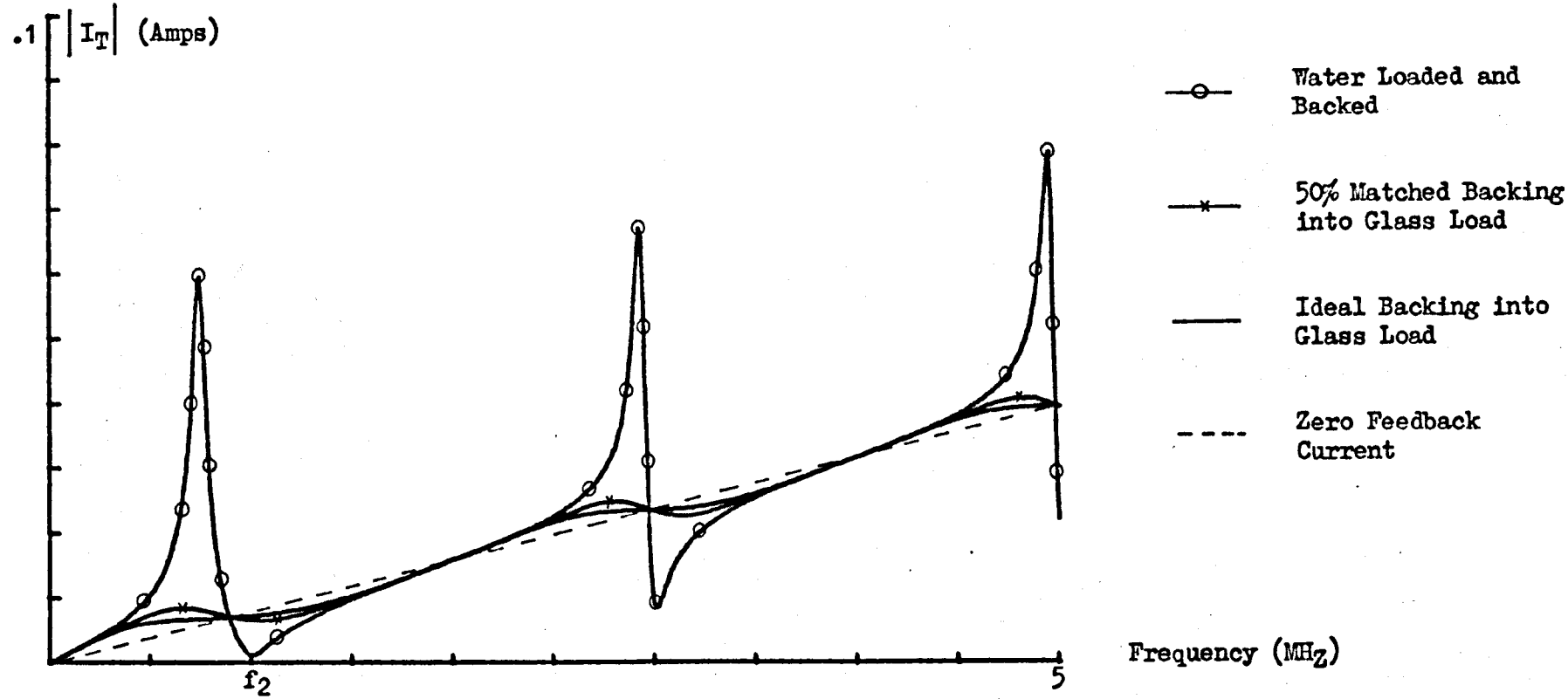

Fig. 7.3. Frequency Characteristics of Transducer Current under Different Conditions of Mechanical Load

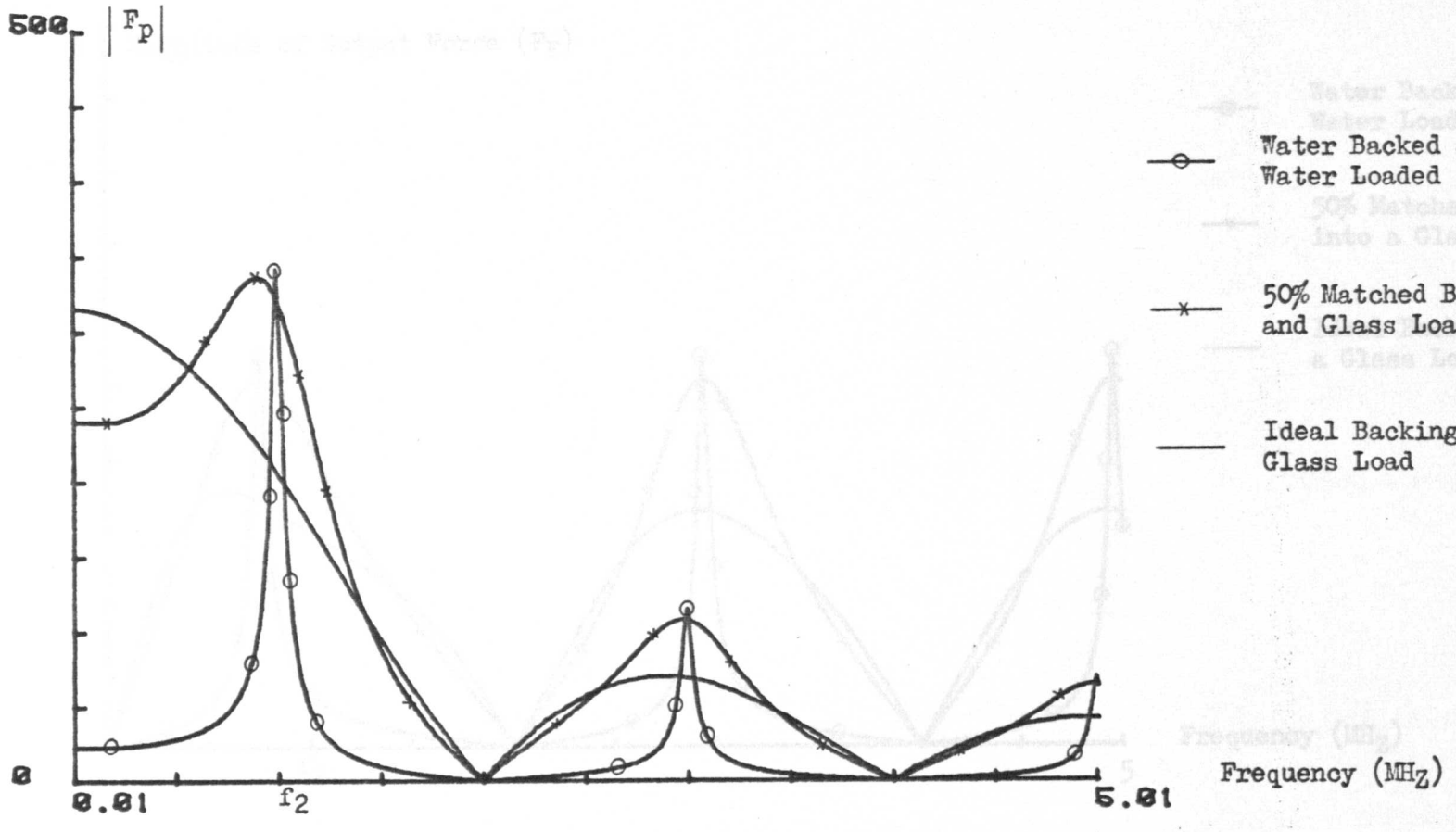

Fig. 7.4. Frequency Characteristics of F_p (Forward Path Transmission Parameter)

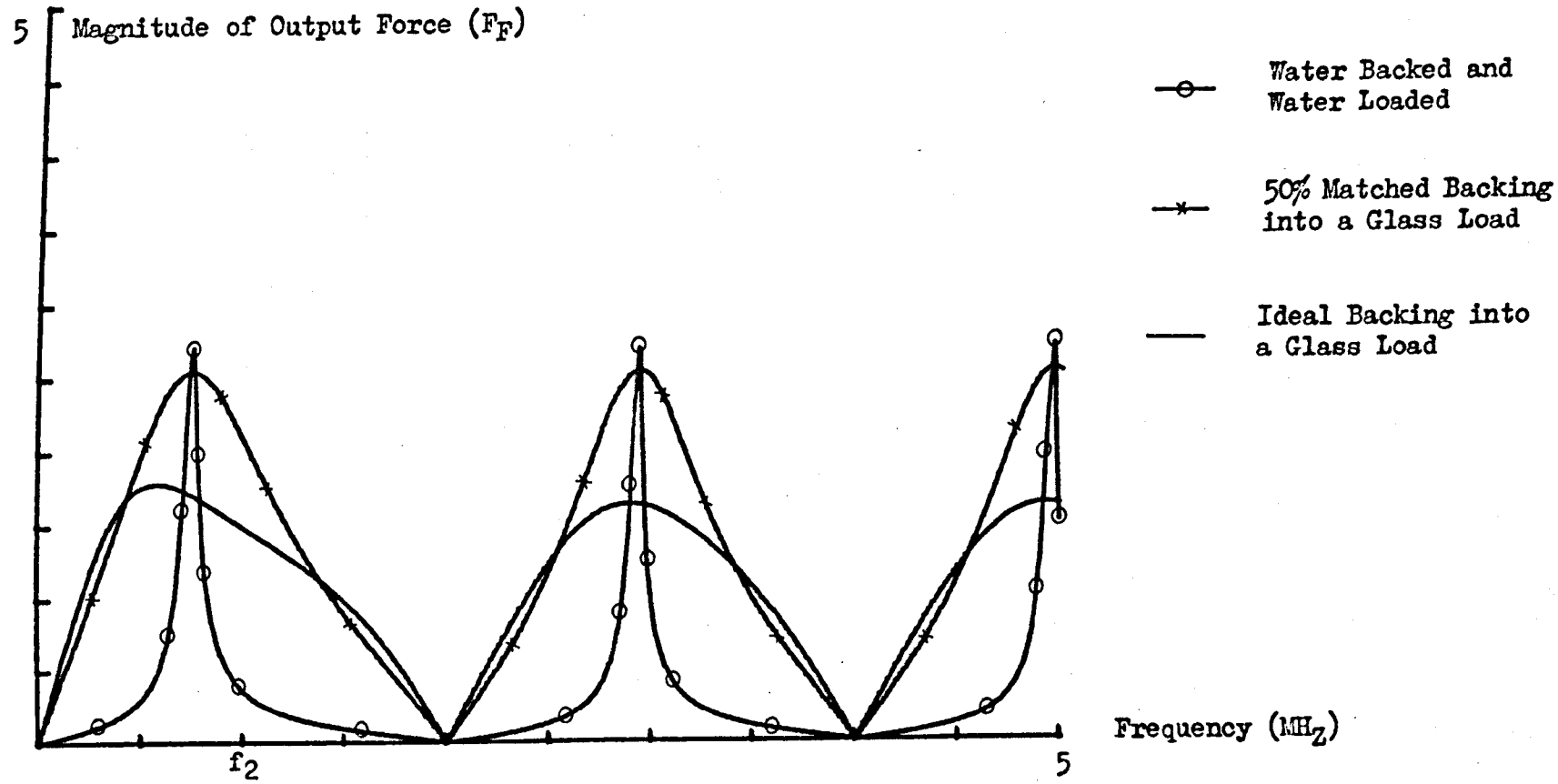

Fig. 7.5. Transmitter Frequency Characteristics under Different Conditions of Mechanical Load

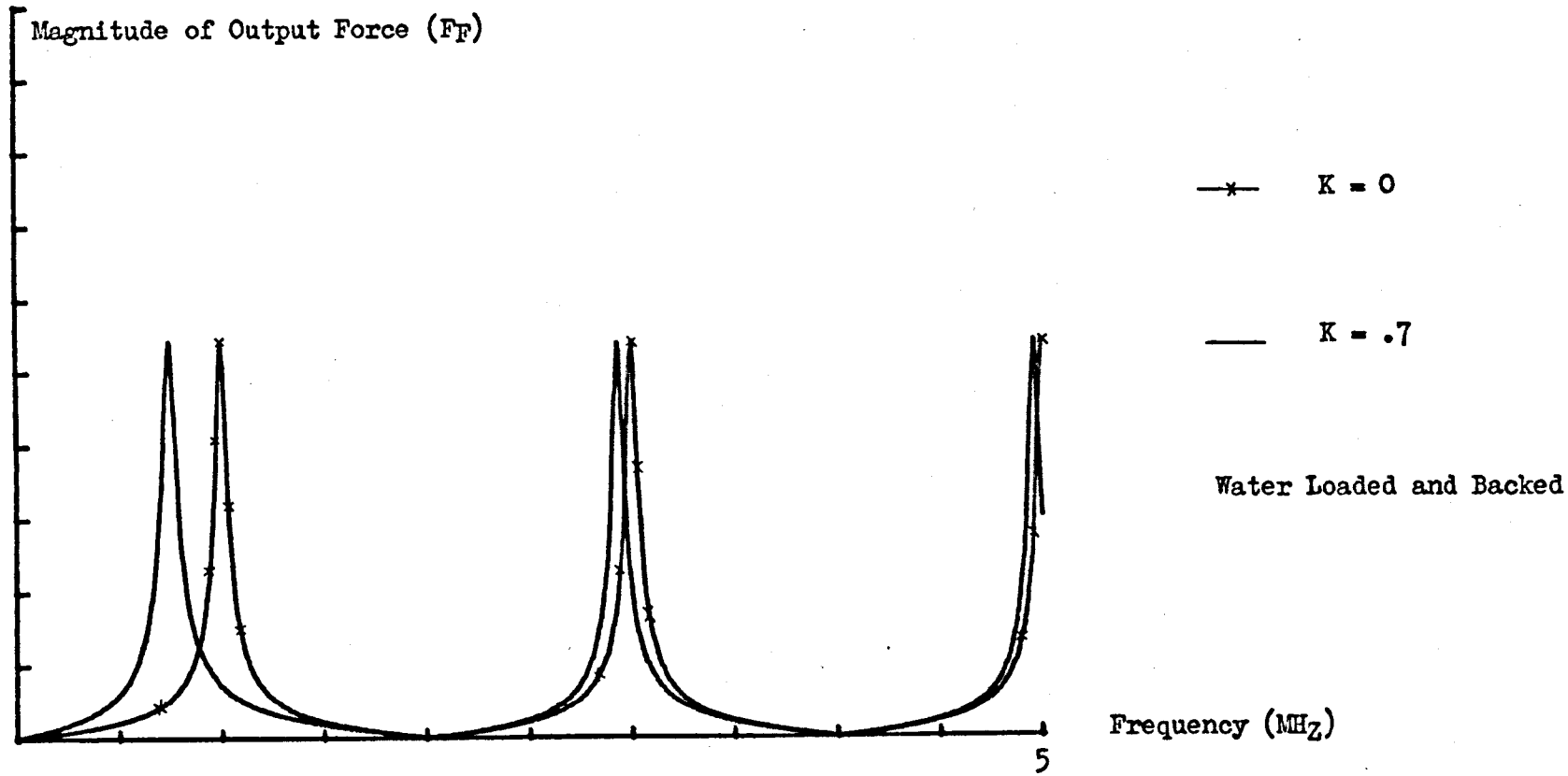

Fig. 7.6. Variation in Output Force Frequency Response with Coupling Coefficient

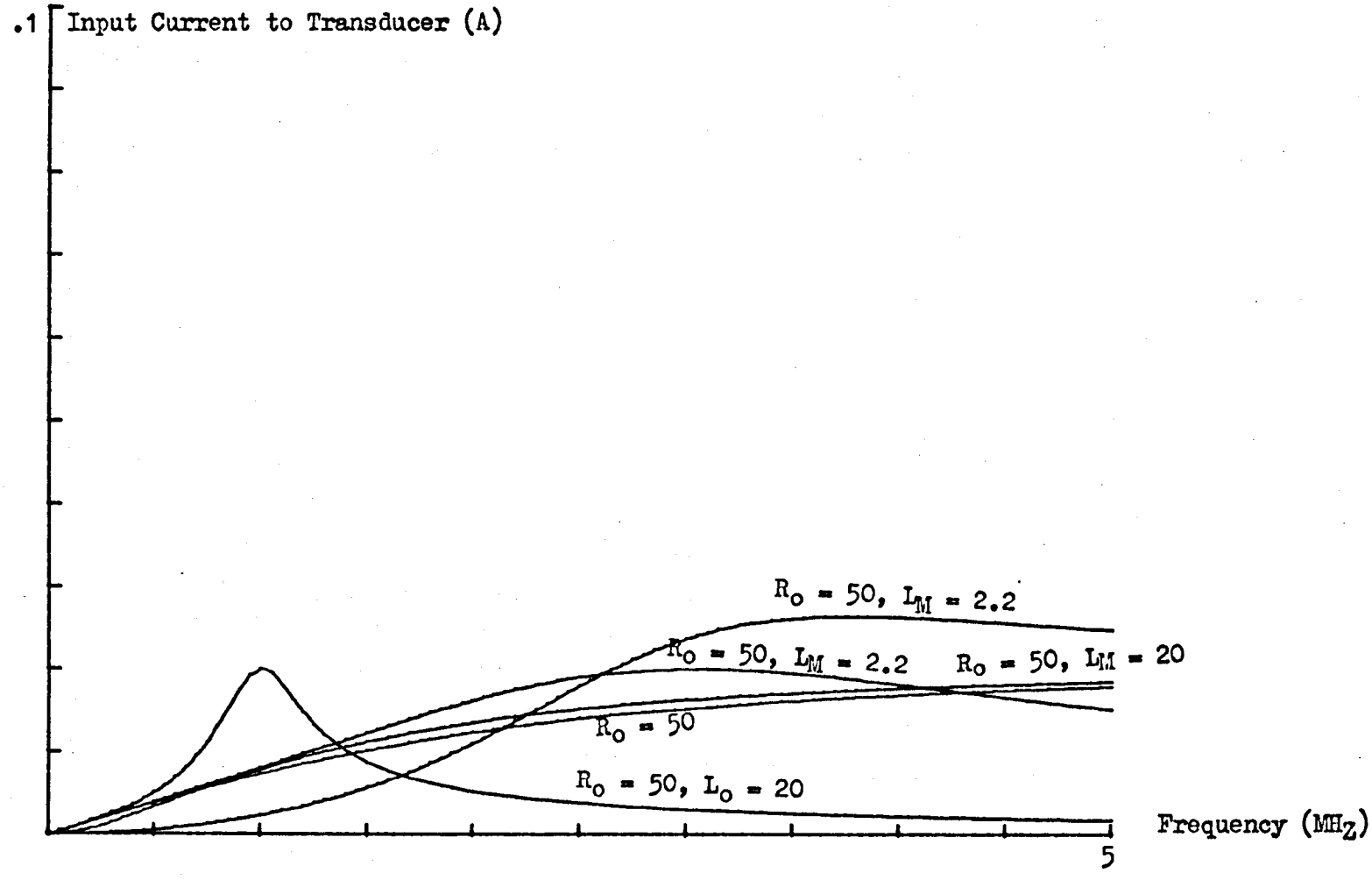

Fig. 7.7. Magnitude of Transducer Input Current for a Variety of Electrical Loading Conditions

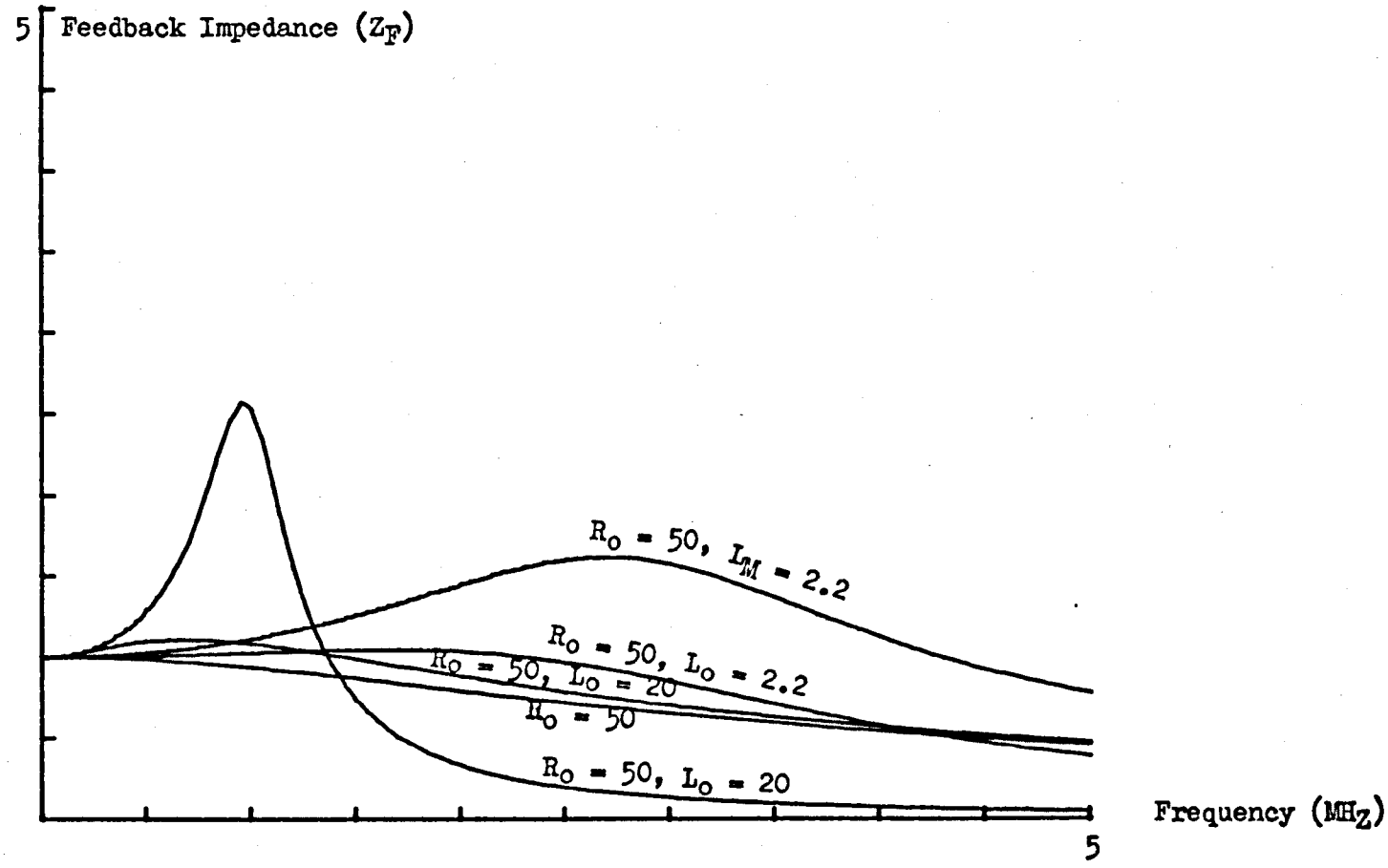

Fig. 7.8. Magnitude of Feedback Impedance V_s Frequency for a Variety of Electrical Load Conditions

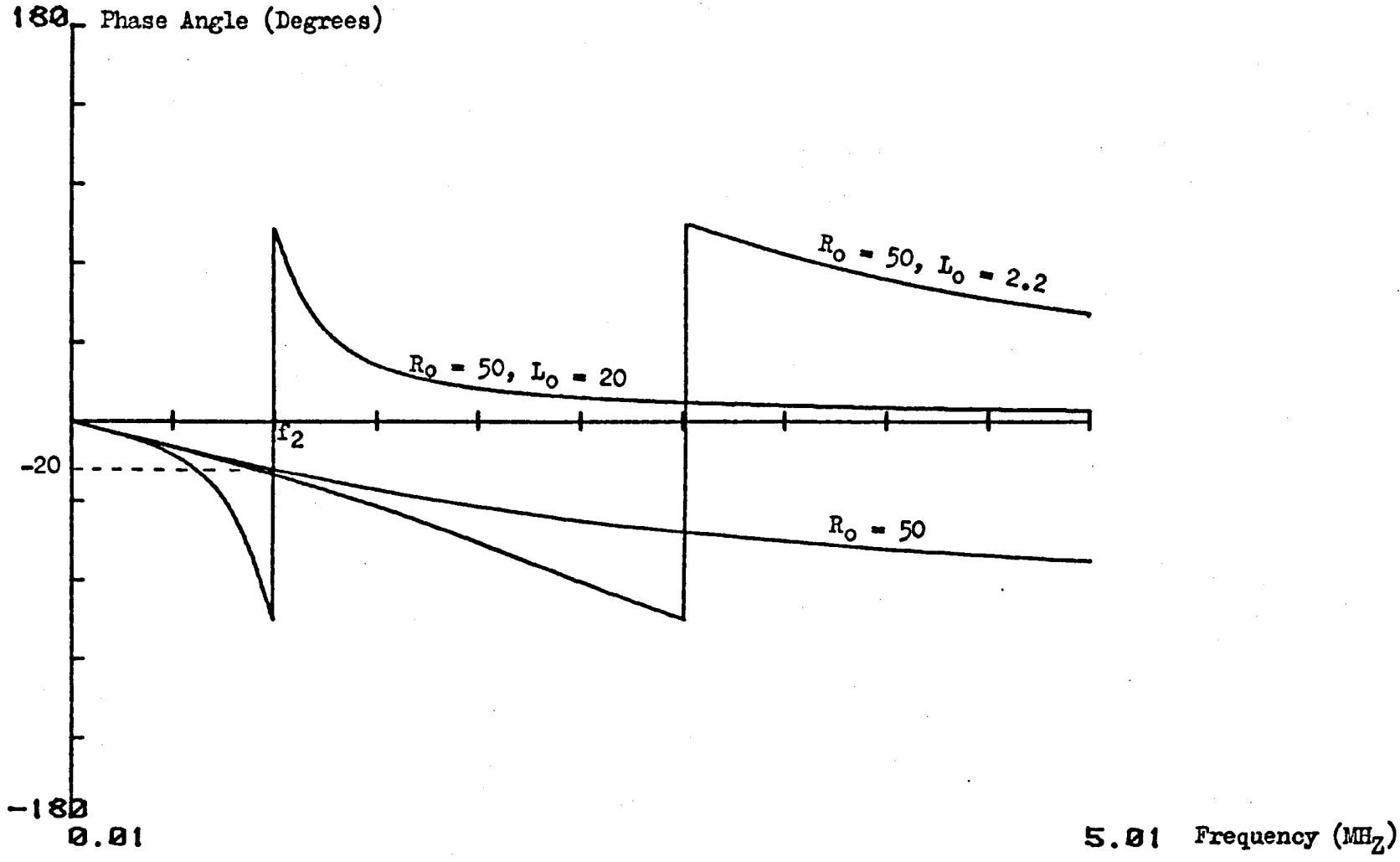

Fig. 7.9a. Phase of Feedback Impedance V_s Frequency for a Variety of Electrical Load Conditions

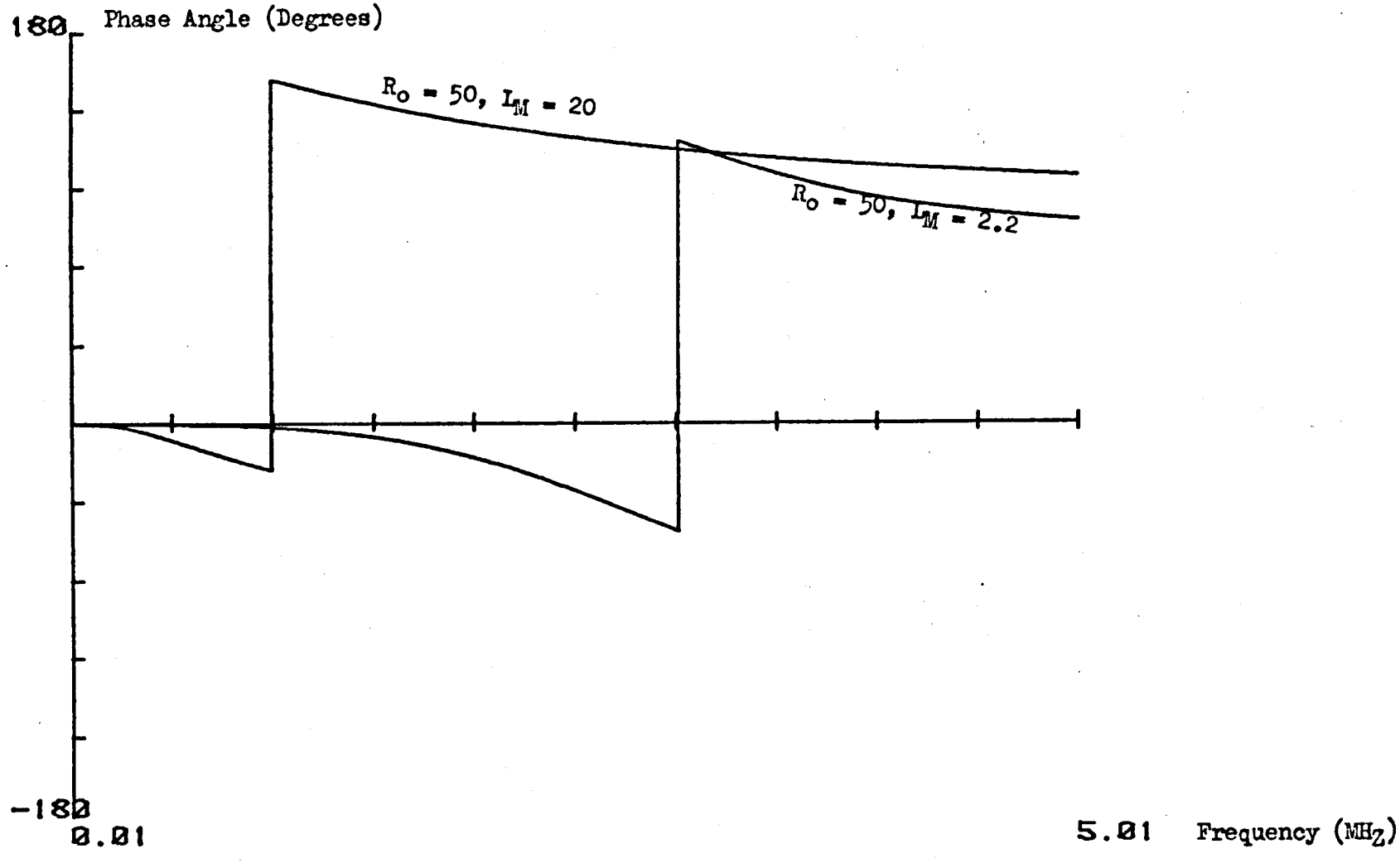

Fig. 7.9b. Phase of Feedback Impedance V_s Frequency for a Variety of Electrical Load Conditions

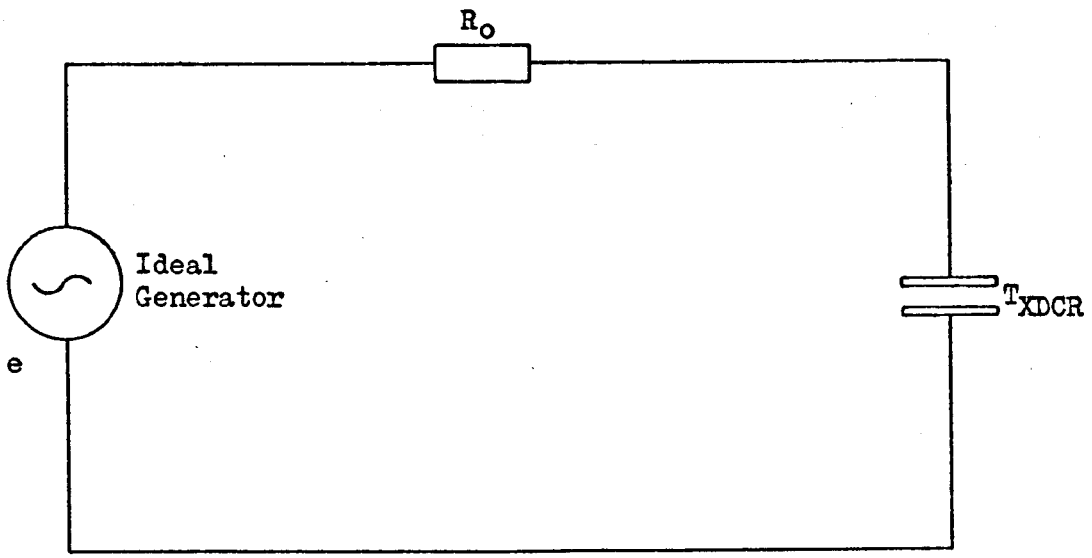

Fig. 7.10. Transducer Driven from a Non-Ideal Voltage Generator

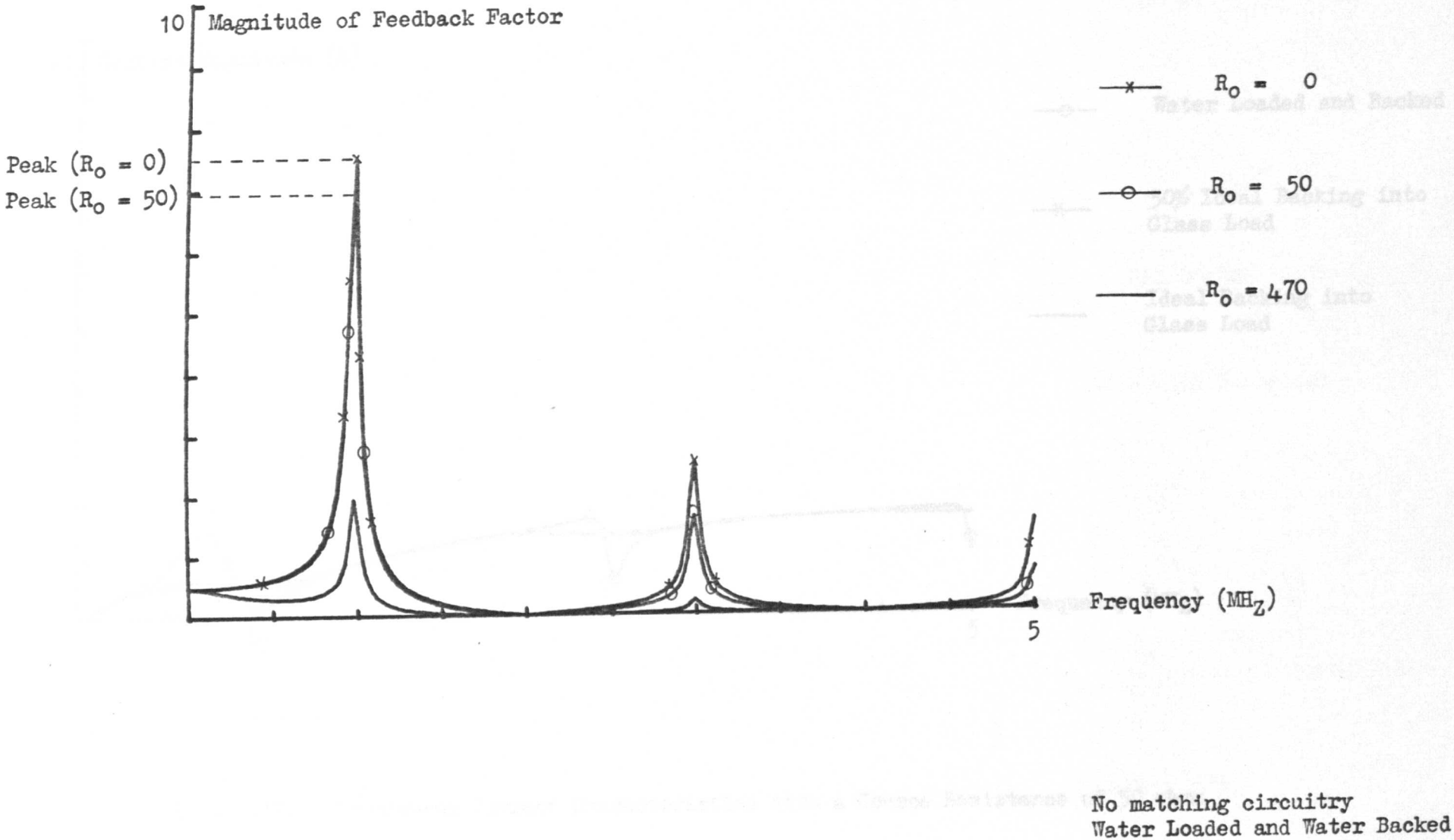

Fig. 7.11. Variation in Feedback Factor with Source Resistance

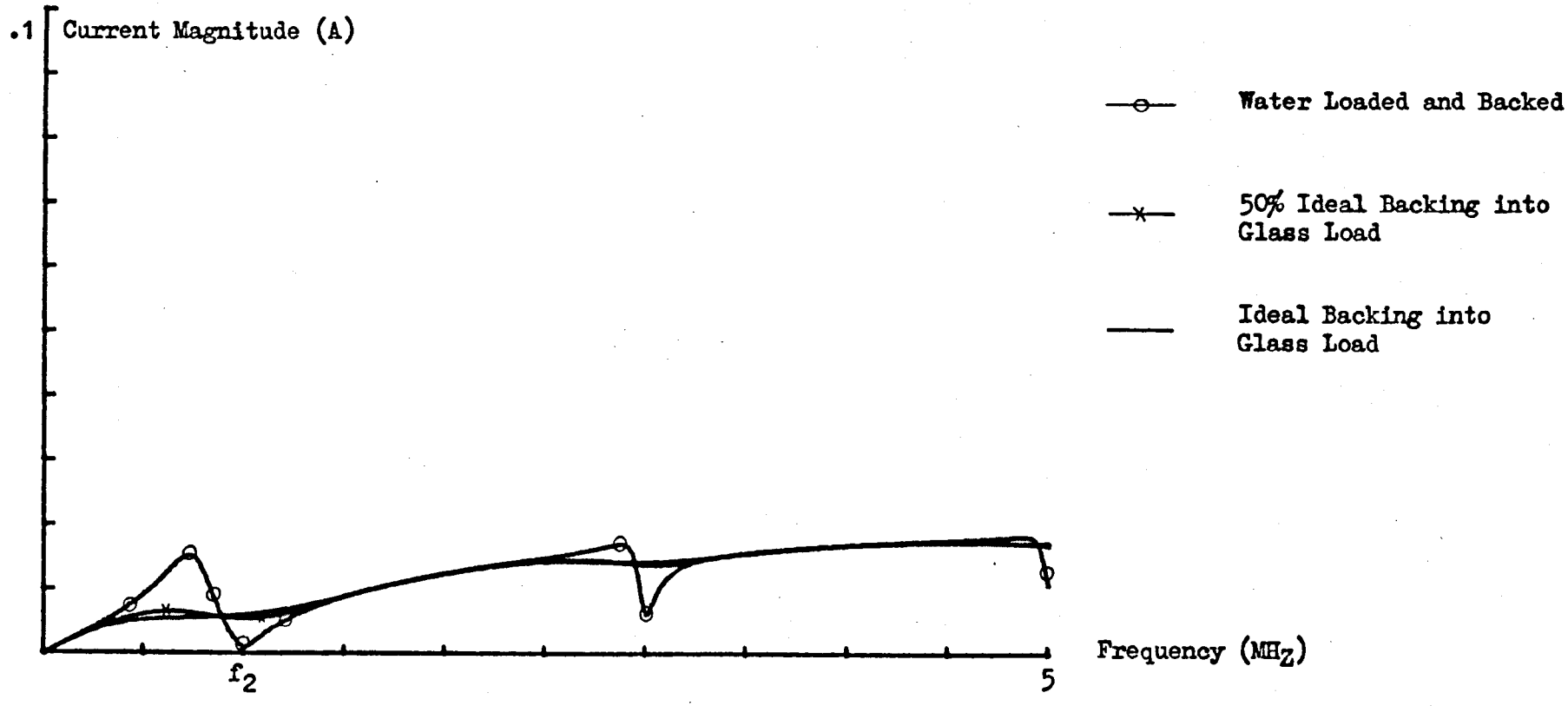

Fig. 7.12. Transducer Current Characteristics with a Source Resistance of 50 ohms

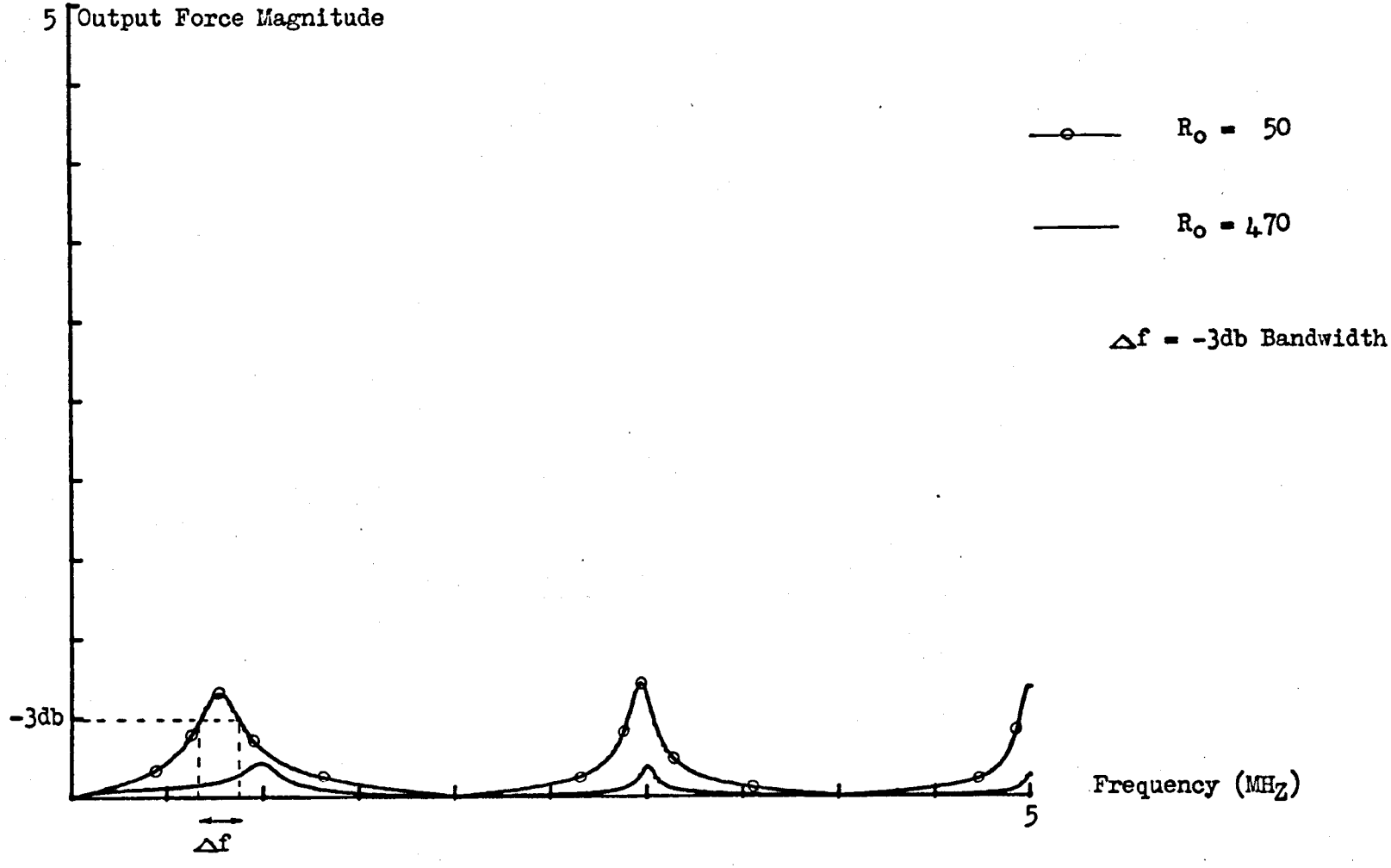

Fig. 7.13a. Variation in Output Force Response with Source Resistance
(Water Backing, Water Load)

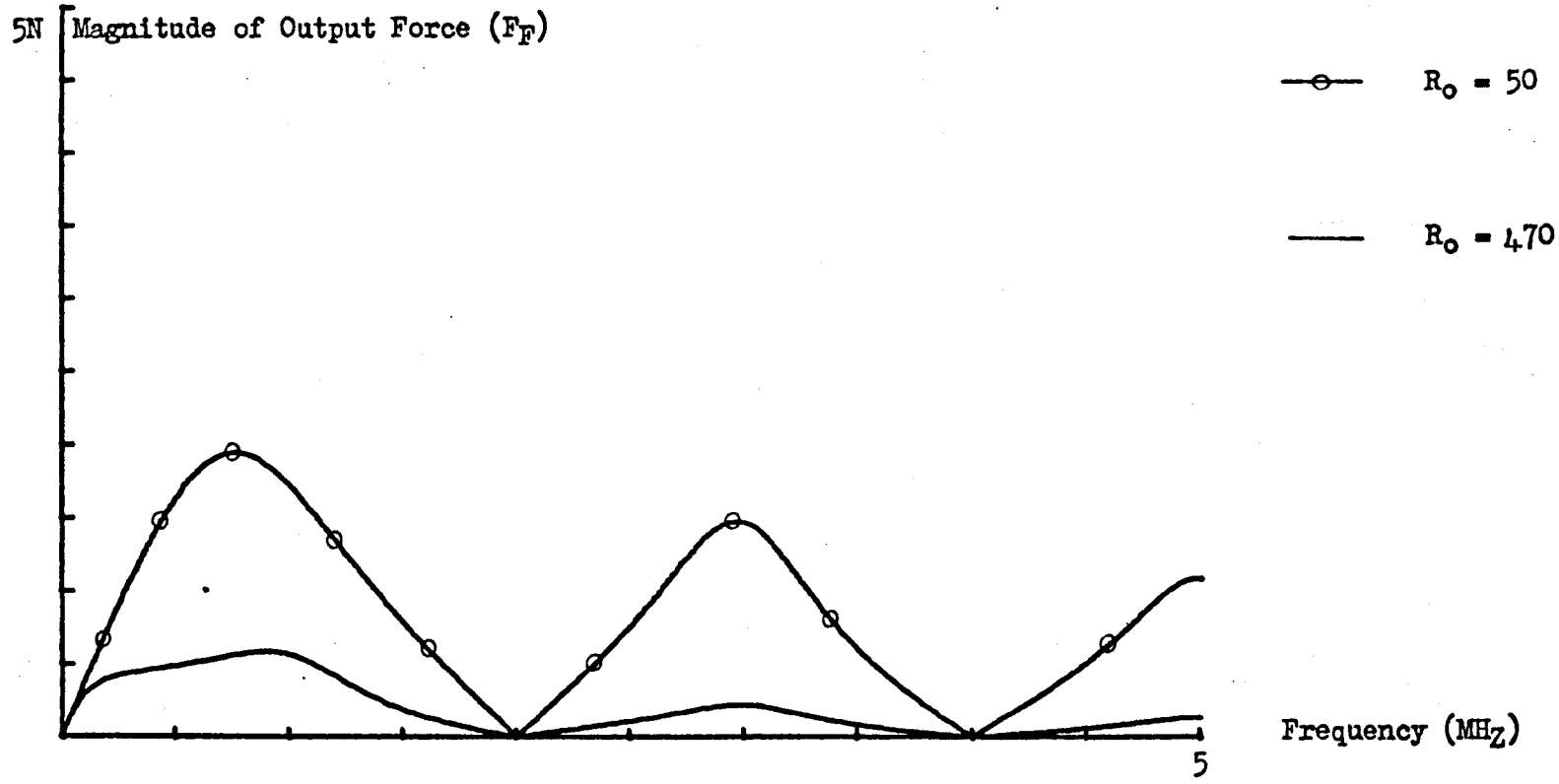

Fig. 7.13b. Variation in Output Force with Source Resistance
(50% Matched Backing, Glass Load)

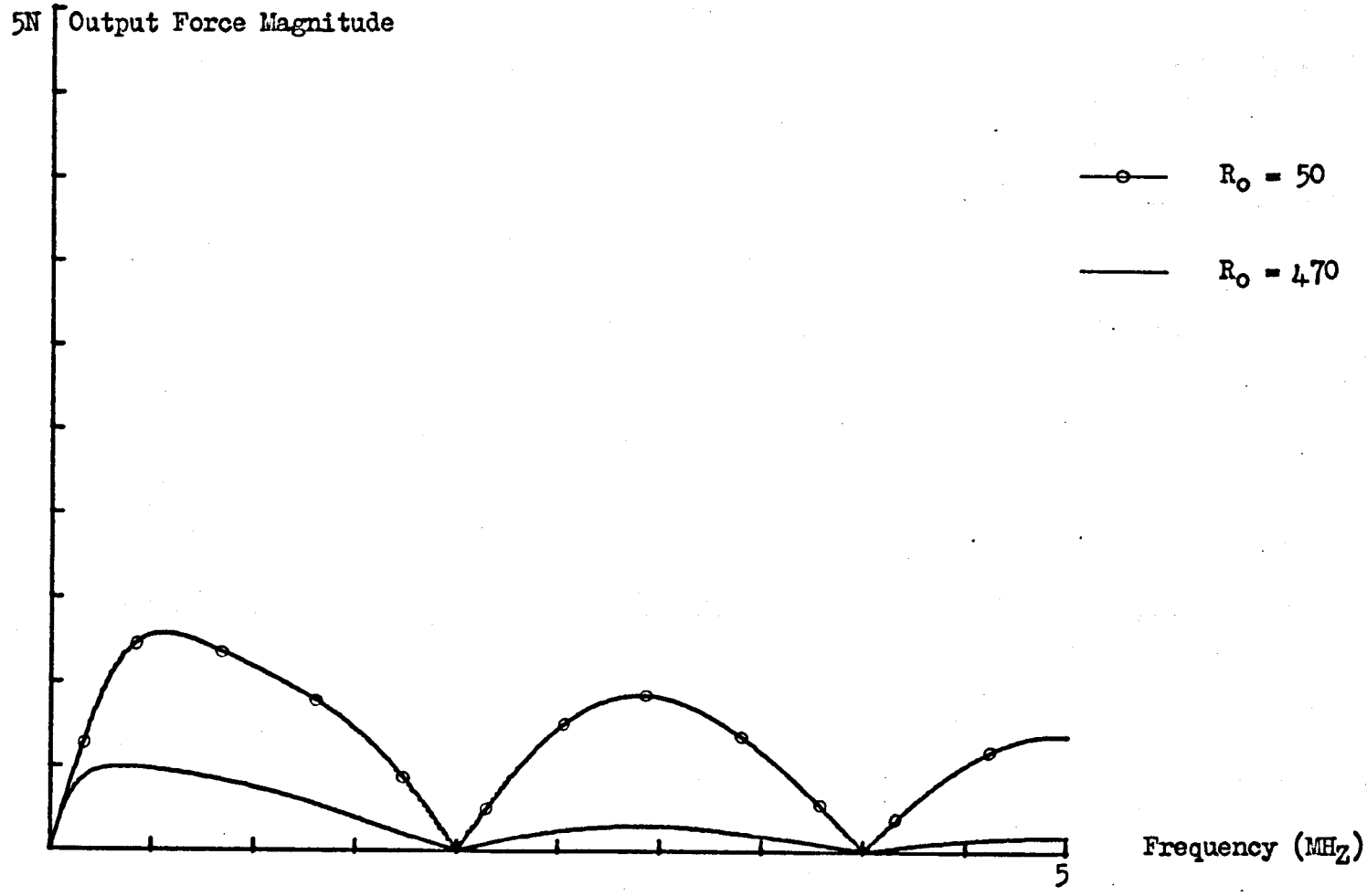

Fig. 7.13c. Variation in Output Force Response with Source Resistance (Ideal Backing, Glass Load)

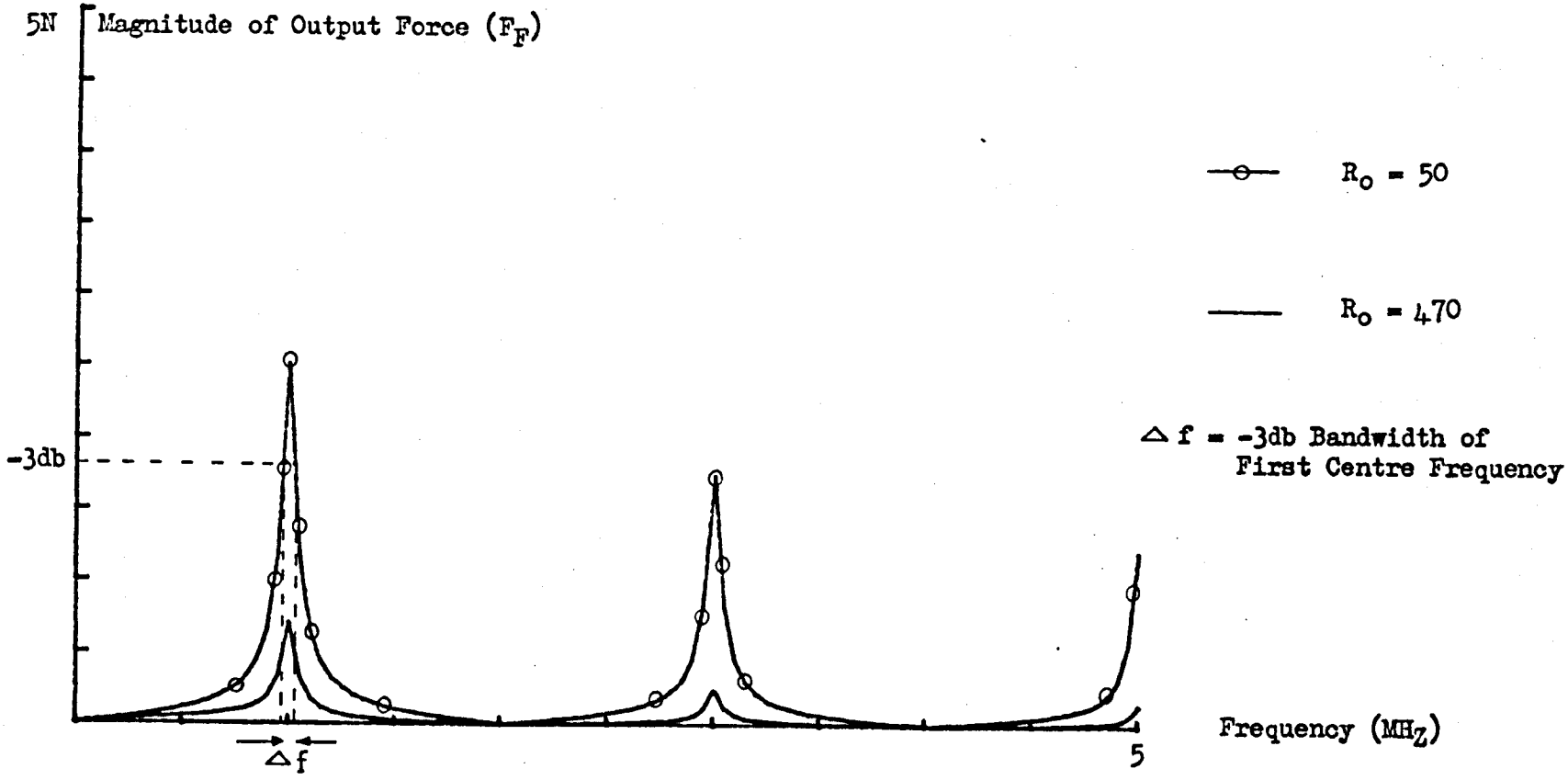

Fig. 7.14a. Output Force in the Absence of Feedback (Water Backing, Water Load)

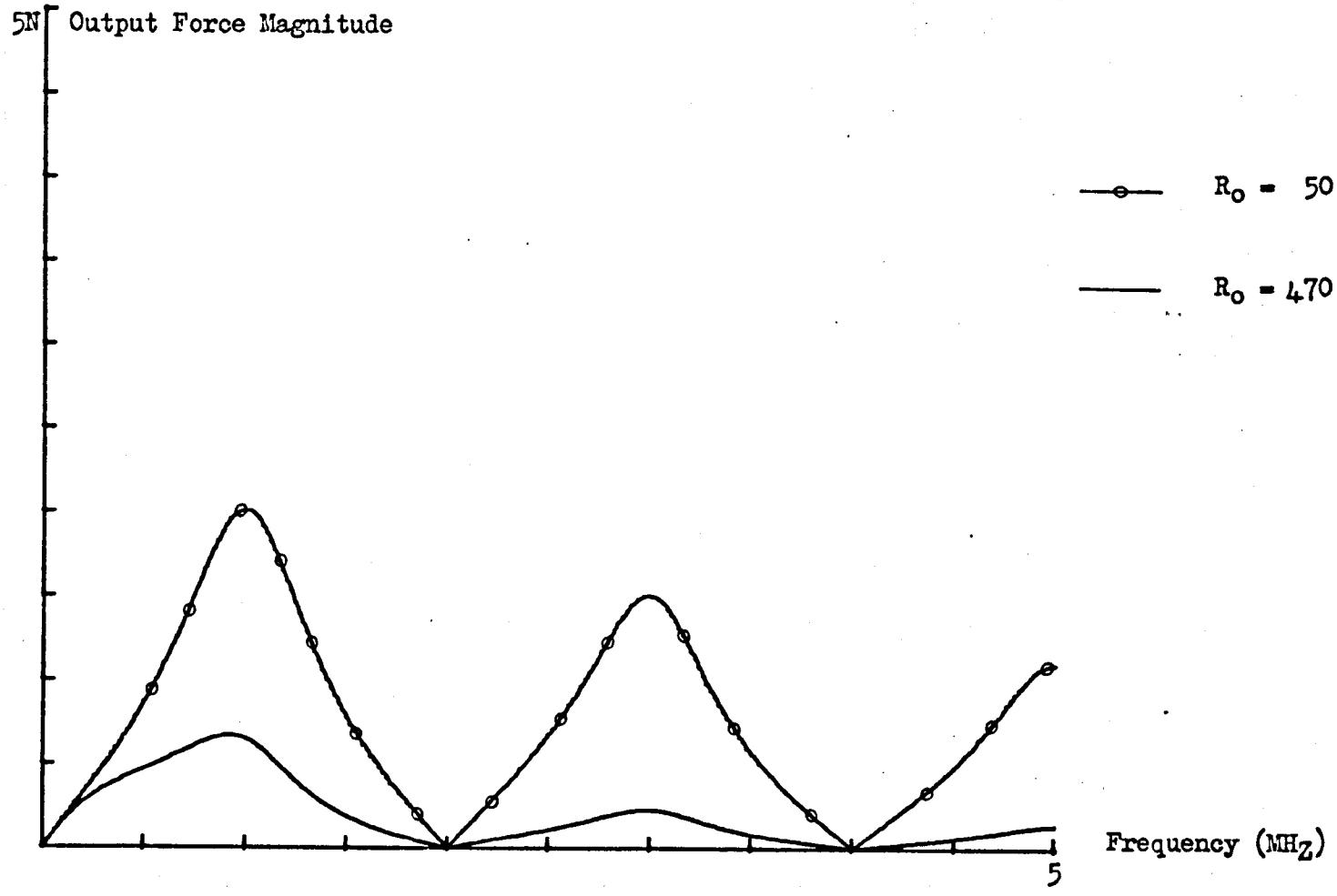

Fig. 7.14b. Output Force in Absence of Feedback (50% Matched Backing, Glass Load)

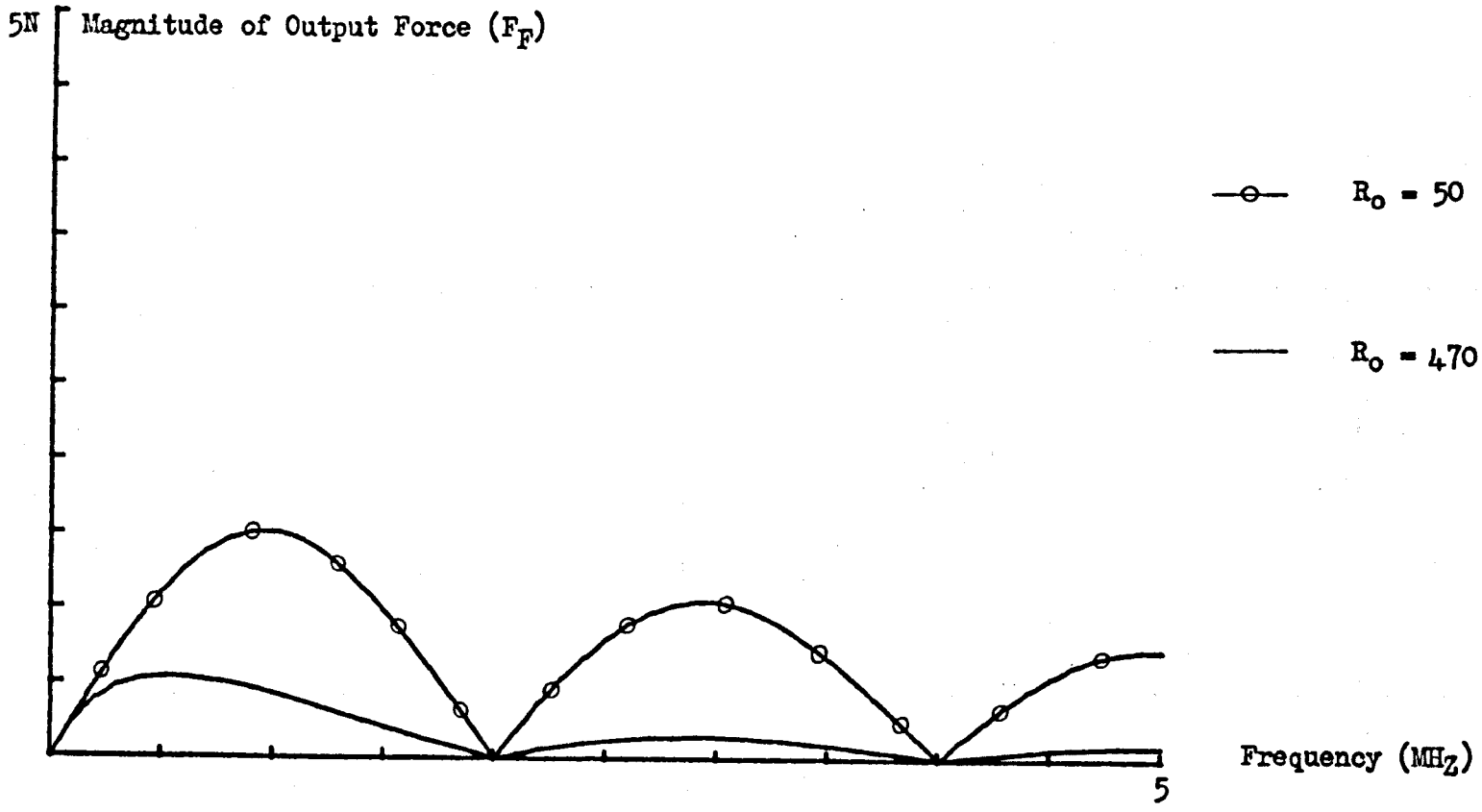

Fig. 7.14c. Output Force in Absence of Feedback (Ideal Backing, Glass Load)

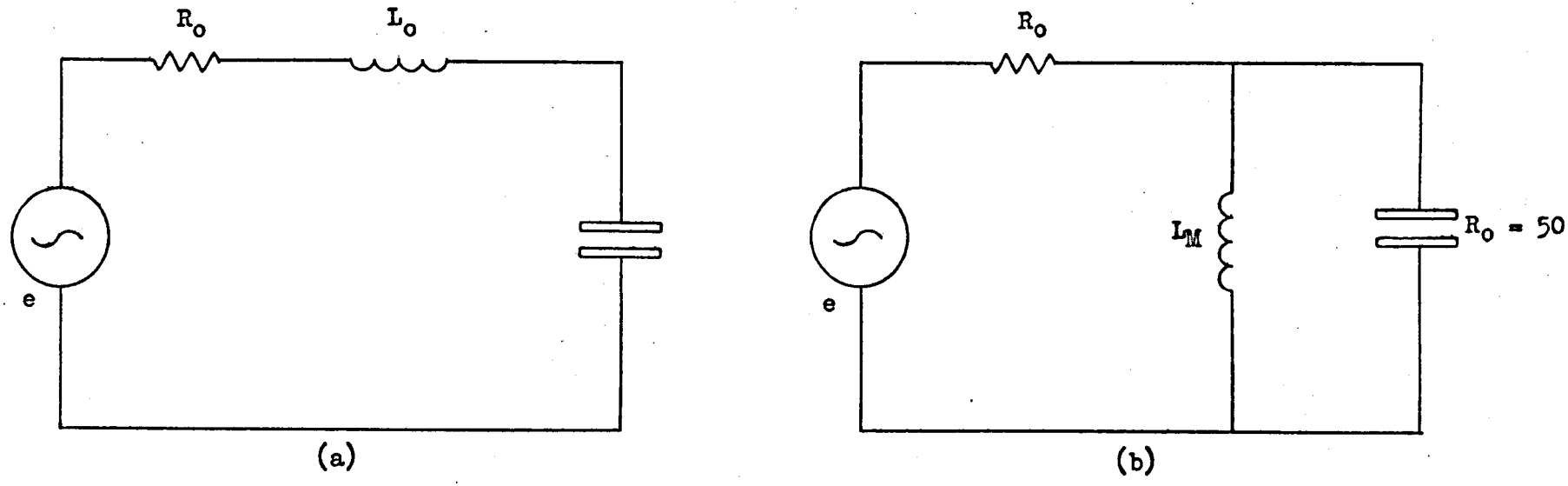

Fig. 7.15. Transducer-Generator Configuration with Inductive Loading

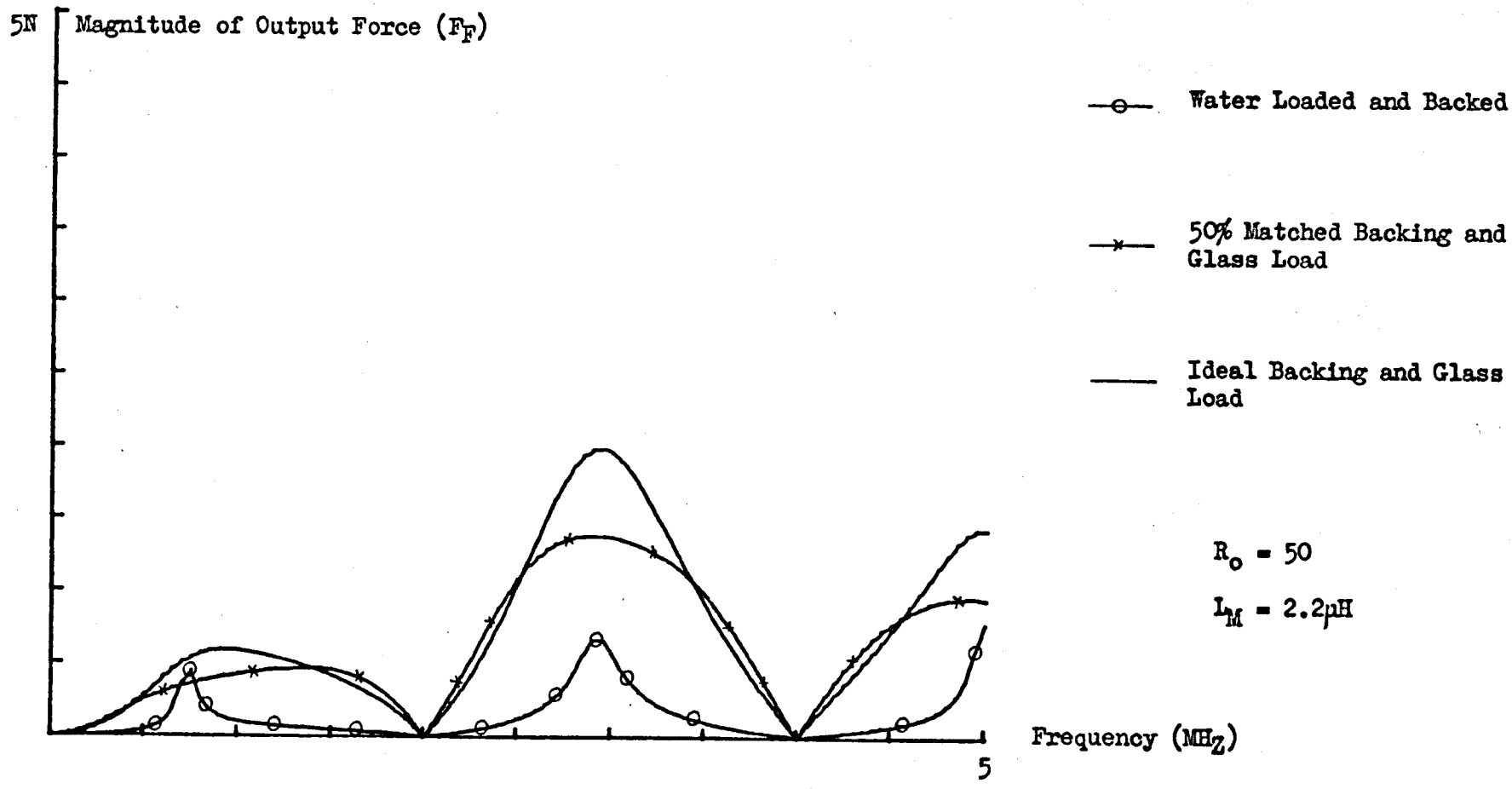

Fig. 7.16. Output Force Frequency Characteristics for a Transducer with Parallel Inductive and Series Resistive Loading

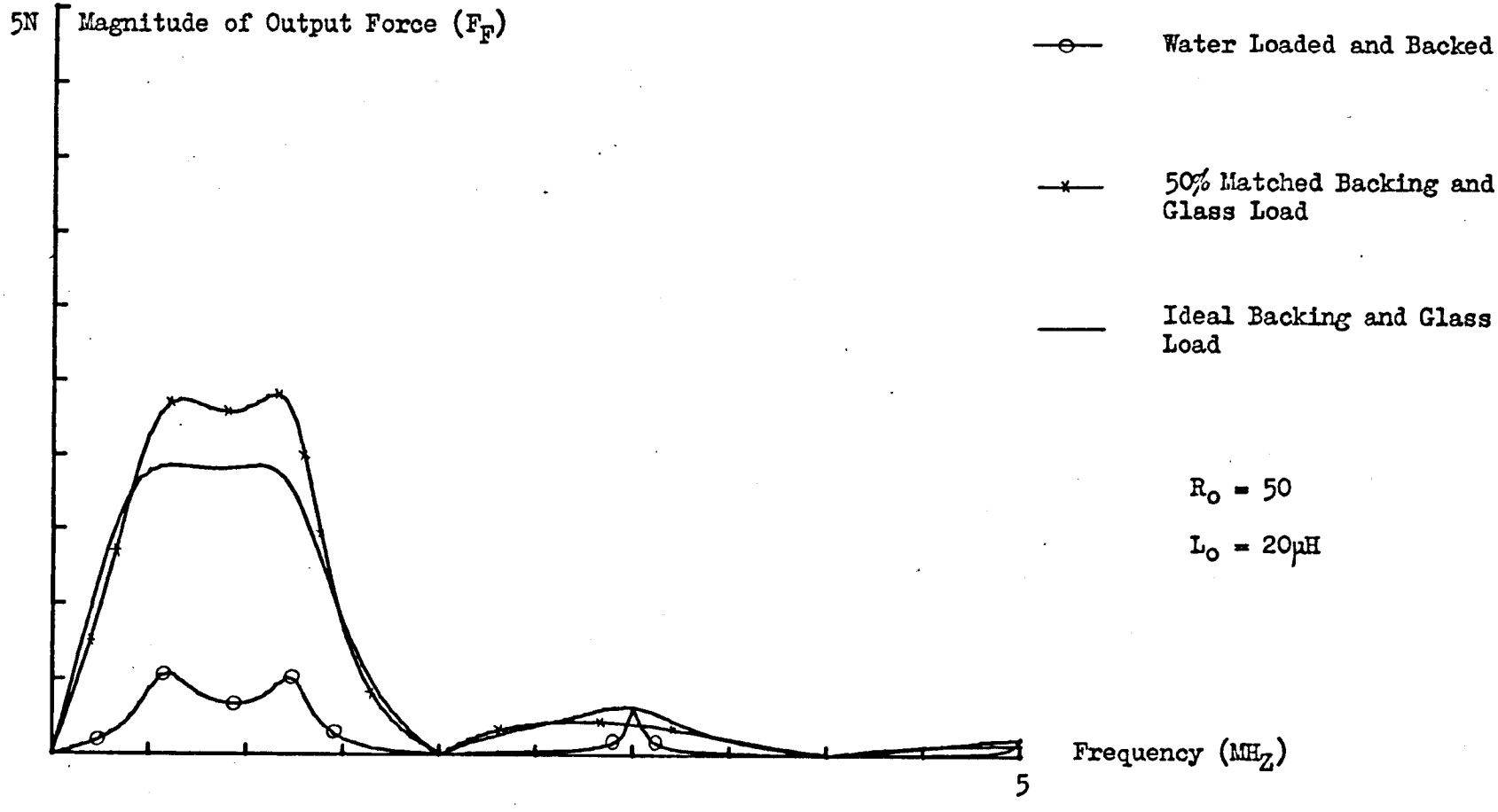

Fig. 7.17. Output Force Frequency Characteristics for a Transducer with Series Resistive and Inductive Loading

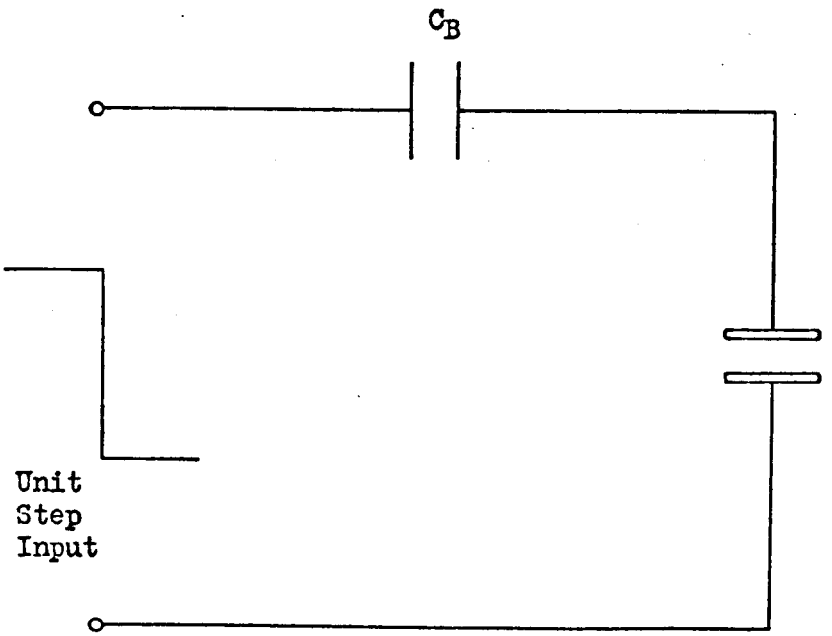

Fig. 7.18. Voltage Step Across Transducer

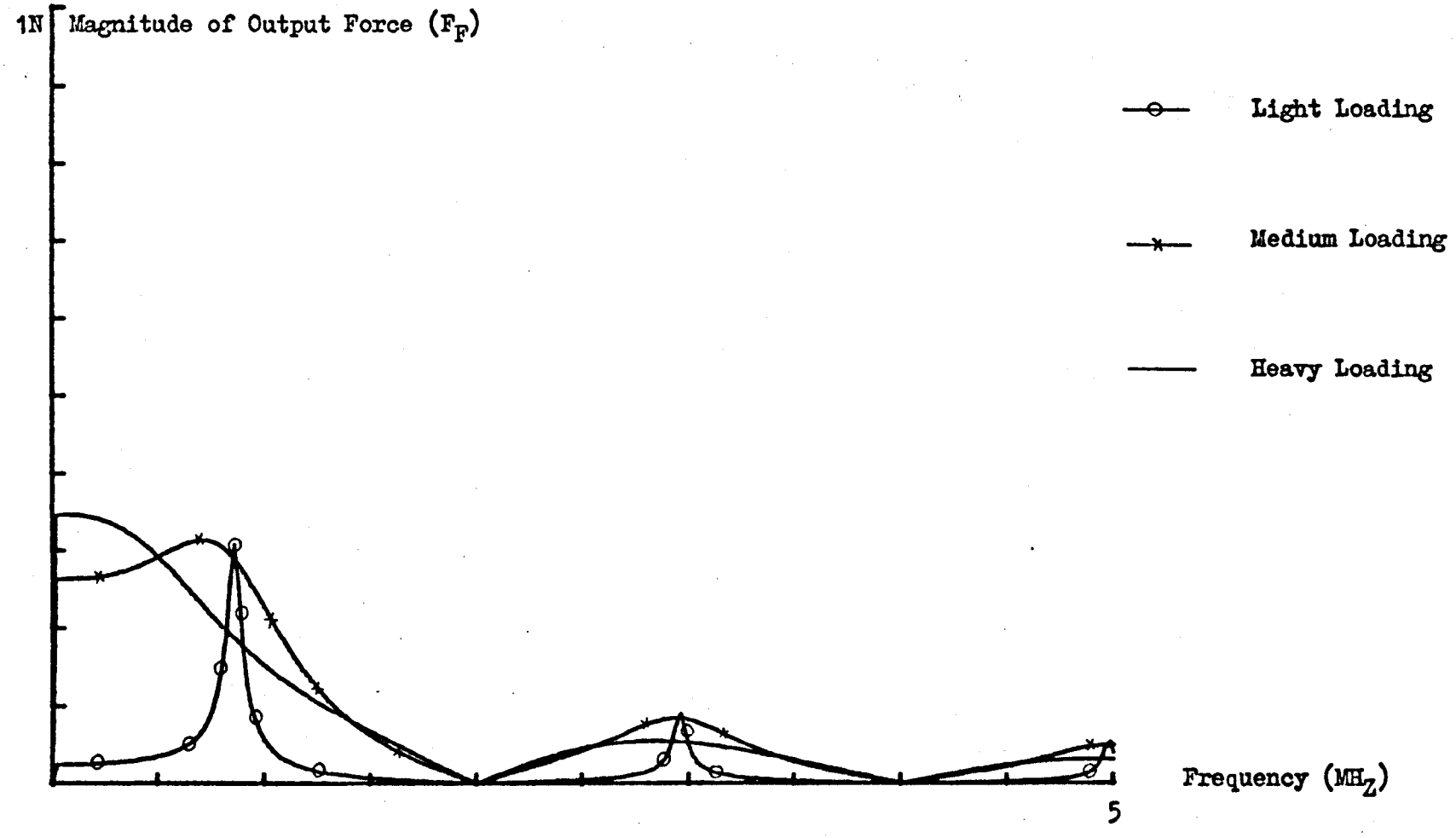

Fig. 7.19a. Transient Frequency Response Characteristics (C_B = 2nF)

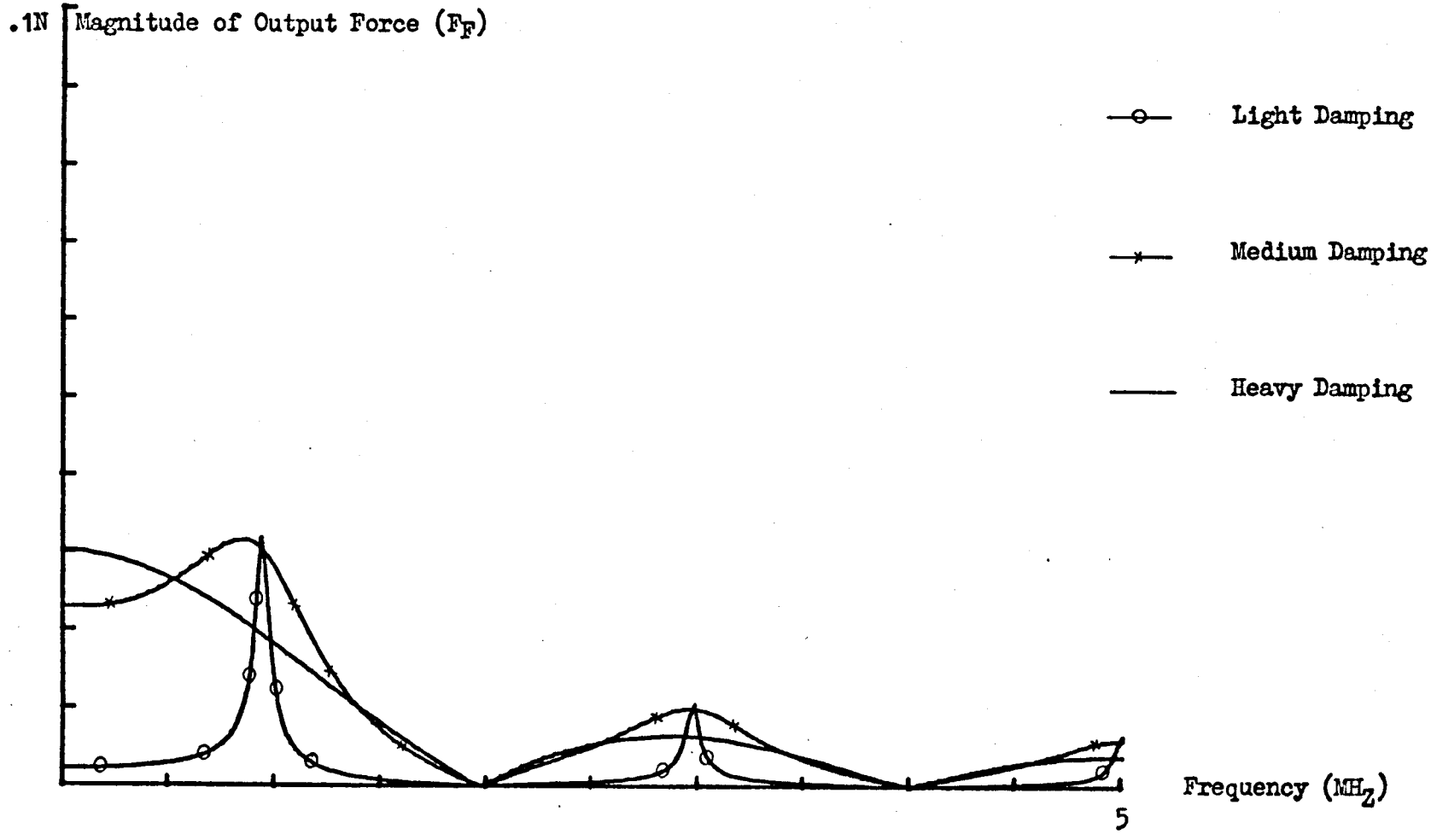

Fig. 7.19b. Transient Frequency Response Characteristics (C_B = .1nF)

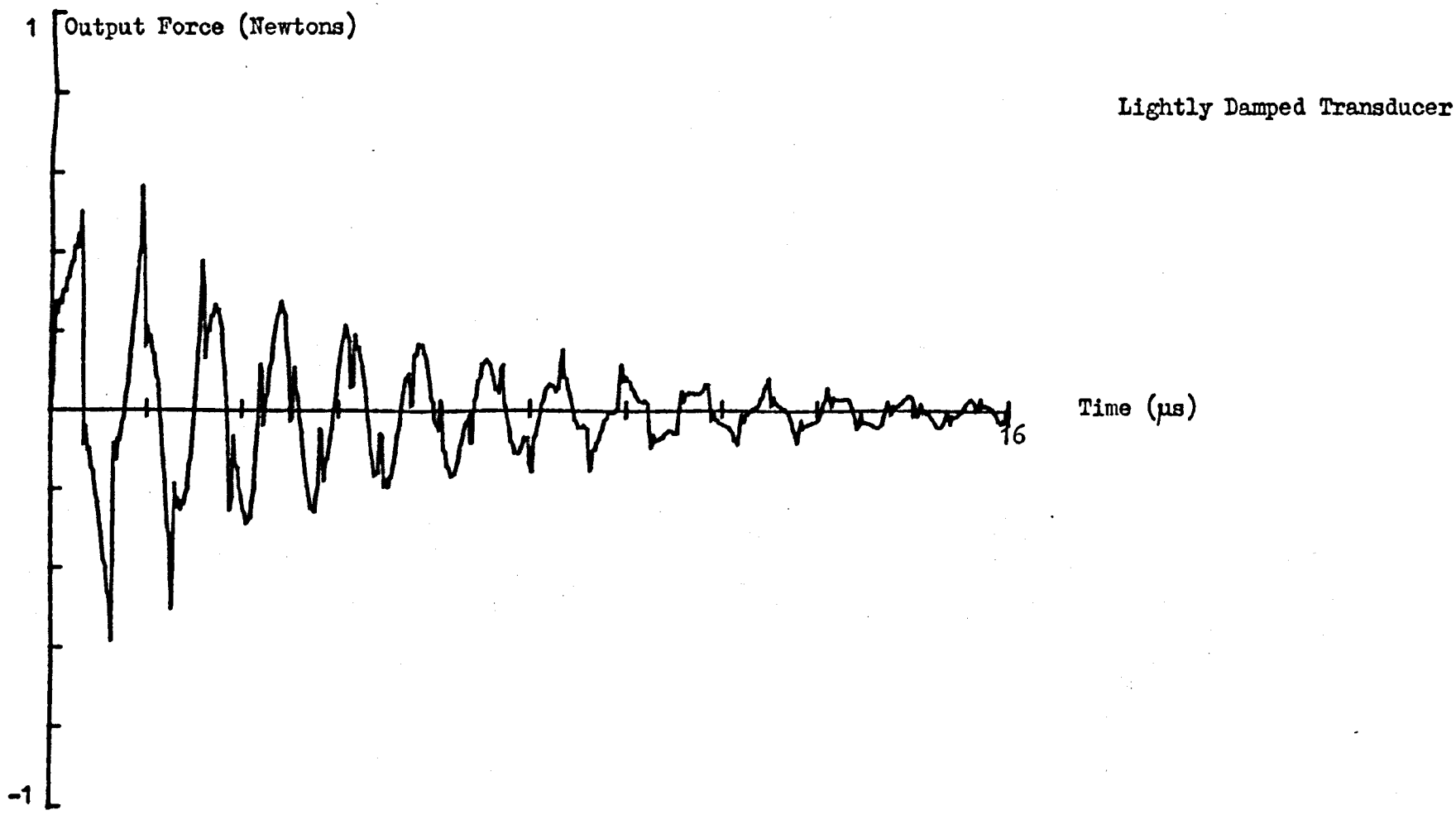

Fig. 7.20a. Time Response of Transducer under Transient Conditions (C_B = 2nF)

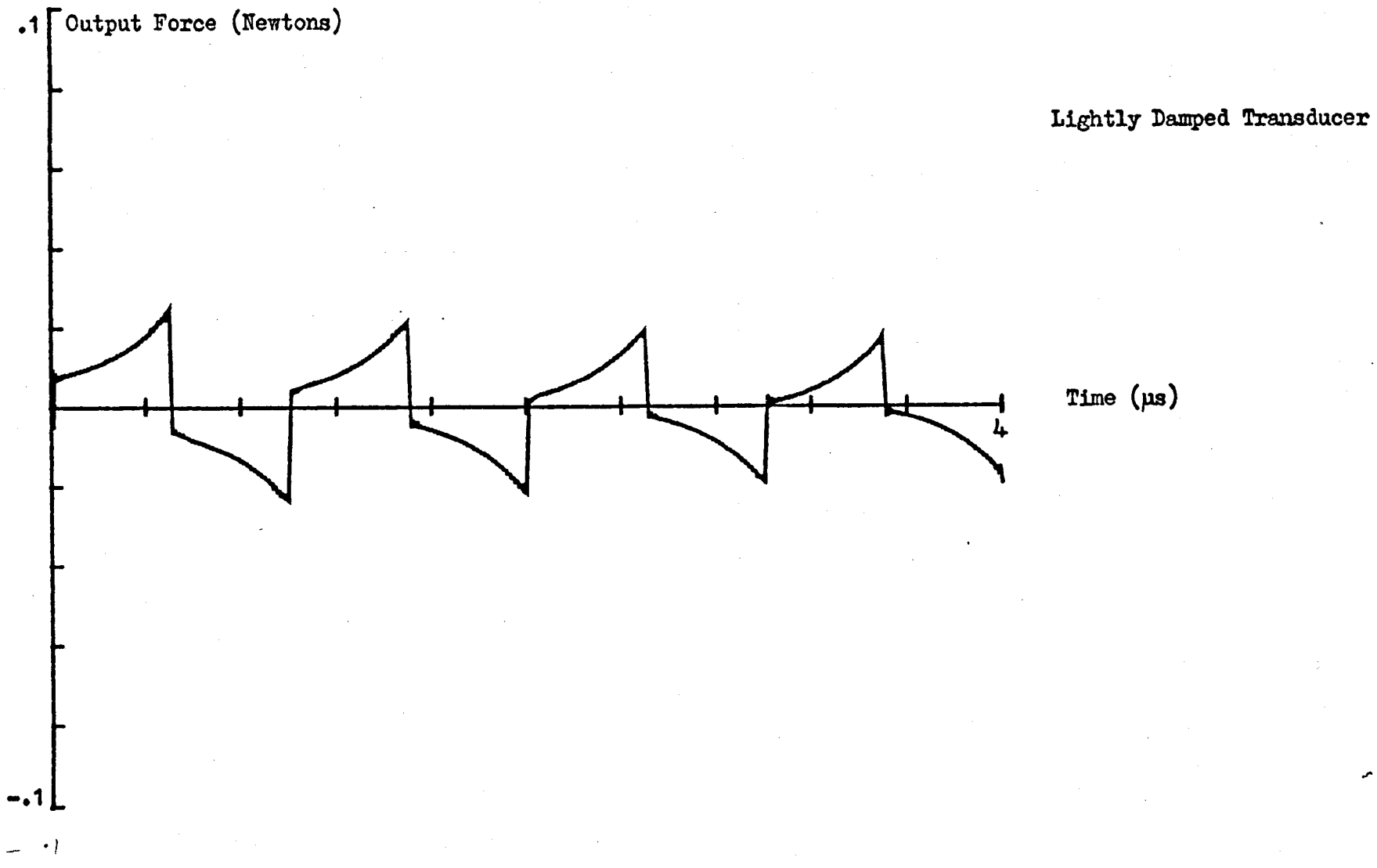

Fig. 7.20b. Time Domain Response of Transducer under Transient Conditions (C_B = .1nF)

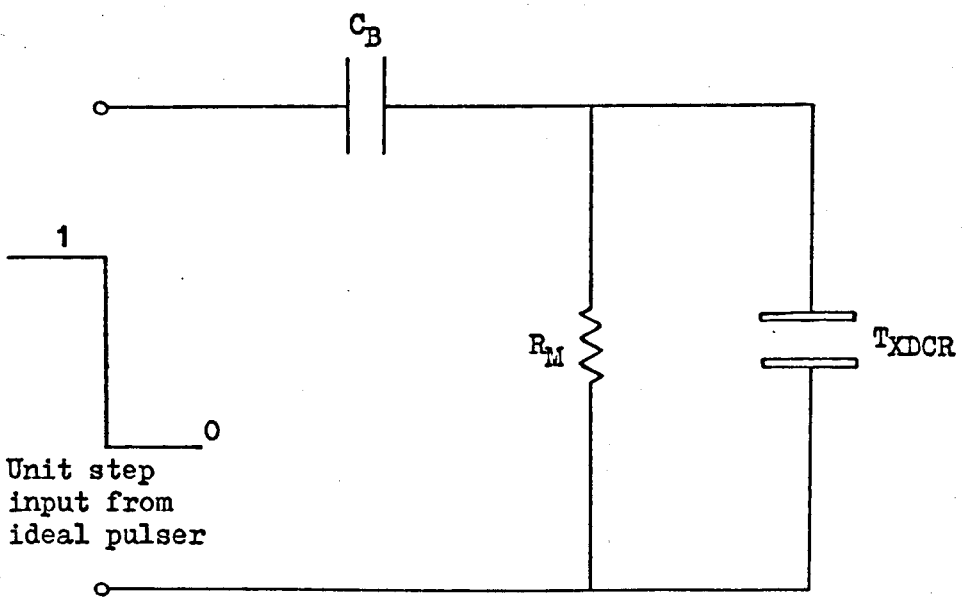

Fig. 7.21. Voltage Step Applied to Resistively Loaded Transducer

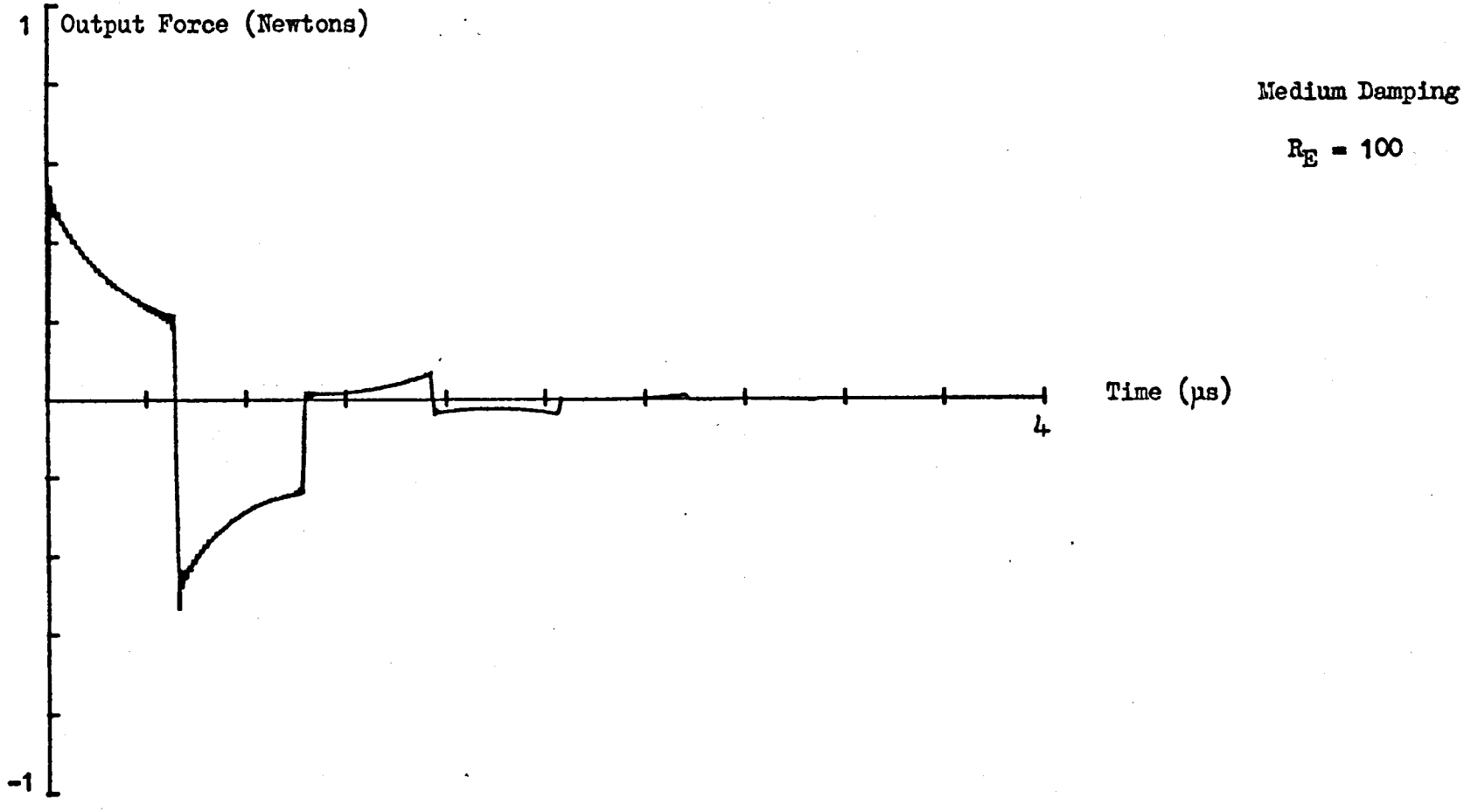

Fig. 7.22a. Output Wave of Force under Transient Conditions

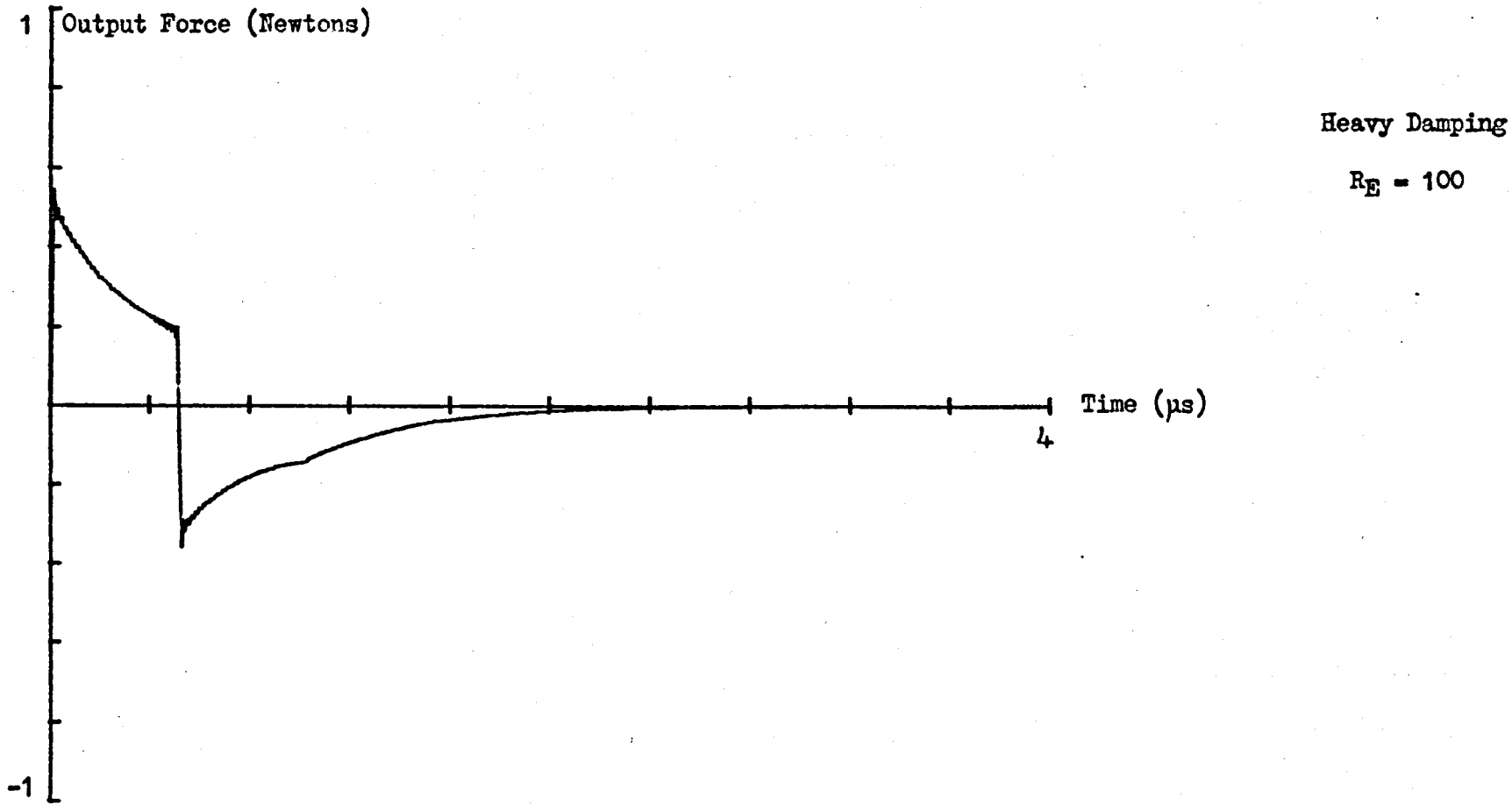

Fig. 7.22b. Output Wave of Force under Transient Conditions

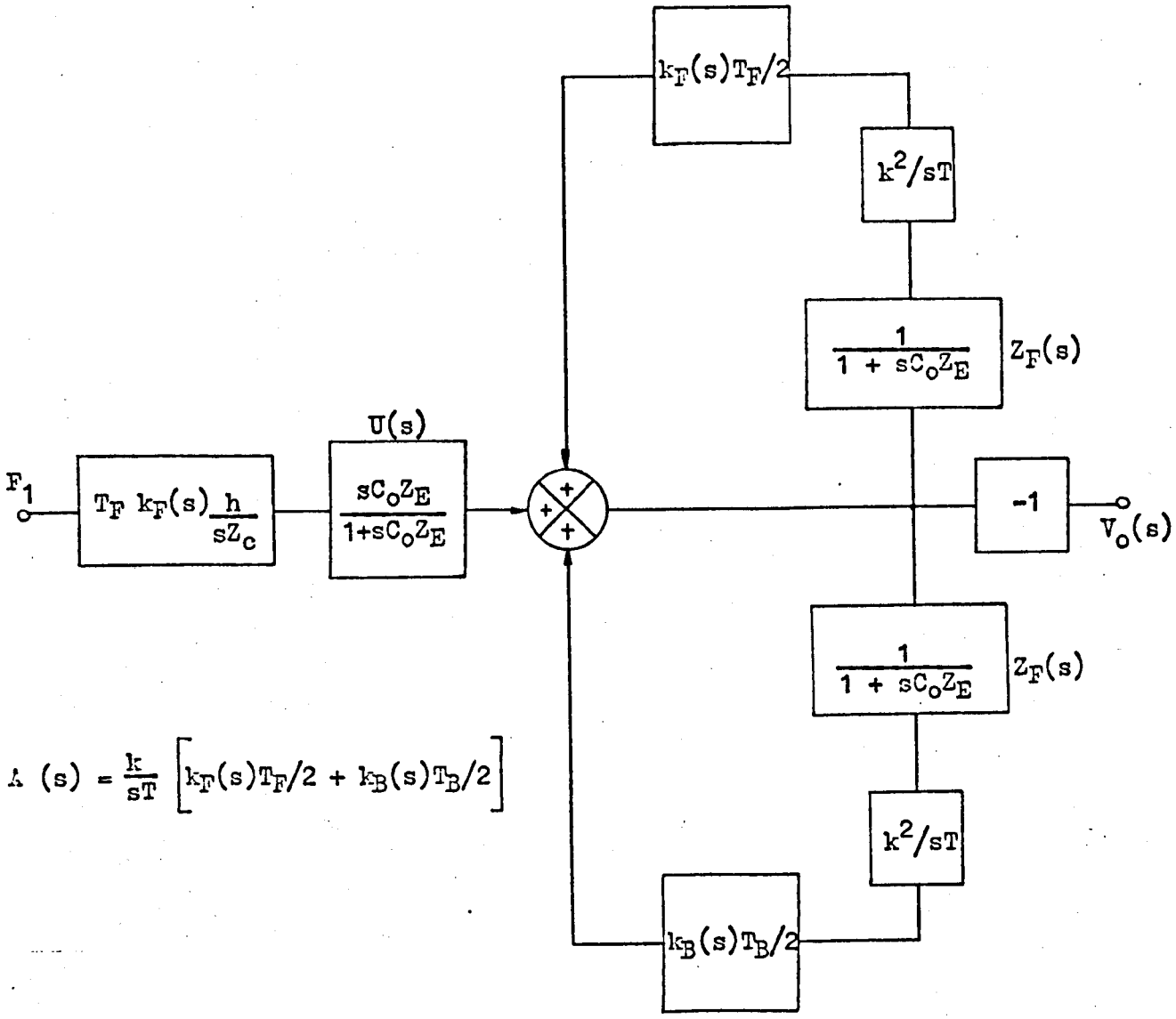

Fig. 7.23. Simplified Block Diagram of a Piezoelectric Transducer in the Receiving Mode

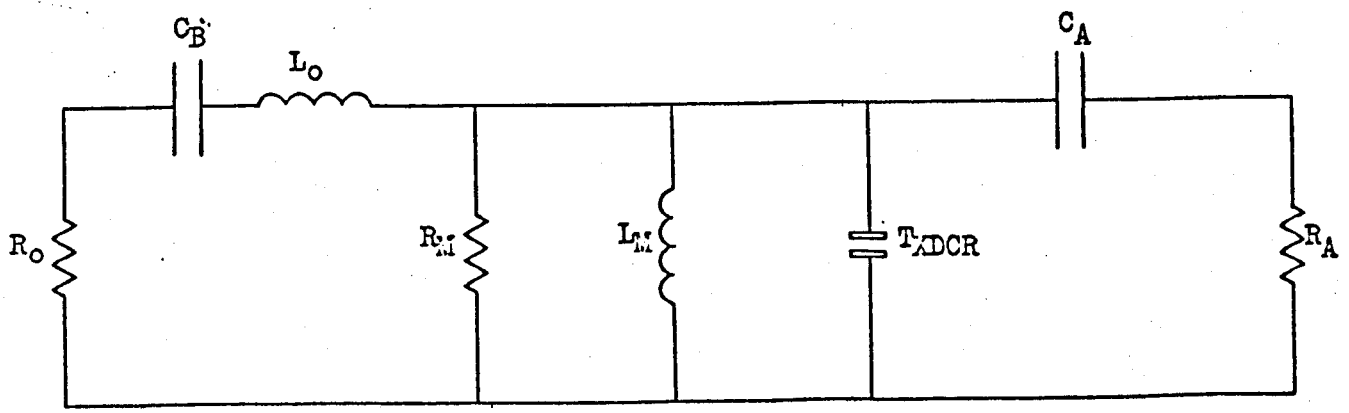

Fig. 7.24. General Electrical Loading Conditions for the Pulse-Echo Receiver

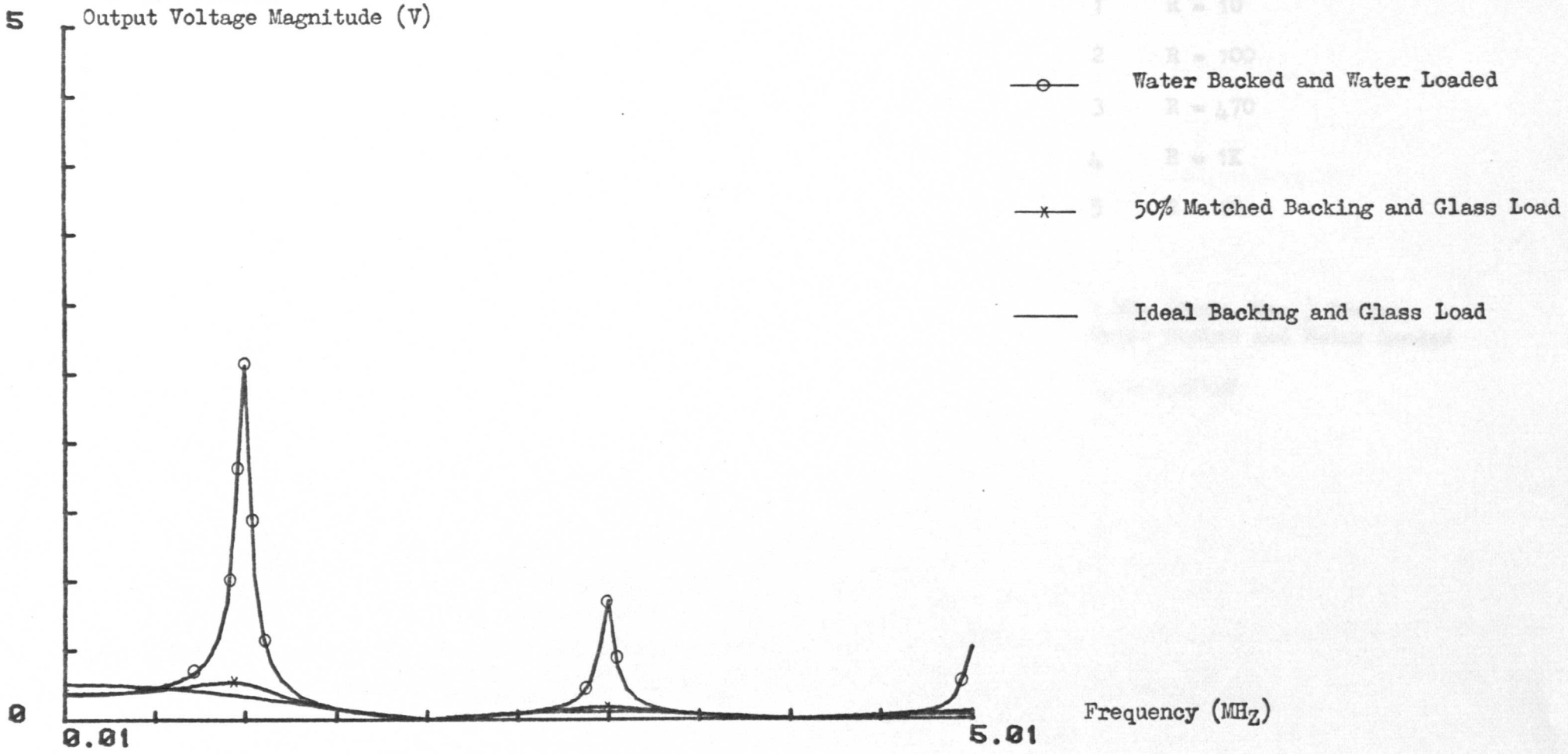

Fig. 7.25. Frequency Characteristics of a Receiver on Electrical Open Circuit

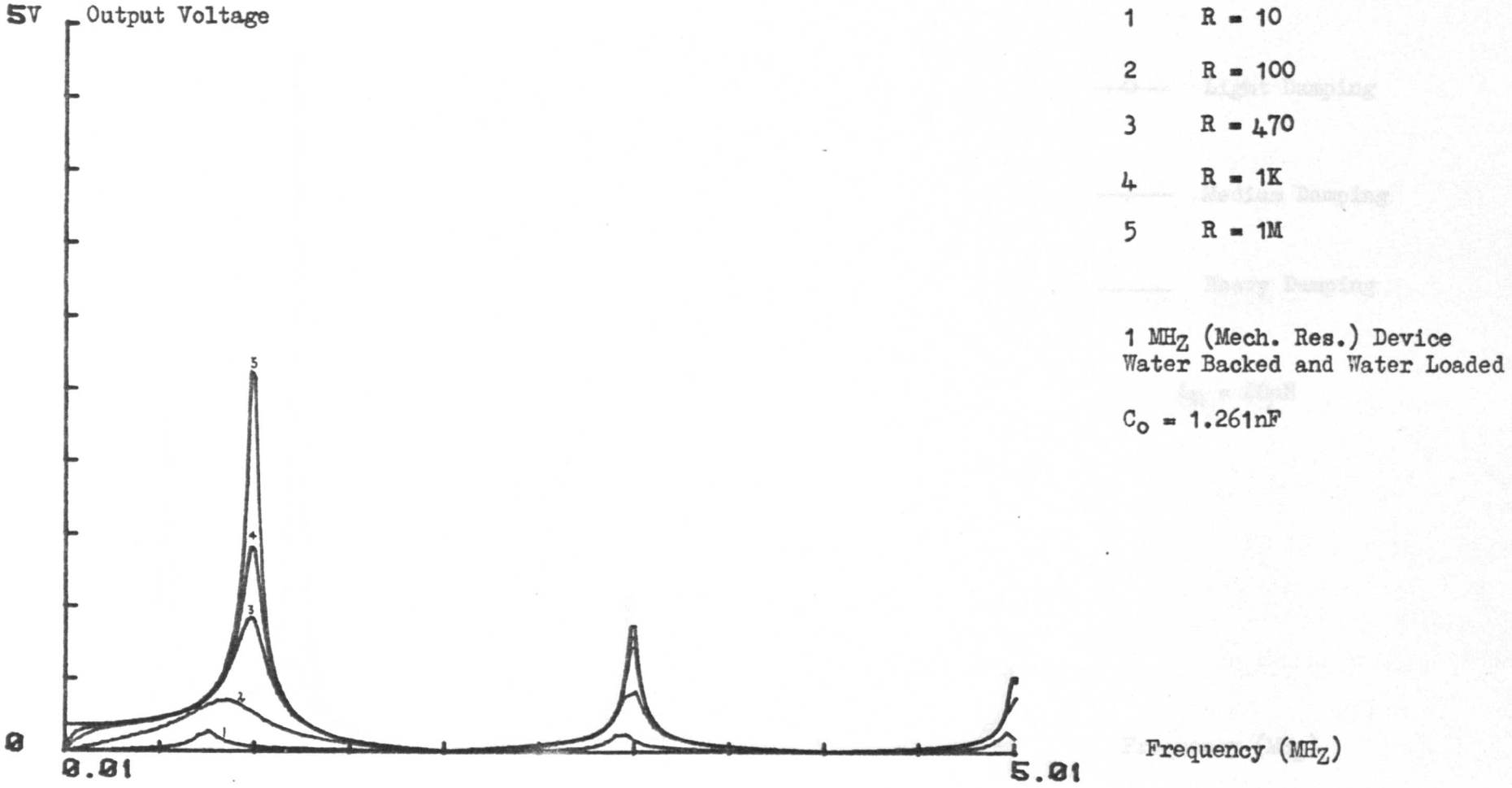

Fig. 7.26. Receiver Frequency Characteristics under Different Conditions of Resistive Load

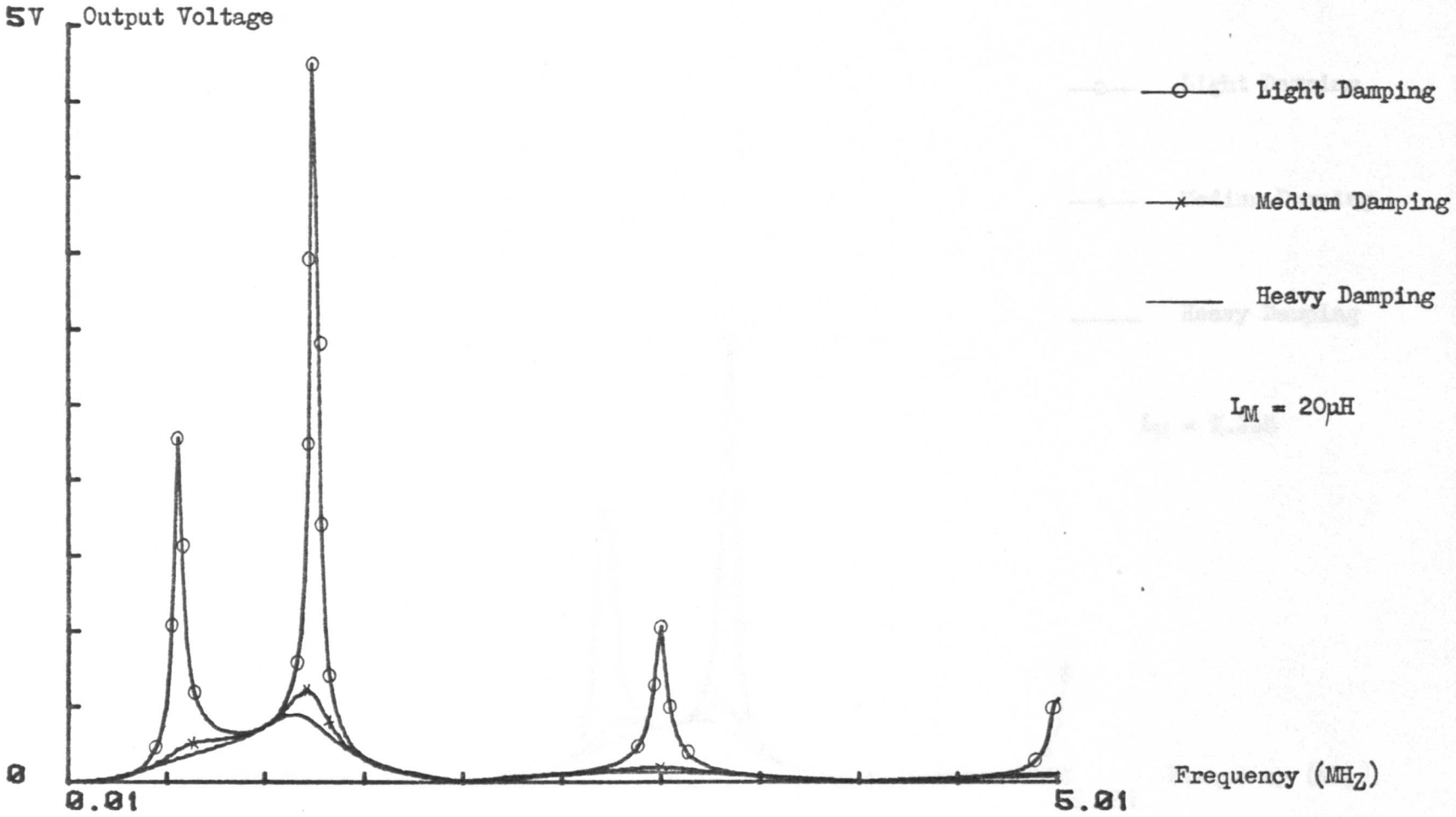

Fig. 7.27a. Frequency Response of a Parallel Inductive Loaded Piezoelectric Receiver

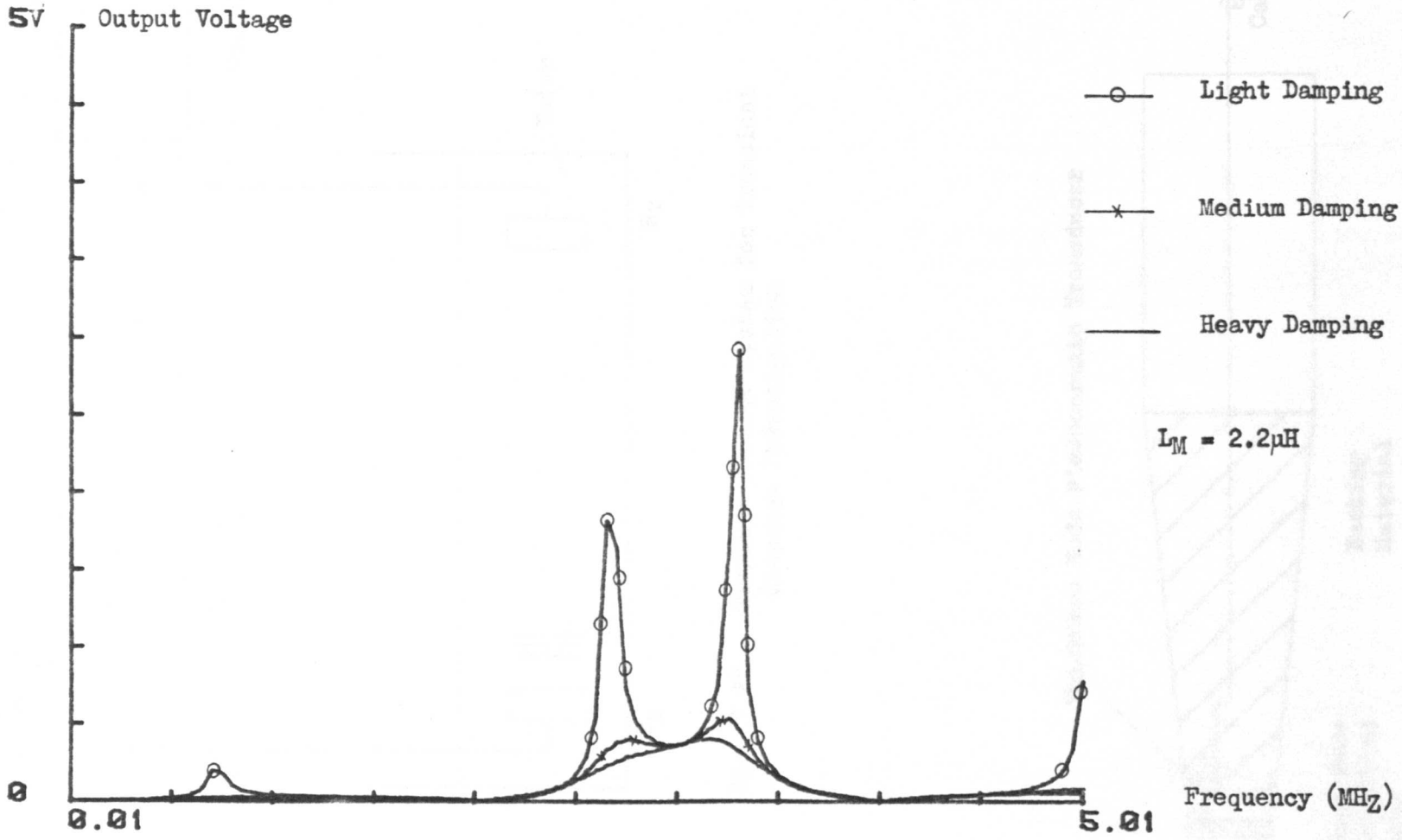

Fig. 7.27b. Frequency Response of a Parallel Inductive Loaded Receiver

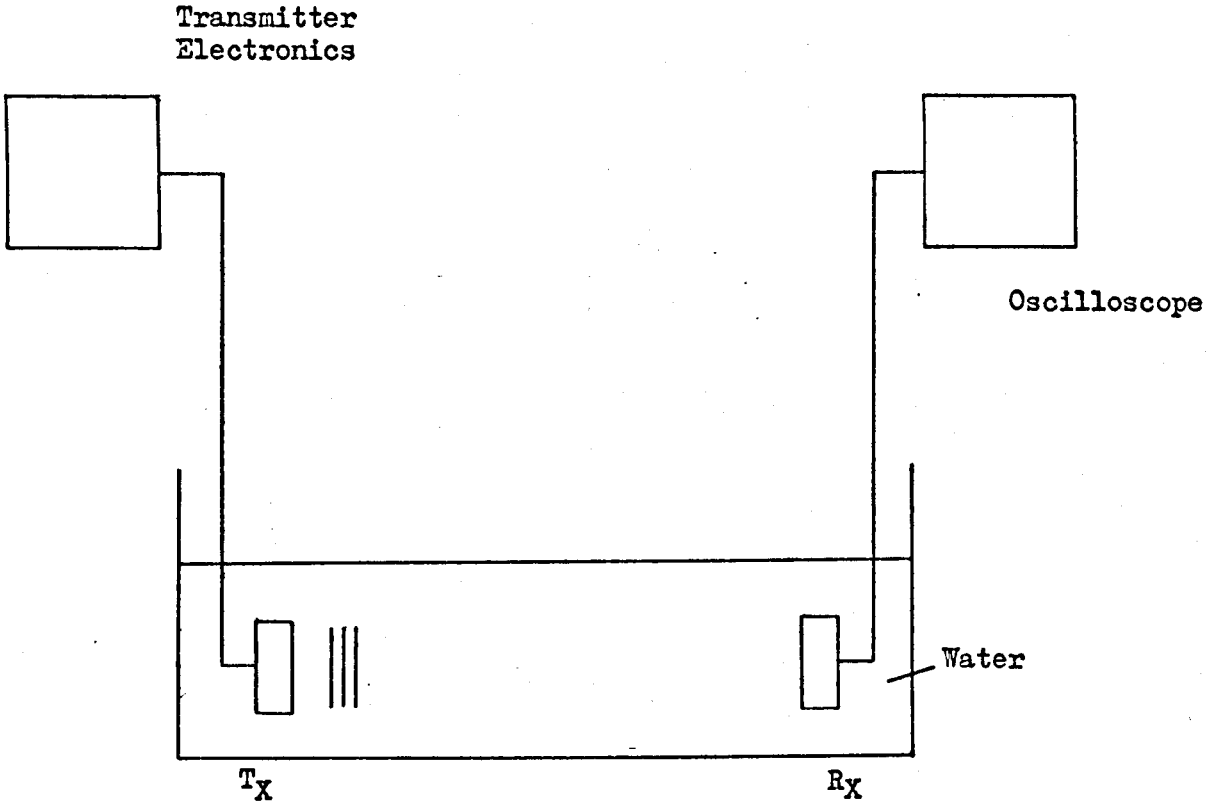

Fig. 7.28. Transmit-Receive System for Transient Response Investigation

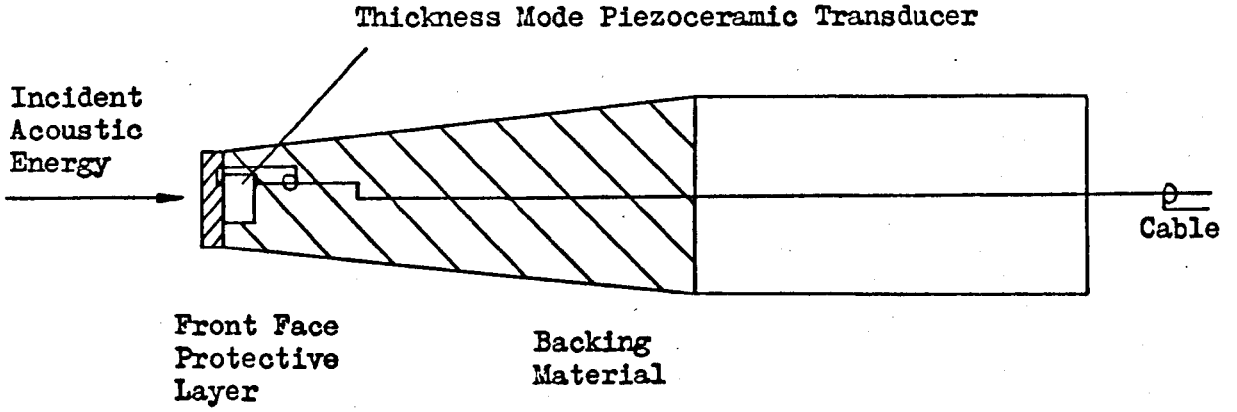

Fig. 7.29. Typical Piezoceramic Hydrophone (Not to Scale)

Longi-tudinal Wave Velocity	Acoustic Impedance	Dielectric Constant	Piezo-electric Constant (h)	Transit Time	Mechanical Resonance	Area of Active Element	Coupling Coefficient	Capacitance (static) of Active Element
m/s	kg/m^2-s		V/m	ns	MHz	m^2		pf
2200	3.916	8	1.65×10^9	11.36	44	$.785 \times 10^{-6}$	.15	2.223

All Parameters Refer to the Thickness Mode

Table 7.1. Physical Properties of the PVDF Membrane Hydrophone

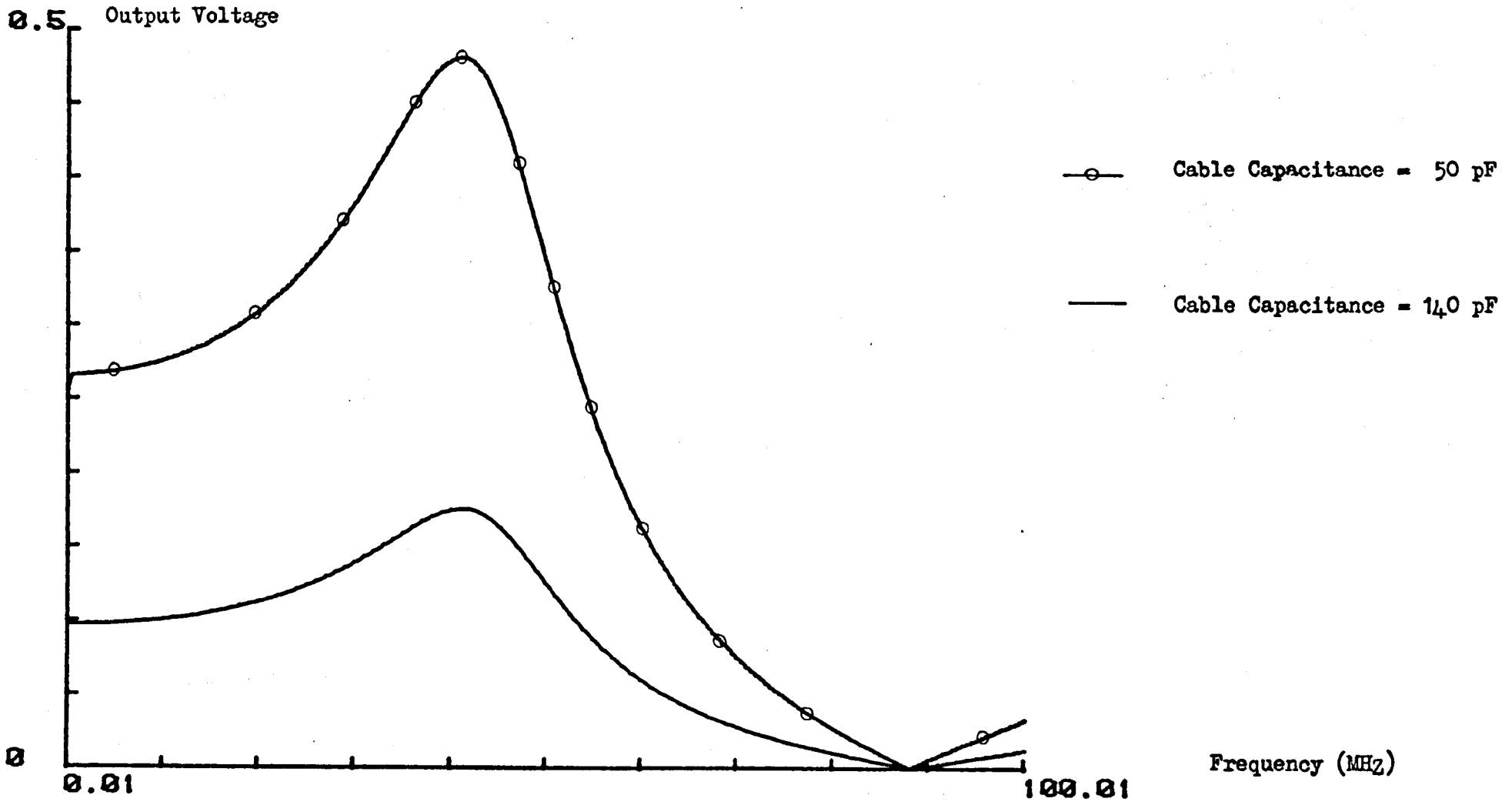

Fig. 7.30. Frequency Response Characteristics of the PVDF Hydrophone/Cable Combination

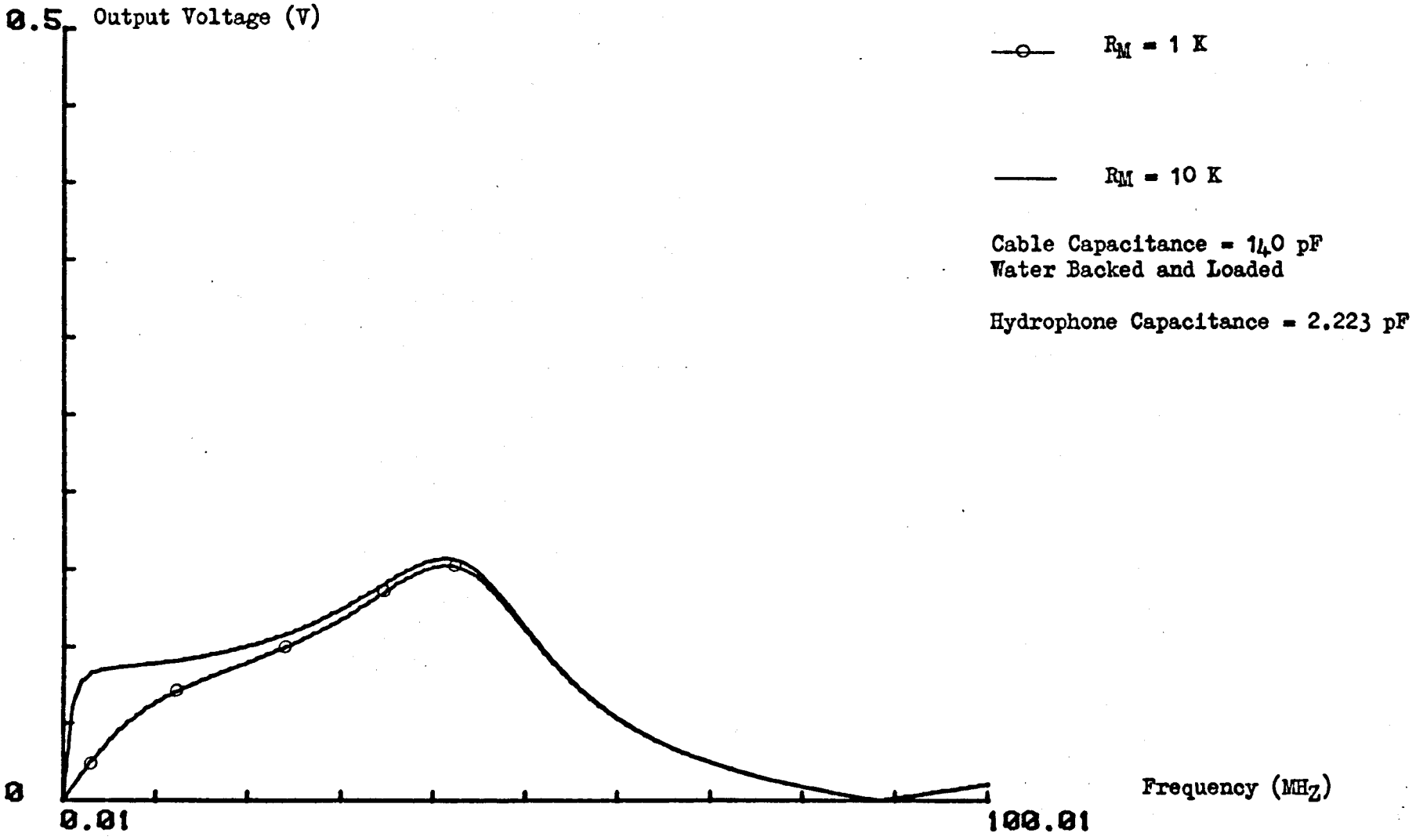

Fig. 7.31. Frequency Response of a Restively Loaded PVDF Hydrophone/Cable Combination

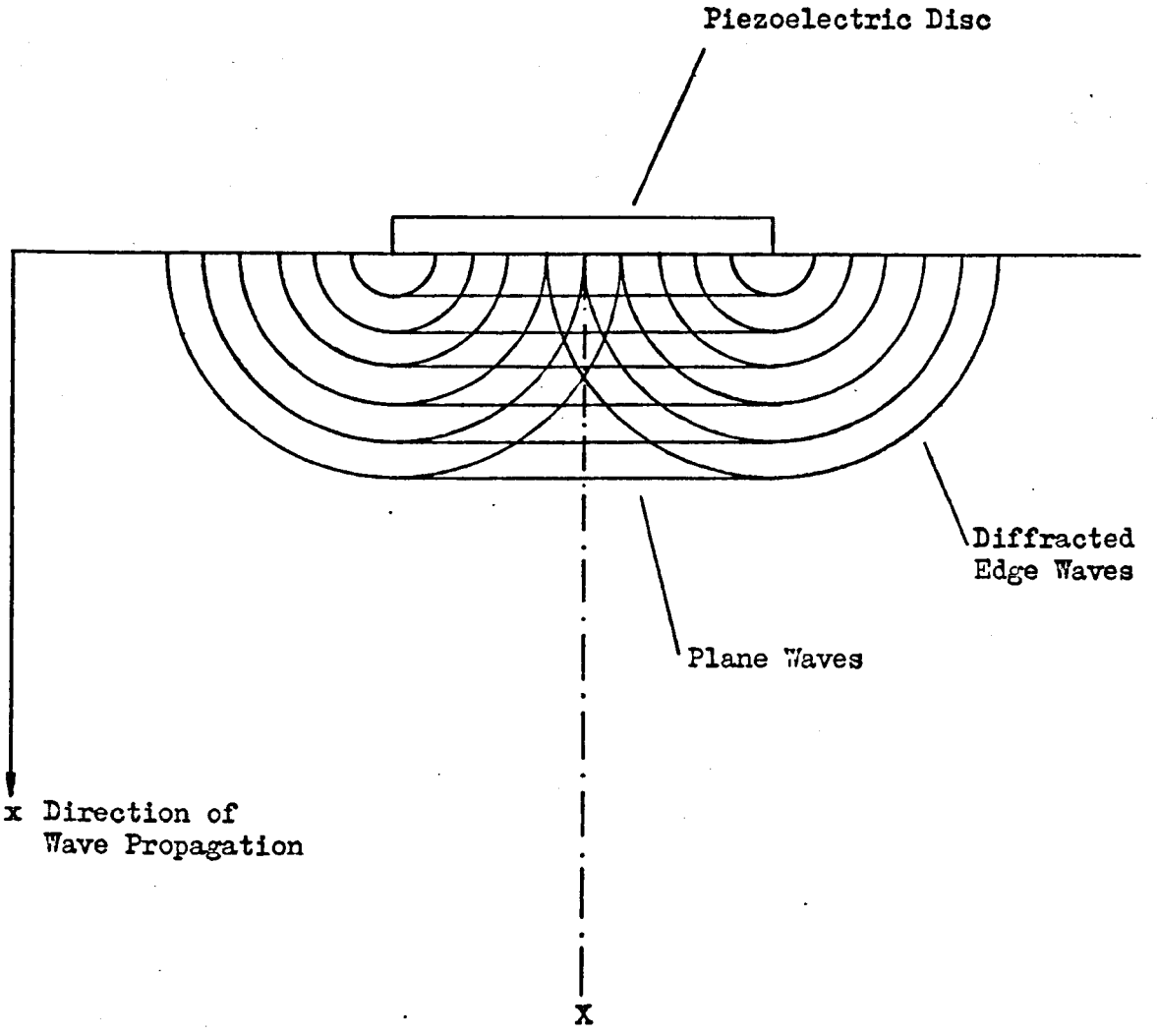

Fig. 7.32. Formation of Plane and Edge Waves in the Piezoelectric Disc Transducer

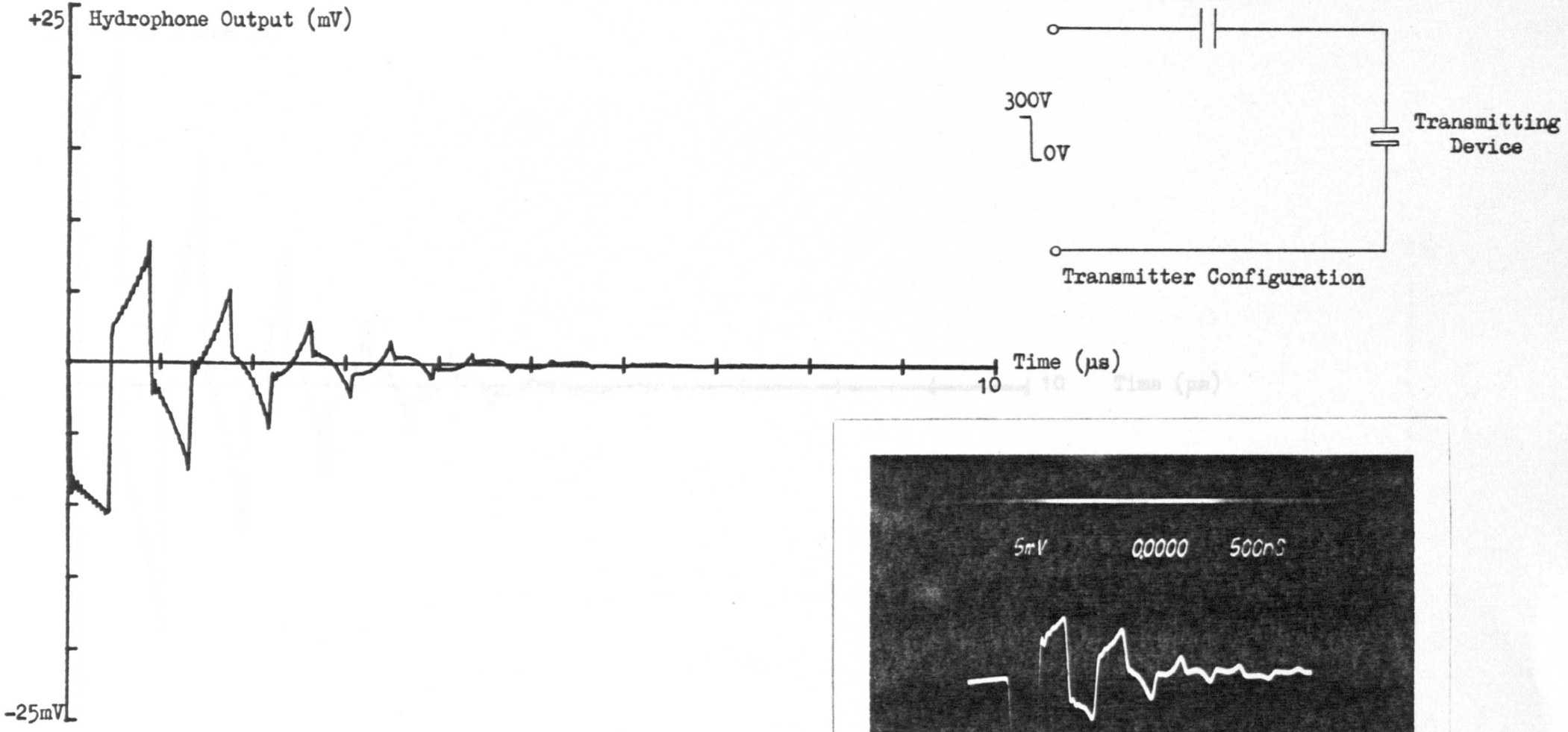

Fig. 7.33. Comparison of Simulated and Experimental Wave Profiles using the PVDF Hydrophone

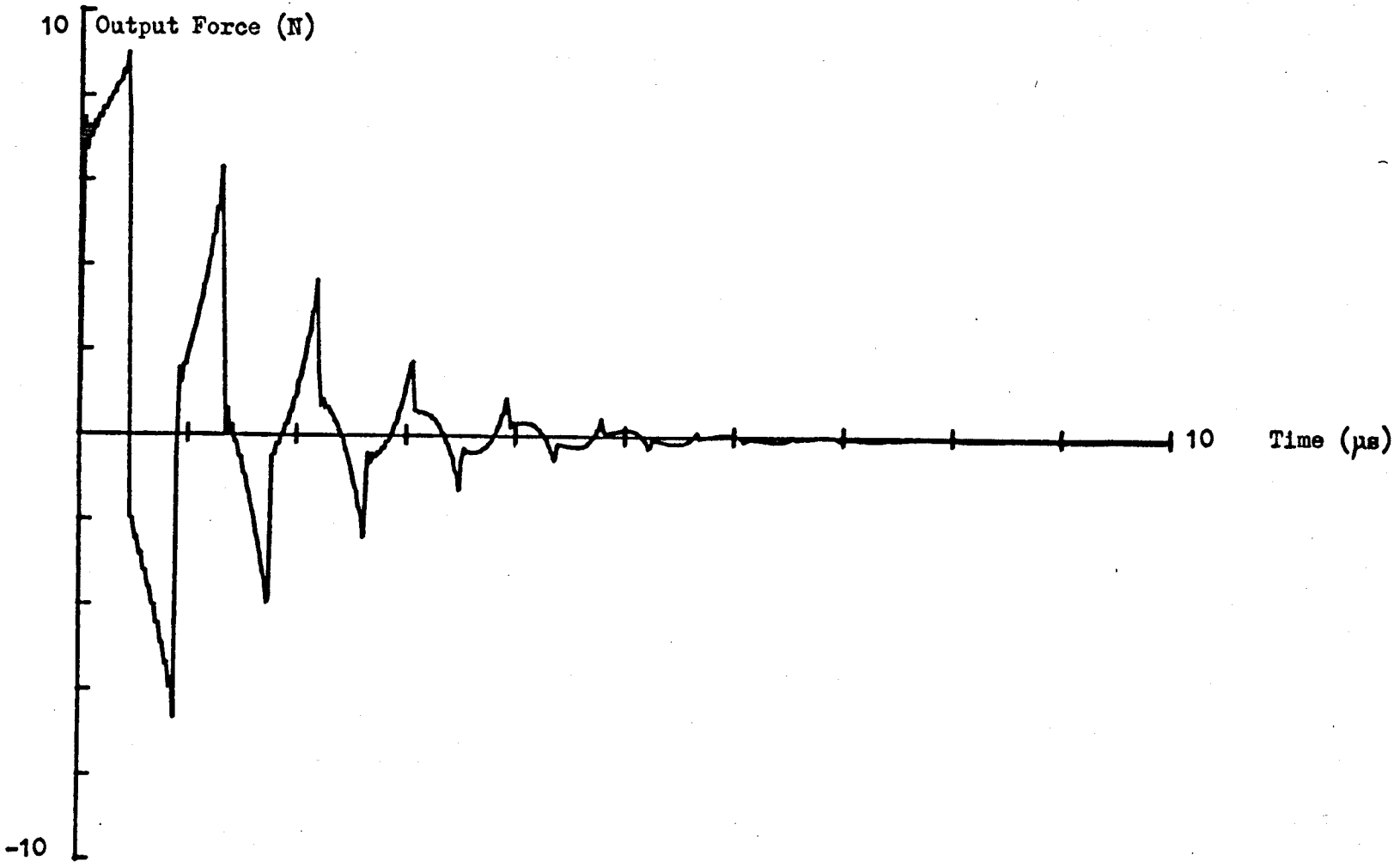

Fig. 7.34. Plane Wave Profile of Output Force (300V Step Input)

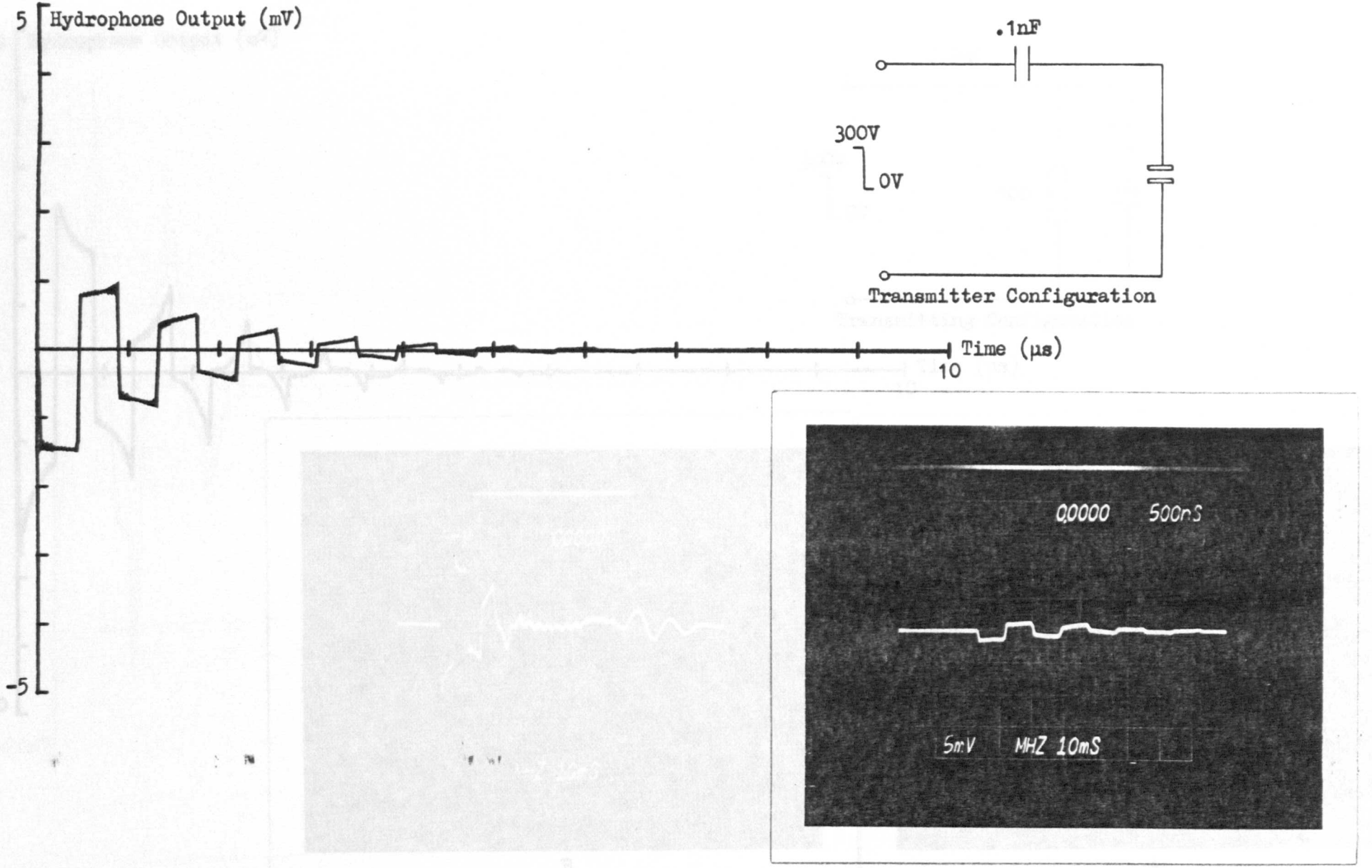

Fig. 7.35. Comparison of Simulated and Experimental Results using the PVDF Hydrophone

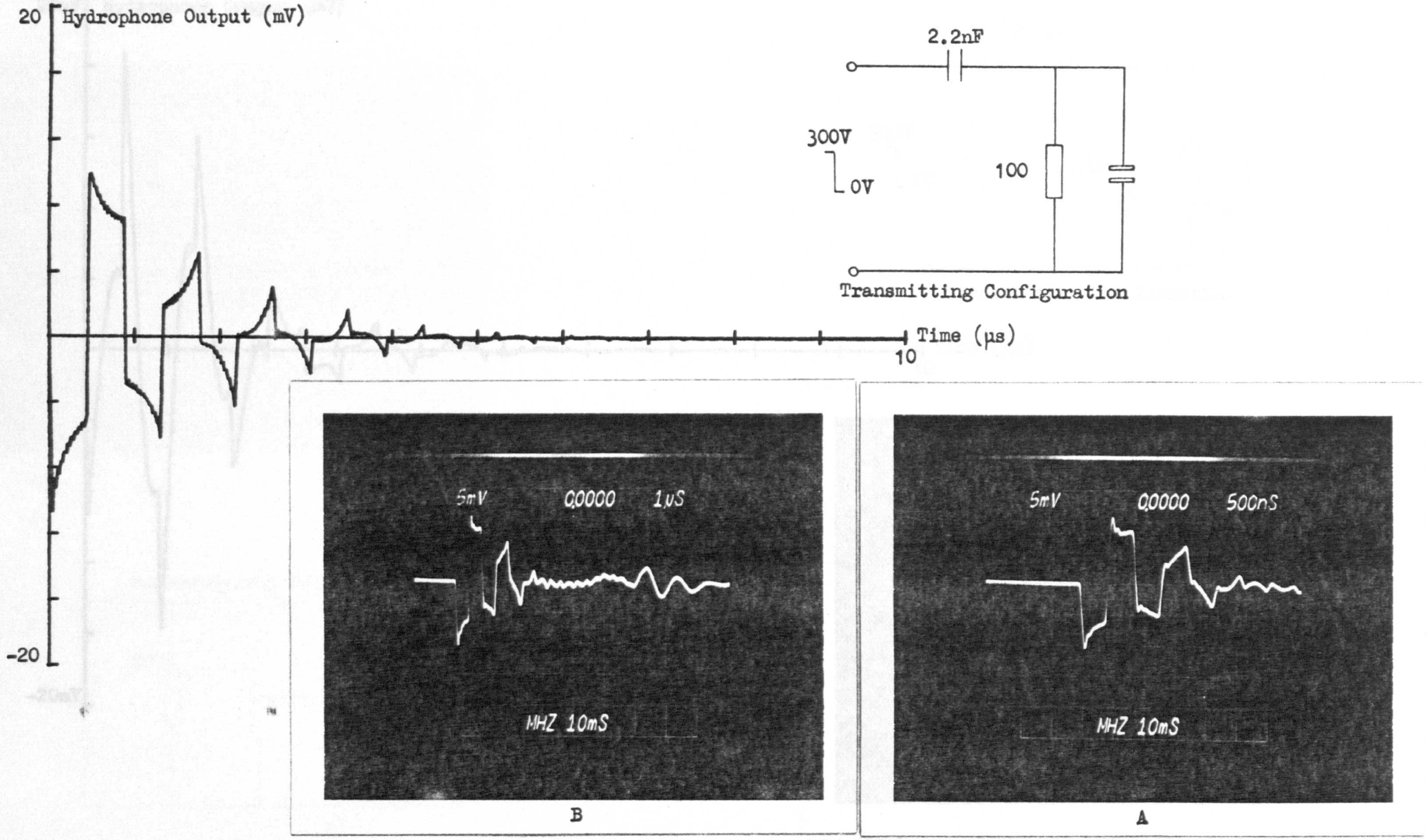

Fig. 7.36. Comparison of Simulated and Experimental Results using the PVDF Hydrophone

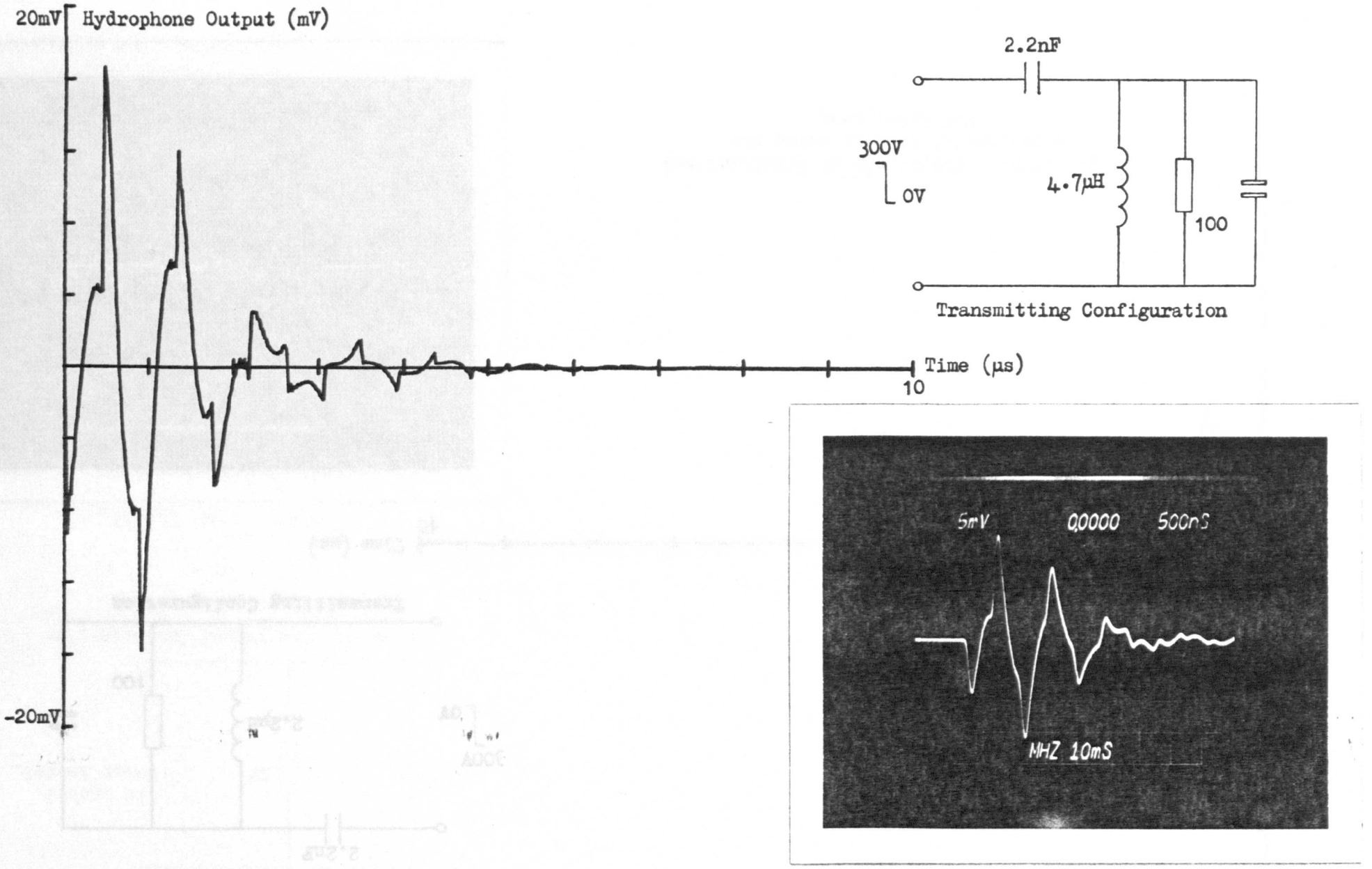

Fig. 7.37a. Comparison of Simulated and Experimental Results using the PVDF Hydrophone

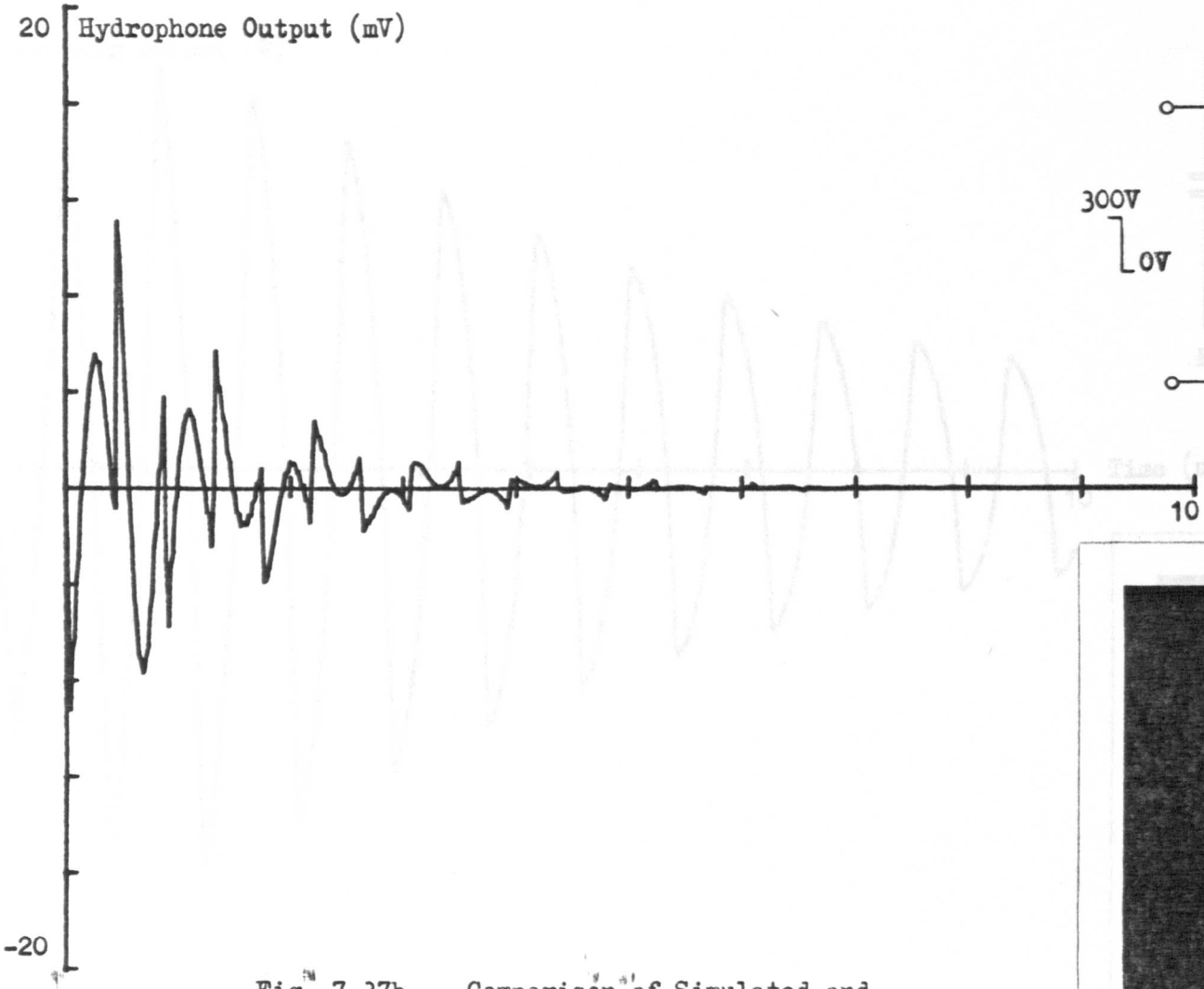

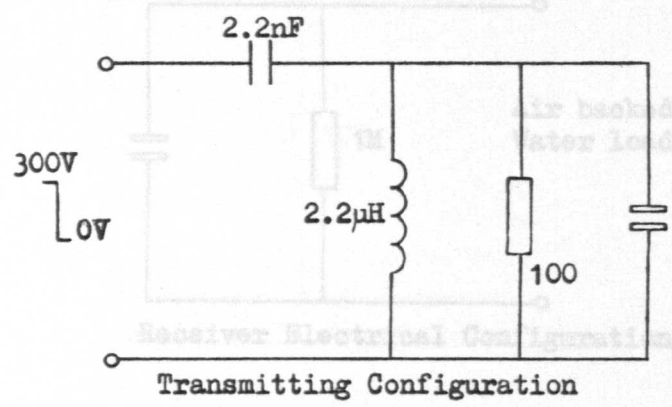

Transmitting Configuration

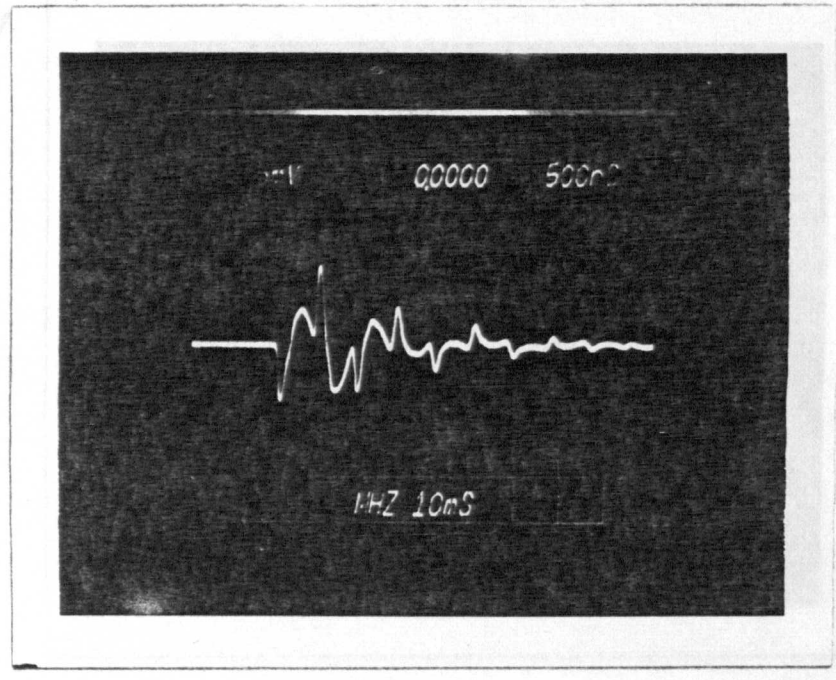

Fig. 7.37b. Comparison of Simulated and Experimental Results using the PVDF Hydrophone

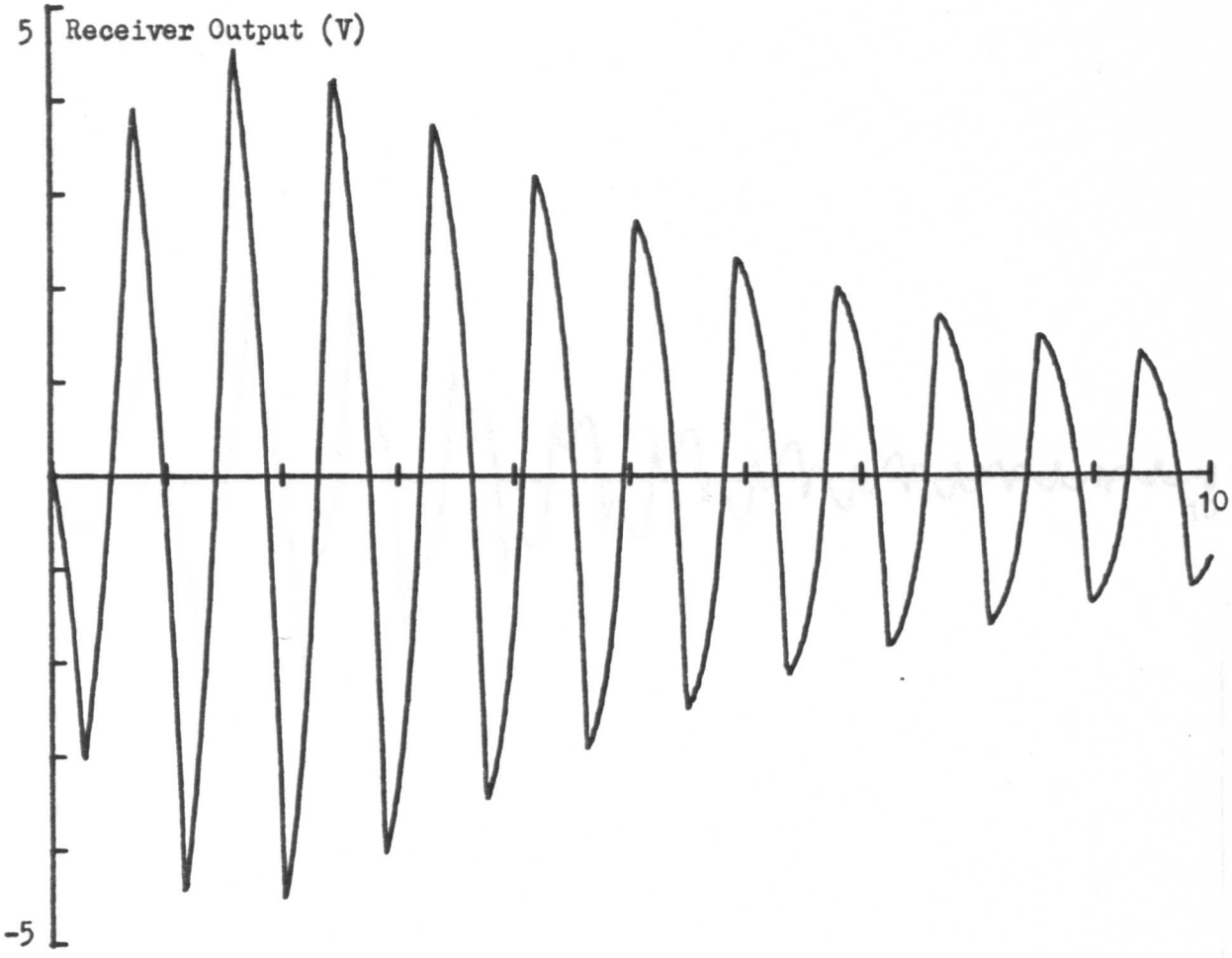

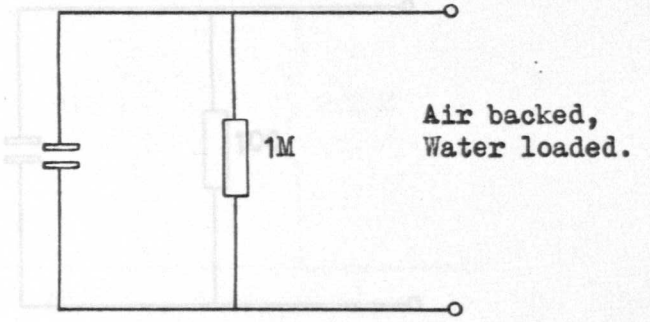

Receiver Electrical Configuration

Scale: Inner Graticule

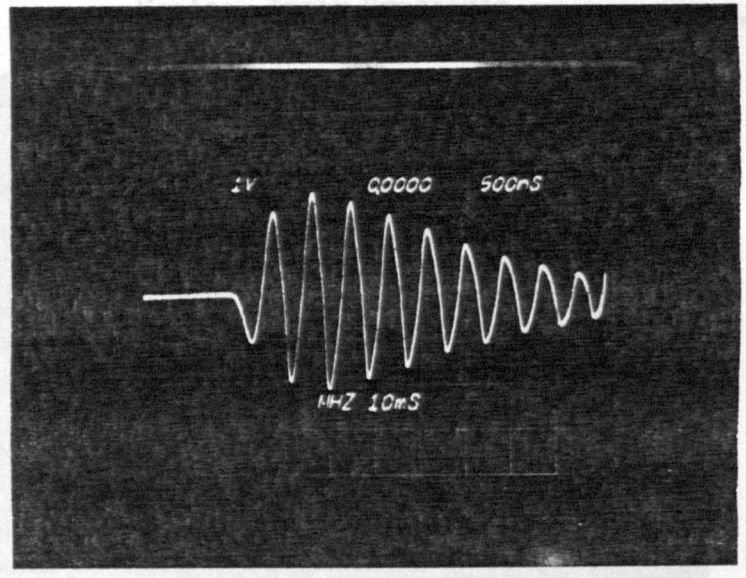

Fig. 7.38 Comparison of Experimental and Simulated Loop Responses

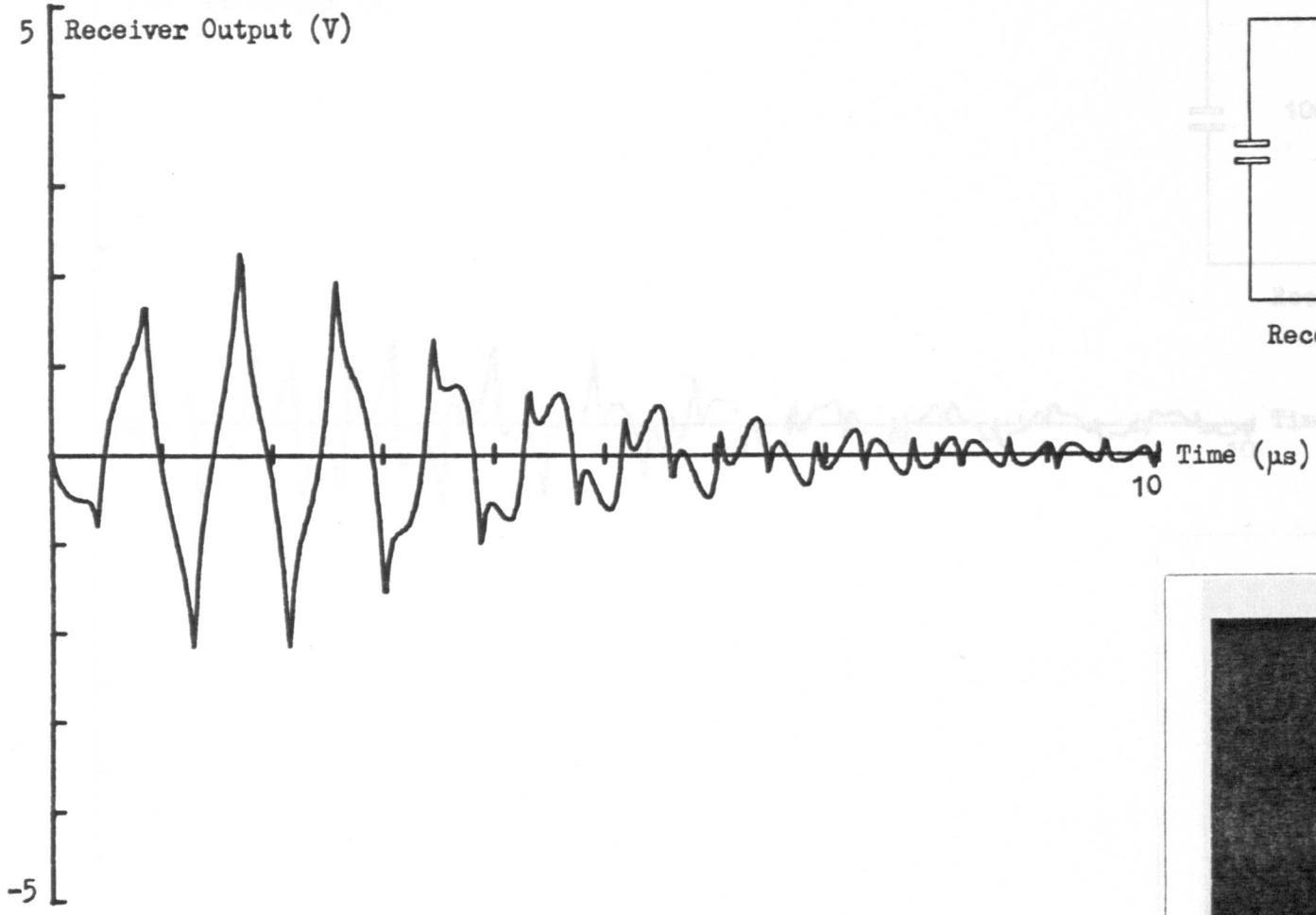

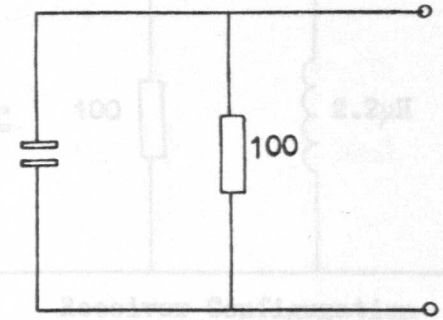

Receiver Configuration

Scale: Inner Graticule

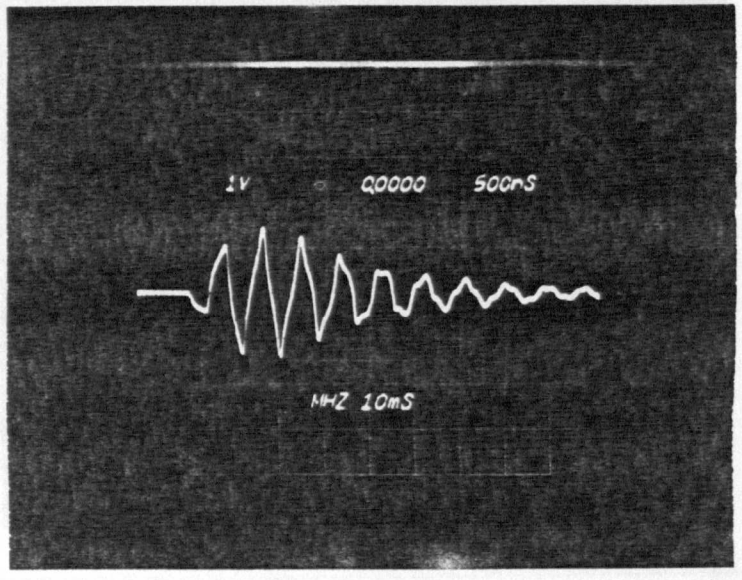

Fig. 7.39 Comparison of Experimental and Simulated Loop Response Characteristics

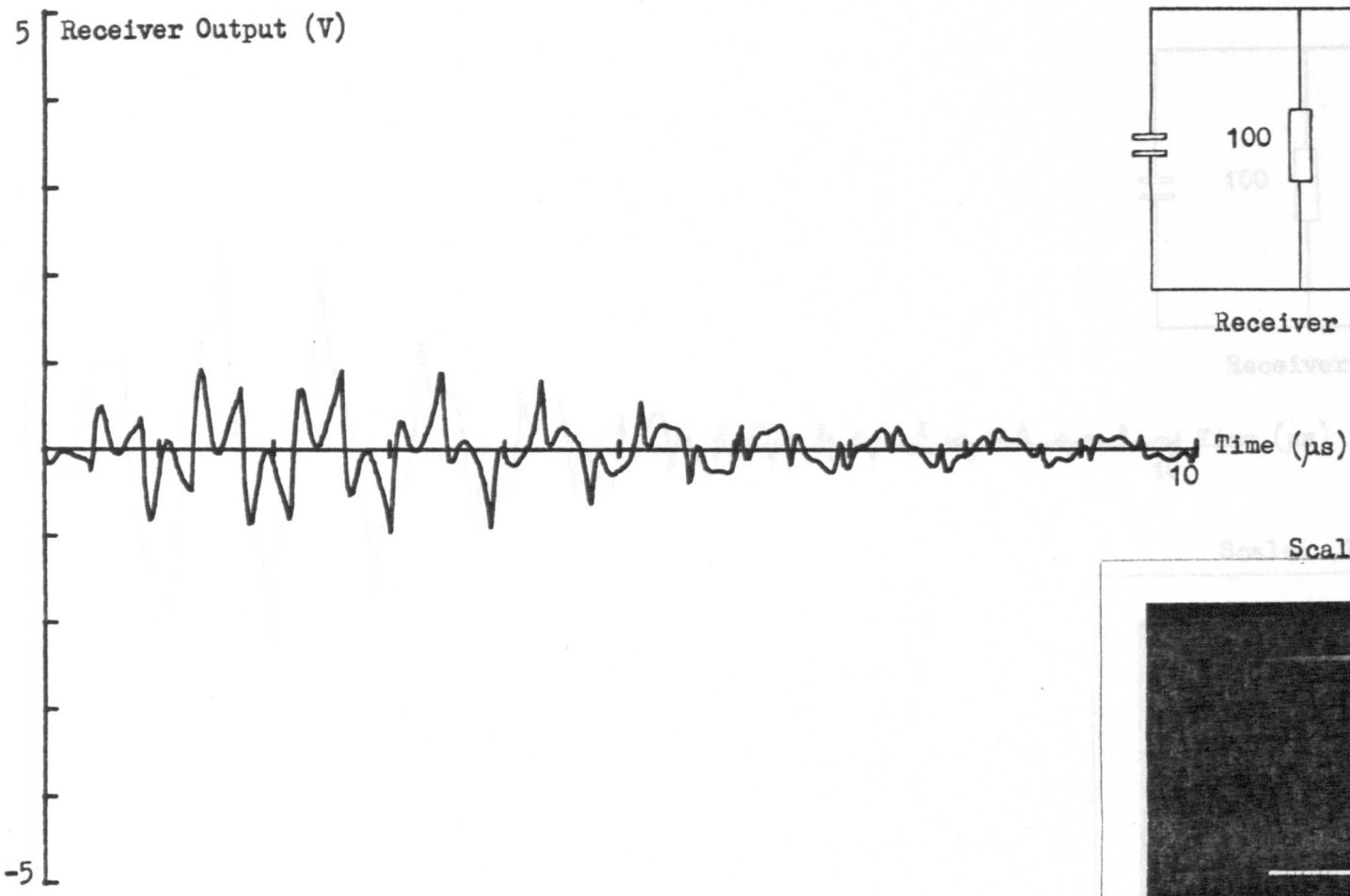

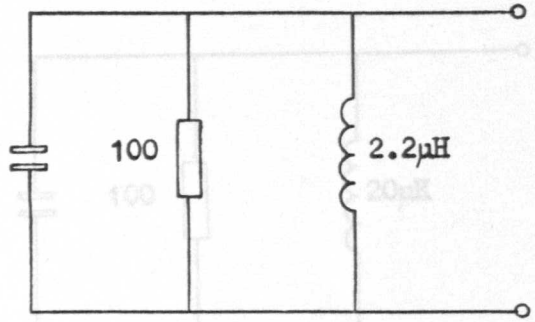

Receiver Configuration

Scale: Inner Graticule

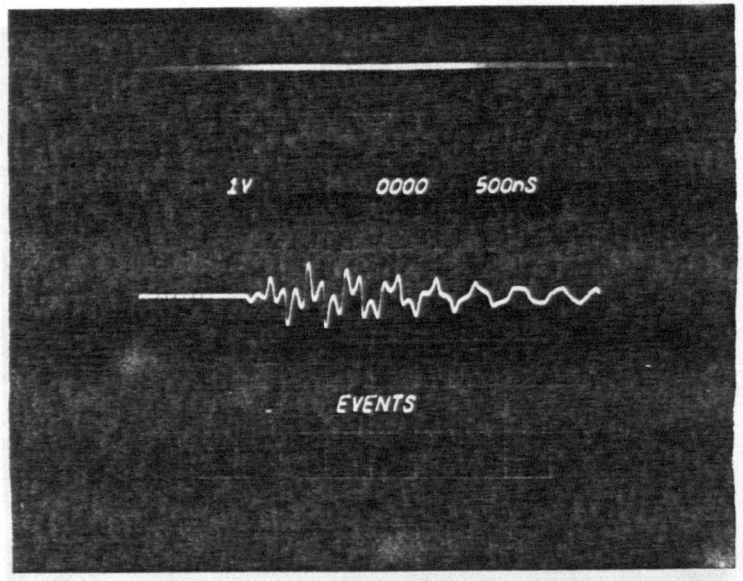

Fig. 7.40a Comparison of Experimental and Simulated Loop Response Characteristics

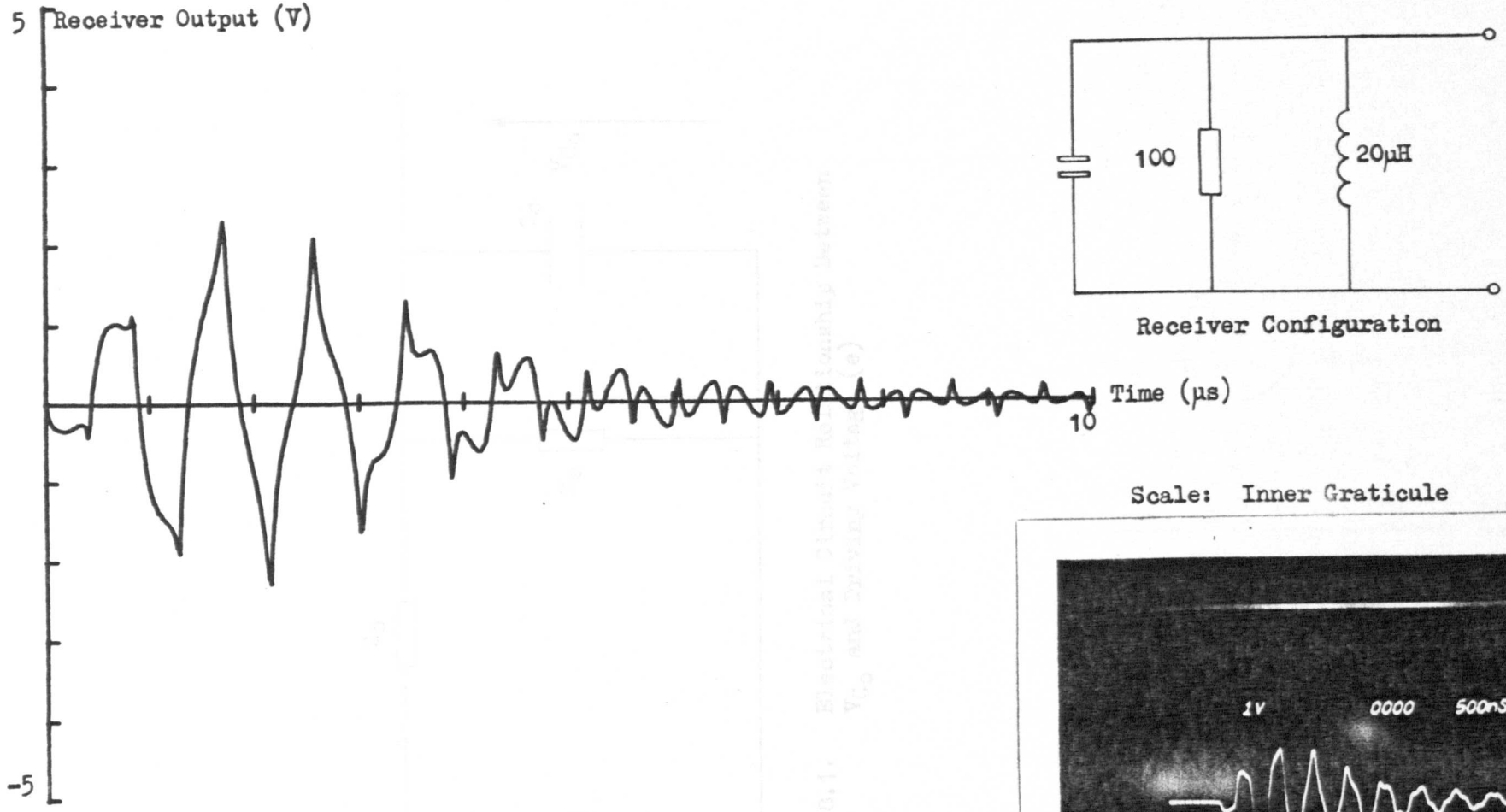

Receiver Configuration

Scale: Inner Graticule

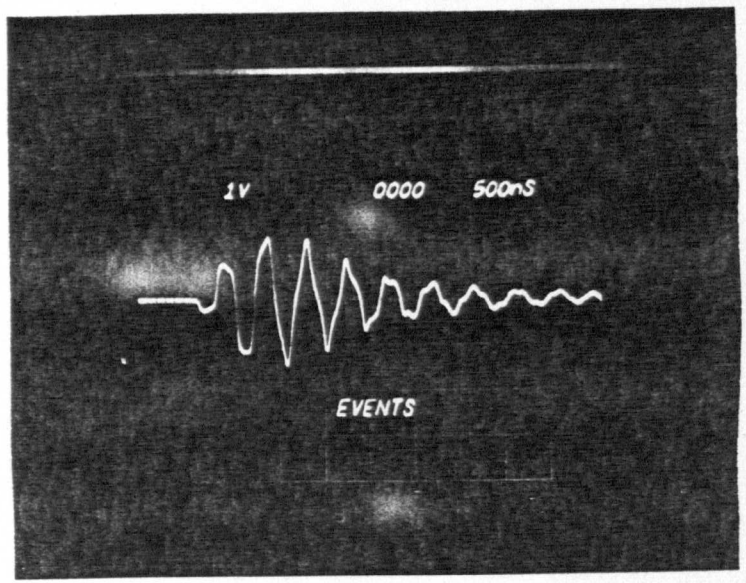

Fig. 7.4Ob Comparison of Experimental and Simulated Loop Response Characteristics

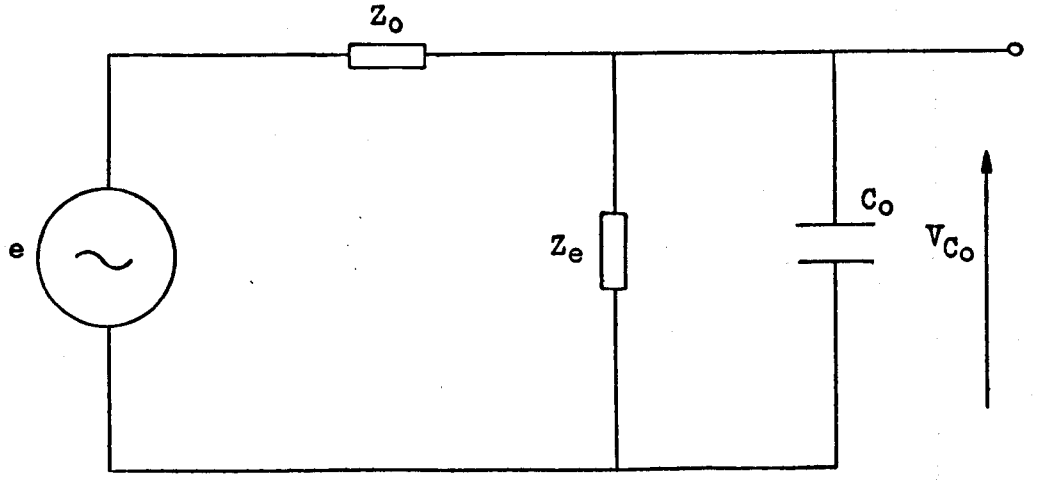

Fig. 8.1. Electrical Circuit Relationship Between V_{C_o} and Driving Voltage (e)

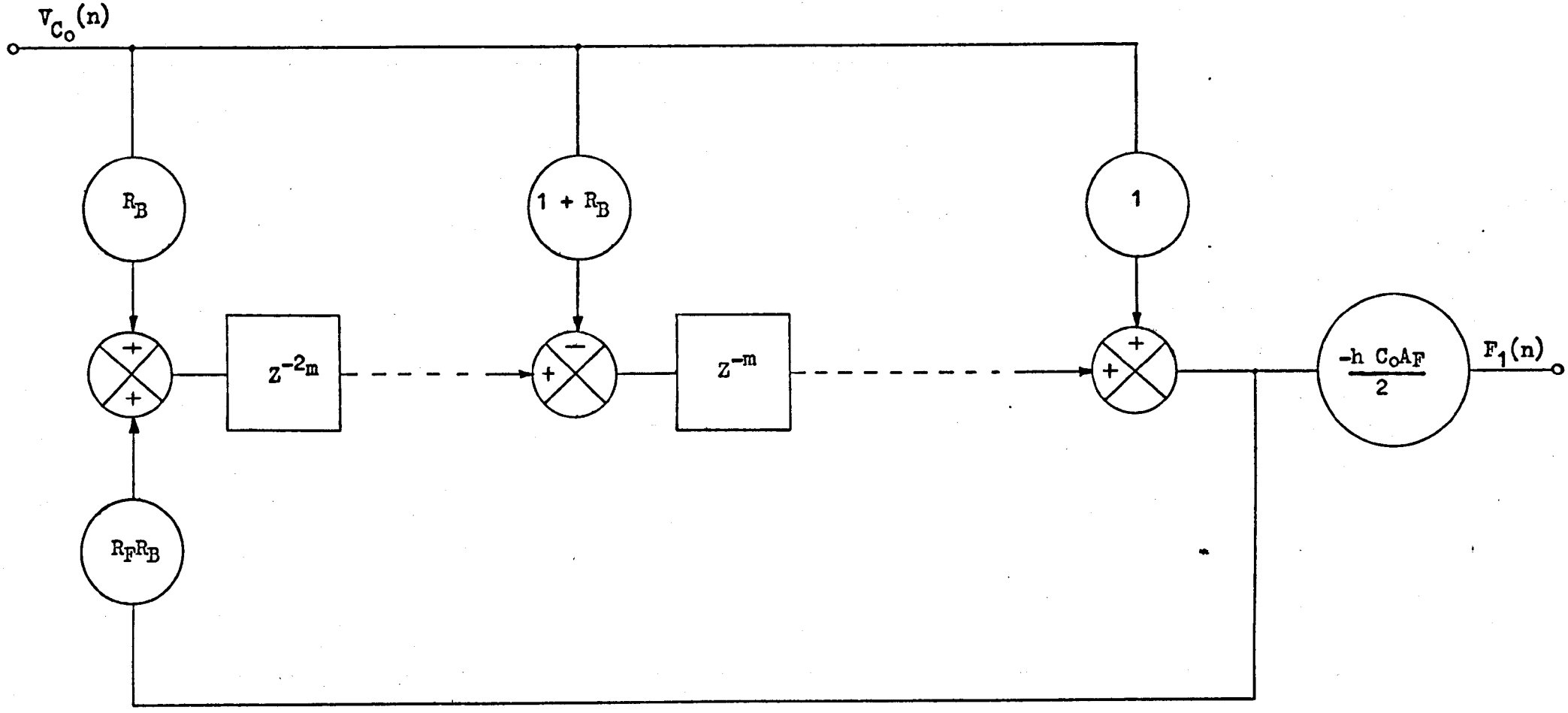

Fig. 8.2. Recursive Model for the Open Loop Transmitter

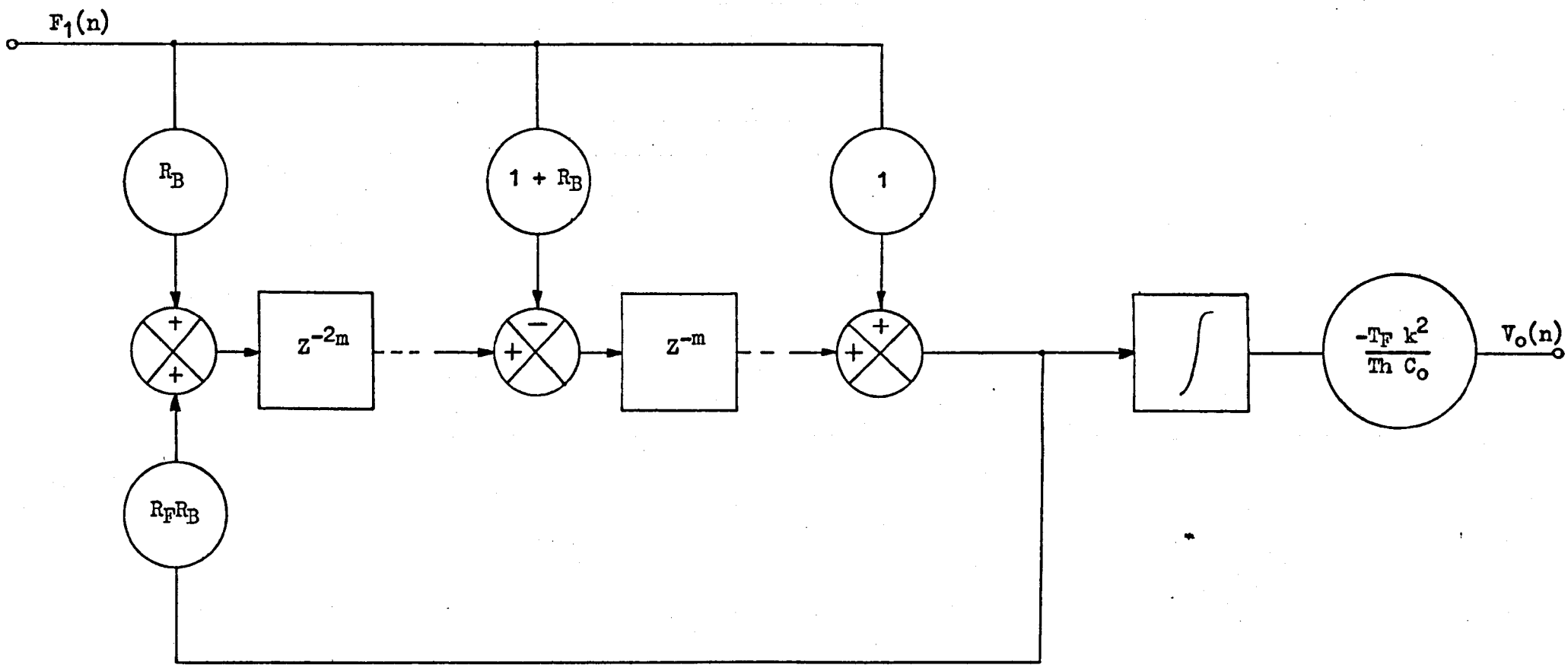

Fig. 8.3. Recursive Model for the Open Loop Receiver

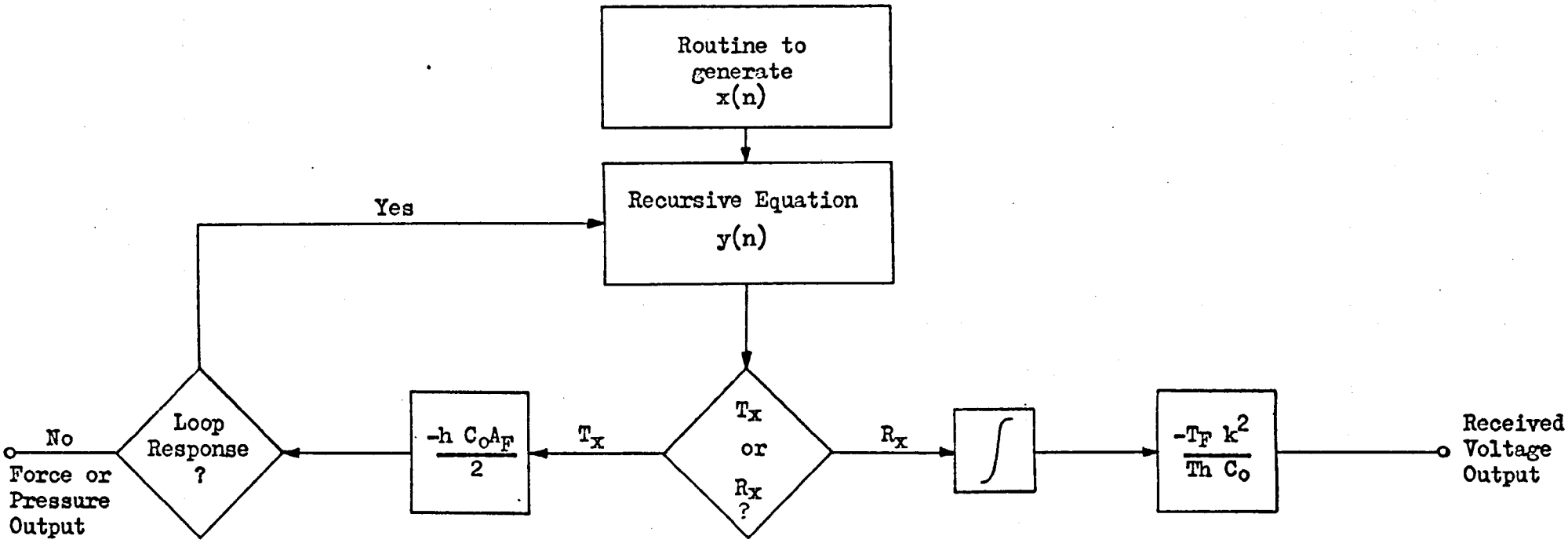

Fig. 8.4. Program Flowchart

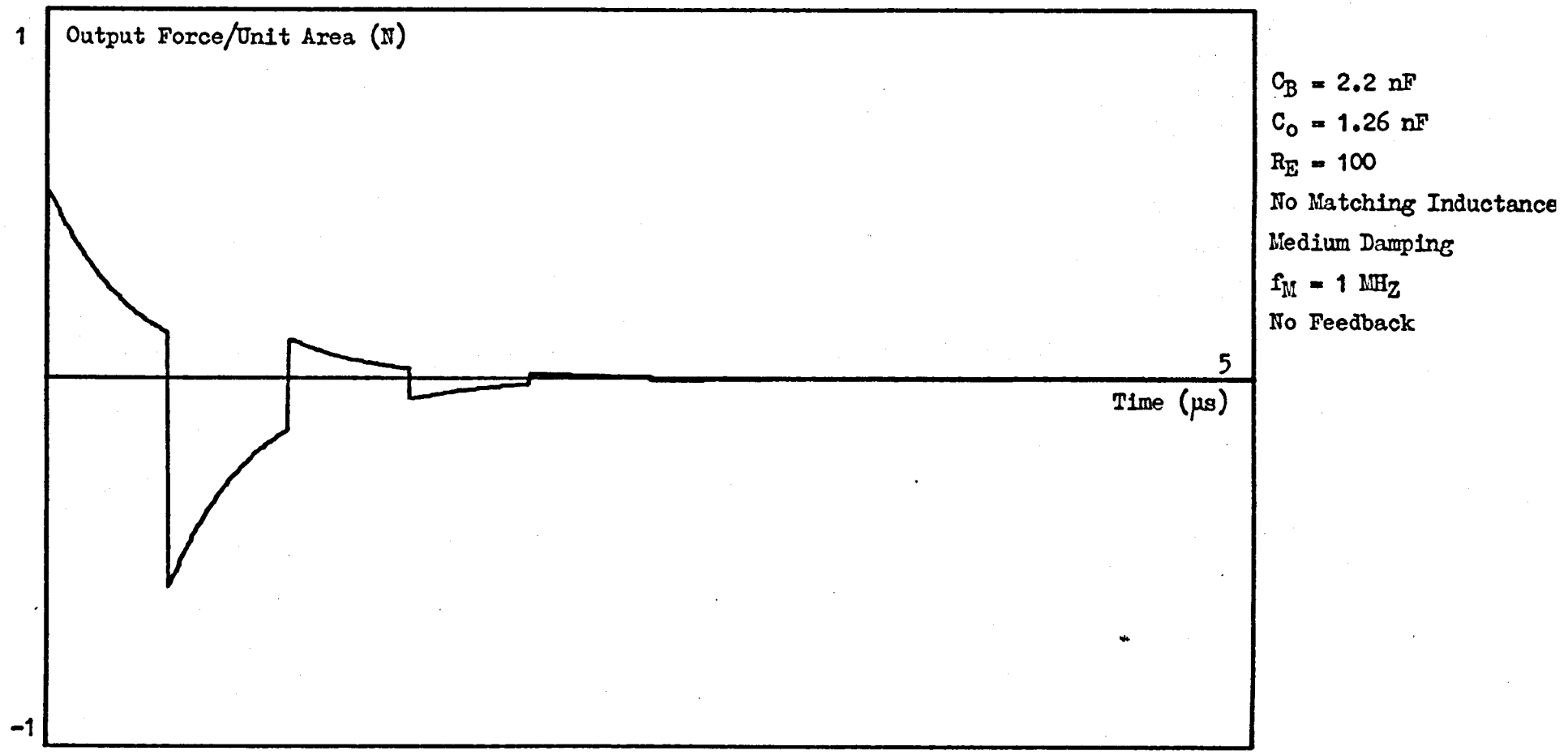

Fig. 8.5a. Approximate Form of Output Force (Z-Transform Solution)

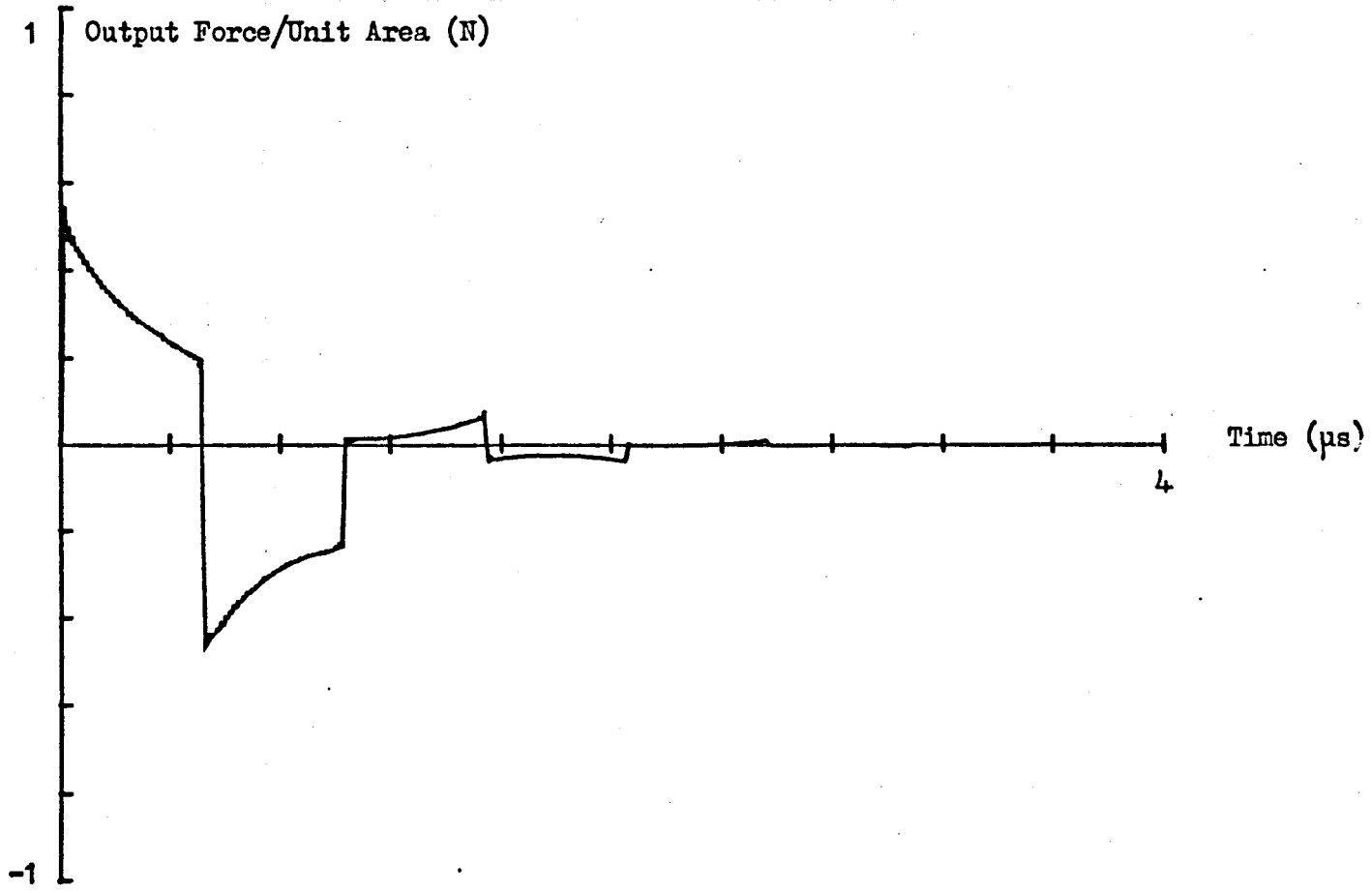

K = 0.48
C_B = 2.2 nF
C_o = 1.26 nF
R_E = 100
No Matching Inductance
Medium Damping
f_M = 1 MHz

Fig. 8.5b. Exact Form of Output Force (IFFT Solution)

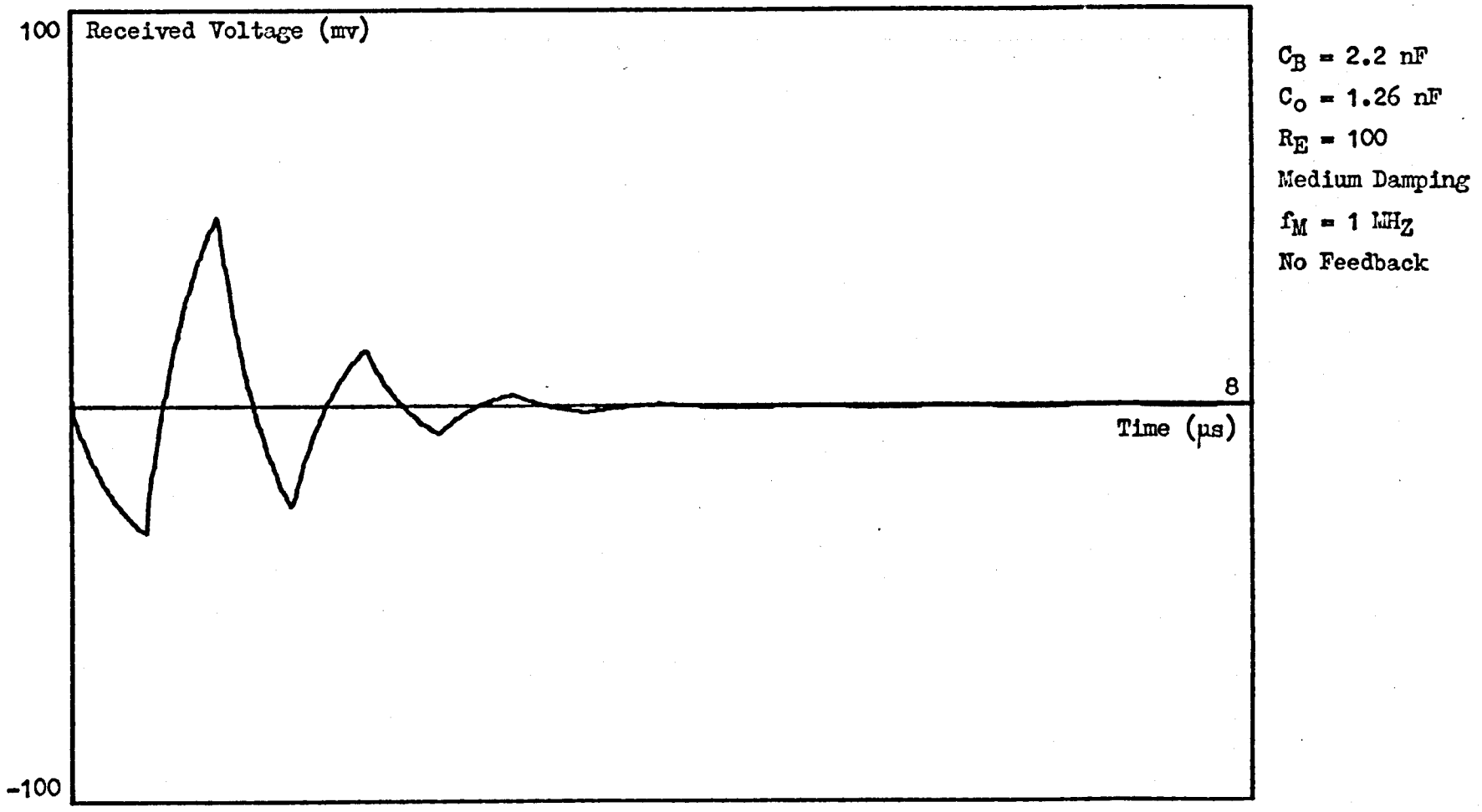

Fig. 8.5c. Received Voltage Waveform (Z-Transform Solution)

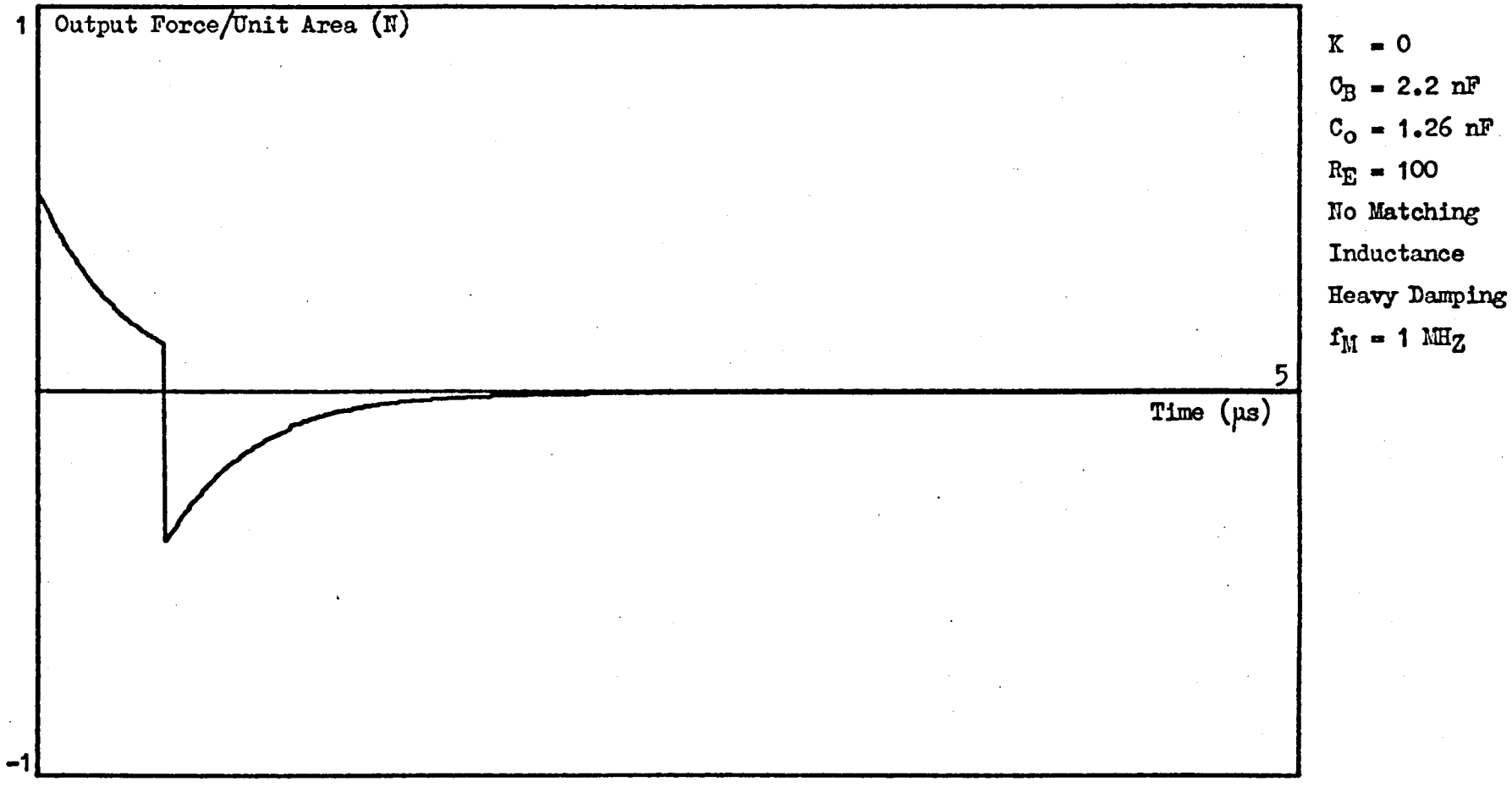

Fig. 8.6a. Approximate Form of Output Force (Z-Transform Solution)

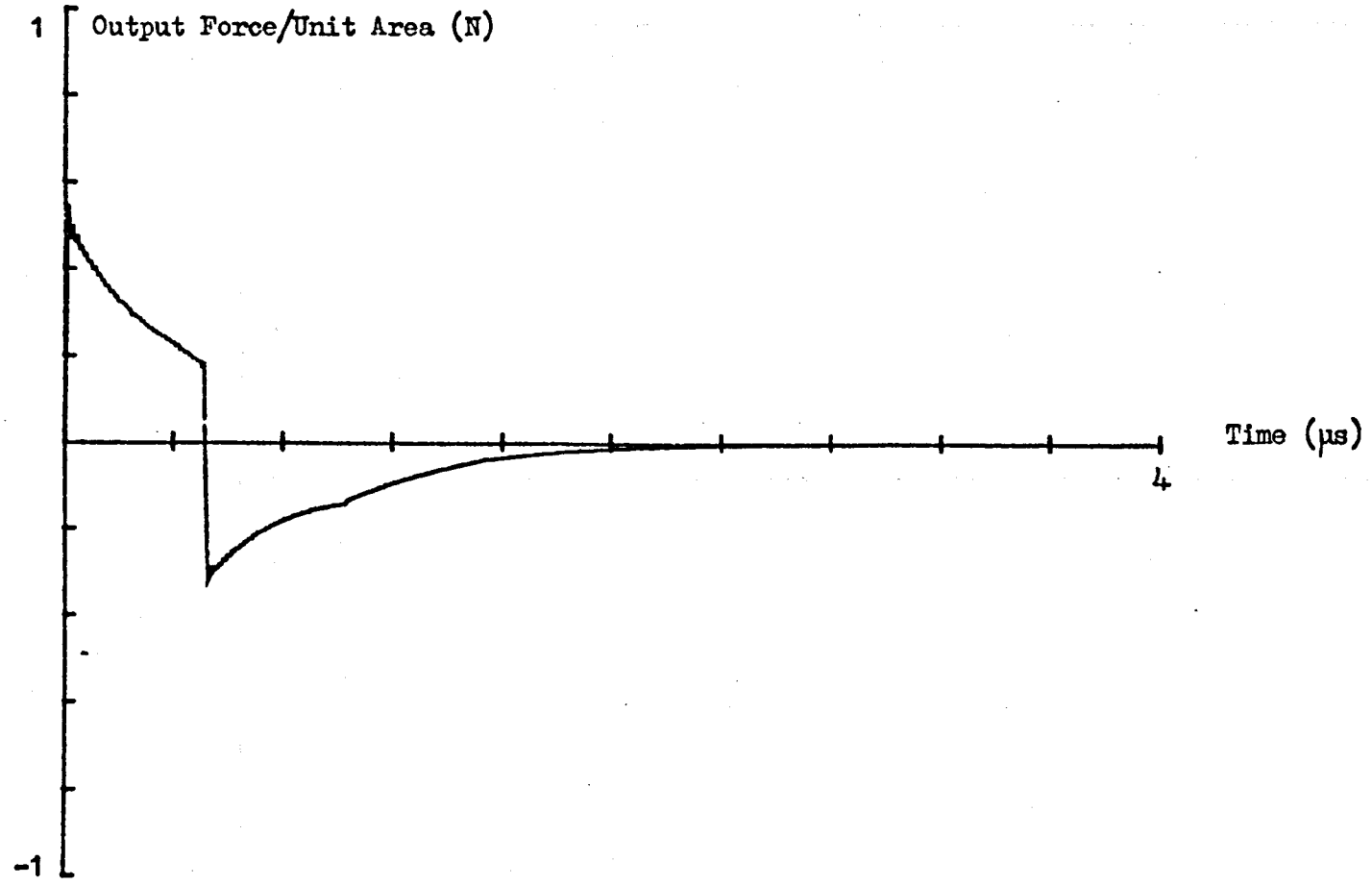

$K = 0.48$

$C_B = 2.2$ nF

$C_o = 1.26$ nF

$R_E = 100$

No Matching Inductance

Heavy Damping

$f_M = 1$ MHz

Fig. 8.6b. Exact Form of Output Force (IFFT Solution)

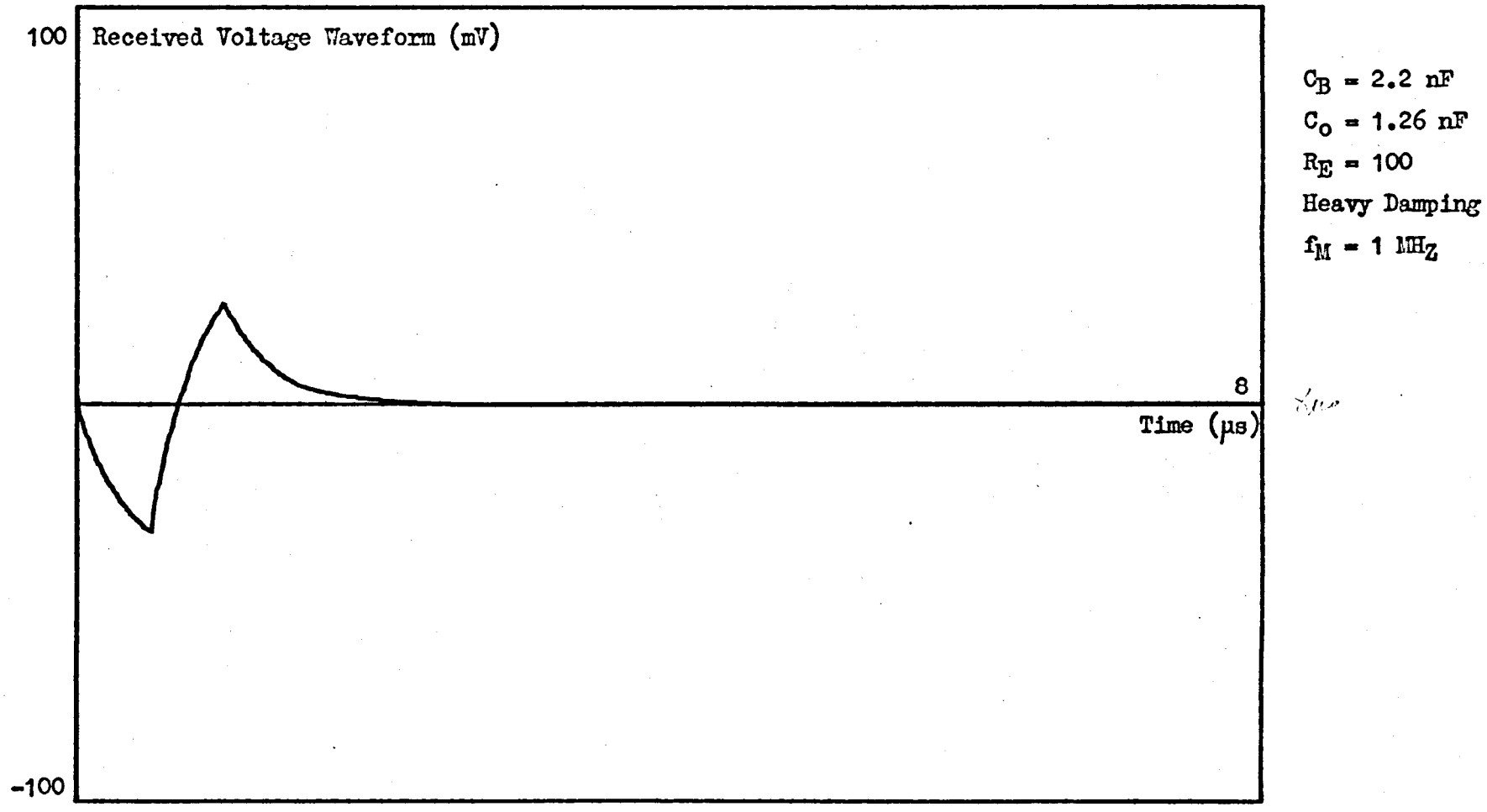

Fig. 8.6c. Received Voltage Waveform (Z-Transform Solution)

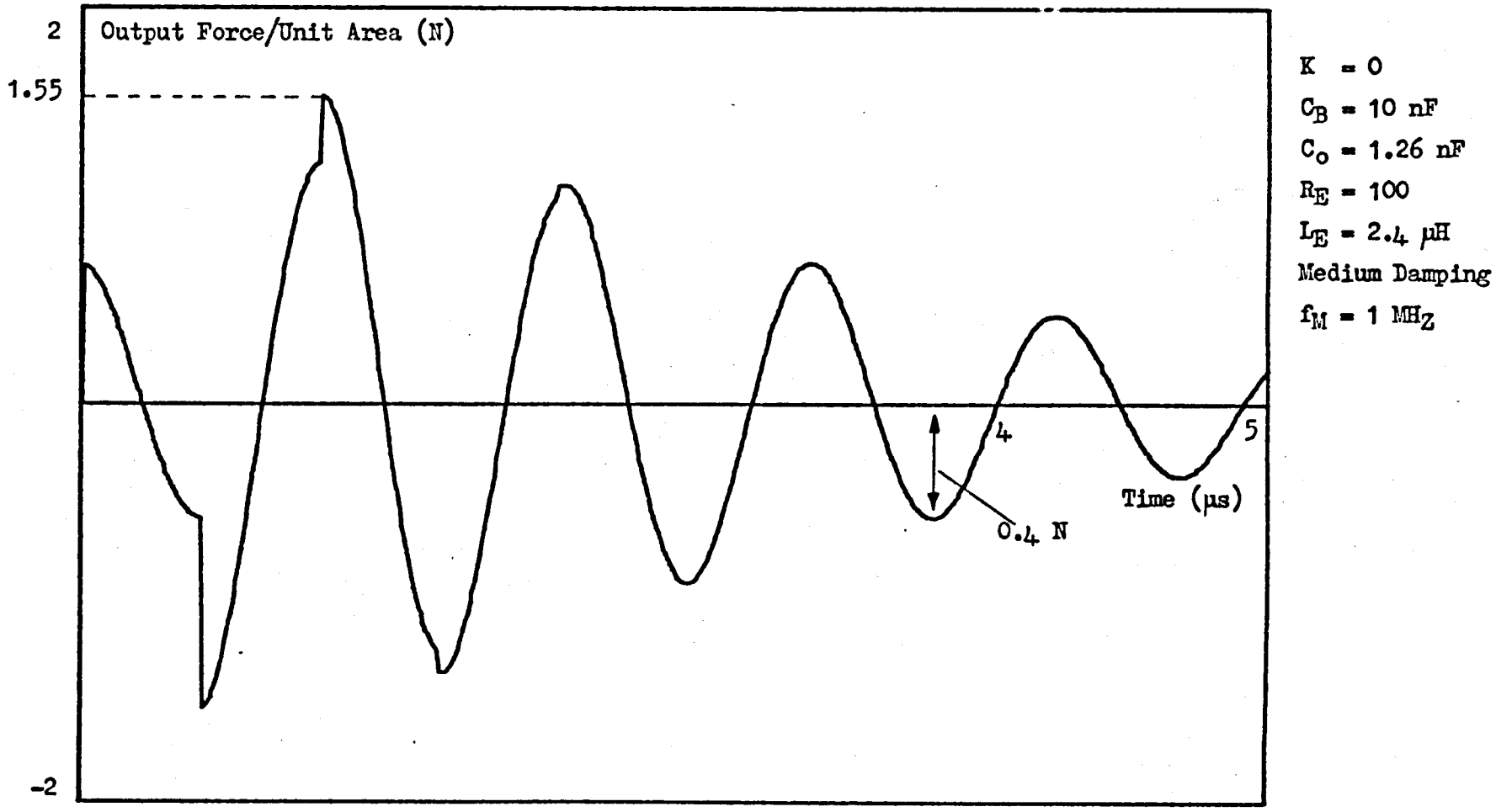

Fig. 8.7a. Approximate Form of Output Force

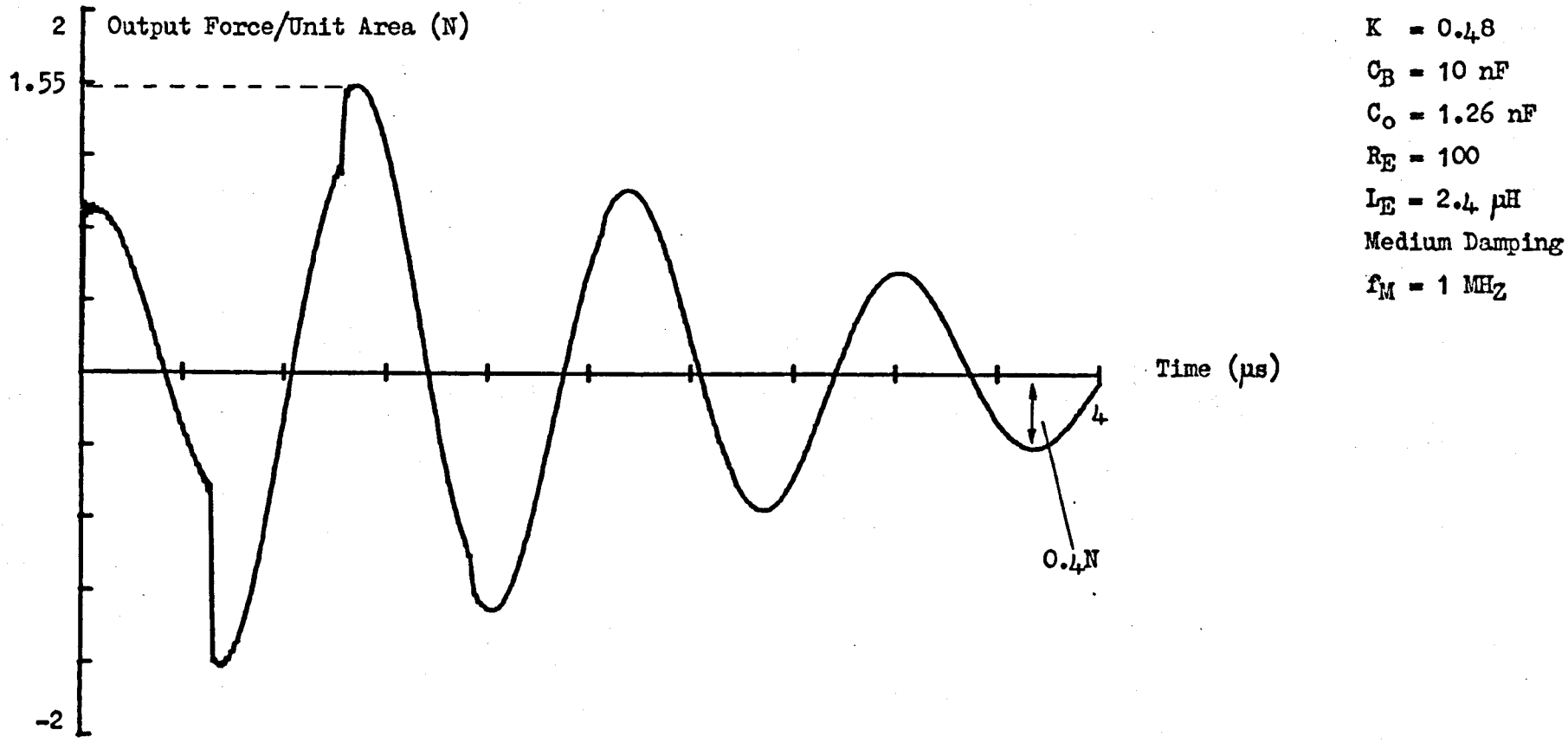

Fig. 8.7b. Exact Form of Output Force (IFFT Solution)

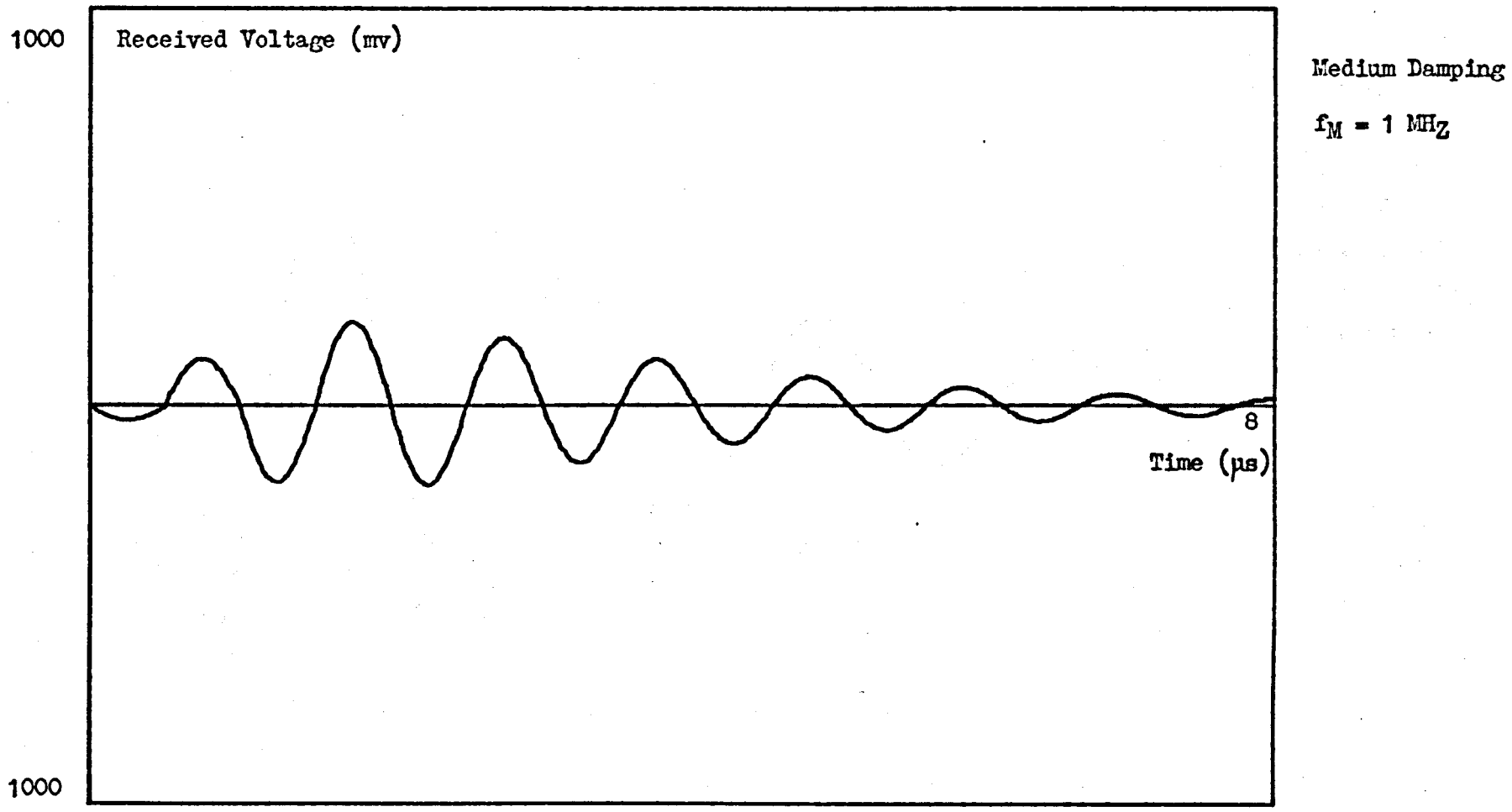

Fig. 8.7c. Received Voltage Waveform (Loop Response)

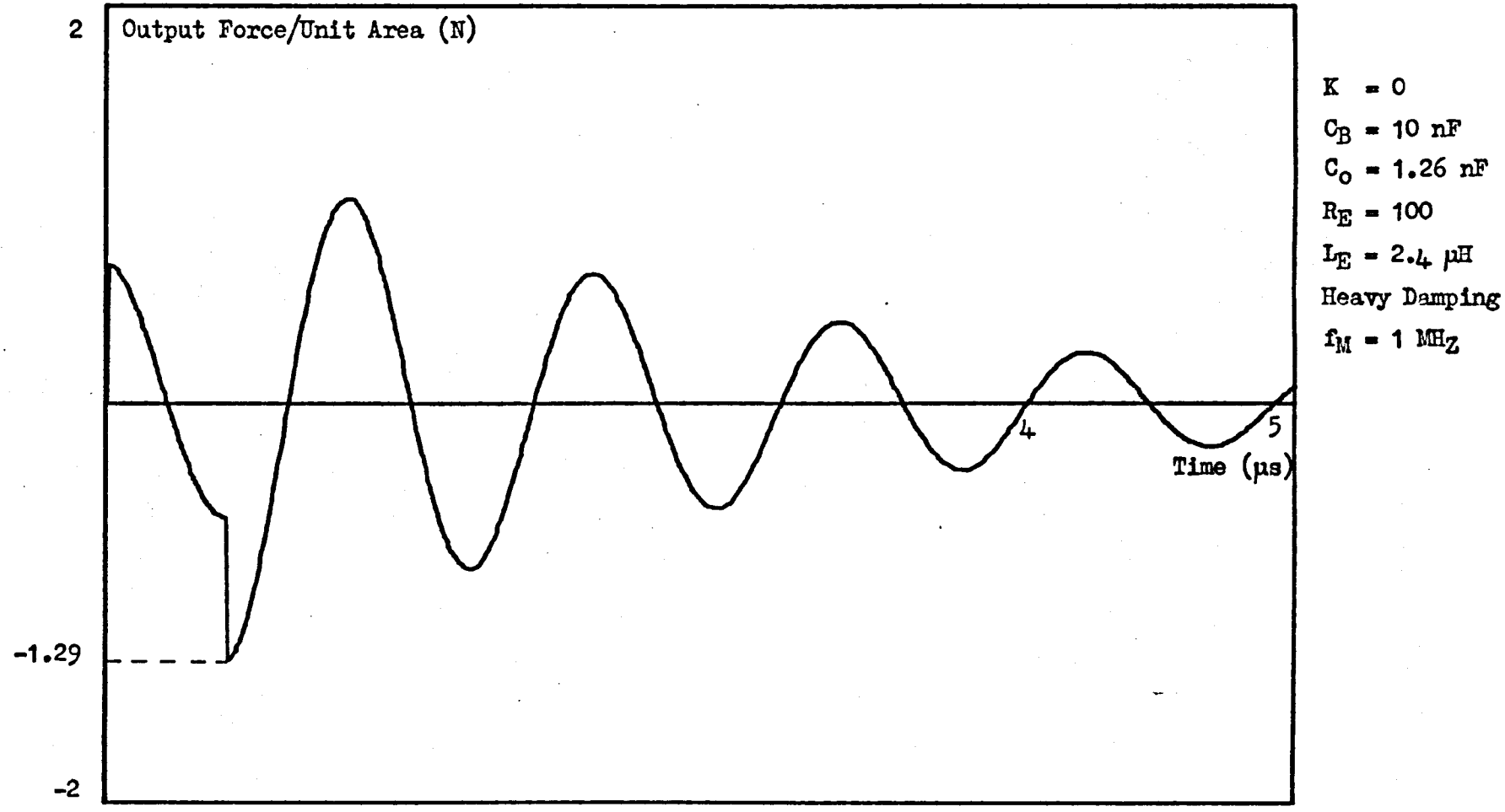

Fig. 8.8a. Approximate Form of Output Force (Z-Transform Solution)

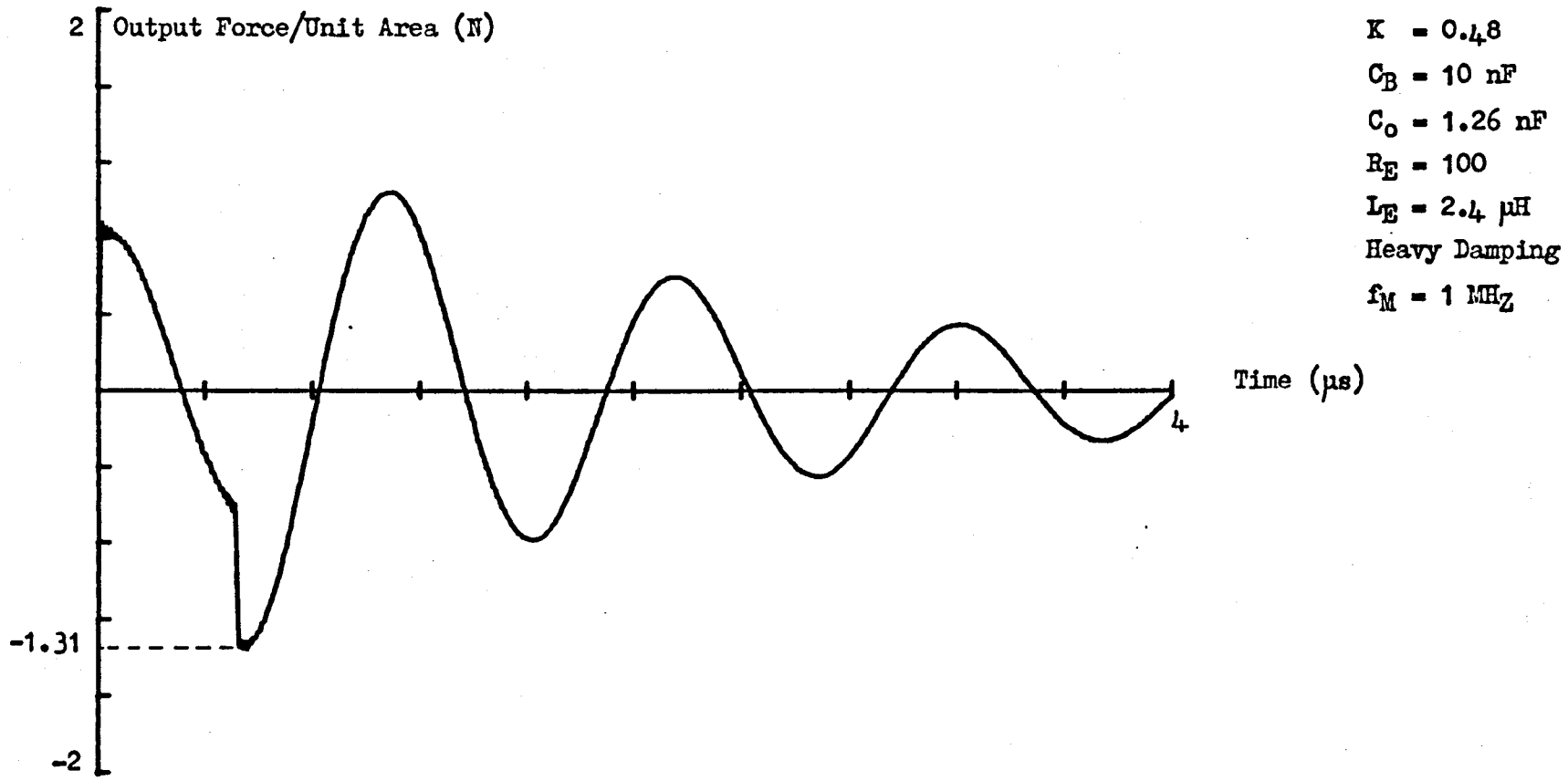

Fig. 8.8b. Exact Form of Output Force (IFFT Solution)

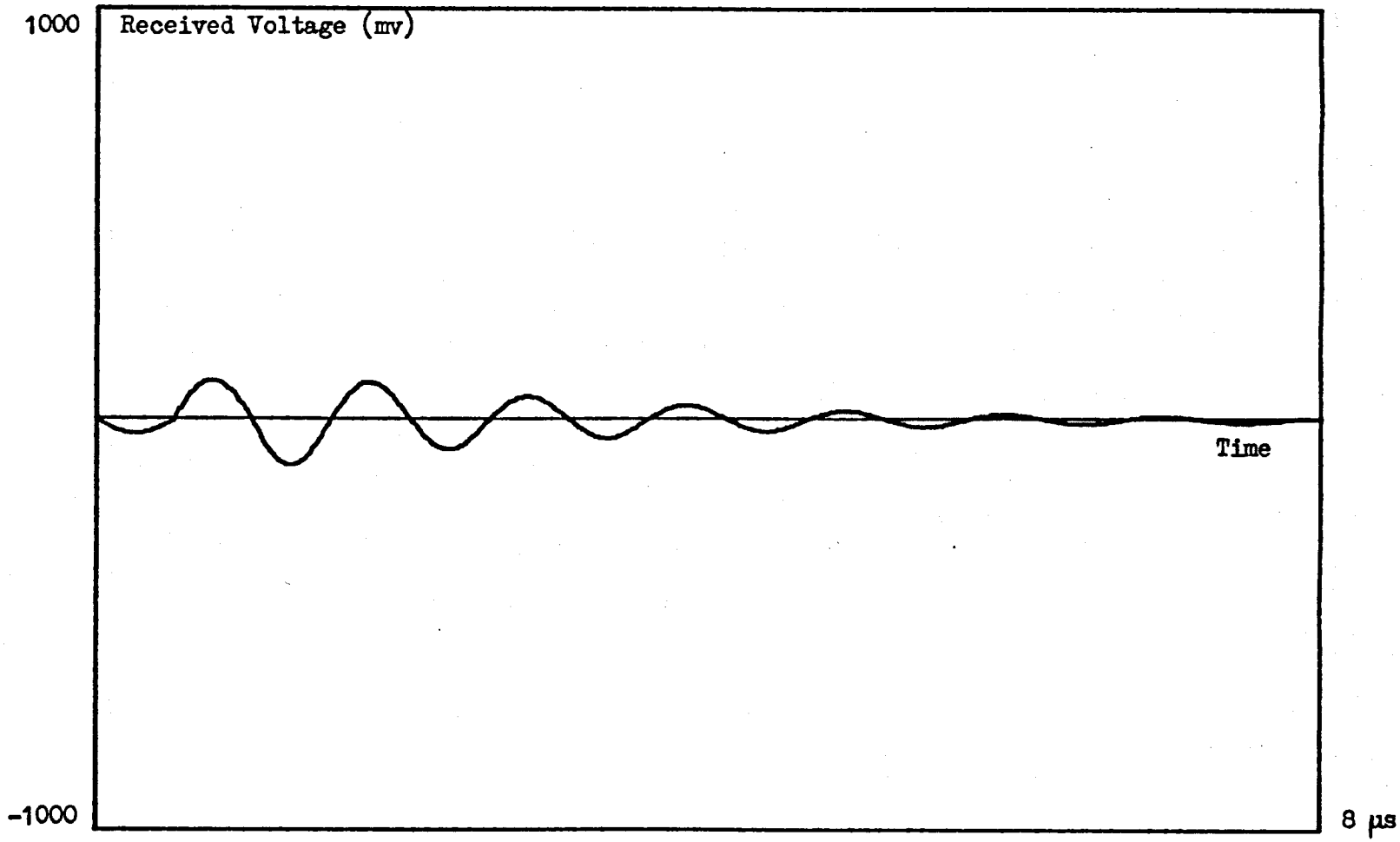

Fig. 8.8c. Received Voltage Waveform (Loop Response) for Heavy Damping

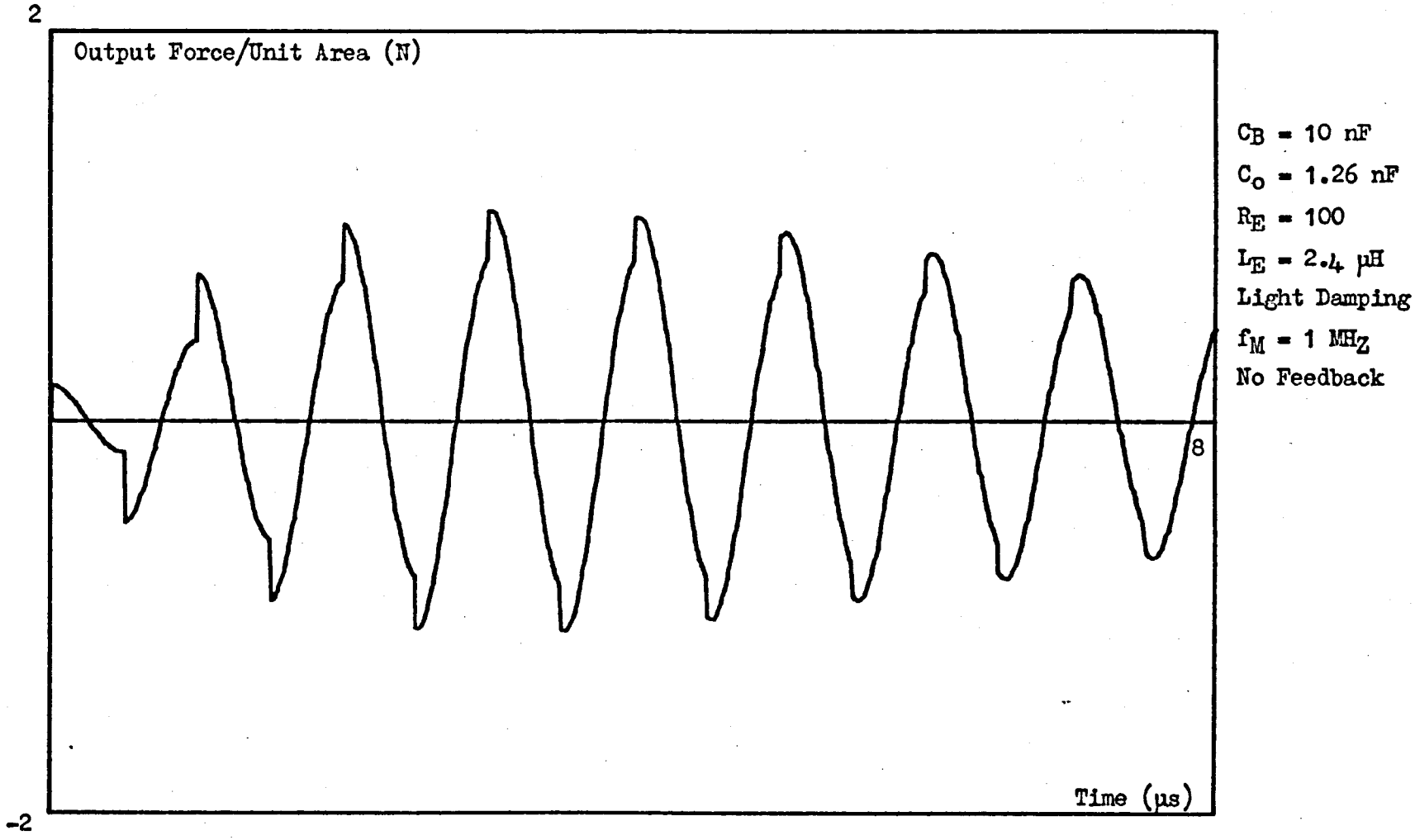

Fig. 8.9a. Approximate Form of Output Force (Z-Transform Solution)

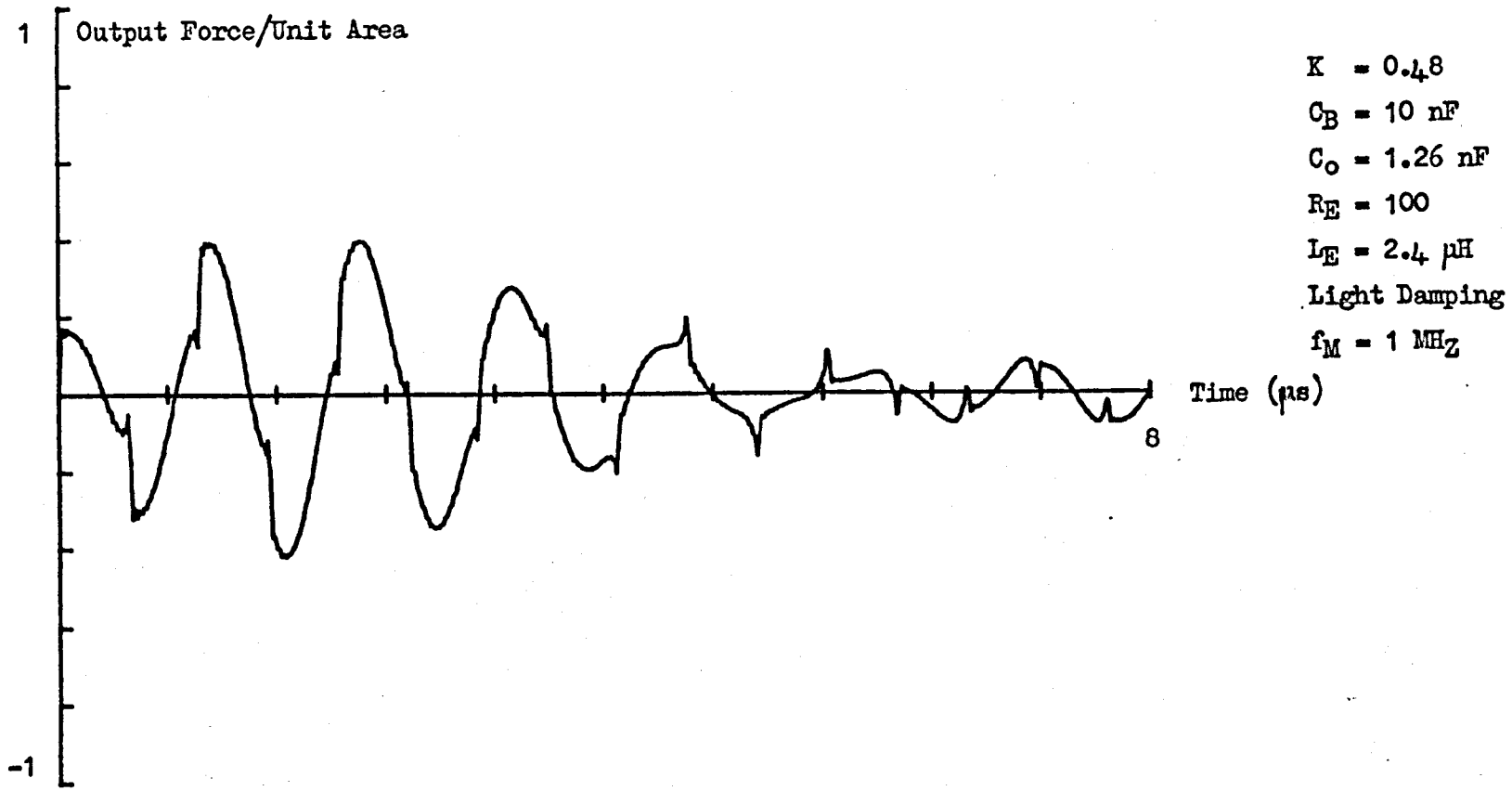

Fig. 8.9b. Exact Form of Output Force (IFFT Solution)

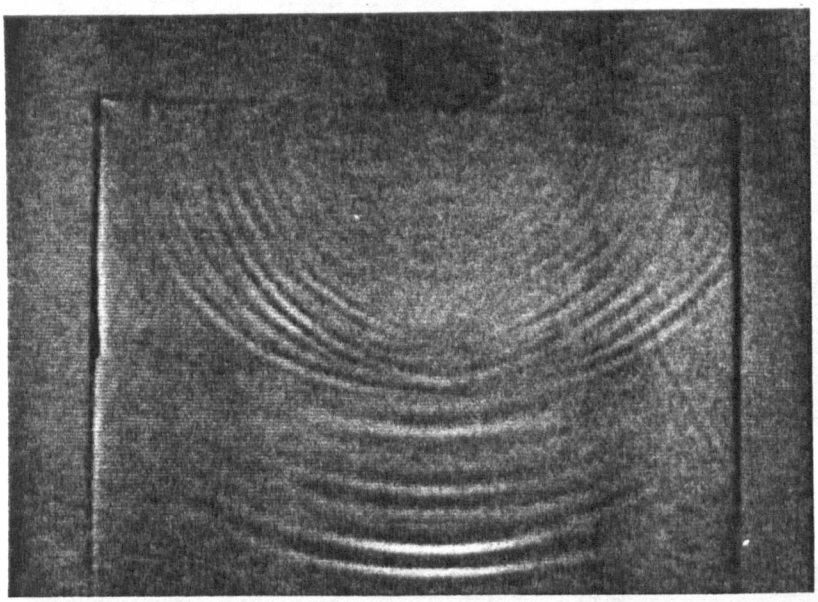

Fig. 9.1 Photoelastic Study of the Transient Far Field of a 1 MHz Transducer

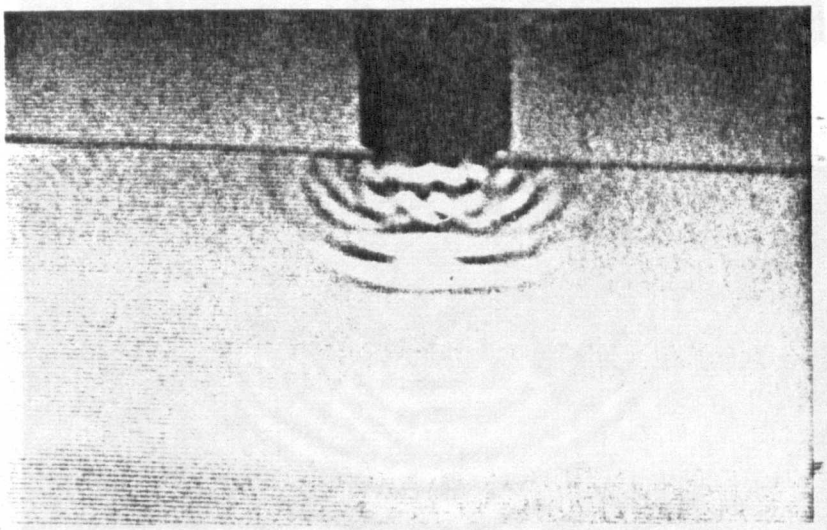

Fig. 9.2 Photoelastic Study of the Transient Near Field of a 1 MHz Transducer

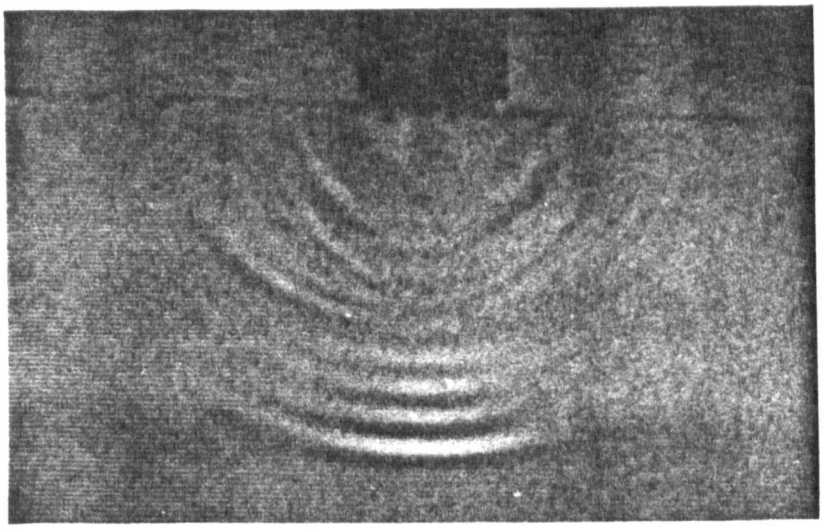

9.3a

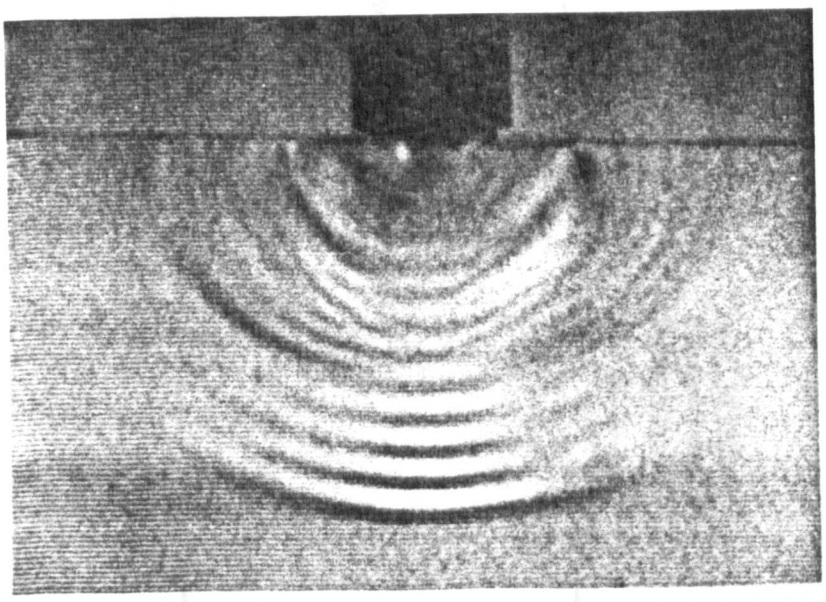

9.3b

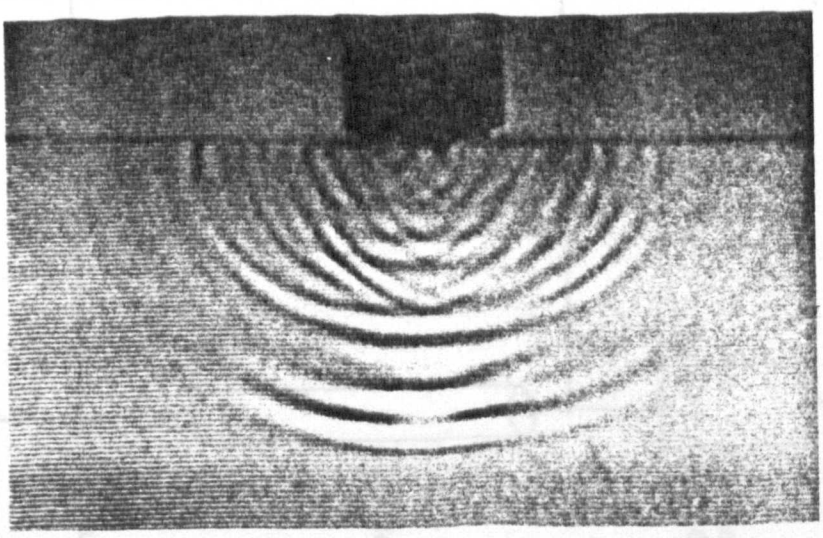

9.3c

Photoelastic Studies of the Transient
Field of a 1 MHz Transducer

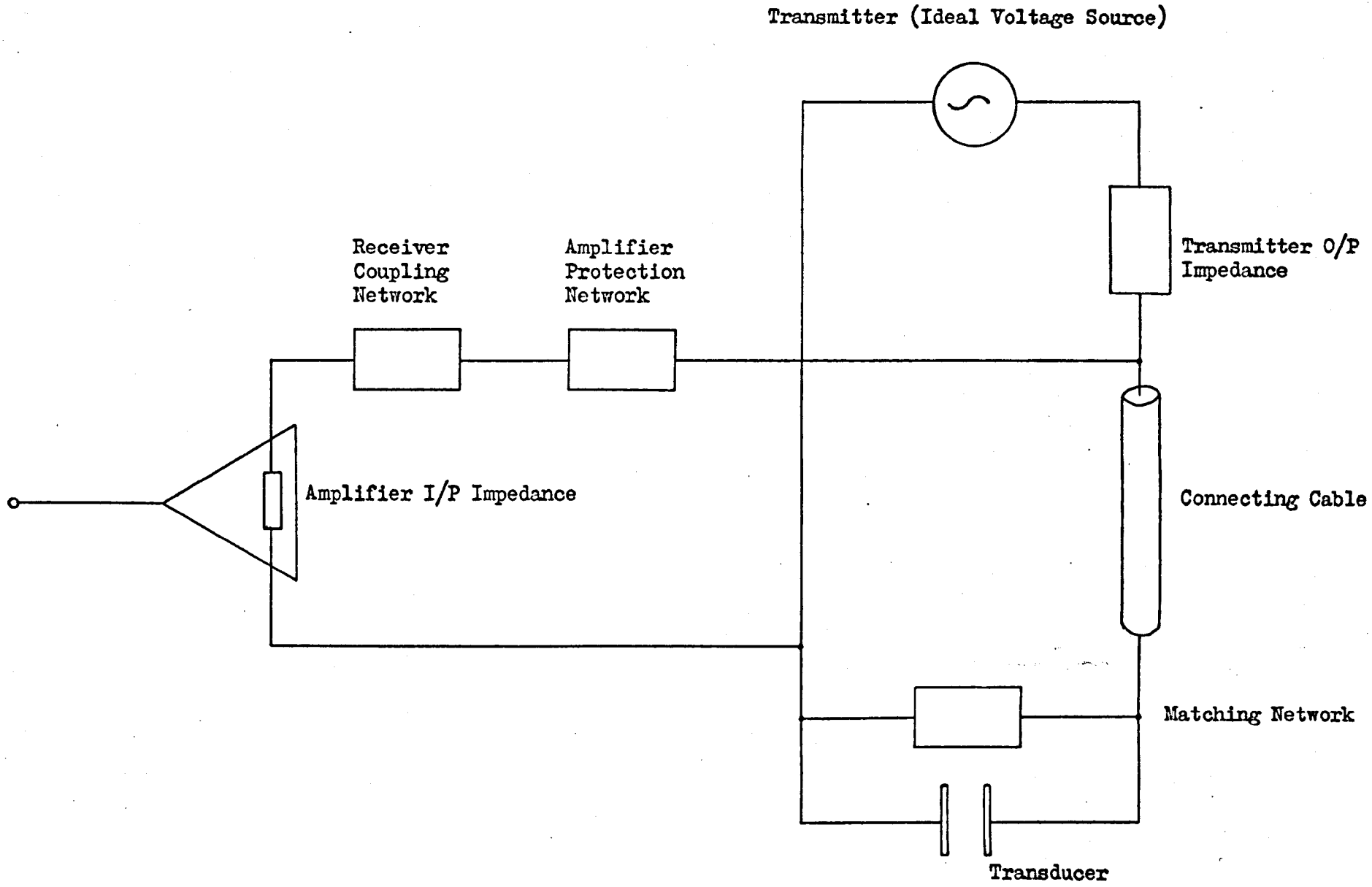

Fig. B1. Electrical Load Configuration for Pulse-Echo Operation

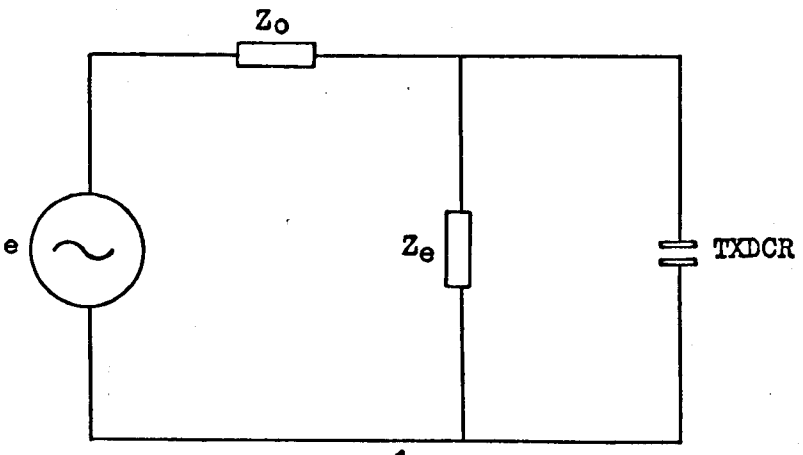

Fig. B2a. Electrical Loading for the Transmitting Mode

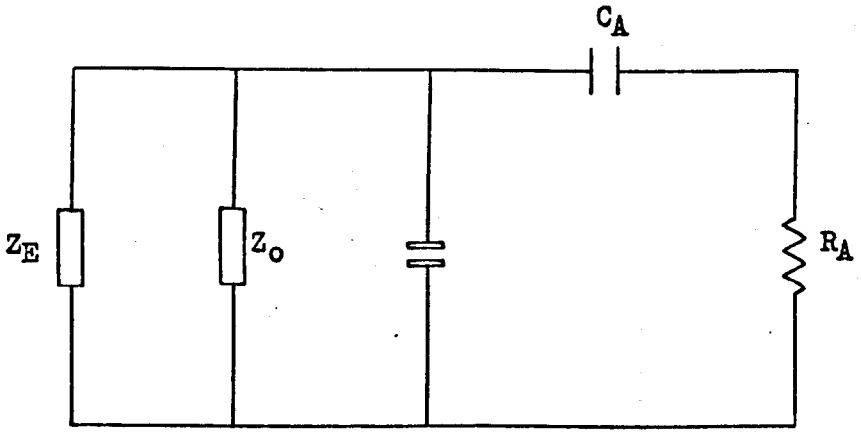

R_A - C_A represent amplifier and coupling impedance elements

Fig. B2b. Electrical Loading for the Receiving Mode

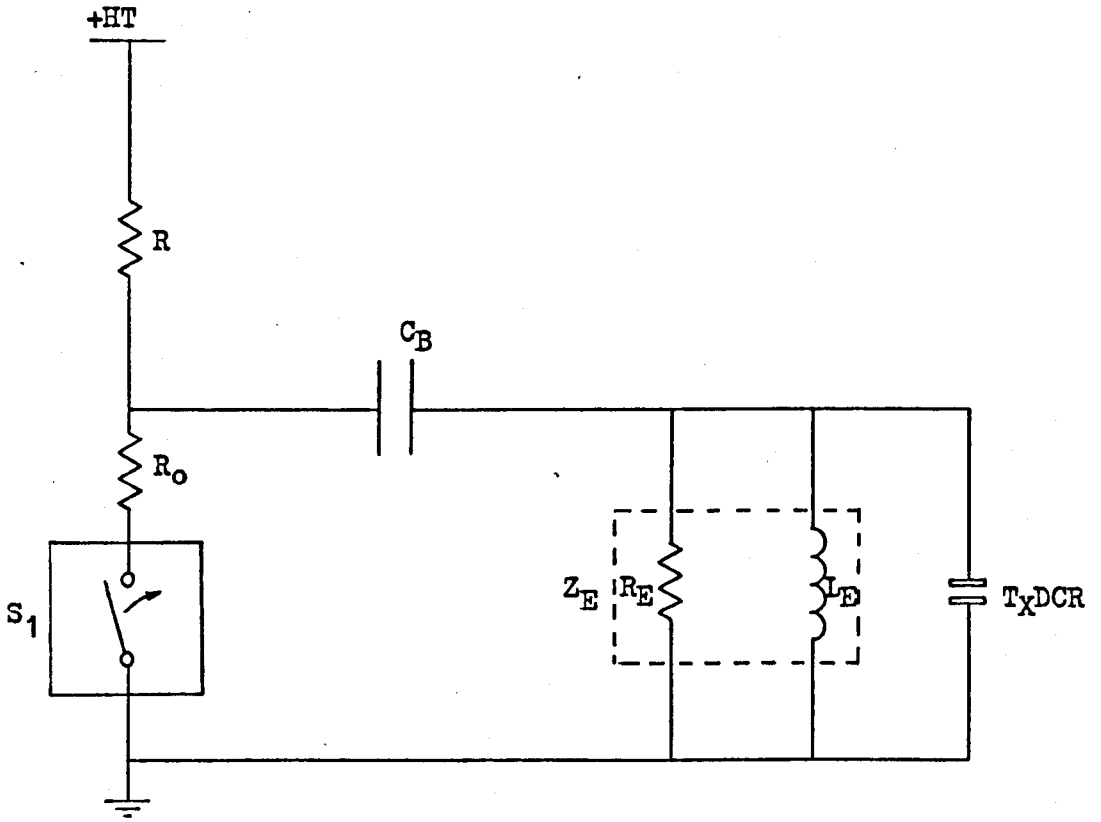

R_o = Pulser 'on' Resistance $R_o \ll R$, $R_o \ll R_E$

Fig. C1. Circuit Configuration for Transient Operation

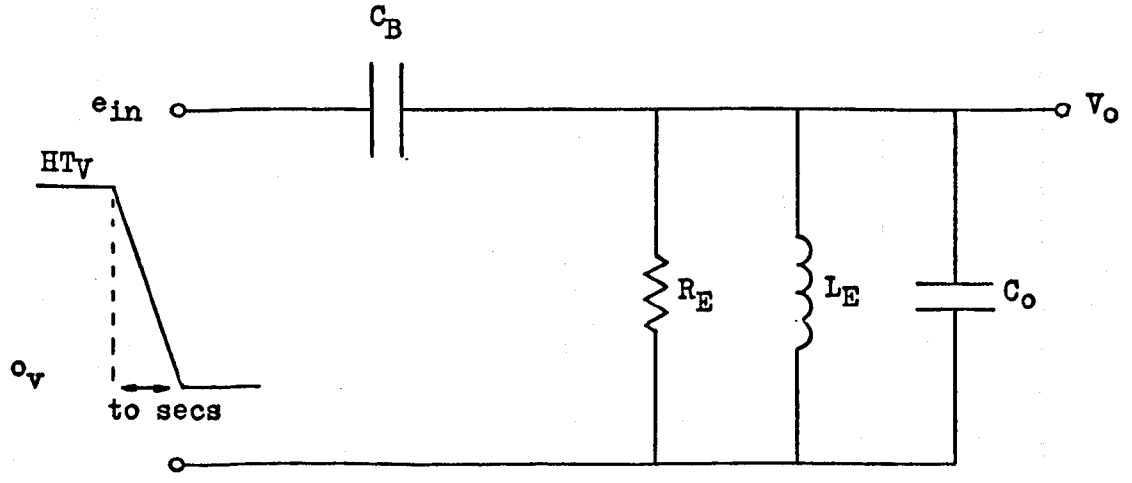

Fig. C2. Equivalent Circuit for Transient Operation

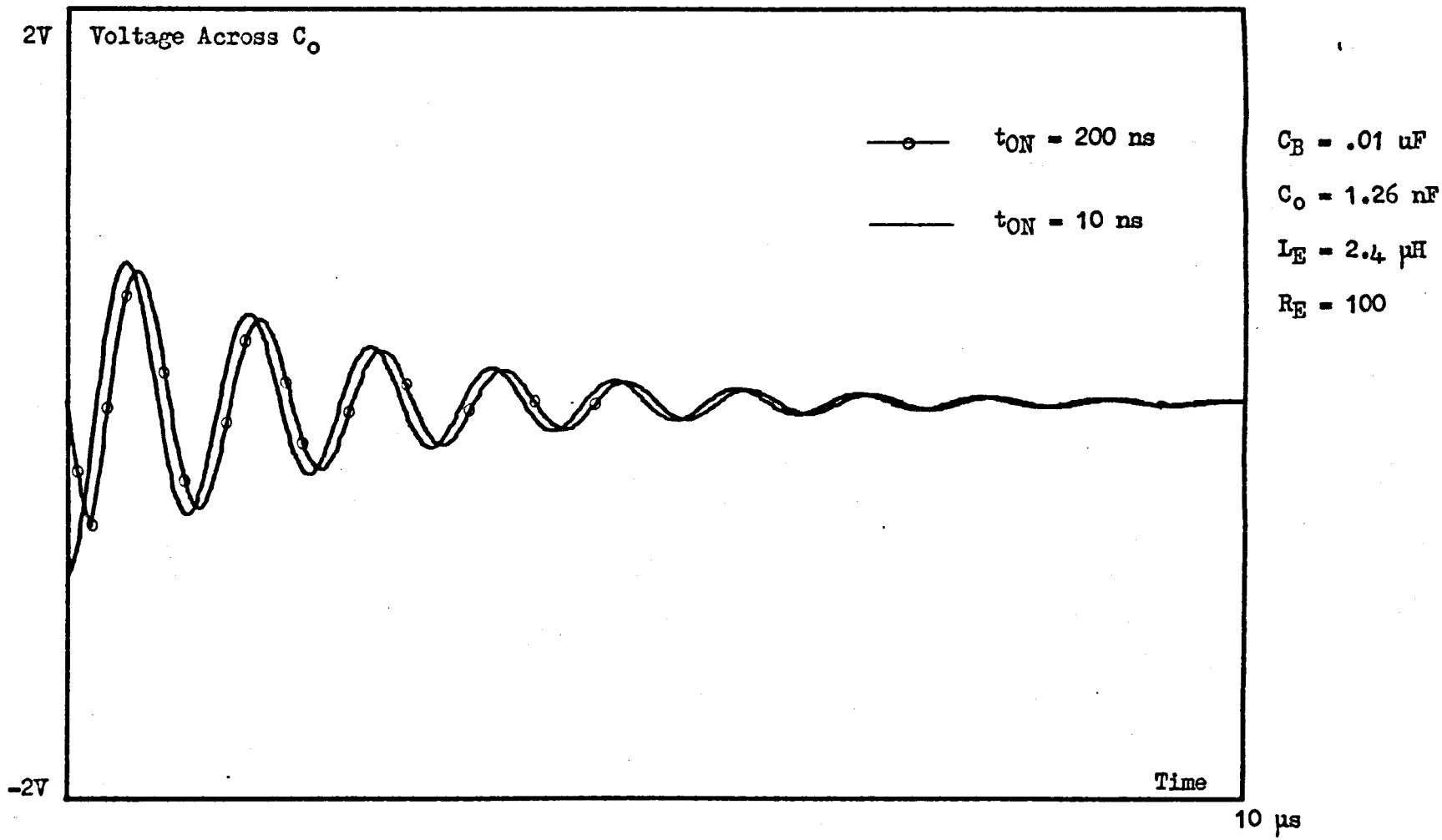

Fig. C3. Variation in Voltage Across C_o with Pulser Turn-on Time

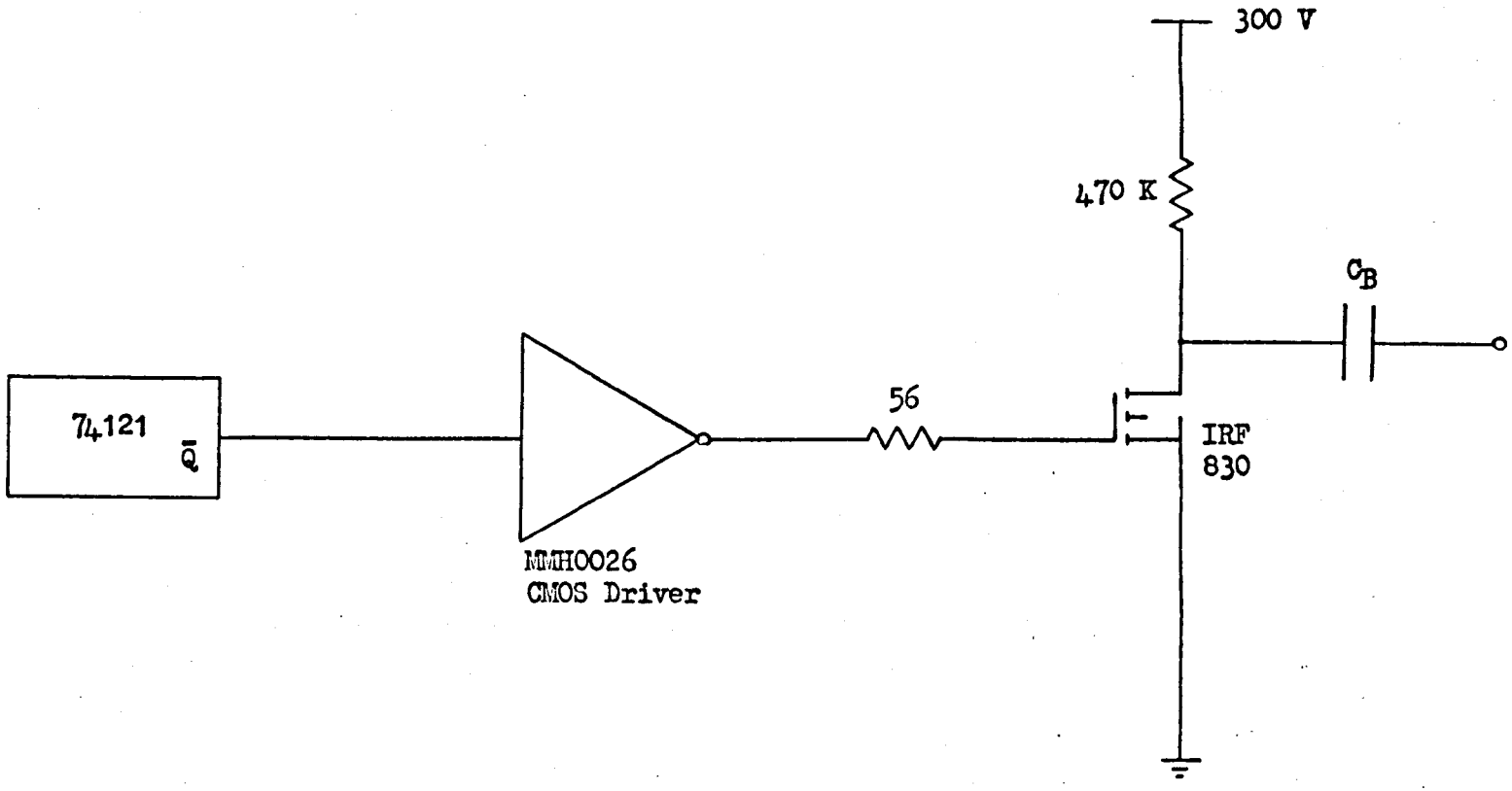

Fig. C4. Schematic of Transducer Firing Circuit

ρ kg/m^3	V_t^D m/s	Z_c kg/s-m^2	ε^T_{33}	$\tan\delta$	ε^s_{33}	h_{33} V/m	$N_3 t$ H_Z-m	k	Y^D_{33} N/m^2
7.75	4350	33.712×10^6	1700	.02	830	21.5	1890	0.486	14.7×10^{10}

Table D1. Standard Transducer Parameters

Electrical Resonance MHz	Thickness mm	Diameter mm	Transit Time μs	Mechanical Resonance MHz	Free Capacitance nF	Clamped Capacitance nF	Diam/ Thickness Ratio
.5	3.75	20	.869	.5754	Theoretical 1.2504	Theoretical .6105	5.333
					Measured 1.188	.57	
1	1.87	20	.4345	1.1508	2.5008	1.221	10.69
					2.2520	1.05	
2	.945	20	.2172	2.3016	5.002	2.4420	21.16
					4.353	1.87	
4	.4575	20	.1051724	4.754	10.0032	4.884	43.716
					8.163	3.7723	

Table D2. Characteristics of Transducers Employed in Experimental Work